Durham University

Durham E-Theses

NEW TECHNIQUES FOR TRACE ELEMENT AND RADIOGENIC ISOTOPE MEASUREMENT OF DIAMONDS: THEIR APPLICATION TO DIAMOND PETROGENESIS AND SOURCE TRACING

MCNEILL, JOHN,CHARLES,ROBERT

How to cite:

MCNEILL, JOHN,CHARLES,ROBERT (2011) *NEW TECHNIQUES FOR TRACE ELEMENT AND RADIOGENIC ISOTOPE MEASUREMENT OF DIAMONDS: THEIR APPLICATION TO DIAMOND PETROGENESIS AND SOURCE TRACING*, Durham theses, Durham University. Available at Durham E-Theses Online: http://etheses.dur.ac.uk/713/

Use policy

The full-text may be used and/or reproduced, and given to third parties in any format or medium, without prior permission or charge, for personal research or study, educational, or not-for-profit purposes provided that:

- a full bibliographic reference is made to the original source
- a link is made to the metadata record in Durham E-Theses
- the full-text is not changed in any way

The full-text must not be sold in any format or medium without the formal permission of the copyright holders.

Please consult the full Durham E-Theses policy for further details.

Academic Support Office, Durham University, University Office, Old Elvet, Durham DH1 3HP
e-mail: e-theses.admin@dur.ac.uk Tel: +44 0191 334 6107
http://etheses.dur.ac.uk

NEW TECHNIQUES FOR TRACE ELEMENT AND RADIOGENIC ISOTOPE MEASUREMENT OF DIAMONDS: THEIR APPLICATION TO DIAMOND PETROGENESIS AND SOURCE TRACING

John McNeill

A thesis submitted in partial fulfilment of the requirements for the degree of Doctor of Philosophy at Durham University

Department of Earth Sciences
Durham University
England
2011

Thesis Abstract

To investigate impurities in diamond we have developed an offline laser ablation method to acquire radiogenic isotope compositions and quantitative trace element determinations on diamond. This information has the potential to be used as both a petrogenetic tracer and as a tool in determining the geographic region of origin of particular diamonds. Trace element abundances are determined by sector-field ICPMS and isotope ratios are analysed via TIMS (Sr) and multi-collector ICPMS (Nd-Pb). To report quantitative trace element data the analyte mass we require from a given ablated sample volume is <1 pg for most elements, except for Sr, Zr, Ba which require between 2 – 30 pg, and for Pb ~40 pg.

Diamonds show broad LILE and LREE enrichment and HFSE and HREE depletion. Trace element systematics in fibrous diamonds are mimicked in monocrystalline diamonds. Monocrystalline diamonds display $^{87}Sr/^{86}Sr_{(i)}$ = 0.7014±0.0010 to 0.70864±0.00004 and fibrous diamonds display $^{87}Sr/^{86}Sr_{(i)}$ = 0.70386±0.00005 to 0.712406±0.00007. The isotope data show no defined isochron systematics that could be used for dating purposes. The parental fluids of fibrous and monocrystalline diamonds are thought to be derived through a similar multi-component mechanism. Diamond formation will result from the interaction between 1) a primitive, volatile and carbonate-rich, silicate liquid with an unradiogenic Sr signature ascending from the asthenosphere and 2) other components with more radiogenic Sr, akin to more ancient, enriched and vein-dominated lower lithosphere e.g. glimmerite/ PIC assemblages and the sources of Group II kimberlites.

We have demonstrated, using >100 diamonds from the Ekati, Diavik, Snap Lake and Congo kimberlites, that statistical processing of data using analysis of variance and logistic regression can allow source discrimination of ‘unknown’ samples. For logistic regression the most successful models focus on differences in Nb, Eu, Rb and Th data. This method shows good potential for use in a diamond fingerprinting programme.

Declaration

The research and discussion presented in this thesis are the original work of the author and have not been submitted at any institute of learning for any other award. Any material by any person or institute which has been presented is duly referenced, and a complete list of all references is presented in the bibliography.

John McNeill
Durham University

2011

The copyright of this thesis rests with the author. No quotation from it should be published without prior written consent and information derived from it should be acknowledged.

Acknowledgments

This work was completed during the tenure of a Diamond Trading Company / De Beers student scholarship for JM at Durham University. The sponsors are thanked for their generosity with sample provision, enthusiasm for the work being done, and their commitment to understanding the problems faced and helping to overcome obstacles. Dr. Philip Martineau, Dr. Simon Lawson, Dr. David Fisher, Dr Ingrid Chinn and Andy Davis are owed particular gratitude for their help and advice throughout the project. Dr Chinn and the staff at Harry Oppenheimer House, Kimberly, RSA, organized a fantastic tour of the facilities and a hands-on viewing of their 616 ct. and Eureka diamonds. Dr Chinn and Trevor Rowlands are thanked for a memorable tour of the Finsch diamond mine, Cape Province, RSA.

Principle supervisor Professor D. Graham Pearson and supervisors Dr. Geoff M. Nowell and Dr. Chris J. Ottley conceived the project and were actively involved in all aspects of the study. This thesis would not have been possible without the time and effort that they invested in me and in the work. Professor Pearson was always available for conversation, brainstorming and problem-solving and is thanked for his thoroughness and patience when reviewing my manuscripts. Professor Pearson is also thanked for the countless experiences and opportunities for travel and learning that he has generously facilitated. Dr. Nowell freely shared his analytical expertise and experience, provided full instruction and help in instrumental analysis and low-level chemistry and spent many hours working through thesis drafts and helping me

fully understand large data sets. Dr. Ottley is thanked for his patience and assistance with sector-field ICPMS, data processing and guidance on low-level chemistry.

Dr. Ofra Klein-BenDavid was directly involved in the initial method development during a Marie Curie fellowship at Durham. Dr. Klein-BenDavid is thanked in particular for the help, advice and teaching in the laboratory and for constructive conversation on data interpretation. Yakov Weiss at the Hebrew University of Jerusalem is thanked for kindly taking the time to acquire EMP analyses on a number of fibrous diamond samples. Dr. Fred Worrall at Durham University spent many hours running statistical models to help understand the potential for source discrimination of diamond. Dr Worrall freely shared his experience and expertise in a very challenging field.

Several other individuals have provided useful, insightful and encouraging comments or instruction throughout the course of this project. Dr. Fernando Laiginhas provided assistance and expertise in visual diamond characterization, diamond cracking procedures and diamond combustion methods. Dr Colin Macpherson is thanked for the use of a stable isotope gas prep line for diamond combustion experiments. Professor Lutz Nasdala provided assistance and training in Raman microscopy at the University of Vienna, Austria.

Samples used in the method development and applied studies were generously supplied by several companies, research institutes and individuals. DTC / De Beers

supplied large high quality diamonds from the Cullinan mine in the Republic of South Africa, and from the Snap Lake mine in the Northwest Territories, Canada. CVD diamonds and diamond grown in HPHT conditions were provided by DTC. BHP Billiton and Professor John Gurney of the University of Cape Town provided an array of diamonds from the Ekati property, Northwest Territories, Canada. Rio Tinto provided a large number of high quality diamonds from the Diavik property, Northwest Territories, Canada. Dr. Mark Hutchison and Dr Felix Kaminsky provided ultra-high pressure diamonds. Peter Nixon, formerly of the University of Leeds, UK, and Galina Bulanova at the Institute of Diamonds, Yakutsk, RF, are also thanked for provision of samples.

Completion of this thesis would have been almost impossible without Alice Rogers and she deserves my unending gratitude for her unquestionable support, patience, understanding and kindness of heart over the past 38 months.

CONTENTS LIST

An **electronic supplement** contains a full copy of the thesis and an excel file containing LOQ calculations as well as trace element concentrations filtered and non-filtered by LOQ for reference.

LIST OF FIGURES

Page

Chapter 2

Chapter 3

Chapter 4

LIST OF TABLES

Page

Chapter 2

Chapter 3

Chapter 4

Chapter 5

CHAPTER 1

Introduction: Current diamond science and the rationale for continuing research

The extreme physical properties of diamond, and thus the high expectations for application to technological solutions, continues to drive current diamond research into a new age. This has been aided by discoveries of chemical vapor deposition (CVD) methods for synthesis of diamond and industrial processes for producing diamond powder by detonation of explosives (Butler et al., 2009; Kong and Cheng, 2010). The clear technology drivers for the 21st century come from biomedical engineering, the demand for energy (fusion reactors), and the information technologies where perhaps diamond will provide the major progress-enabling component. Understanding and quantifying the impurity levels in synthetic diamond products is a critical issue in all these potential applications because of the way that impurities affect the resulting physical properties.

The characterization of *natural* diamonds is equally important. Continued research can help to develop a further understanding of diamond formation and in turn support development of new exploration models. Chemical and physical characterization of natural diamond is also currently addressing the feasibility of acquiring a diamond's 'fingerprint'. Using this study's approach, the multiple

constraints offered by combined trace element and radiogenic isotope measurements of lattice impurities within natural diamonds make it an extremely promising tool for such chemical fingerprinting, especially when coupled to other physical measurements. The principle use of this information might lie in the geographical discrimination of diamond sources but there are other applications such as determination of synthetic from natural diamond and the discrimination of physio-chemically treated from untreated diamonds as a means to enhance value. An analytical method to reliably identify conflict diamonds and thus stem their illegal trade was a key mandate of the European Commission Workshop on Conflict Diamonds held in Geel, Belgium, October 2007.

The first models of diamond genesis constrained by modern petrological and geochemical data made significant progress in establishing a clear framework of diamond petrogenesis, dominantly in the lithospheric mantle (Meyer & Boyd, 1972; Gurney et al., 1974; Sobolev et al., 1974; Gurney and Harte, 1980; Deines, 1980; Richardson et al., 1984; Harte, 1983; Meyer, 1985; Navon et al., 1988). More recent review papers now provide in-depth detail on the chemical and petrological aspects of natural diamonds, their inclusions, their host rocks and their possible origin; diamond genesis models (Navon, 1999; Stachel et al., 2004; Gurney et al., 2010); carbon sources in diamond (Cartigny, 2005; Stachel et al, 2009); diamond and inclusion chemistry (Stachel and Harris, 2008); diamond host rocks (Pearson et al., 2003; Gurney et al., 2005; Kjarsgaard, 2007); ultra-deep diamonds (Harte, 2010).

In this study I focus on the analysis of the trace element and radiogenic isotope signatures of lattice impurities in diamond, with the aim of constraining further the nature and origin of diamond-forming fluids. A method is developed that can be applied to both natural and synthetic diamonds, ranging from highly impure (e.g., fluid-rich diamonds of fibrous growth form) to octahedral smooth-faced diamonds of the highest gem quality. From a genetic standpoint, impurities, whether solid or fluid, represent some sort of sample of the diamond growth medium. At the pressures and temperatures of the diamond stability field, parental melts and fluids are fully miscible (Wyllie and Ryabchikov, 2000; Kessel et al., 2005). Fluids present during diamond growth therefore would be trapped as uniform, highly concentrated, high density fluids (HDFs) that are similar to sub-critical melts, but with higher volatile content. Included fluids may have since fully or partially crystallized. Pioneering studies of diamond-forming fluids have mainly focussed on fluid-inclusions in fibrous diamonds where they are present at high density;

- FTIR and TEM studies indicate the presence of multiphase mineral assemblages variably comprising silicates, carbonates, and apatite, along with water, carbonate, residual LDFs and minor molecular CO_2 (Chrenko et al., 1967; Navon et al., 1988; Lang and Walmsley, 1983; Guthrie et al., 1991; Walmsley and Lang, 1992; Zedgenizov et al., 2004; Shiryaev et al 2005; Klein-BenDavid et al., 2006).
- EMPA studies report that the bulk compositions of the fluid-inclusions present in fibrous diamonds are volatile rich (up to 50 wt. %) and vary between carbonatitic components, high in Ca, P, Fe, Mg, alkalies and carbonate (CO_2),

silicate components, dominated by Si, Al, K and H_2O, and saline components rich in K, Cl and H_2O (Navon, 1999; Izraeli et al., 2001, 2004; Klein-BenDavid et al., 2007, 2009).

- Trace elements measured in diamond HDFs from worldwide sources display a general LILE enrichment, HFSE depletion and REE depletion (INAA - Schrauder et al., 1996; LA-ICPMS methods - Rege et al., 2005, 2008, 2010; Tomlinson et al., 2005, 2006, 2009; Zedgenizov et al., 2007; McNeill et al., 2009; Weiss et al., 2009; Klein-BenDavid et al., 2010).
- Halogens are enriched in the HDFs relative to Primitive Mantle and Noble gas isotopic ratios are close to those accepted for convecting mantle (Turner et al., 1990; Johnson et al., 2000; Burgess et al., 2002, 2009).
- Sr-isotope measurements of combusted Congo fibrous diamonds bulk sample these fluid-inclusions as well as other impurities and display $^{87}Sr/^{86}Sr = 0.70360$ to 0.70516 (Akagi and Matsuda, 1998; Akagi, 1999).

All of this information has led most authors to link the fluids that are parental to fluid-rich fibrous diamonds with chemically similar and spatially associated carbonatites and kimberlites (Navon et al., 1988; Schrauder et al., 1996; Izraeli et al., 2001, 2004; Klein-BenDavid et al., 2004, 2007; Weiss et al., 2008, 2009). However, the large spectrum in bulk composition of diamond-forming fluids (e.g., Klein BenDavid et al., 2010) together with a significant range in Sr-Nd-Pb isotope compositions, that vary from those typical of the convecting mantle to extremely

enriched compositions suggest a role for several deep-seated and mobile components in the generation of diamond-forming fluids (Klein-BenDavid et al., 2010).

In contrast to the relative abundance of geochemical data for fluid-rich fibrous diamonds, available data for fluid-poor monocrystalline diamonds are very sparse, largely because of the exceedingly low levels of elemental impurities that they contain (INAA - Fesq et al., 1975; Bibby, 1982; LAM-ICPMS - Watling et al., 1995; Resano et al., 2003; Araujo et al., 2009b; Rege et al., 2010). Much of the data in these studies are unlikely to be above limits of quantitation and hence are of restricted use in constructing petrogenetic models. To address the very low levels of trace element analyte present in 'gem' diamonds, this study describes a new laser-based method for the quantitative analysis of diamonds at lower concentrations than possible with other methods. We present, compare, and contrast, for the first time, quantitative trace element concentrations and coupled radiogenic isotope information on both fibrous and monocrystalline diamonds. We use this information to develop a diamond genesis model and also to address the possibility of using statistical processing of the data to discriminate diamond source regions.

CHAPTER 2

A method for the combined radiogenic isotope and trace element analysis of diamond

2.1 Introduction

Whereas a great deal of chemical information has been acquired for fluid inclusions in fluid-rich, fibrous diamonds, the scarcity of fluid inclusions in white monocrystalline diamonds has hindered attempts to analyze them. Established LA-ICPMS techniques are hampered by the low volume of material provided to the mass spectrometer per second of analysis, resulting in elemental data that are rarely demonstrably quantitative.

In this study, we employ a closed-system laser ablation cell in which a diamond is ablated and the bulk products trapped to collect enough fluid-inclusion material for a precise analysis. The pre-concentrated diamond material is collected into solutions that are analyzed by sector-field ICPMS in the same short analysis time as conventional ICPMS techniques. Signal sizes and, critically, signal to background ratios are therefore much higher and greatly increase the chance of producing quantitative data. We show that the individual analyte mass we require from an ablated volume in order to report quantitative data is <1 pg for most of the analyzed elements, except for Sr, Zr, Ba which range between 2 – 30 pg, and for Pb ~40 pg. These values represent the method limits of quantitation (LOQ). We discuss the limitations of applying only "limits of detection" as a criterion for screening data. We demonstrate that this method can produce quantitative data on 'gem' monocrystalline diamonds that display trace element concentrations up to 2 orders of magnitude lower than the current LOQ values of other existing online LA-ICPMS techniques.

An additional advantage of the new method is that an analyte collected into solution also allows radiogenic isotope compositions for Sr, Nd and Pb to be acquired. The methodology is based on that found to be successful by Klein-BenDavid et al. (2010) when analyzing fibrous, micro-inclusion rich diamonds and is a development of that described in detail by McNeill et al. (2009).

2.1.1 Aims

Three main aims are addressed in this chapter;

- To evaluate the accuracy of published laser ablation trace element concentrations in diamond and compare the new method with alternative, non-laser based techniques, i.e. combustion.
- Establish a Limit of Quantitation for this offline ablation method, below which trace element concentrations are rejected as ether non-quantitative or too heavily influenced by blank/background.
- Perform a reconnaissance study of 'gem' quality monocrystalline diamonds to acquire quantitative trace elements and radiogenic isotope compositions.

Trace element concentrations have been measured in diamonds from multiple regions and in diamonds of various growth forms (Table 2.1). Diamond samples used to validate the method include coated/fibrous octahedral diamonds and monocrystalline diamonds. Monocrystalline diamonds used in this study have been separated into two groups;

- A low-purity group that consists of diamonds that have a high density of fluid inclusions;
- A high-purity group that has an extremely low density of fluid inclusions.

In the text the term *monocrystalline* will refer to both groups, *low-purity* when addressing the first group and '*gem*' is used when referring specifically to the high-purity group for which much more sparse data exist. We have also analyzed fragments of diamond coats that have been previously analyzed using LA-ICPMS, and a variety of synthetic diamonds grown either by Chemical Vapour Deposition (CVD) or High Pressure High Temperature (HPHT) processes.

	Location	Fibrous	Monocrystalline	Cube	Octahedron	Dodecahedron	Macle	White	Yellow	Brown	Black	Grey
Canada	Diavik	7	20	4	23			20			7	
Canada	Ekati	12	30	7	28	6	1	22	2	9	2	7
Canada	Snap Lake		49		49			30	5	7		7
Africa	Congo	10			10				2			8
Africa	Jwaneng	1			1							1
Africa	Cullinan		10		10			10				
Africa	DRC	1			1					1		
Siberia	Udachnaya		1		1			1				
Siberia	Mir		1		1			1				
S.America	Venuela		1		1			1				
Synthetic	CVD		3		3			2	1			
Synthetic	HPHT		1		1						1	
Synthetic	Silicon Wafer		-	-	-							5

Table 2.1. Characteristics of the diamond samples used in this study.

2.2 Analytical methods and instrumentation

2.2.1 Trace element analysis – A new approach: Closed-system laser sampling

2.2.1.1 Experimental.

All laboratory and analytical work for this study was carried out in the Arthur Holmes Isotope Geology Laboratory at the Department of Earth Science, Durham University. All low concentration work is conducted in custom-built class 100 laminar flow environments. Dedicated reagent bottles and teflon beakers are used to obtain consistent ultra low-level chemistry. Ultra-pure water with a resistivity of ~ 18.2 MΩ is obtained from a Milli-Q Element system. Reagents used for sample recovery and dilution for mass spectrometry are ultra purity triple-distilled acids (UpA) manufactured by Romil Ltd. Working solutions of reagents are made up from these stock acids by diluting with Milli-Q purity water.

2.2.1.2 Laser Ablation techniques

2.2.1.2.1 Off-line ablation cell. While we use both laser ablation and ICPMS for multi-element trace analysis of diamonds we differ from previous approaches (e.g. Resano et al., 2003; Tomlinson et al., 2005; 2006; 2009; Rege et al., 2005, 2010; Weiss et al. 2008, 2009) in that we utilize an "off-line", closed system ablation cell that is not connected to the mass spectrometer. This allows us to control analyte levels by varying the duration of ablations. The resulting signals for most analytes are considerably elevated above instrumental background compared with direct-ablation techniques, permitting more precise quantitative measurement. The defining

parameter for quantitative data then becomes the reproducibility of the analytical blanks arising from the chemistry.

For this study we employed a New Wave™ Nd:YAG 213 nm laser to ablate all diamonds. The standard New Wave™ open-system ablation cell is replaced with a custom-manufactured cell of our own design that consists of a PTFE body that can be acid-cleaned between ablations, and a laser-glass-window lid. Since our offline ablation cell is a sealed unit, material is retained within the cell during the ablation such that laser-induced elemental fractionation at the ablation site, which is a major problem for on-line laser ablation analysis, poses no problem. This system was originally developed for the analysis of Sr-Nd-Pb isotopic ratios in fluid-rich fibrous diamonds (Klein BenDavid et al., 2008) and has been adapted for trace element determinations.

The internal volume of our off-line ablation cell is approximately 5 mls. It comprises three components - a main vessel that houses the sample, a removable laser window/ PTFE cap and a screw cap, which retains the laser window (Figure 2.1). The laser window is UV grade fused silica and is coated on the upper surface, which faces the incident laser beam, with an anti-reflection coating transparent to wavelengths of 193-248 nm. The main vessel has an outer diameter of ~ 30 mm and a similar depth. An internal plinth with a slight central recess allows controlled placement of the sample in the centre of the cell.

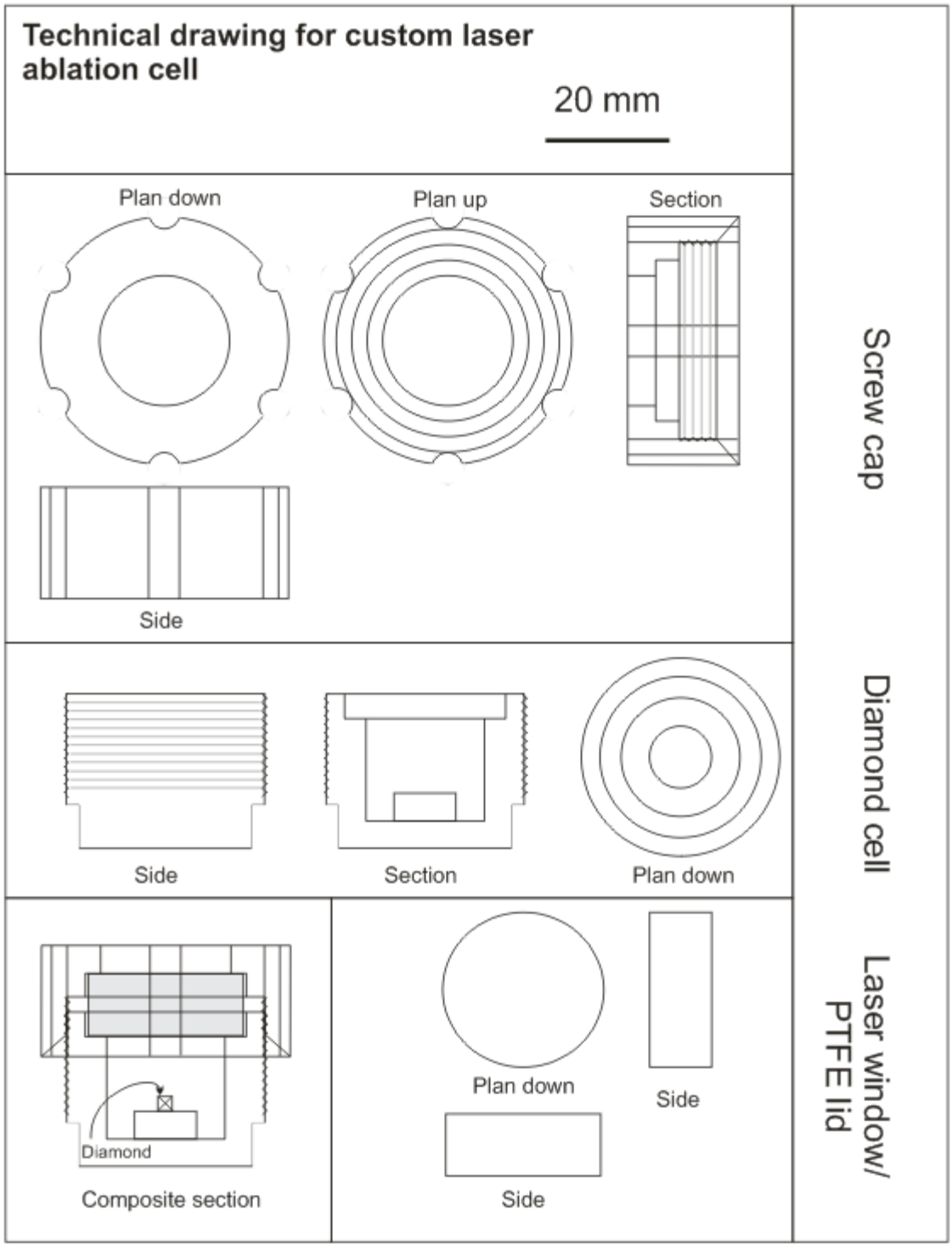

Figure 2.1. Ablation cell schematic is to scale. All components are constructed from PTFE except for the laser glass which is made from silica and has the same dimensions as the PTFE cap.

Prior to each ablation the cell is leached in 6N HCl (2 x 24 hrs) at 120℃ to remove any memory of a previous sample. The main compartment and parts are then immersed in 2N HNO_3 for 24 hrs at 80°C followed by a Milli-Q H_2O bath (2 x 24hrs). The last stage involves a further 120℃ leach in UpA 6N HCl (2 x 24 hrs). This process is detailed in Process 1 (Appendix).

2.2.1.2.2 Sample preparation and ablation.

Samples are first characterized under a microscope and then washed, weighed and loaded into the ablation cell, Process 2 (Appendix).

2.2.1.2.3 Laser parameters. A series of experiments was carried out to determine which laser parameters would provide optimum results for the diamond analysis. These experiments involved the ablation of a diamond sample at varying laser frequencies, spot sizes and energies. Diamond 3812P, a colourless, monocrystalline plate was used throughout the laser parameterization. This sample shows no macroinclusions and no visible microinclusions or cracks. Weight lost from the diamond as a result of ablation in the closed cell increased positively with laser spot size until 200 μm (Figure 2.2). At this point increasing the spot size did not result in greater diamond weight loss over a twenty minute ablation period. This marks the juncture where the fluence or energy density at the sample surface decreases below the ablation threshold for diamond and we no longer get efficient coupling with the diamond and therefore inefficient ablation.

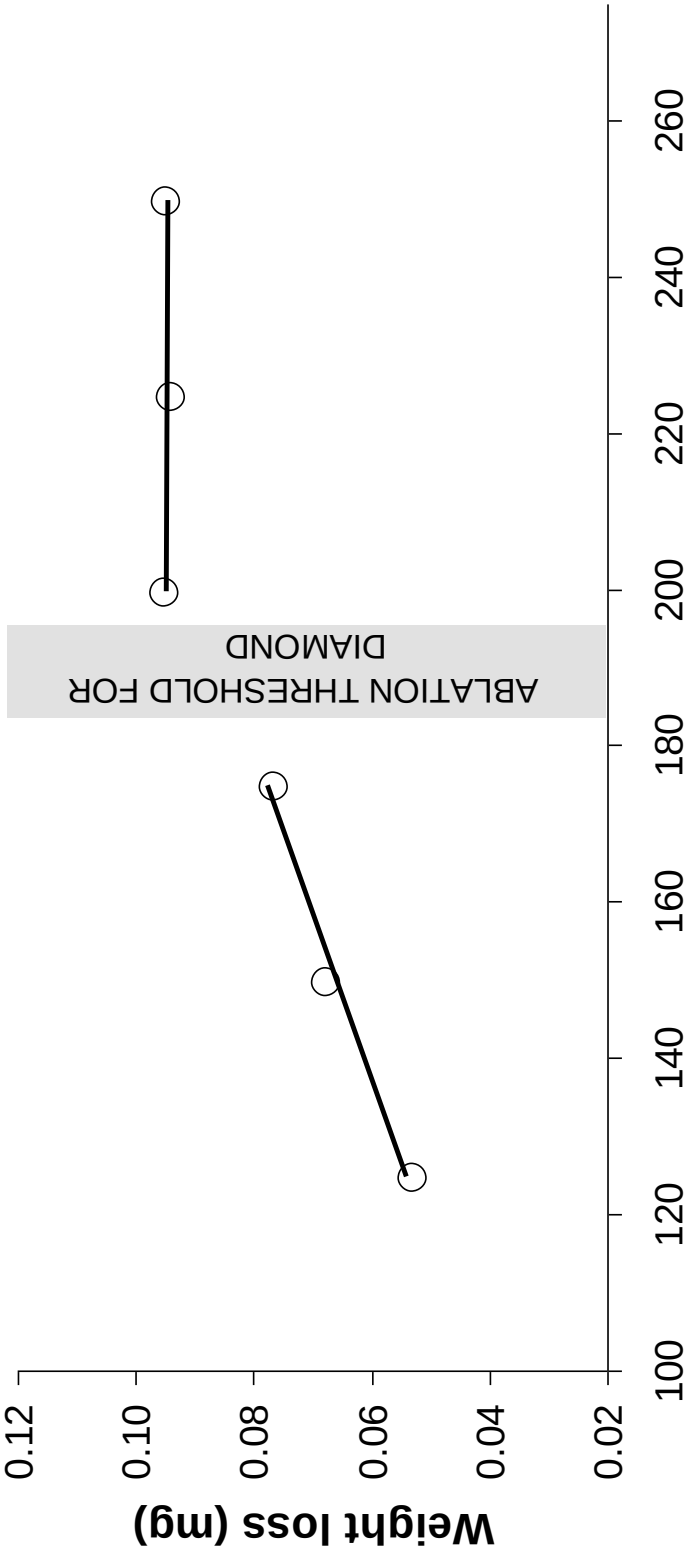

Figure 2.2. Laser parameters tests defined a laser head size of 160um-200um on the sample surface as the most efficient setting. Each analysis was a 20 minute ablation followed by sample weight loss measurement.

This energy density cannot be directly measured at the sample surface using our current experimental set up since the only measurement of laser energy takes place prior to the final objective. It is also likely that this ablation threshold will occur at different spots sizes for different diamonds due to variations in the density of inclusions and hence efficiency of coupling and may be different for different customer UP213 units. At the time of these experiments the output of the Tempest laser unit on our UP213 was depleted by approximately 60%. At any given spot size diamond weight loss is also proportional to ablation duration (Figure 2.3). This straightforward observation is important to verify since it confirms that ablated material is not recondensing in the ablation pit to be reworked by subsequent laser pulses, thereby decreasing the efficiency of the ablation. Figure 2.3 also demonstrates that weight loss does not follow a consistent proportional change for all diamond types. This is likely to be due to variations in the efficiency of coupling between the laser and diamond as a result of variations in micro-inclusion density, lattice defects, other irregularities and fundamental growth form (fibrous vs monocrystalline).

During ablation we operate the New Wave Nd:YAG UP213 nm laser at a repetition rate of 20Hz at 100% output, producing a laser energy of ~1 mJ and an estimated fluence (energy density on the sample) of 3-6 J/cm^2 based on a beam diameter of 160 μm (Table 2.2). If the parameters are set lower than these values we find that the desired weight loss from the diamond takes longer to achieve.

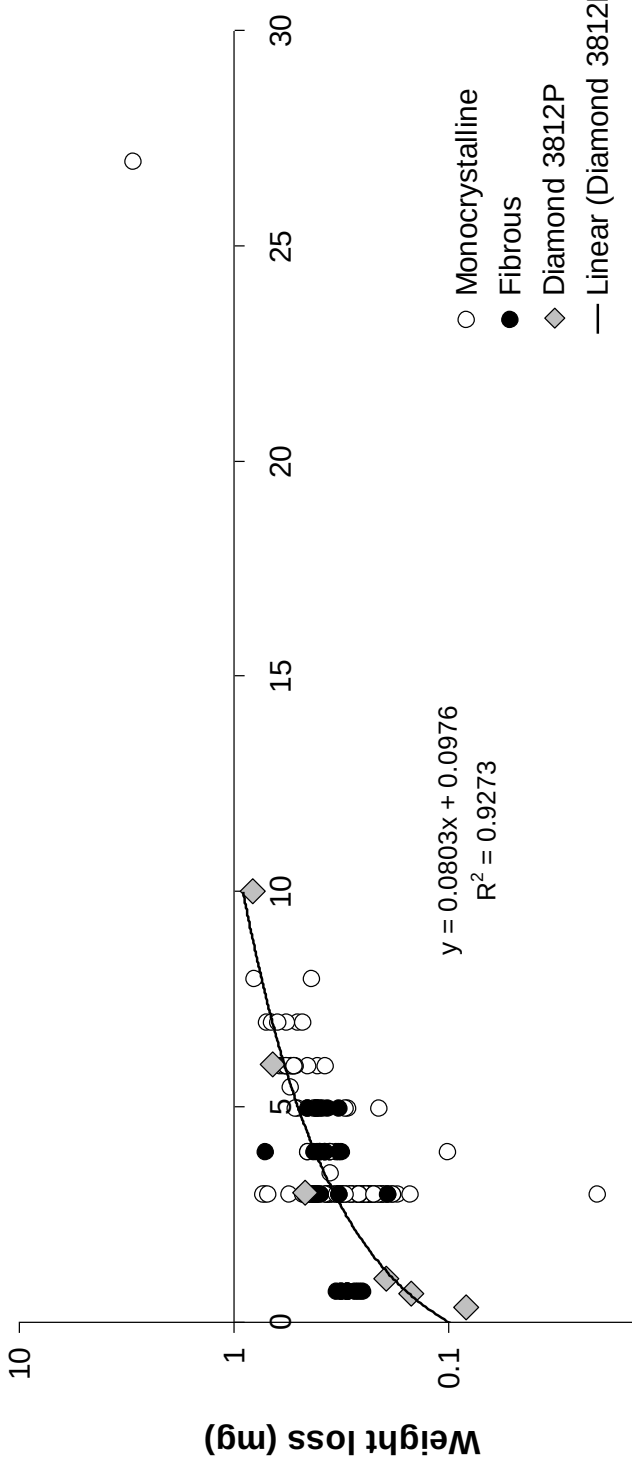

Figure 2.3. Ablation time vs. resulting weight loss from the diamond sample. A clear linear trend is unlikely to be observed as each diamonds structure is non-perfect, whether monocrystalline or fibrous and each sample will have a variable density of fluid inclusions throughout its body. Grey diamond shaped symbols displays a better trend as they represent multiple analyses on one monocrystalline stone.

LA *New Wave Nd:YAG*		**ICP-MS** *Thermo ELEMENT2*	
Laser source	New Wave	Nebuliser	25 ul min-1 micromist
Wavelength	213 nm		Teflon PFA concentric nebuliser
		Spray chamber	ESI stable introduction
Power			system quartz dual spray chamber
Energy	0.0-1.1 mj		
Energy density	3-6 J cm-2	RF Power	1300 watts
Output	100%	Plasma gas flow	16 L min-1
Rep. Rate	20 Hz	Auxillary gas flow	1 L min-1
		Nebuliser gas flow	~ 0.95 L min-1
Spot size	160 um	Resolution	300 (low)
Scan speed	50 um s-1		
Depth/pass	2 um	Isotopes measured	Ti47, Ti48, Ti49, Rb85, Sr88, Y89, Zr90, In115, Cs133, Ba137, La139, Ce140, Pr141, Nb93, Nd143, Nd144, Nd145, Sm147, Sm149, Eu151, Gd157, Dy161, Er166, Yb172, Lu175, Hf179, Pb208, Th232, U238, Tb159, Ca44, Sn118
Raster (average)			
W	500.9 um		
H	500.9 um		
A	2.509e5 um-2		
D	200-400 um	Sample time	10-60 ms
		Samples per peak	20
		Mass window	60
		Runs	4
		Passes	3
		Total time per sample	01:51

Table 2.2. Instrumental parameters typical during a full-method analysis of diamond samples.

The duration of the ablation is varied depending on the expected analyte levels within the diamond and the signal intensity that we are aiming for. These factors also control the size of the resulting ablation pits. For the analysis of gem diamonds with extremely low trace element concentrations we employ a raster pattern that avoids any visible solid inclusions. Typical ablation pits on the diamond surface have X-Y dimensions of 150 to 700 μm and a depth of 150 to 500 μm. For the analysis of samples with very low suspected trace element abundances, larger raster patterns (X-Y: 750 x 750 μm) were used requiring ablation times of ≥180 minutes. While this extended ablation time is considerably longer than that used in recently published "direct ablation" studies (i.e. normal LA-ICMPS techniques; Rege et al,

2005; Zedgenizov et al, 2007; Weiss et al, 2008), which are typically ~130 seconds, the advantage is in the much larger measured analyte signals during mass spectrometry, with resulting gains in limits of quantification (see below).

2.2.1.2.4. Elemental Fractionation. A critical aim in laser sampling for elemental analysis is to optimize the laser coupling efficiency for ablation with minimal inter-element fractionation. This ensures that all the material collected has been successfully volatilized and therefore can enter and be ionized efficiently by the mass spectrometer. Arguably one of the outstanding significant problems with LAM-ICPMS is elemental fractionation at the ablation site arising through different elemental volatilities.

An empirical measure of the homogeneity of ablation efficiency in any solid material is the symmetry of the ablation pit geometry. A comparison of ablation pit geometries made using our offline measurement routine and ablation parameters compared with those of the online ablation approach of Rege at al. (2005) is given in Figures 2.4 and 2.5. The irregularity of the base and the morphological variability between pits made during the Rege et al. measurement routine (2.4B) is very likely to cause elemental fractionation problems. In addition the pits show extensive areas of collateral damage and re-deposition (over 100 μm) that must be removed by polishing if other spectroscopic measurements are to be made in these areas (2.5A+C). This re-deposited material may account for a significant percentage of the volume of total material ejected from the laser pit during the ablation. In itself this

may create elemental fractionation problems if certain elements remain in transport while others get recondensed onto the diamond surface. An additional conclusion to be drawn from these images is that even though the direct LAICPMS technique typically uses much shorter ablation times than the off-line method presented here, the resulting collateral damage to the host diamond can cover as large an area and may be cosmetically much worse. An amount of material is therefore not entering the mass spectrometer and must result in a weaker analyte signal. Ablation pit geometry and differential elemental volatility is not such a critical parameter for our closed system method as the volatilized material is contained within the cell and completely collected before being presented to the mass spectrometer (2.4A+C and 2.5B+D). Ablation pits produced via this routine are geometrically regular, with minimal areas of collateral damage. These pits are based on a raster pattern and yield much more reproducible pit morphologies.

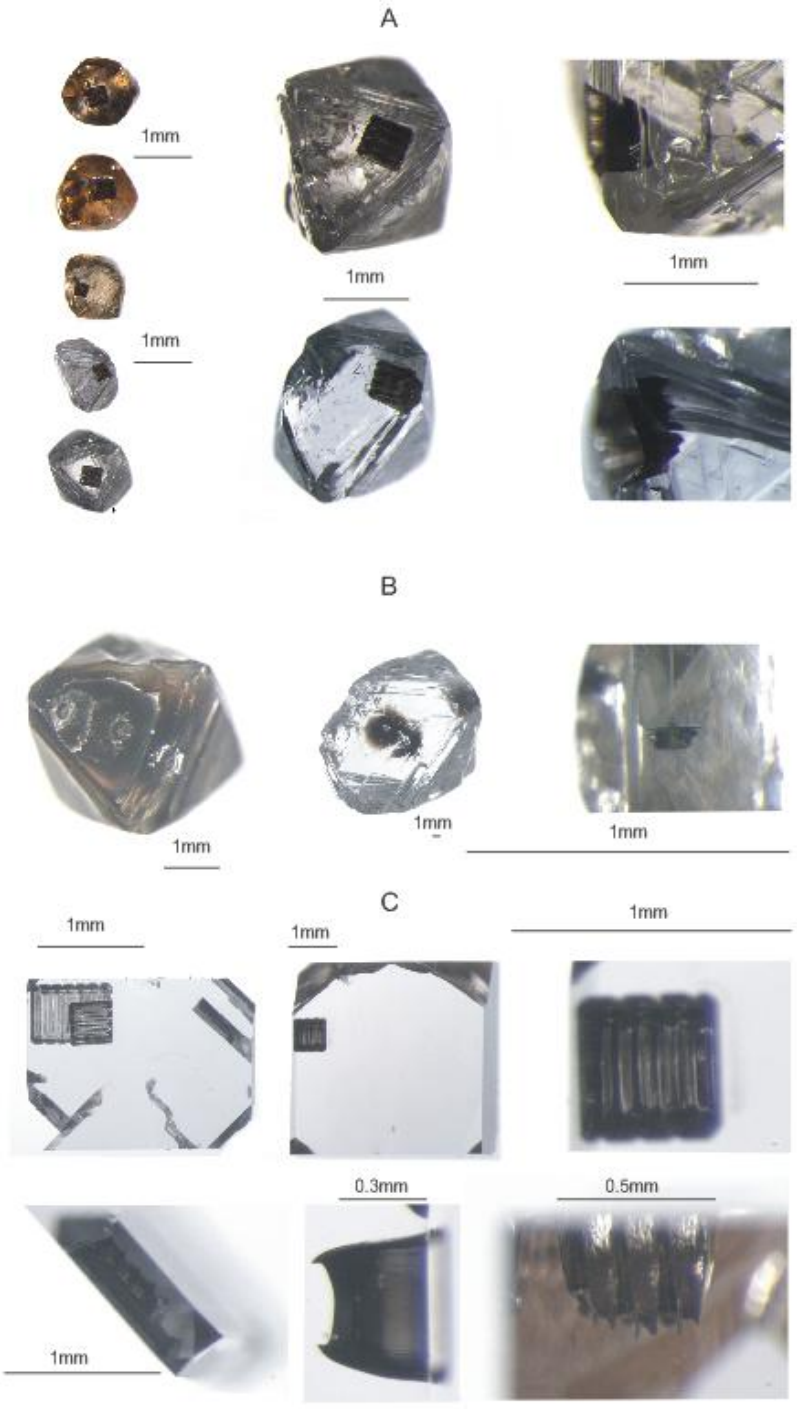

Figure 2.4. Diamonds in this study. A - Diamonds from Canada demonstrating the size of the offline ablation pit. B – Diamonds from Diavik previously analyzed by the GEMOC group using the online laser ablation method. Note the ejecta material remaining behind after ablation. C – Synthetic diamonds analyzed in this study which demonstrate the well proportioned and clean laser pits resulting from the offline ablation technique.

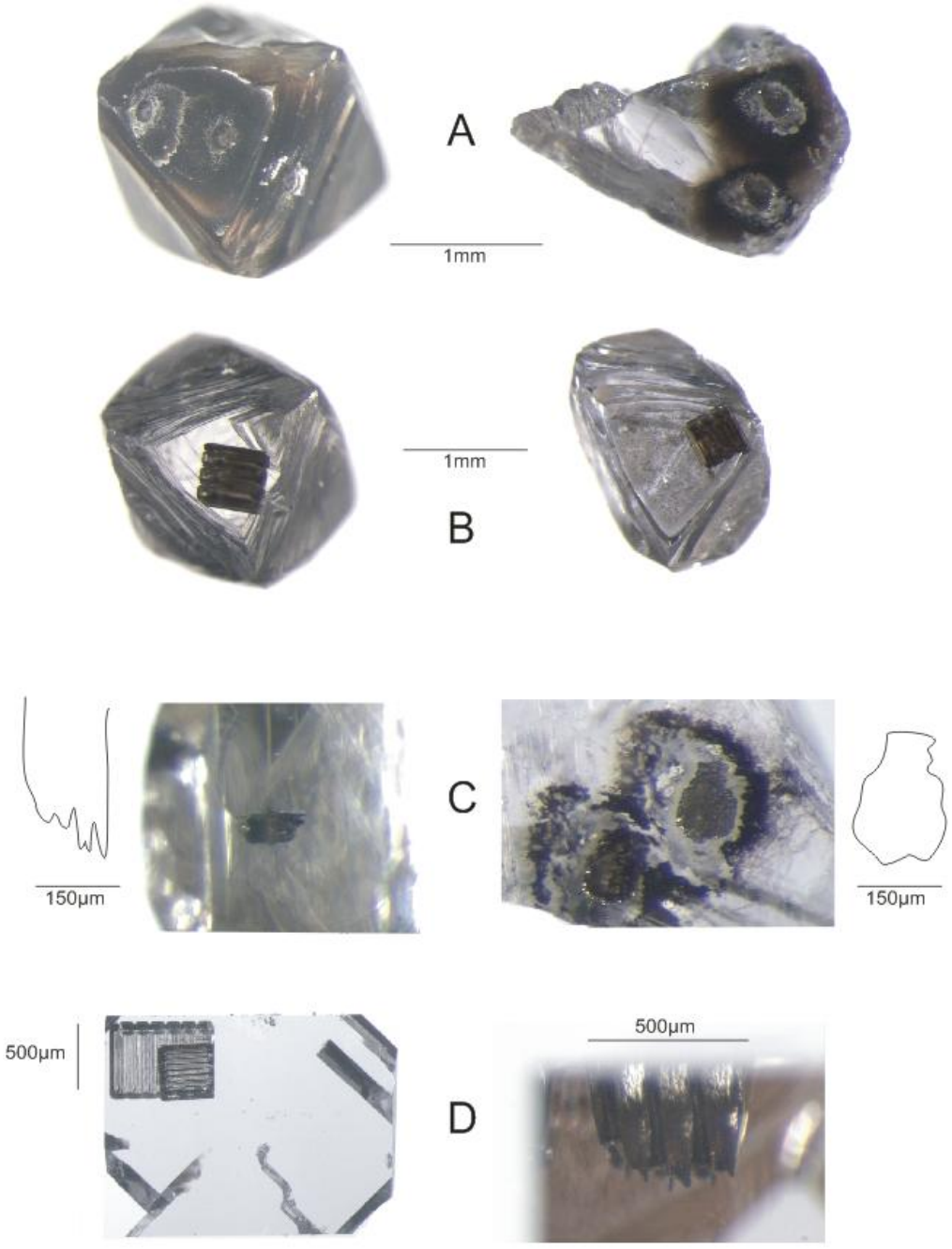

Figure 2.5. Ablation pits created by the GEMOC online laser ablation technique and the Durham Offline ablation technique. A - Diamond surface after a complete diamond ablation analysis using the direct laser technique and B – the offline technique. C – Profile and plan diagrams of an ablation pit after complete analysis by the online laser ablation method. D - Ablation pits after a full analysis by the offline technique demonstrating the more stable pit profile created.

2.2.1.2.5. Post-ablation procedure.

After the period of ablation is complete the material is collected from the ablation cell in UpA 6N HCl and prepared for elemental abundance analysis. The process is detailed in Process 3 (Appendix).

2.2.1.2.6. Diamond Combustion procedure

In order to confirm that trace element concentrations acquired via the offline ablation method are accurate it was necessary to verify them using a different method. A diamond combustion system was designed in-house for this purpose (Figure 2.6). A crucible in which to burn the diamond was fabricated from high purity platinum foil (Advent Research Material, 99.95% Pt.). This foil was formed around a 3 mm diameter flat head screw driver. The overlapping joint sections were spot welded. Dimensions for the crucible were designed such that it could be placed inside a quartz combustion tube with 4 mm inner diameter via the open top end (the end attached to the gas line). Each diamond fragment was between 1.5 and 11 mg. The diamond and crucible were cleaned in HF / HNO_3, HCl and MQ H_2O as for laser ablation analysis. The quartz combustion tube was cleaned in a 3N HNO_3 bath for 24 hrs at 100 ^{0}C. The inside of the quartz tube was further cleaned with UpA 6N HCl acid for 3 hrs before a final MQ H_2O rinse. The diamond is placed in the crucible and the crucible into the quartz combustion tube. This is carried out in a Class100 workstation. The quartz combustion tube was then attached to a port on a modified stable isotope gas prep line. The quartz combustion tube and prep line were then purged with high purity oxygen for 5 minutes before being sealed.

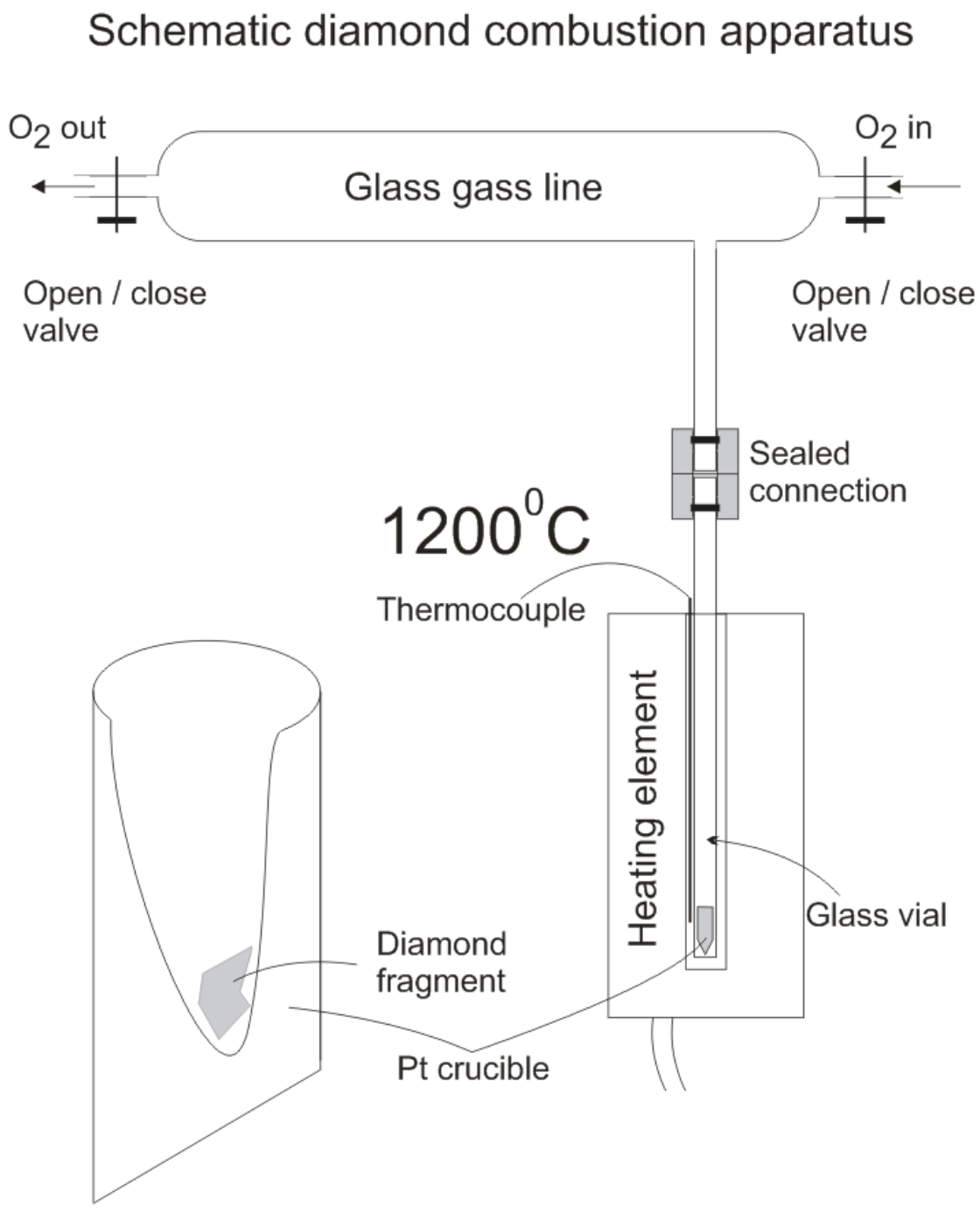

Figure 2.6. Combustion set-up at Durham University. Schematic showing relative location of gas-in and gas-out as well as the 'docking' port for the glass vial that contains the Platinum crucible and diamond fragment.

The heating component was designed in-house at Durham University and consisted of a temperature modulator, a transformer and a high temperature element with an inner ceramic lined sample port. This heating component was positioned over the glass tube and diamond crucible. The modulation system allowed the temperature to reach 1200 ^{0}C in less than 60 seconds and to be held stable at 1200 ^{0}C over a 30 minute period. Diamond fragments under 5 mg fully combusted over this time. Larger diamonds require the combustion process to continue. The oxygen port can be re-opened, the gas recharged and the procedure continued.

Once the diamond has fully combusted and the heating system switched off, removed and allowed to cool, the glass tube may be removed. The oxygen exhaust port is opened to allow any residual gas pressure to be released. Then the glass tube is removed from its port. Once in an ultra clean environment the tube can be unsealed and the crucible can be tipped into a clean teflon beaker. The crucible which contains the combusted material should now be treated as laser ablated material. The contents are covered in acid, sonicated and collected. This solution is then dried and can then be prepared for trace element analysis. Due to the high temperature during the combustion and the open nature of the crucible it is possible that some volatile elements such as Rb and Pb may be lost from the crucible to condense elsewhere in the gas prep line.

2.2.2 ICPMS analysis.

At the start of each analytical session a Ce solution was aspirated and the Element II optimized for sensitivity and minimal oxide generation with a typical CeO/Ce ratio of < 2%. Oxide production rates were then determined for various key elements (Ba, La, Ce, Pr, Nd, Sm and Gd) using single element 1 ppb solutions (Harlou et al, 2009). Elemental and oxide interferences on the mass spectrum of interest were monitored and corrected using the methods outlined in Font et al. (2007) and Harlou et al. (2009). The technique as currently applied collects data on 32 isotopes of 27 elements (See Table 2.2 for isotopes measured) with sampling times of 10-60 milliseconds per isotope per scan depending on the abundance of the isotope (see Table A5 and A6 (Appendix) for details on specific dwell times for each isotope). Instrumental accuracy in the determination of trace element ratios in the ppt concentration range in solution is documented by Harlou et al. (2009) and for most elemental ratios of interest is between 5 and 15%.

Samples were analyzed against a multi-point (at least 6 points) calibration line derived from several dilutions of standard USGS rock solutions of AGV-1, BHVO-1, and W2 prepared in a HF/HNO_3 digest. Initially these were diluted by a factor of 1000 such that the total dissolved solid (TDS) concentrations were 2 μg/ml, and then diluted further to provide a more appropriate TDS-match with the samples. This yielded calibration lines that required little or no extrapolation down to the trace element concentrations typical of gem diamonds. The accuracy of these calibrations has been documented in detail by Harlou et al. (2009). Samples were analyzed in

batches of five, each sample running for 111 seconds. A rinse solution of 3% UpA HNO_3 (made with UpA H_2O) is run in between every sample for 180 seconds. The USGS rock standards were re-analyzed as 'unknowns' after each batch to check the consistency of the calibration line. The original calibration blank and separate wash blanks are also run at this stage to monitor and later correct potential analytical drift through the session. The limits of quantification based on our total procedural blanks are described below.

An In internal spike was the main control on the drift of instrumental sensitivity. In was selected because it is mono-isotopic and in the middle of the mass range of interest. All samples and standards were spiked to achieve an In concentration of 0.2 ppb in the 0.5 ml solution presented to the mass spectrometer. This resulted in approximately 100,000 counts per second at mass 115 for the typical instrument parameters given in Table 2.2. Figure 2.7 demonstrates that the In spike had no measureable background impurities that affected our analysis. Post analysis, all samples were blank and drift corrected.

2.2.2.1 Analytical blanks

2.2.2.1.1 Limits of detection and limits of quantification.

The high purity of gem quality diamonds indicated by the early study of Fesq et al. (1975) and more recently by Araujo et al. (2009) in combination with our preliminary studies (McNeill et al., 2009), demonstrates the need for an analytical method with very low limits of quantification (LOQ) that allow the acquisition of

data that are quantitative, rather than semi quantitative or even qualitative in nature. When examining this requirement it is important to adhere to a common set of definitions, namely those outlined by Currie (1968, 1999a-c) and adopted by IUPAC, the International Union of Pure and Applied Chemistry. The numerous recent publications reporting methods and data for fibrous, fluid rich diamonds, do not quote or use the concept of the limit of quantification (e.g., Rege et al., 2005; Tomlinson et al., 2005; Zedgenizov et al., 2007). Despite claiming to produce quantitative data these studies have actually only reported the limits of detection (LOD) for their particular method and often do not even make a clear statement about how the LOD were derived. Rege et al. (2010) discuss in detail their derivation of LOD but then displays the result against a fibrous diamond with very high fluid inclusion density and then only with regards to the elements in highest concentrations in the diamond. Scrutiny of the Rege et al (2010) limits of quantitation reveals that only a very few elements in a small number of gem diamonds they analyzed are likely to be quantitative.

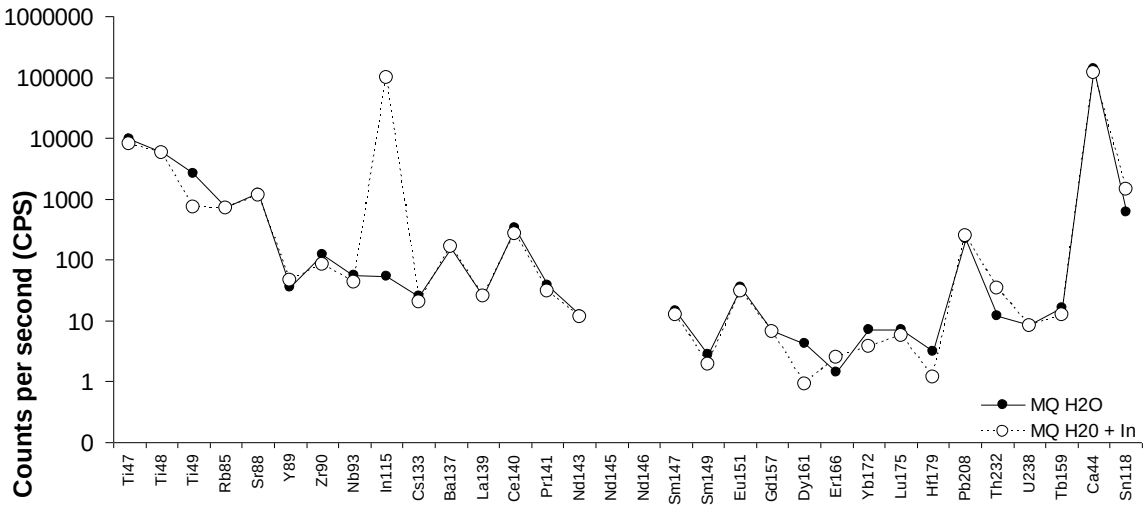

Figure 2.7. ICPMS reported counts per second values for a MQH_2O solution both with and without an ^{115}In spike.

The definition of the LOD is:- "the true net signal level that may be expected *a priori* to lead to *detection*" (Currie, 1968, p587). The implication is that while data reported from signals above LOD are detectable they cannot be described as being quantitative unless they exceed a more rigorous threshold, the LOQ, defined as:- "the signal level above which a quantitative measurement can be performed with a stated relative uncertainty" (Currie, 1968, p587). While Currie's efforts have brought clarity to the definitions, within the field of analytical geochemistry there is still widespread use of the LOD as some sort of validation that quantitative data are being presented when this may not be the case. The LOD defines only the limit of the inherent detection capability in any chemical measurement procedure (Currie, 1968; 1999a-c; Olivieri et al., 2006). Data must exceed LOQ (the minimum quantifiable accurate value) if it is to be referred to as truly quantitative (Figure 2.8, 2.9a+b).

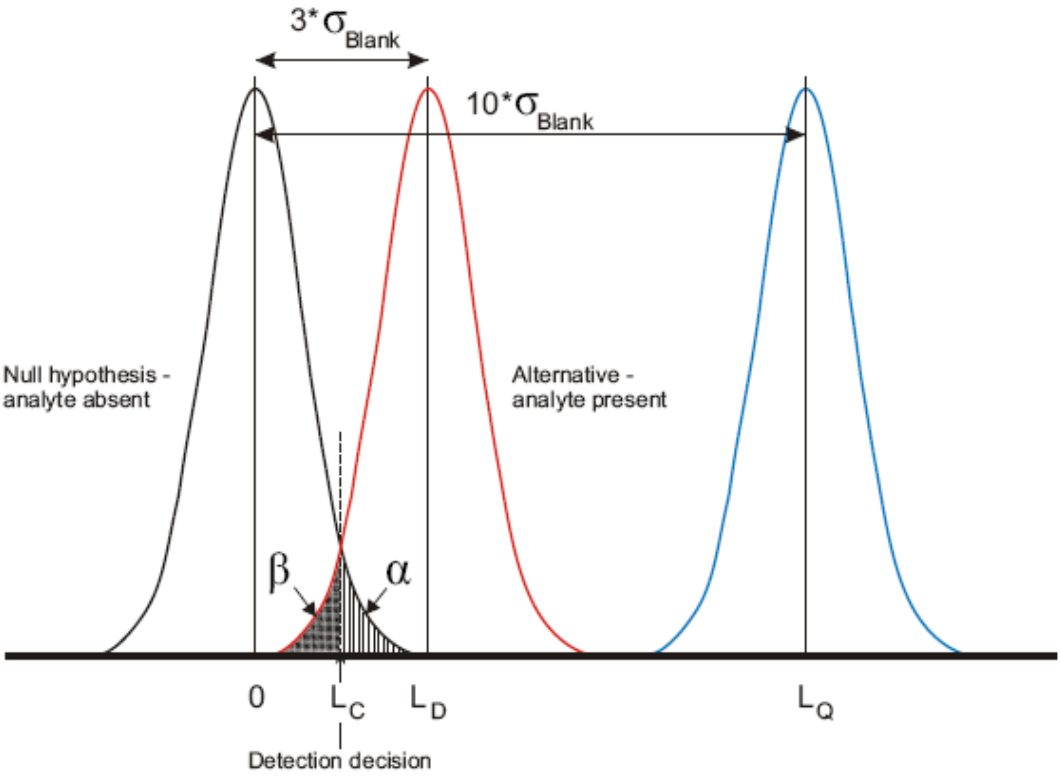

Figure 2.8. Illustration of the definitions of LOD and LOQ used in the text. For presentation of the defining relations, L is used as the generic symbol for the quantity of interest. Subscripts C, D, and Q are used to denote the critical value, detection limit, and quantification limit, respectively. The maximum acceptable false positive together with the standard deviation of the net signal of the null establish the critical value, L_C (detection decision), upon which decisions may be based. An observed signal must exceed L_C to be detected. Once L_C has been defined, the detection limit L_D may be established by specifying L_C, the acceptable level, β and the standard deviation σ_D which characterizes the probability distribution of the net blank signal when its true value is equal to L_D.

Here we use the expressions derived by Currie (1968, 1999a-c) to derive LOD and LOQ for our new "off-line" laser sampling method. These expressions are based on hypothesis-testing, and their graphical expressions together with the underlying assumptions are outlined in Figure 2.8. We employ the expressions for these parameters derived for a situation where the analytical blank is "well known" and normally distributed. We estimate blank parameters by the "external approach", i.e., by statistical processing of multiple measurements (n=103) of the total procedural blank analyzed in the 3 year period of this study, that encompasses all elements of our chemical and instrumental procedures. For this situation we take our LOQ value to be:-

$$LOQ = 10\sigma_{blank} \quad (1)$$

And LOD is defined as

$$LOD = 3\sigma_{blank} \quad (2)$$

Where σ_{blank} is the standard deviation of the mass of each element reported in the total procedural blank set. Following Currie (1999a-c), we attribute errors of 5% to Type I, or "false positive" decisions and 5% for Type II errors, or false negative errors (Figure 2.8) and assign an error for the resulting quantification at 10% or less (Currie, 1999b). We note that for other methods, such as direct laser ablation ICPMS, where only LOD is usually presented, there is often inadequate information provided to fully evaluate how the "blank" is defined, making it difficult to judge how adequate the "blank" will be at capturing the true variability within the system. More importantly this lack of detailed information prevents the independent

assessment of whether the stated LOD values are likely to be meaningful. For our measurements, repeatability of total procedural blanks yielded consistently low values so that our limits of quantification (LOQ) in terms of how much total analyte we require from the ablated volume = <1 pg for most of the analyzed elements, except for Sr, Zr, Ce, Ba which range between 2 – 20 pg, and for Pb ~40 pg (Table A1. Appendix, p228). The LOQ values are presented in pg rather than as a concentration in the solid since total procedural blanks are largely independent of sample weight ablated with our off-line ablation method. These LOQ values are calculated from the instrument report and are applied as a filter to the blank corrected data at that stage. LOQs estimated as ppm are presented in Section *2.3.2* and Table A1 (Appendix)). These levels are consistent with our expectations based on total procedural blank variability for other procedures established in our laboratory. Such LOQ values in ppm are considerably less than the analyte levels present in most fibrous diamonds. Lower-purity monocrystalline diamonds are closer to this limit but still above it although only a small number of white 'gem-monocrystalline' diamonds exceed these LOQ values given our typical ablation times (Figure 2.9a). Increasing ablation times considerably or improving the reproducibility of chemistry blanks would allow quantitative values to be achieved for every element.

Figure 2.9 ►. LOQ comparison; A) Blank-corrected concentration (total amount from ablation) of measured trace elements in this study normalized to the LOQ. Values above the LOQ are quantitative and those below can only be at best classified as qualitative. Most data representing the highest-purity 'gem-monocrystalline' diamonds falls below this limit. A small number of gem diamonds have concentrations above this limit. B) Quantitative ppm data from this study normalized to the ppm LOQ of Rege et al., 2010 (represented by the '1' line). REE concentrations up to 2 orders of magnitude below the Rege et al. (2010) LOQ can be quantitatively measured using our offline method.

Figure 2.9b highlights the values in this study that were reported above our LOQ normalized to the LOQ of the online direct laser ablation method of Rege et al. (2010). It is clear, that if using the online method of ablation analysis, many of the elemental concentrations that we acquired by the offline method would not have been reported above LOQ. This would be most significantly manifested in the 'gem' monocrystalline samples of this study, i.e. using the offline method we can acquire quantitative measurements on a number of elemental concentrations up to 2 orders of magnitude lower than the online ablation method. (***See Section 2.3.2 for a more direct comparison between online and offline ablation methods***).

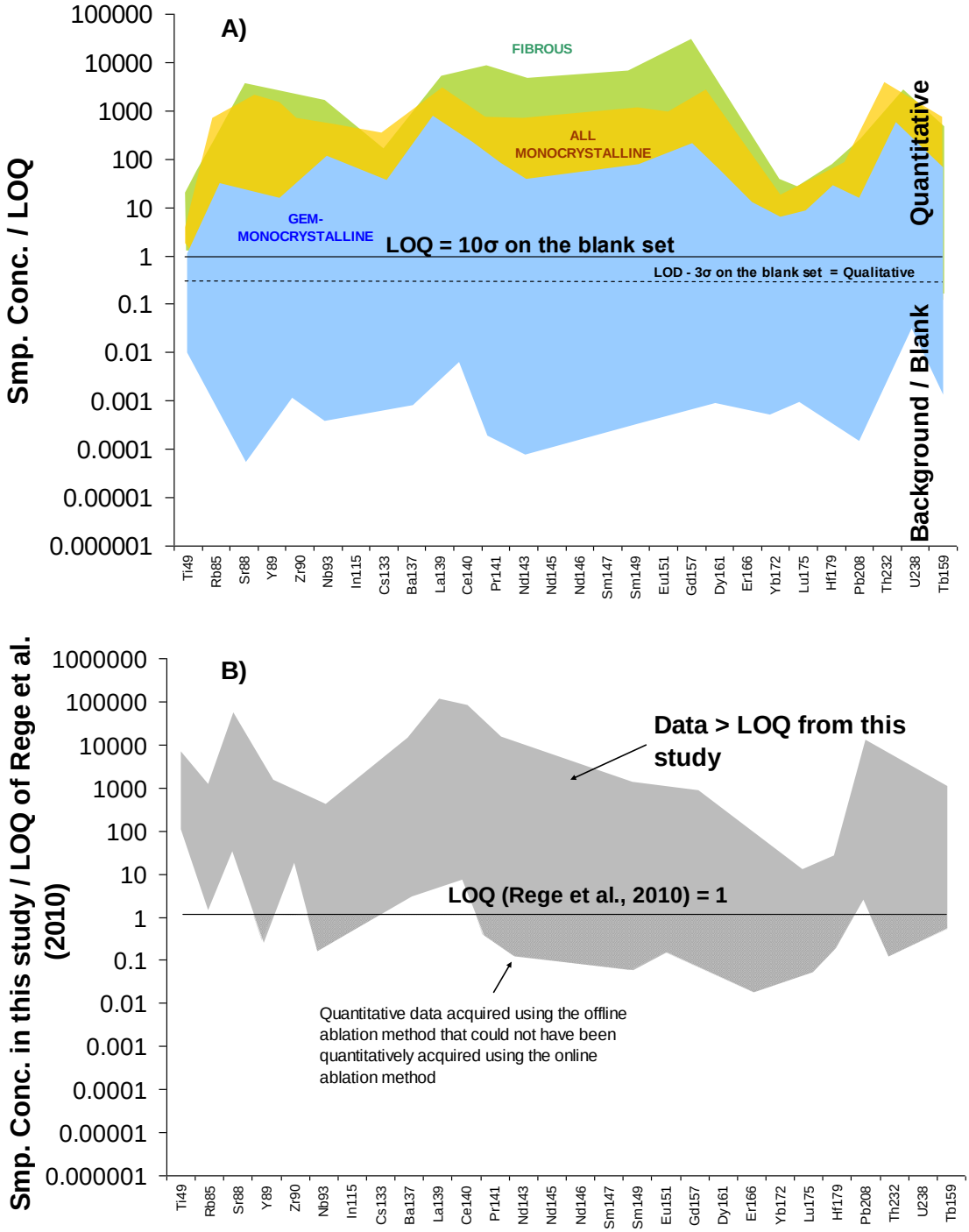
A)
Smp. Conc. / LOQ
100000
10000
1000
100
10
1
0.1
0.01
0.001
0.0001
0.00001
0.000001
FIBROUS
ALL MONOCRYSTALLINE
GEM-MONOCRYSTALLINE
LOQ = 10σ on the blank set
LOD - 3σ on the blank set = Qualitative
Quantitative
Background / Blank
Ti49 Rb85 Sr88 Y89 Zr90 Nb93 In115 Cs133 Ba137 La139 Ce140 Pr141 Nd143 Nd145 Nd146 Sm147 Sm149 Eu151 Gd157 Dy161 Er166 Yb172 Lu175 Hf179 Pb208 Th232 U238 Tb159
B)
Smp. Conc. in this study / LOQ of Rege et al. (2010)
1000000
100000
10000
1000
100
10
1
0.1
0.01
0.001
0.0001
0.00001
0.000001
Data > LOQ from this study
LOQ (Rege et al., 2010) = 1
Quantitative data acquired using the offline ablation method that could not have been quantitatively acquired using the online ablation method
Ti49 Rb85 Sr88 Y89 Zr90 Nb93 In115 Cs133 Ba137 La139 Ce140 Pr141 Nd143 Nd145 Nd146 Sm147 Sm149 Eu151 Gd157 Dy161 Er166 Yb172 Lu175 Hf179 Pb208 Th232 U238 Tb159

Perhaps the major control on our LOQ values is the reproducibility of the chemistry blanks. Figure 2.10a displays counts per second (cps) measurements on the elements analyzed in the 3% nitric acid solvent containing no ablation solute as well as the cps values for an averaged total procedural blank set from May 2010. As the sensitivity of the ICPMS can vary with each analytical session, the exact cps values are not representative of absolute concentrations and only once they are converted to concentrations using a standard based calibration curve and corrected for instrument drift can they provide information on trace element content. However for comparative purposes cps plots are useful to illustrate the differing levels of impurities in the various reagents used. The acid blank is comparable to the total procedural blank and highlights that the limiting factors in the achievement of even lower blank levels are the acids used in the method chemistry. The counts for ^{115}In are always very high because it is used as an internal spike. Ensuring that the In solution yields the expected level of detector counts acts as a check that low counts of other elements are not merely a result of suppression.

Within individual blank sets the elements that display the greatest variation are the M- and HREEs. Figure 2.10b shows a typical blank dataset of six TPBs and highlights that this variation is contained within 5 to 10 cps. As such blanks are highly repeatable and allow for very low LOQ values to be calculated. The observation that most ‘gem-monocrystalline’ diamonds analyzed in this study display trace element concentrations that fall below this limit highlights that there are extremely low concentrations of impurity in ‘gem’ diamond.

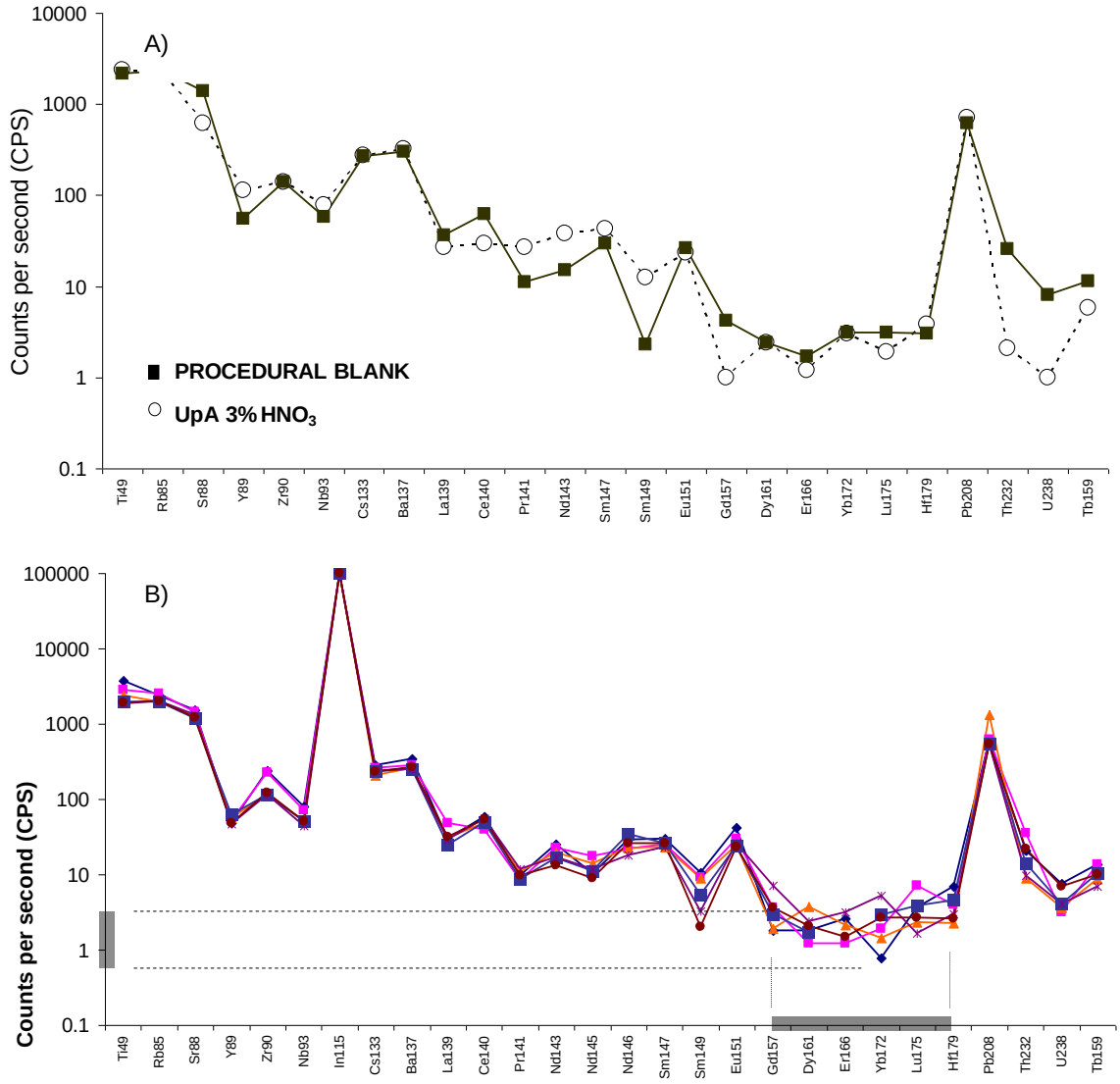

Figure 2.10. CPS values for an acid solvent introduced to the ICPMS and typical blank set values run during an ICPMS sample analysis session. A) Romil UpA 3% HNO_3 solvent values compared to a total procedural blank for trace element analysis. B) Typical Total Procedural Blank values. Grey bars highlight that blank variation even at low CPS levels is contained within 5 – 10 CPS. This is important as REE concentrations are also relatively low in natural diamond.

Figure 2.11 ►. Uncertainties associated with trace element analyses. A – ppm concentration with 2σ error to demonstrate that the uncertainty is essentially as small as the symbol used. B – The error as a percentage of the sample concentration. C, D – Error relationships to individual elemental concentration in the diamond. ON-JWN-110 also shown as this diamond has been analyzed by Rege et al. (2010).

2.2.2.1.2 Sample concentration uncertainties

2σ errors for each elemental concentration are calculated based on the standard deviation reported by the ICPMS for each samples analytical run. This error is reported for any sample that is above the method LOQ (Table A2: Appendix). Figure 2.11a shows an example of a fibrous diamond as well as monocrystalline diamonds with uncertainty bars on data points, and typically covered by the datapoints. D186 is one of the highest purity diamonds analyzed in this volume. 2σ errors are less than the size of the data point except for Eu, Dy, Er and Hf which are only a little outside the symbol. As such, these errors are not plotted on multi-element graphs throughout this volume as errors are consistently smaller than the data point. It is useful to represent the error in terms of the relative % of the concentration (Figure 2.11b). In diamond D186 and D104 errors average 10% of the sample value but can be up to 70%, e.g., for Er. Figure 2.11c demonstrates that there is a linear decrease in 2σ error with decreasing concentration. Figure 2.11d displays the relative precision versus concentration to show that precision is generally independent of concentration down to ~0.01 ppm, and then rises as concentration decreases.

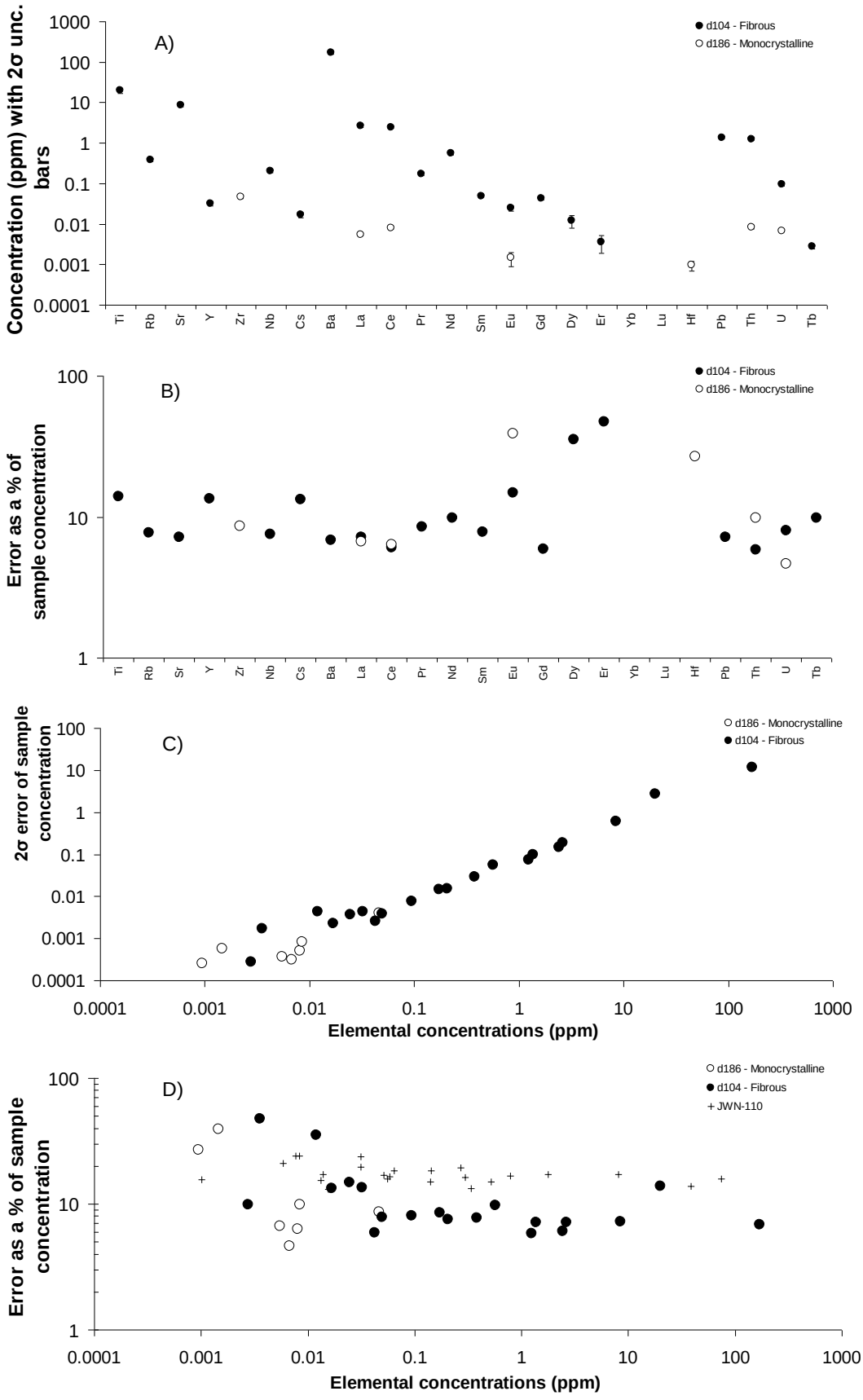
A)
Concentration (ppm) with 2σ unc. bars
1000
100
10
1
0.1
0.01
0.001
0.0001
d104 - Fibrous
d186 - Monocrystalline
Ti Rb Sr Y Zr Nb Cs Ba La Ce Pr Nd Sm Eu Gd Dy Er Yb Lu Hf Pb Th U Tb
B)
Error as a % of sample concentration
100
10
1
d104 - Fibrous
d186 - Monocrystalline
Ti Rb Sr Y Zr Nb Cs Ba La Ce Pr Nd Sm Eu Gd Dy Er Yb Lu Hf Pb Th U Tb
C)
2σ error of sample concentration
100
10
1
0.1
0.01
0.001
0.0001
d186 - Monocrystalline
d104 - Fibrous
0.0001 0.001 0.01 0.1 1 10 100 1000
Elemental concentrations (ppm)
D)
Error as a % of sample concentration
100
10
1
d186 - Monocrystalline
d104 - Fibrous
JWN-110
0.0001 0.001 0.01 0.1 1 10 100 1000
Elemental concentrations (ppm)

2.2.2.1.3 Suitability of CVD diamond or Silicon wafer as an ablation blank

Our Total Procedural Blanks, which are important in establishing the LOD and LOQ for our offline ablation method necessarily omit the step of ablating a solid. To include this step would require a solid that is essentially devoid of all trace elements, or have trace element concentrations below the LOD of our method. Two forms of solid were ablated to test their suitability as solid ablation blanks..

Repeat ablations of an ultrapure single crystal semi-conductor-grade silicon yielded Ti concentrations of up to 16 ppm and Sr up to 0.02 ppm. Other elements for which count rates allowed qualitative and even quantitative analysis yielded concentrations of 60 ppt to 0.5 ppm. Although a number of other elements are not reported above LOD the semi-conductor grade silicon wafer does not appear to be a higher purity than the majority of gem-monocrystalline diamonds and as such it is unsuitable as an ablation blank.

Synthetic diamonds grown via chemical vapour deposition (CVD) in an ultra-pure environment are currently being used as a solid blank for online laser ablation techniques and also as doped analytical standards (C. Dalpe, personal communication, 2009). The CVD diamonds analyzed in this study, donated by Element 6, were found to have concentrations of several elements within the range determined for ‘gem’ diamonds (Table A1 - Appendix). Figure 2.12 demonstrates that although many elements below LOQ in the CVD diamonds, a significant number of elements (e.g., Ti, Y, Zr, Ba, Pb, Th, and U) were reported above LOD

and therefore these synthetic diamonds cannot be used for a solid ablation blank. Using our parameters, synthetic diamonds cannot be distinguished from natural diamonds.

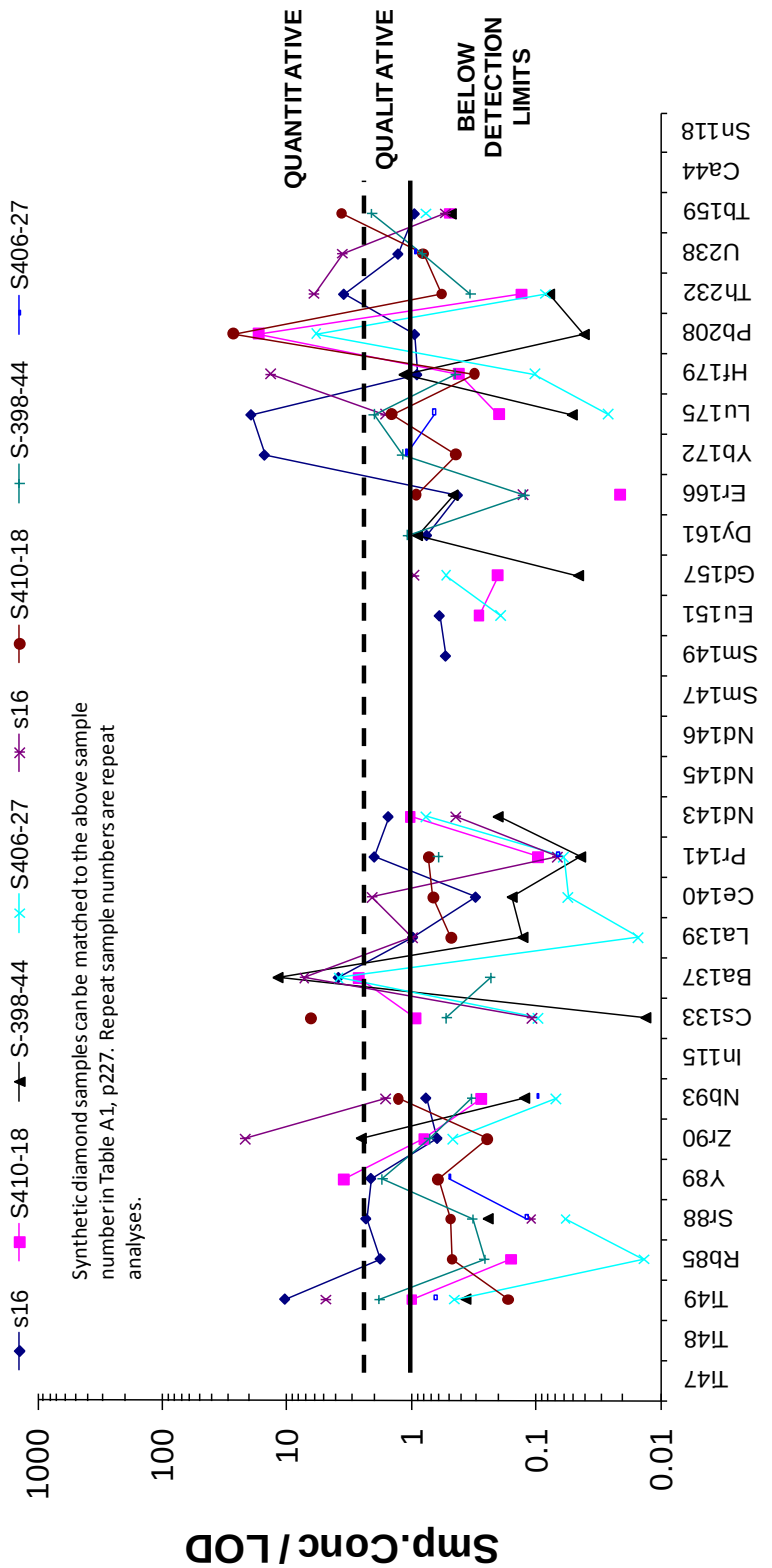

Figure 2.12. Synthetic diamond blank corrected concentrations (total amount from ablation) normalized to the limits of detection for offline laser ablation. Values above 1 indicate an element that is reported at levels high enough to be considered qualitative. Values above 3.33 are quantitative. This demonstrates that these synthetic diamonds are unsuitable as blanks considering the concentration range reported by natural diamonds in this study.

2.2.3 Isotopic analysis

Acquiring radiogenic isotope ratios on diamonds will not only provide useful information on mantle processes but may also prove to be a potentially invaluable fingerprinting tool. In contrast to trace element analyses where just a few pg of analyte provides quantitative data, obtaining precise and accurate isotope ratios for the most commonly used radiogenic isotope systems (Sr, Nd and Pb) requires on the order of several 100 pg to several ng depending on the method of analysis. On average, after a 20 minute ablation of a brown translucent fibrous surface on a coated diamond from the Congo a sufficient amount of material is collected to acquire both a trace element analysis and $^{87}Sr/^{86}Sr$ ratios (e.g., Klein BenDavid et al., 2010). The amount of Sr analyzed in this case is between 2 and 12 ng absolute Sr, well above the minimum 0.1 ng required by TIMS for a straightforward analysis *G.Nowell, pers comm.*). 'Gem' quality diamonds have significantly lower concentrations of Sr and hence require much longer ablation times to yield this quantity of Sr. Over 70 monocrystalline diamonds were ablated for between 6 and 30 hrs each with the amount of Sr collected from an ablation reaching a maximum of 1 ng Sr, but was typically 50 to 300 pg for the lower purity diamonds and typically <2 pg for 'gem' monocrystalline diamonds (the latter being considered essentially blank) (Figure 2.13. See also Figures 2.3 and 2.14). As such isotopic analysis is only possible on diamonds that appear to have a high density of fluid inclusions or microinclusion impurity. Only one 'gem' diamond, sample 153, from Ekati yielded enough Sr for isotopic analysis.

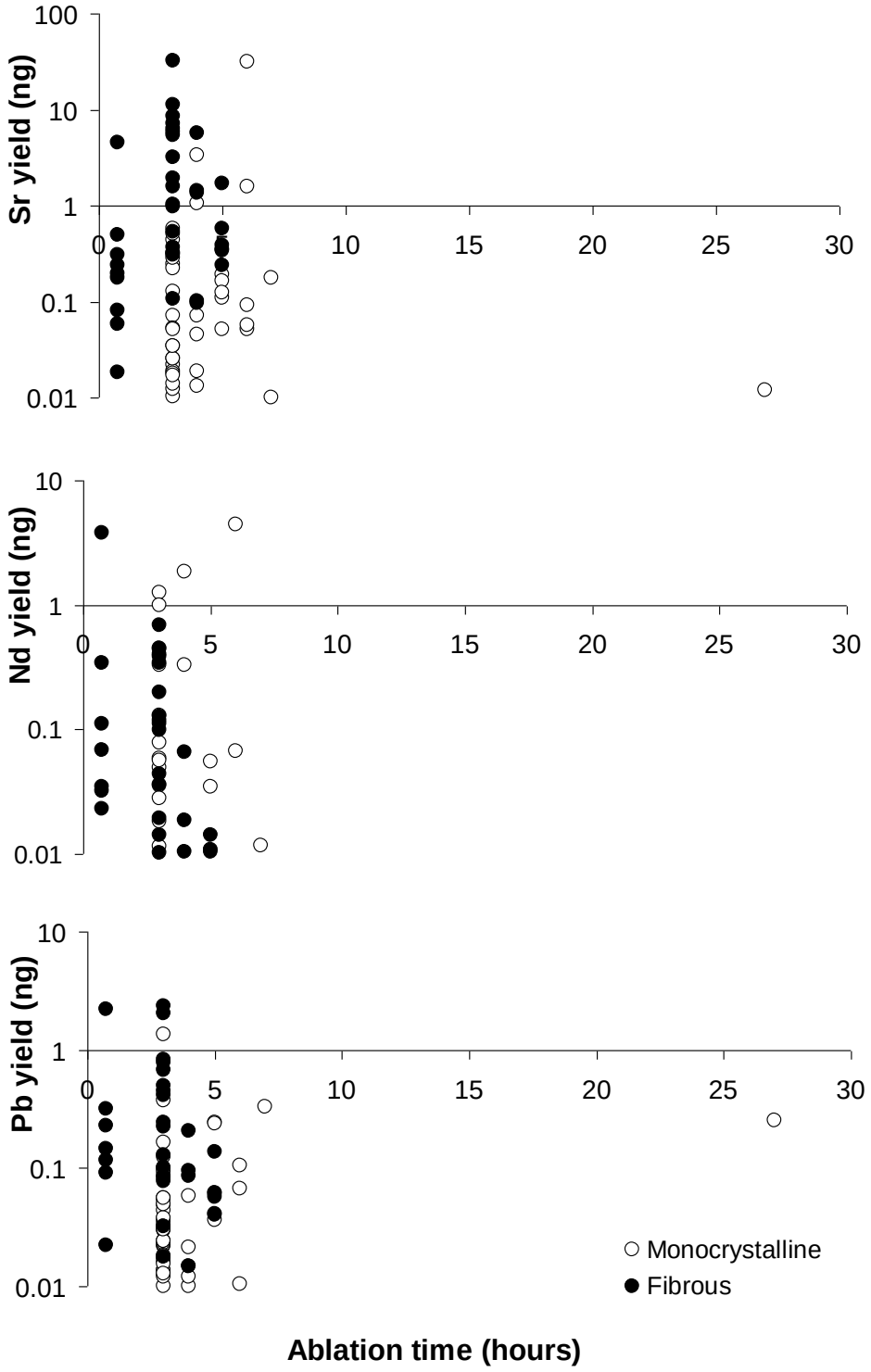

Figure 2.13. Sr-Nd-Pb yield from diamond after given ablation times under the laser. This demonstrates the effect of diamond heterogeneity that creates uncorrelated results.

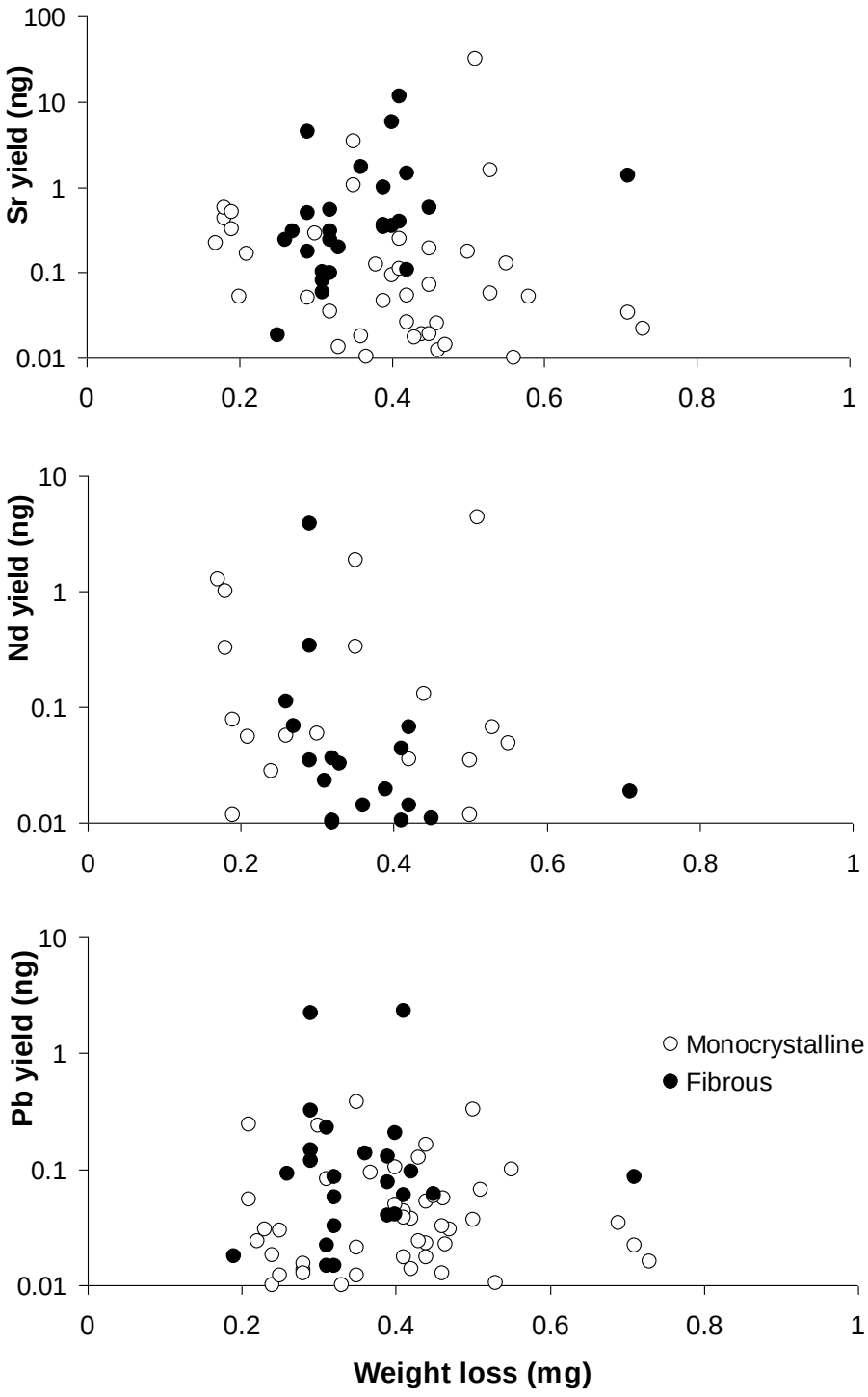

Figure 2.14. The yields of Sr, Nd and Pb in ng from diamond versus ablated sample weight. This demonstrates the effect of diamond heterogeneity that creates uncorrelated results.

To avoid issues of sample heterogeneity, isotope ratios for fluid inclusion-rich diamonds were determined on an aliquot of the sample dissolution used for determining the trace element composition. Since higher analyte amounts are required for an isotope analysis the sample dissolution was split e.g. 80:20 or 50:50 isotopes/trace elements.

The process for separating the solution for trace element and isotopic analysis is detailed in Process 4 (Appendix). Given the extremely low trace element contents of 'Gem' diamonds such samples were not aliquoted for trace elements and isotopes. Instead if the trace element analysis of a gem diamond showed Sr contents were high enough to be able to yield sufficient Sr for an isotopic analysis then it could be re-ablated specifically to acquire material for a Sr isotope measurement.

2.2.3.1 Column chemistry: Sr, Pb, Nd separation

The Sr separation procedure used in this study was based on the micro-Sr column chemistry method described by Charlier et al. (2006) and applied to ng to sub-ng samples by Harlou et al. (2009). Each new batch of Sr Spec™ resin is cleaned thoroughly before use. 2–3ml of new resin slurried with water is placed in a 2-ml Biorad™ column with a 225-ml reservoir attached. Full reservoir volumes of 0.05M HNO_3, 0.1M H_2SO_4, 6M HCl and water are passed in succession until a total of ca. 6L of the above reagents have been passed through the column. This procedure is required to remove traces of labile organic compounds, and to minimize the Sr blank contribution from the resin which can be substantial in the uncleaned resin (Charlier et al., 2006). The cleaned resin is stored as slurry with water in a 50 ml FEP dropper

bottle ready for use. Columns are made up from standard 1ml pipette tips with a circular piece of polypropylene frit (30μm pore-size) material fitted into the tapered end (Figure 2.15). The area of the pipette tip below the frit material is cut diagonally with a scalpel as this both facilitates emptying of the column during elution and reduces the 'dead' volume of reagent between the frit and the column tip. Once made and checked for flow rate by filling with water, columns are washed several times in dilute HCl in a 1-L teflon jar. The full separation procedure is detailed in Process 5 (Appendix) and is summarized in Figure 2.15.

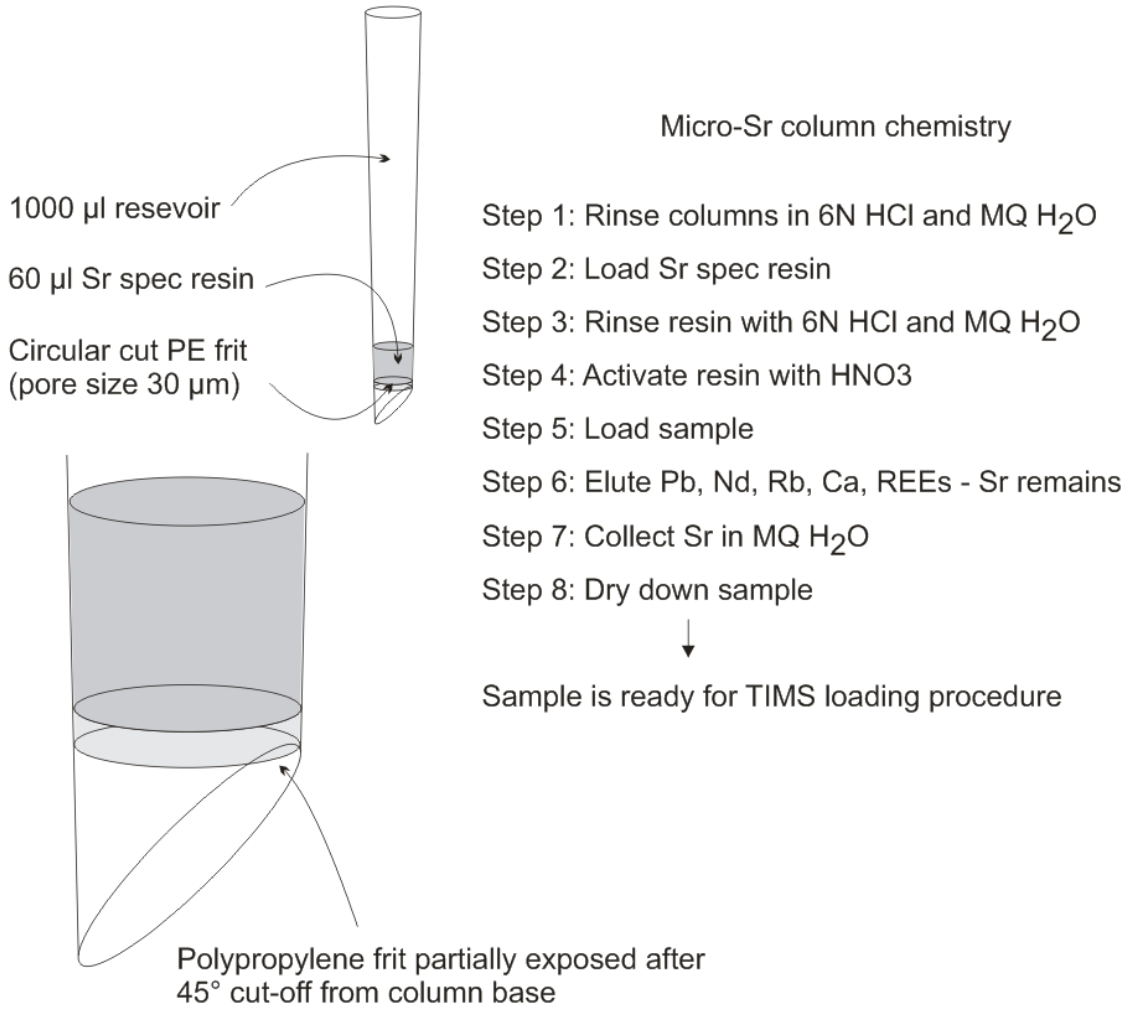

Figure 2.15. Schematic summary diagram of Sr-separation set-up, procedure and chemistry. (After Harlou et al., 2009)

2.2.3.2 Sr isotope measurement

Sr fractions (CB2 – Process 5 (Appendix)) were loaded on single Re filaments for TIMS analysis using procedures described in detail by Charlier et al. (2006) and Font et al. (2007). Enhanced ionization is achieved by employing a purified TaF_5 activator. Rhenium ribbon of 99.98% purity was sourced from Advent Research Materials and has a thickness of 0.025 mm and a width of 0.75 mm. Filaments were cut from the ribbon in ~ 20 mm strips. Re filaments were outgassed at 4.2 A for 20min prior to loading. The procedure is detailed in Process 6 (Appendix).

Sr isotope ratios were measured on a ThermoFisher Triton TIMS at Durham University, UK. Standard and sample evaporation filament currents were increased at a rate of 100 mA min^{-1} until a Rb signal was observed (typically 700 - 1200 mA) at which point the current was held constant while the Rb was allowed to 'burn off'. The filament current was increased at the same rate until an ^{88}Sr intensity of 0.001 V was obtained. Using the ^{88}Sr beam in the high mass 3 (H3) Faraday cup as the control isotope, the filament was automatically focused and the 88Sr peak centered to update the mass calibration.

Sr isotope measurements were measured using a static multi-collection routine (Cup configuration - Table 2.3). Each sample measurement consisted of between 70 and 250 ratios, depending on the amount of Sr on the filament, with an integration time of 4s per ratio; total analysis time approximately 5 to 17 min. Mass fractionation was corrected using an exponential law and an $^{86}Sr/^{88}Sr$ ratio of 0.1194. Multiple loads

(n=43) of NBS987 of between 0.5 and 3 ng size gave an average value of 0.710260±0.00002 (2SD; n=43). As the Durham laboratory reports NBS 987 Sr data relative to an $^{87}Sr/^{86}Sr$ ratio of 0.710240 no additional normalization was performed. Average signal size of ^{88}Sr for the 0.5 and 3 ng standards were 0.8±0.4 V and 5±1.3 V respectively. Signal sizes for samples were on average 0.2±1 V. Harlou et al. (2009) documented in detail the levels of accuracy and repeatability for samples and standards at these low signal intensities.

Cup	Analyte	Interference
L2	^{84}Sr	
L1		^{85}Rb
C	^{86}Sr	
H1	^{87}Sr	^{87}Rb
H3	^{88}Sr	

Table 2.3. Cup configuration used for the analysis of Sr on the TIMS. Species in italics is the monitor isotope used for the correction of ^{87}Rb on ^{87}Sr.

2.2.3.3 Nd isotope analysis

Nd fractions (CB1 from Process 5 (Appendix)) were analyzed on the ThermoFisher Neptune Multi Collector ICP Mass Spectrometer (MC-ICPMS) at Durham University following the procedure of Nowell et al. (2004). Samples were aspirated using an ESI PFA-50 nebulizer in conjunction with a 'cinnabar' micro-cyclonic borosilicate spray chamber. Nd isotope measurements were carried out using a static multi-collection routine comprising 50 ratios and a 4 second integration time per ratio; total analysis time of ~3.5 min. Instrumental mass bias was corrected using an

exponential law and the Sm-free isotope pair $^{146}Nd/^{145}Nd$ assuming a ratio of 2.071943 (equivalent to a $^{146}Nd/^{144}Nd$ ratio of 0.7219). Nd is analyzed as part of a total REE column cut necessitating a Sm interference correction on Nd; 9 Nd standards were run, of which 3 were doped with Sm (with a Sm/Nd ratio of 0.2) to monitor the accuracy of the Sm interference correction on Nd. The average $^{143}Nd/^{144}Nd$ ratio for pure and doped standards was 0.511123 ± 0.0000160 (2SD; n=9) with a reproducibility of 30.7 ppm, which compares very favorably with the long-term value reported by Pearson and Nowell (2005). Average signal size for the ^{146}Nd in the standards was 2.4±0.3 V and was 1±0.5 V for the sample. Sample data are reported relative to a J&M $^{143}Nd/^{144}Nd$ ratio of 0.511110 (equivalent to a La Jolla value of 0.511862; Royse et al., 1998).

Nd isotope compositions were acquired on only one combusted diamond in this study as offline ablations were unable to yield sufficient Nd. CNG-1, a fibrous stone yielded a $^{143}Nd/^{144}Nd$ ratio of 0.511121±0.0000388 (2SE). Since this Nd isotope ratio was not obtained on more samples using the offline ablation method, it is not used in any petrogenetic model in this study. Klein-BenDavid et al. (2010) used this offline laser ablation methodology to acquire Nd isotopes on multiple spots on three non-typical fibrous diamonds from Botswana.

2.2.3.4 Pb isotope analysis

Pb fractions (CB3 from Process 5 (Appendix)) were analyzed on the ThermoFisher Neptune MC-ICPMS at Durham. Samples and standards were aspirated using an ESI

PFA-50 nebulizer in conjunction with a 'cinnabar' micro-cyclonic borosilicate spray chamber. Pb isotope measurements are carried out using a static multi-collection routine comprising 50 ratios and a 4 second integration time per ratio; total analysis time of ~3.5 min. Samples were run in a single analytical session along with five NBS981 Pb standards. Mass bias for Pb was corrected using an exponential law and a $^{205}Tl/^{203}Tl$ ratio of 2.3881. The average $^{206}Pb/^{204}Pb$, $^{207}Pb/^{204}Pb$ and $^{208}Pb/^{204}Pb$ values for NBS981 were 16.9410±0.0019, 15.4966±0.0012 and 36.7123±0.0033 respectively. Average ^{208}Pb signal intensities for the NBS981 standards were 2.8±0.07 V.

Pb compositions were not successfully acquired on any diamond samples in this study. Klein-BenDavid et al. (2010) used this offline laser ablation methodology to acquire Pb isotopes on multiple spots on two non-typical fibrous diamonds from Botswana. These samples were not analyzed in this study and are not used in any petrogenetic model in this study.

2.2.3.5 Total procedural Sr, Nd and Pb blanks and sample processing

Very low total analyte sizes for Sr (from 0.02 ng to >1 ng), Nd (0.02 ng to 2 ng) and Pb (0.02 ng to 2 ng) make it imperative to monitor both the size of the total procedural blank contribution from the dissolution and column chemistry procedure and the isotopic composition of that blank. Thus several total procedural blanks (TPBs) were carried out to determine the average size of the blank. The TPBs were prepared following the same sample digestion and column procedure used for all

samples. The Sr, Nd and Pb elemental fractions were analyzed by ICPMS to determine the elemental concentration in the TPB and hence overall blank size (Background Equivalent Concentration, BEC, is included). The Sr TPBs during this study averaged 5 pg (n = 12). The isotopic composition of the lab blank was determined periodically by combining the equivalent of 60 TPBs to yield sufficient Sr for a precise and accurate TIMS analysis. The average $^{87}Sr/^{86}Sr$ composition of the lab blank during this study was 0.710853 ± 0.000194 (2SE). The Nd TPBs averaged 1.1±0.8 pg (n=4) and the Pb TPBs averaged 15.7+17.6 pg (n=4). We were unable to accurately determine the isotopic compositions of the Pb and Nd blanks but note that assuming typical crustal compositions for both these elements results in insignificant corrections to the reported data and hence no corrections are made.

Nd and Pb isotopes have only been acquired in non-typical, enriched diamonds that are not a part of the subsequent applied study. The MC-ICPMS at Durham University is also used for the analysis of Os-rich metal alloys. Residual Os sits in the instrument for several weeks following analysis and resulting Os-oxide ions severely interfere with the Pb mass spectrum. As such Pb analyte levels of less than 1 ng do not result in reliable data. Most samples in this study fell into that category (Fig. 2.13). Nd analyte levels for the samples in this study were mainly too low to attempt analysis (Fig. 2.13). Sr isotopes are run via TIMS, and as such are much less susceptible to memory effects and isobaric interferences. Sr yields ranged from 0.01 to 31 ng and hence allowed for more successful data collection of Sr isotopic compositions. It may be possible to measure Nd oxide by TIMS.

It is important to monitor data accuracy at the very low Sr signals resulting from sub-ng levels of Sr. Harlou et al. (2009) demonstrated that, for the Durham Triton TIMS instrument used in this study, 0.1 Sr ng loads of the NBS 987 standard gave an average $^{87}Sr/^{86}Sr$ of 0.710261 ± 0.000042 (2SD; 59 ppm, n = 91) and that standards below this amount begin to be influenced to a progressively greater degree by loading blank. Using varying aliquots of a natural sample with a very unradiogenic Sr isotope composition (making it very sensitive to chemistry blank addition), using the methods and reagents described here, Harlou et al (2009) demonstrated that very small sample sizes, to as little as 0.02 ng, can yield $^{87}Sr/^{86}Sr$ values that are within 500ppm of the reference value, once blank corrected (Figure 2.16). This result was produced when a TPB for Sr of 4.7 pg +/- 1 pg was reported, identical to the blank data derived here. As such, we have accepted as accurate Sr isotope compositions that contained 0.02 ng or more of Sr.

Figure 2.16 ►. Non blank corrected (top) and blank corrected (bottom) $^{87}Sr/^{86}Sr$ versus Sr concentration for eclogitic clinopyroxene aliquots (after Harlou et al., 2009). The two curves illustrate the expected effect of a 4.75 pg (dotted) and 10 pg (broken) Sr TPB with $^{87}Sr/^{86}Sr$ ratio of 0.7129±0.0002 (2σ – Harlou study) on decreasing aliquot sizes of the reference isotope composition. The non blank-corrected data points show the expected level of displacement away from the 'true' values, indicating that the measured TPB is a realistic estimate of the TPB pertaining to a typical sample analysis. The blank correction on the samples is based on a TPB of 4.75pg Sr with an $^{87}Sr/^{86}Sr$ ratio of 0.7129 (±0.0002). The blank-corrected data show that it is possible to measure Sr isotope compositions of sub-ng samples sizes. The grey shaded zone represents the expected theoretical increase in uncertainty on the $^{87}Sr/^{86}Sr$ resulting from the blank correction at decreasing Sr aliquot sizes.

Uncertainty includes the ±2σ error on the size and composition of the blank and assumes an analyte composition equal to the reference value.

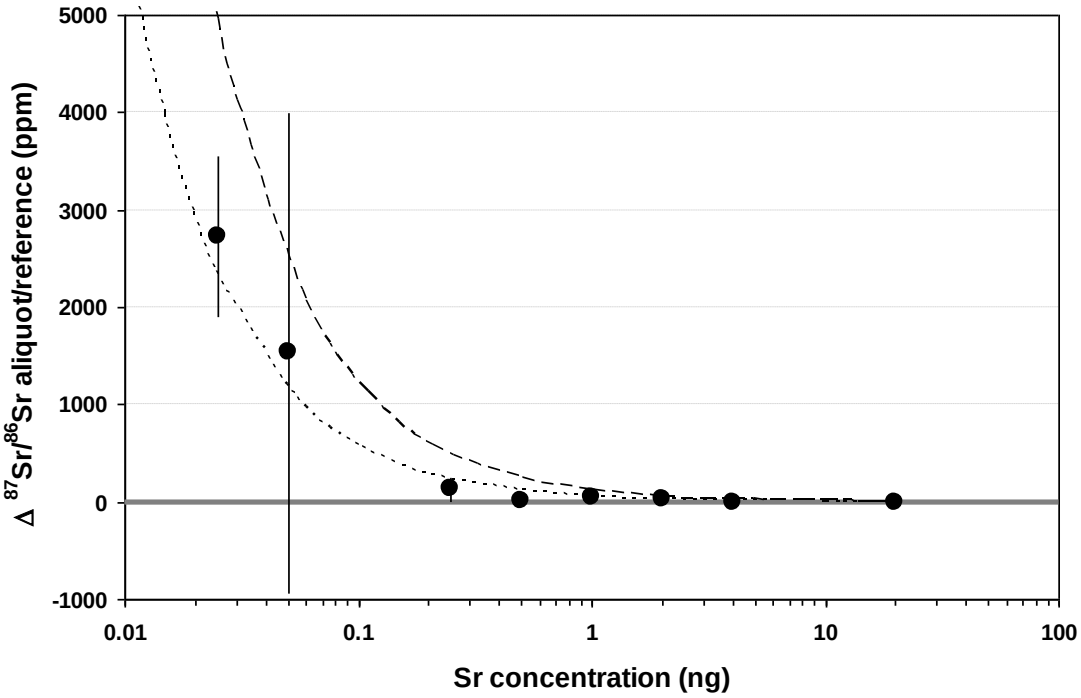

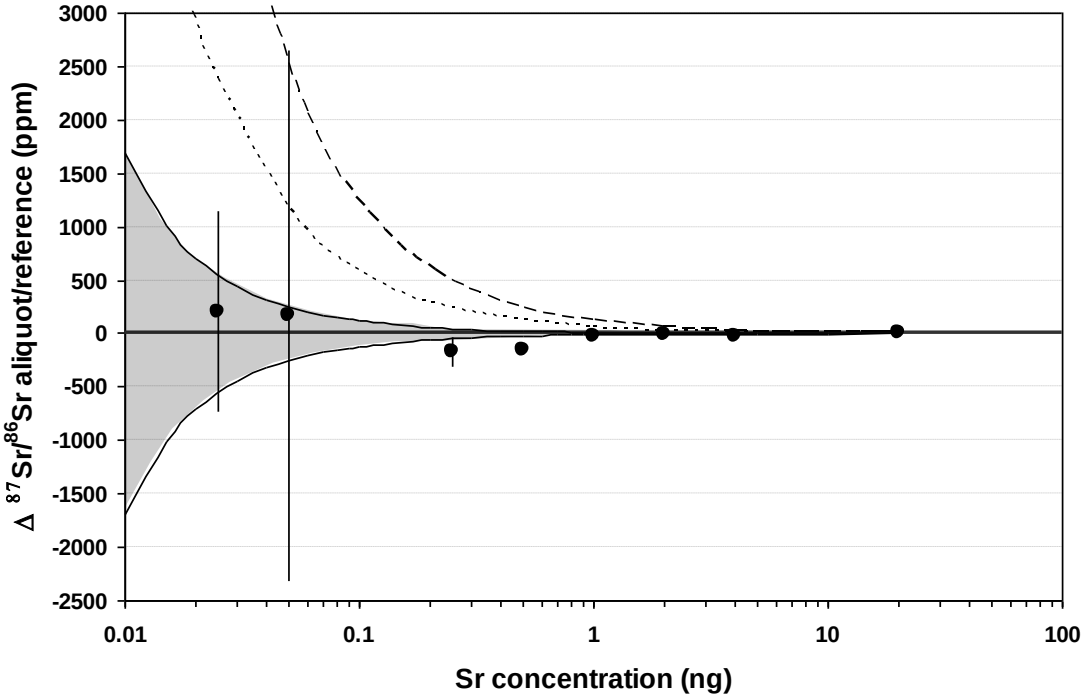

Figure 2.17 shows the 1σ internal, or within-run, precision of diamonds analyzed in this study (open circles) versus the average ^{88}Sr beam intensity during the analysis. Also shown are data for various sizes (0.5-12ng Sr) of the NBS987 standard analyzed on the Triton over the last 4 years. As expected from counting statistics the internal precision for both samples and standards increases as the Sr beam size decreases. Although there is some scatter on the regression line through the standard analyses and it is sparsely populated below ~0.2V ^{88}Sr it is nevertheless clear that the samples define a steeper trend to that of the standards. This is due to the propagation of the additional uncertainty arising from the application of Total Procedural Blank corrections on the diamond analyses, which increase with magnitude as the sample size decreases (Fig. 2.16). TPB corrections are not applied to standard analyses since they are only subject to filament and loading blank which are only a fraction of the TPB and it is extremely difficult to determine their isotopic composition.

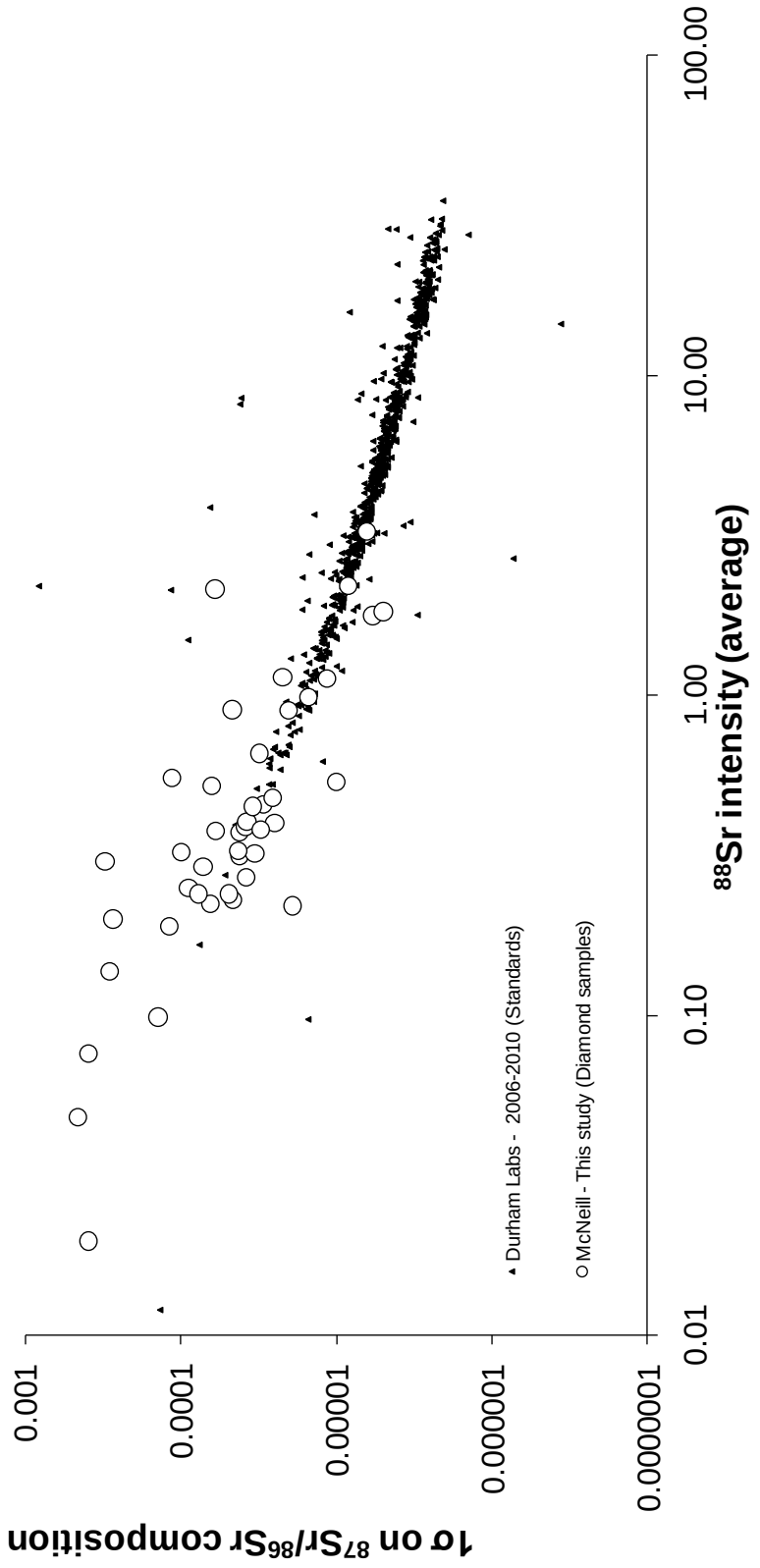

Figure 2.17. Propagated error on isotopic composition as a function of 88Sr intensity during TIMS analysis. Diamond samples do not deviate from the standards to a significant degree and both groups follow a similar trend indicating stable measurements to relatively high errors of 0.001 on a given diamond isotopic composition.

Figure 2.18 shows typical Sr isotope analyses for a 0.5 ng NBS987 standard, a fibrous diamond and a monocrystalline diamond. The amount of Sr recovered from the ablation of fibrous diamonds for isotopic analysis is generally sufficient for them to run like 0.5ng NBS987 standards in as much as the ^{88}Sr beam size is usually on the order of several 100mV and usually lasts approximately 200 integrations. Although relative to a standard they are occasionally more fractionated at the start of the analysis ($^{86}Sr/^{88}Sr$ ~0.12) and always more fractionated at the end ($^{86}Sr/^{88}Sr$ <0.118) the fractionation is similarly smooth and temporally consistent. In contrast, the recovery of Sr from monocrystalline diamonds can be extremely variable, even with extended ablation times, and as a result we take a very precautionary approach to the analysis and start acquiring isotope ratios when the ^{88}Sr beam size is very small. Despite this monocrystalline diamond analyses rarely last more than 100 integrations and the Sr beam usually becomes quite unstable toward the end of the analysis and often dies catastrophically (1.18c). For monocrystalline diamond analyses the $^{86}Sr/^{88}Sr$ fractionation ratio is usually very erratic at the start of the analysis, due to the very low beam size, and at the end of the analysis as the beam size decreases due to the exhaustion of the Sr on the filament. As such monocrystalline stones often require greater degrees of post-analytical time-resolved processing. In the typical example shown in Figure 2.18 only the $^{87}Sr/^{86}Sr$ ratios between cycle 30 and 120 are accepted.

Each integration for both standard and sample analyses is corrected for Rb interference and mass bias. Those integrations that lie outside the two standard

deviations of the mean Sr isotope ratio of the accepted group are rejected. The average $^{87}Sr/^{86}Sr$ composition of the sample is then blank corrected based on a Sr-TPB of 5 pg in this study and the laboratory blank $^{87}Sr/^{86}Sr$ composition of 0.710394. Figure 2.19 shows $^{87}Sr/^{86}Sr$ ratios for diamonds from the Slave craton both uncorrected and corrected for TPB. The change in composition after correction decreases rapidly with increasing Sr content. Samples with lower Sr content display changes in composition that will still place the samples at one or other endmember of a group and are thus not rejected. Diamond sample 153, a 'gem' monocrystalline core of a coated diamond from the Fox pipe on the Ekati Property yielded 82 pg Sr from a 5hr ablation and 0.21 mg of ablated material. This allowed a successful radiogenic isotope measurement to be acquired, $^{87}Sr/^{86}Sr = 0.70603 \pm 0.0002$. This diamond also displays a result above LOQ for most of the trace elements analyzed on that sample. See Table A3 (Appendix) for all sample compositions and Chapter 2 for discussion and interpretation.

Figure 2.18 ►. Typical reports for Standard, Fibrous and Monocrystalline samples by TIMS analysis during this study. Top) ^{88}Sr (primary y-axis, mV) and ^{85}Rb (secondary y-axis, V) intensities obtained during a typical TIMS Sr analysis during this study, shown as a function of number of cycles. Middle) Variation in $^{88}Sr/^{86}Sr$ measured during the course of the analysis to illustrate more unstable fractionation of low Sr samples relative to higher Sr samples and standards. Bottom) Variation in $^{87}Sr/^{86}Sr$ measured during the course of the analysis. The monocrystalline diamond demonstrates that early cycles show considerable spread in $^{87}Sr/^{86}Sr$ ratios primarily as a result of very small Sr beam size, but show much less variation once ^{88}Sr exceeds ~0.2 V. Data are only accepted after a standard 2σ rejection is applied to the stable cycles, in this case between cycles 30 and 120 (black filled circles).

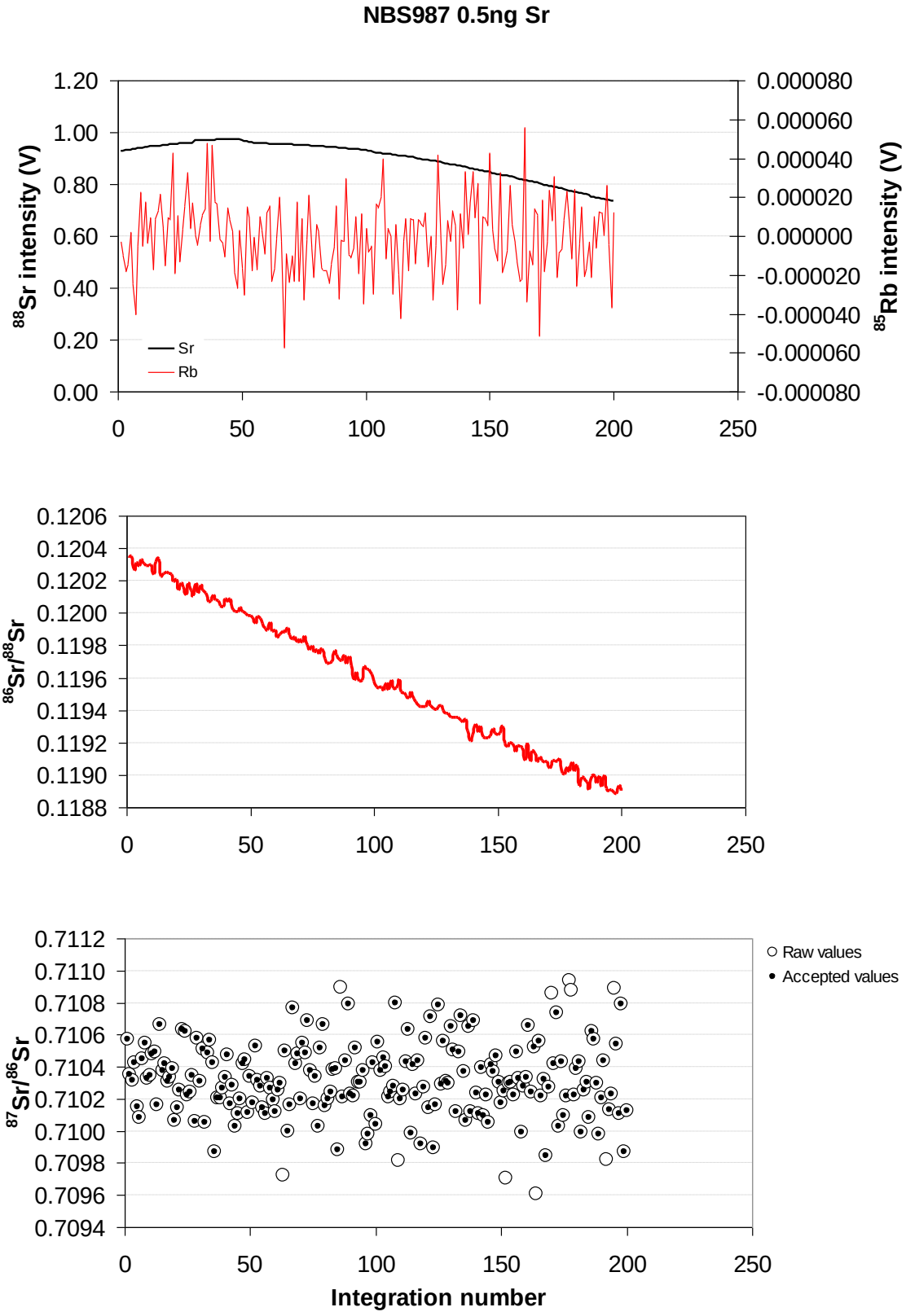
NBS987 0.5ng Sr
88Sr intensity (V)
85Rb intensity (V)
Sr
Rb
86Sr/88Sr
87Sr/86Sr
Raw values
Accepted values
Integration number

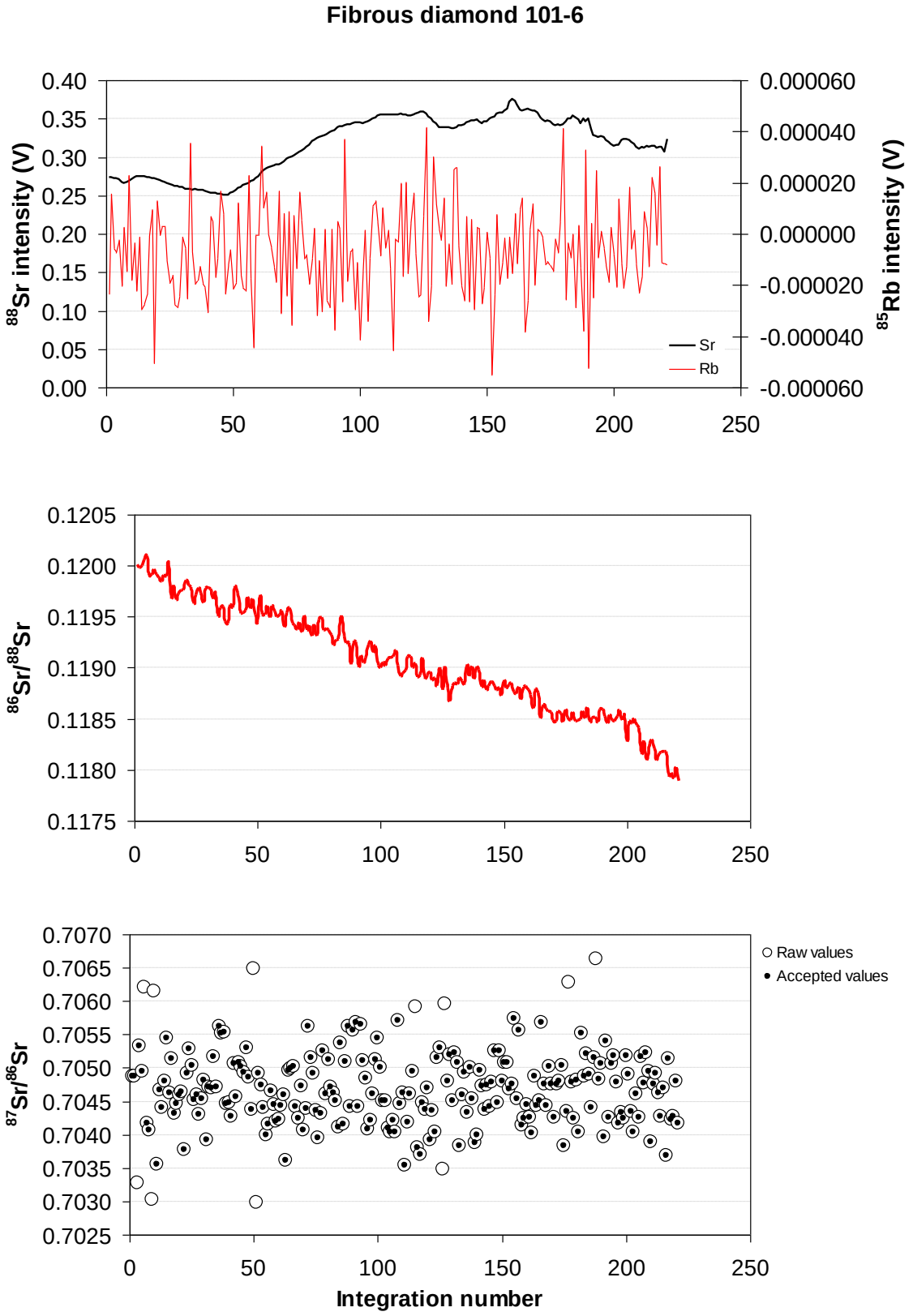
Fibrous diamond 101-6
^{88}Sr intensity (V)
^{85}Rb intensity (V)
Sr
Rb
^{86}Sr/^{88}Sr
^{87}Sr/^{86}Sr
Raw values
Accepted values
Integration number

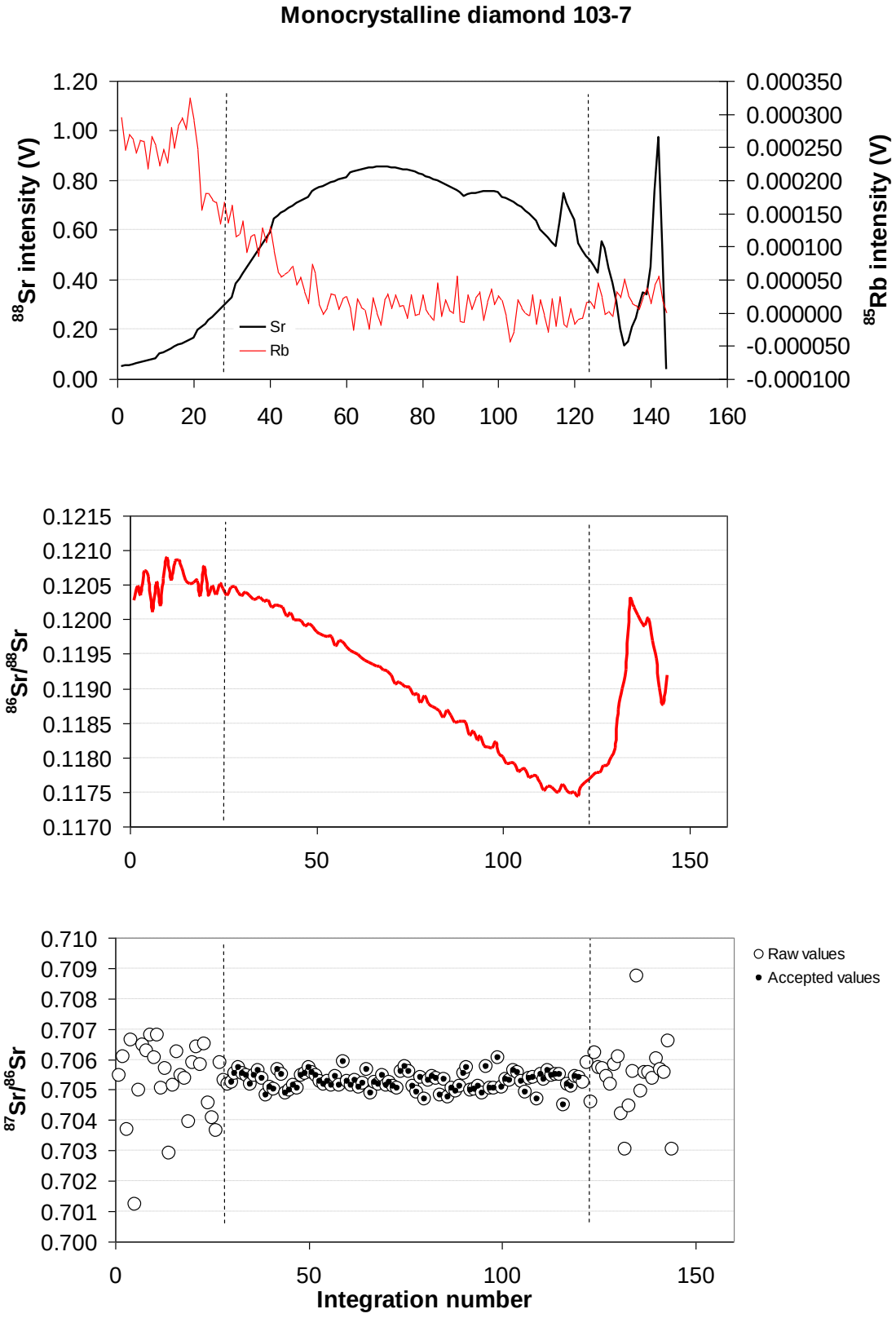
Monocrystalline diamond 103-7
88Sr intensity (V)
85Rb intensity (V)
Sr
Rb
86Sr/88Sr
87Sr/86Sr
Raw values
Accepted values
Integration number

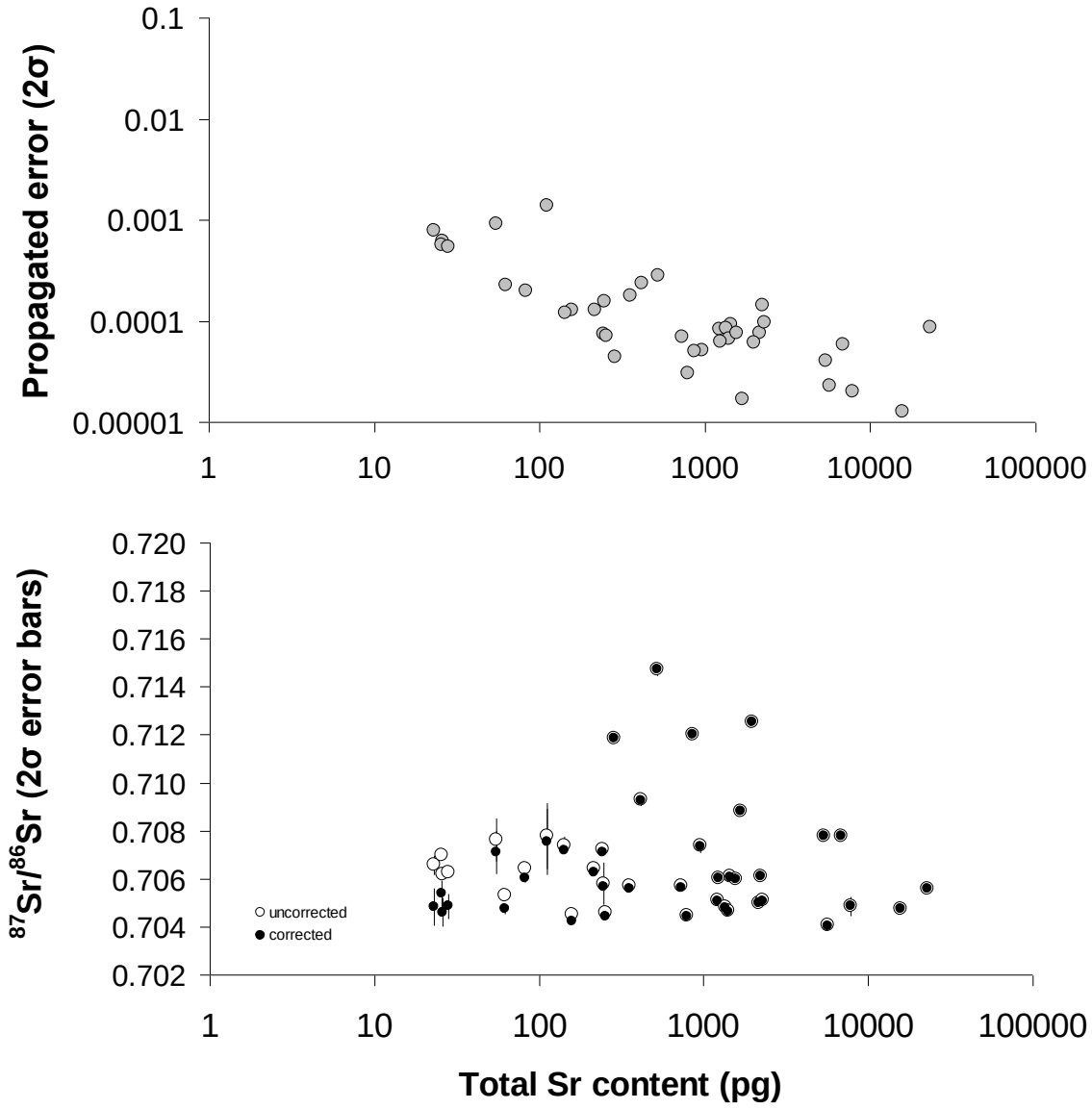

Figure 2.19. Non blank- and blank-corrected accepted sample values from TIMS analysis. The top plot shows the expected decrease in composition uncertainty with increased sample size. The bottom plot illustrates that blank correction has a greater effect on low Sr samples and that the uncertainty on that measurement is higher but that the $^{87}Sr/^{86}Sr$ compositions changes little after correction. Values at the lower analyte levels are still useful in defining an endmember to which the sample belongs in a suite that displays a large range i.e. to an unradiogenic or radiogenic endmember.

2.3 Discussion

This discussion deals with two topics; 1) Data reproducibility and inter-method comparisons and; 2) A comparison of offline and online laser ablation techniques for acquiring in-situ trace element data. The geochemical discussion and interpretation of the sample data is dealt with in Chapter 3.

2.3.1 Reproducibility of trace element concentrations via offline ablation and inter-method comparisons

Assessing data reproducibility is important when establishing any new analytical method and in this case it is likely to depend on the type of diamond being analyzed. There is no a-priori reason to expect high levels of reproducibility in the trace element concentrations of 'gem' diamonds via any in-situ or bulk analysis method since the sampling volumes are very small compared to the inclusion density. In the case of fibrous diamonds the inclusion density is very high relative to the sampling volume so we might expect good reproducibility of trace element concentrations. To investigate the offline ablation method reproducibility repeat ablations were made on two monocrystalline diamonds while 3 ablations were made on a fibrous diamond.

The three repeat offline ablations of the fibrous diamond DCR-2 yield trace element concentrations with 10 to 30% of one another and similar relative fractionation patterns (Figure 2.20). The offline ablation results are also very similar (within 50%) to three combusted fragments of DRC-2 (Figure 2.22A) so although the sampling volumes are different this doesn't bias the trace element concentrations.

Trace element concentrations of ‘gem’ monocrystalline diamonds determined by offline ablation are not reproducible to better than 50 to 150% and that inter-element ratios can display differences of over an order of magnitude. In contrast, combustion of monocrystalline diamond yields more reproducible trace element concentrations (Figure 2.21: Primitive mantle normalized values). This is presumably because the combustion technique samples a very large volume relative to the offline ablation technique (~4 mg compared to ~0.6 for the ablation technique) and despite the low density of inclusions this large combustion volume homogenizes any heterogeneity.

Further comparisons between ablation and combustion analyses are shown for monocrystalline stones from Snap Lake (Figure 2.22B). Discrepancies between the concentrations of monocrystalline diamond B3-6 from Snap Lake are attributed to heterogeneity in the fluid-inclusion density i.e. fluid inclusions are so scarce that small changes in their density make a large difference to the bulk composition. The ablation of diamond B3-6 was located on a fluid inclusion-rich rim whereas the combustion bulk sampled the rim together with core material with much lower fluid inclusion density. When two fragments of this stone and ‘gem’ diamond B4-5 were combusted the separate analyses yield similar concentrations (Figure 2.21) indicating that heterogeneity is averaged.

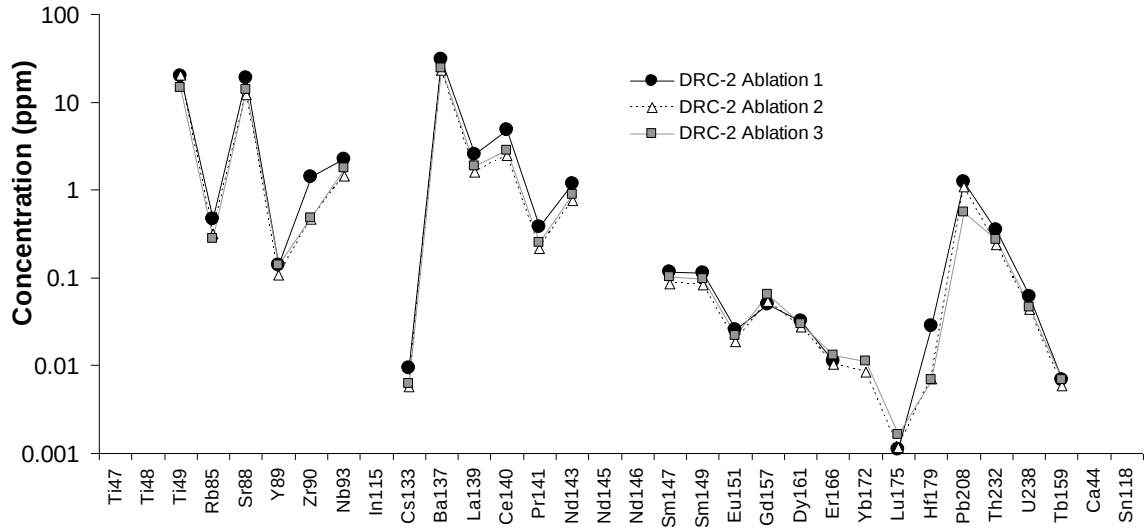

Figure 2.20. Concentrations in three separate ablation analyses of fibrous diamond DRC-2

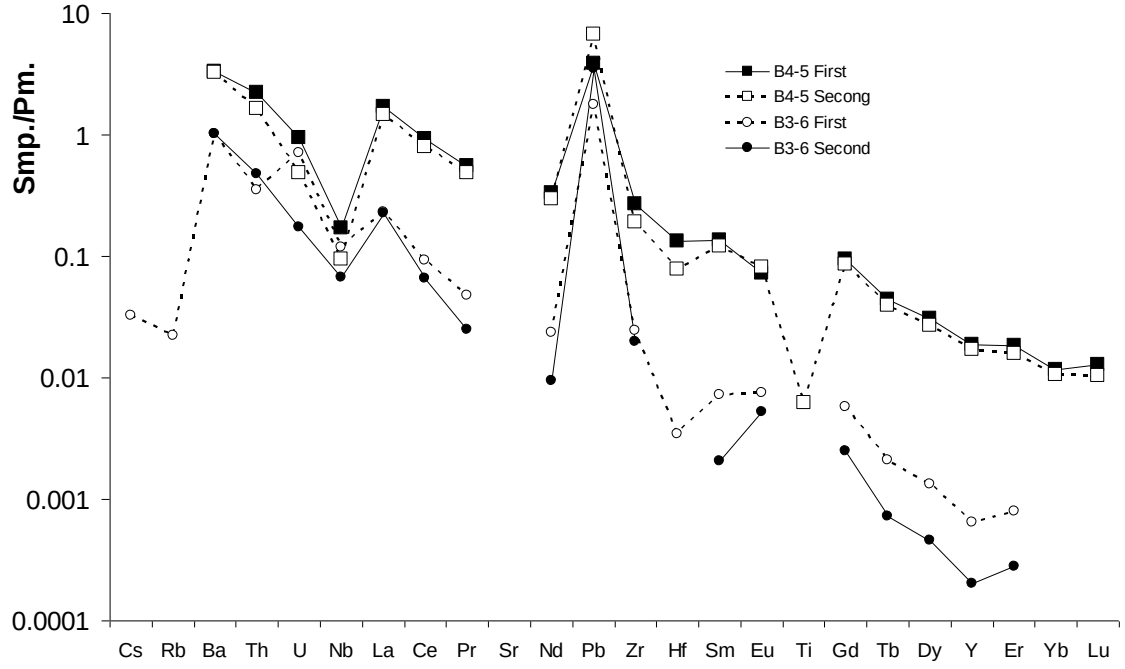

Figure 2.21. Combustion results for 'gem' diamonds B3 (First and second fragment) and B4 (First and second fragment). Sample concentration normalized to primitive mantle (McDonough and Sun, 1995).

Fibrous diamond DRC 2 was also analyzed by Tomlinson et al. (2009) using an online laser-ablation method based loosely on Rege et al. (2005). This allows comparison of the offline and online ablation methods for a fibrous stone with a relatively high density of inclusions and one for which we would therefore expect good inter-method agreement, and in fact comparison reveals close comparability for many key elemental ratios. However, despite the similarity in trace element ratios the online ablation technique of Tomlinson et al. (2009) consistently yields trace element concentrations 1 order of magnitude higher than those obtained with the offline technique. This difference is a result of the use of ^{44}Ca as the internal standard by Tomlinson et al. (2009), as opposed to ^{13}C as used by Rege et al. (2005). While our offline ablation method and online ablation using ^{13}C as the internal standard (Rege et al. 2005, 2010) yield bulk diamond compositions online ablation using ^{44}Ca as the internal standard yields inclusion compositions since the ^{44}Ca resides in the inclusions rather than the diamond lattice.

Diamond ON-JWN-11O was analyzed previously by INAA at the Astra-research reactor at the Forschungszentrum in Seibersdorf near Vienna (Austria) and PIXE at CSIRO, Australia (Schrauder et al., 1994; 1996) and most recently by Rege et al., 2005 using online LAM-ICPMS at GEMOC, Australia.

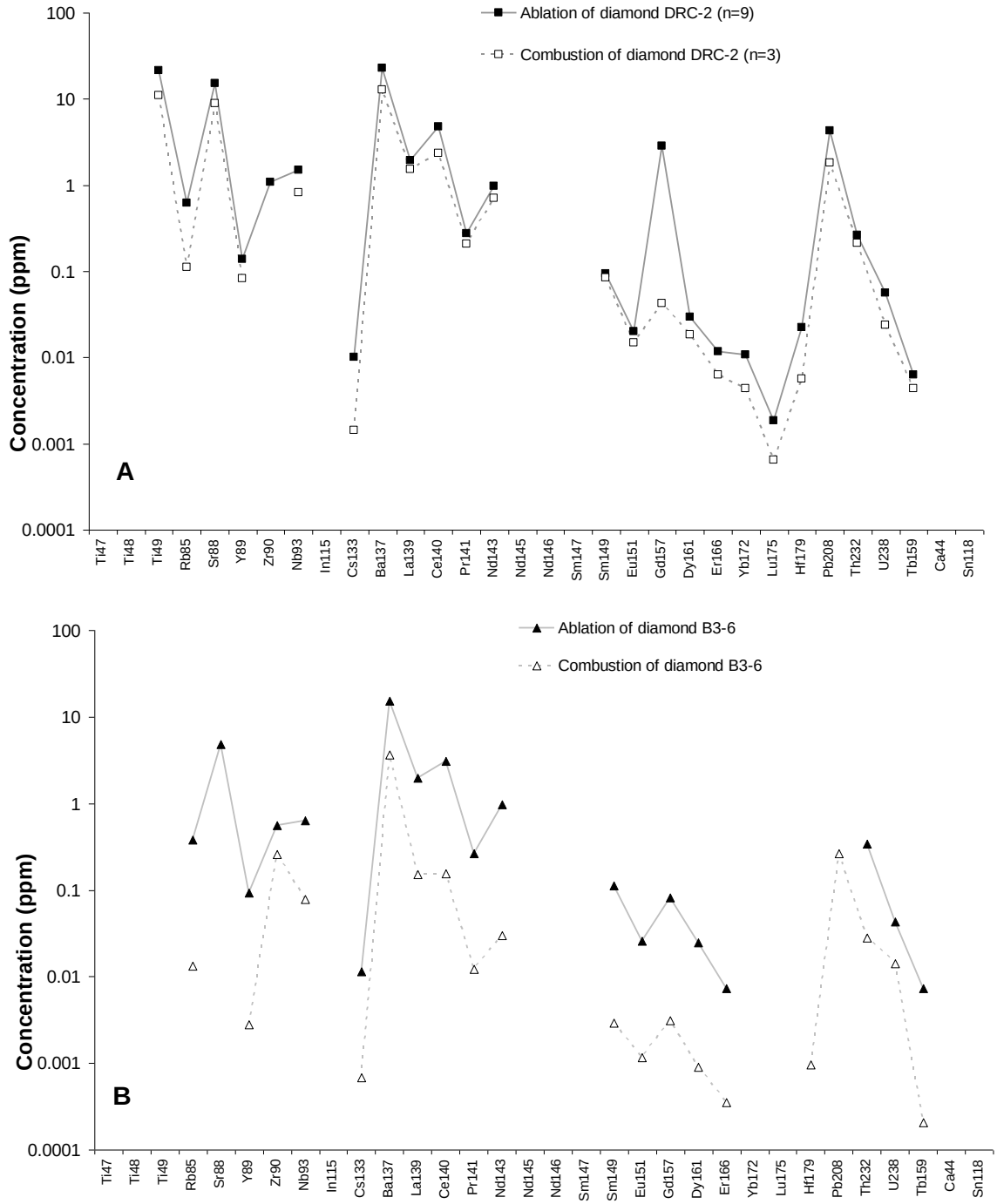

Figure 2.22. Concentrations (ppm) of an ablation analysis and a combustion analysis of the same diamond to demonstrate that the majority of key elemental ratios are maintained and reproducible. A – Fibrous diamond DRC-2. B – Monocrystalline diamond B3-6.

Figure 2.23 shows the trace element data for ON-JWN-11O obtained by each method. In general there is good inter-method agreement and although the concentrations determined by offline ablation are usually higher than for the other methods the overall profile of the trace element plots are similar. The main exceptions to this are Sr and Pb which are 2 orders of magnitude higher in concentration for the offline ablation data (Figure 2.23). However, the diamond coat is not homogeneous so there is no reason to assume that the measured concentrations from each analysis will be identical.

Despite the obvious potential for variations in inclusion density and composition in diamond, the trace element concentrations and patterns obtained by our offline laser ablation method are reproducible between ablations, and can be replicated by combustion analysis. Differences between the off-line ablation method and combustion data are present, as expected, for the volatile elements Rb and Pb due to volatile loss during the open-system combustion process. The offline ablation results also demonstrate good coherence with data obtained by other in-situ techniques and laboratories given the caveat that samples are not completely homogenous. Inter-method and inter-laboratory comparisons of data are currently hampered by the lack of a suitable diamond standard that is known to be homogenous in its concentration of a wide range of elements,

It is useful to compare and contrast the offline method with the main alternative in-situ method i.e. online ablation, to address the suitability or preferability of either

technique to study fibrous and 'gem' diamonds. Combustion techniques, although rapid, require diamond samples to be cracked and a large volume consumed. The combustion method is therefore unsuitable for routine 'gem' diamond analysis.

2.3.2 Comparison of analytical methods for trace element analysis in gem diamonds.

The very low trace element abundances found in this study confirm the earlier indications of the Fesq et al (1975) study, i.e., that 'gem-quality' diamonds contain exceedingly low levels of the incompatible trace elements of interest to geochemists (REE, HFSE, LILE etc). Abundances of almost all incompatible trace elements are in the 10s of ppb to less than 10 ppt range. This presents a considerable analytical challenge for any technique and it is especially severe considering the unusual nature of the diamond matrix that renders it intractable to traditional wet-chemical dissolution techniques that can routinely deal with such low analyte levels (e.g., Font et al., 2007; Harlou et al., 2009). The problem for diamond is further accentuated by the lack of an established diamond analytical standard.

The recent application of on-line laser ablation ICPMS to the analysis of fluid-inclusion-rich diamonds, with trace element abundances in the ppm range, has been successful because of the high concentrations of the elements of interest within such diamonds (trace element abundances in the ppm range; Resano et al., 2003; Tomlinson et al., 2005, 2006, 2009; Rege et al., 2005; Zedgenizov et al., 2007; Weiss et al., 2008). Such studies have produced a wealth of valuable information and advanced our understanding of diamond-forming fluids. However for 'gem'

quality diamonds the situation is quite different because of the extremely low trace element abundances typical of 'gem' diamonds are at the limits of detection/quantification of the current online LA-ICPMS methods.

Proponents of the online ablation technique (Rege et al., 2005, 2010) recognize that the limits of detection (LOD) of this method are primarily controlled by the volume of material ablated per second during the analysis. To improve the LOD of the online ablation method requires an increase in the rate of ablation per unit time, i.e. an increase in ablation volume per second. This can be achieved by increasing the laser energy density at the sample surface. There are two problems with this approach however; 1) If the laser is already operating at maximum energy output then the energy density can only be increased by decreasing the spot size and this does not necessarily increase the rate of ablation; 2) If the energy density is too high the sample can start to fragment and the ablation efficiency decreases. Fragmentation reduces the overall method sensitivity as fragments are not efficiently entrained in the carrier gas flow and the larger fragments are not fully dissociated during their short residence within the ICP-MS plasma. The incomplete dissociation of fragments in the plasma can also lead to inter-element fractionation and the 'spurious signal spikes' they try to avoid with on-line ablation. Increasing the energy density too much is counter productive.

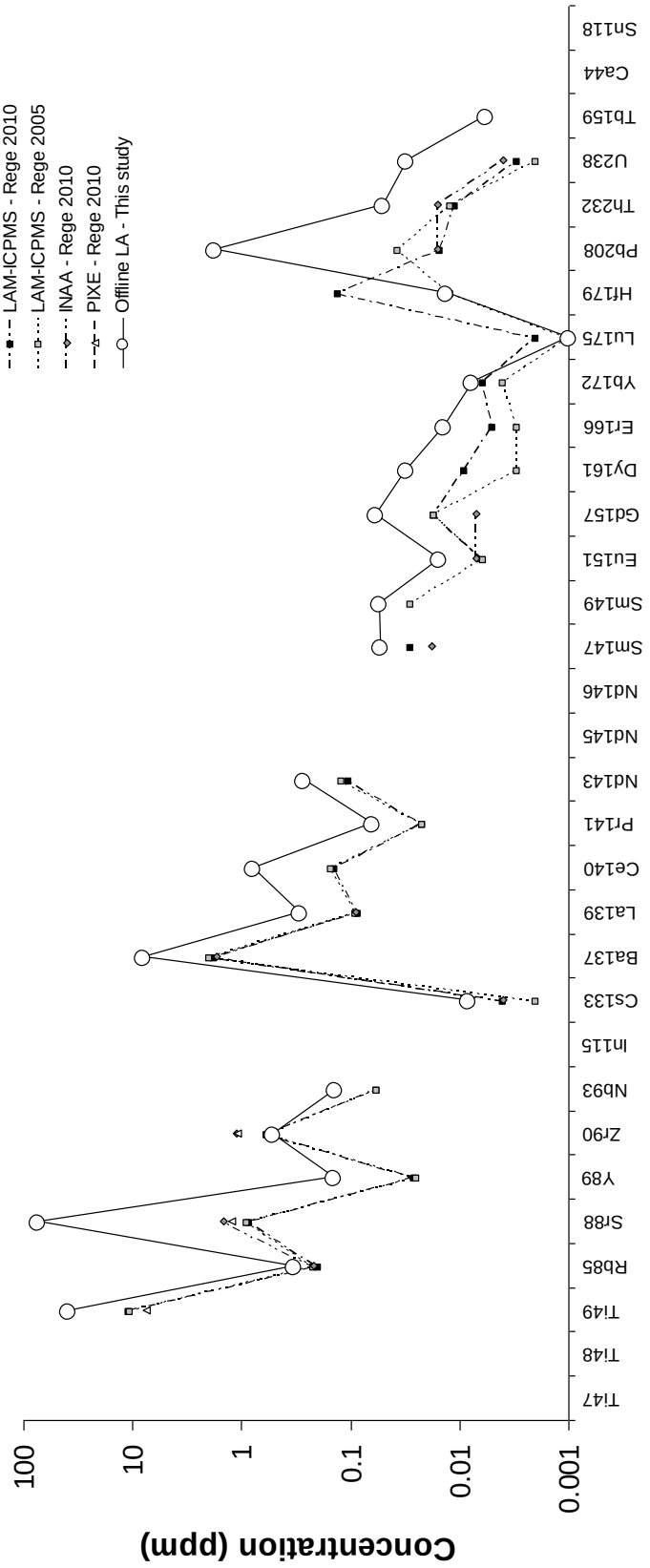

Figure 2.23. Analyses on diamond ON-JWN-110 from Jwaneng, Botswana. Concentrations have been acquired by several authors using a variety of techniques (References on the diagram and in text). The values reported from this study are similar but not fully consistent with previous measurements. This may be due to heterogeneity in the diamond as measurements were on a different half of the fibrous sample.

The online ablation method most recently reported in Rege et al., (2010) has not changed significantly from that of Rege et al. (2005) indicating that they have not resolved/addressed the issue of increasing the ablation volume per unit time. Rege et al. (2010) nevertheless report a one or two orders of magnitude improvement in LOD and LOQ for many trace elements (Figure 2.24) over Rege et al. (2005) although the way in which this was achieved remains unclear.

Improving the LOD and LOQ of our offline ablation method can also be achieved by increasing the volume of sample that is ablated. Indeed this is necessary to compensate for the slightly elevated LOD and LOQ, relative to the online ablation method, due to processing the sample through chemistry and increased TPB. However, with a closed ablation cell we can achieve this without having to increase energy density by simply increasing the ablation time. It is also possible to analyze the collected volume on the ICP-MS in a shorter measurement time. The net result is that the *sample volume per unit time* entering the mass spectrometer is greatly increased relative to the online ablation method.

The main advantages and disadvantages of the offline and direct methods are summarized in Table 2.4 and 2.5.

Table 2.4 ▼. Advantages and disadvantages of the 'offline ablation' method to acquire trace element and isotope compositions in diamond. Numbers are correlated, i.e. 1 to 1 and also with Table 1.7.

	Advantages	Disadvantages
Table 2.4 Offline LA (this study)	1. Collection of ablated material offline allows the ratio of ablation time/analysis time to be variable and *user definable* from 1:1 to ~100:1 +. LOD and LOQ **easily** reduced by increasing ablation/ analysis ratio – best achieved by increasing ablation time.	1. Collection of ablated material offline in sealed ablation cells requires multiple cells which need rigorous cleaning – reduces sample throughput. Decreasing LOD and LOQ by increasing ablation time also reduces sample throughput.
	2. Ablated volume can be aliquoted and analyzed for trace elements *and* isotopes	2. For isotope measurements ablation times must be significantly increased to increase analyte recovery and decreases throughput.
	3. Sample introduced as solution. Signal stability considerably better than with dry LA aerosol. Different nebulizers can be used to enhance efficiencies.	3. Total procedural acid blanks are higher for most elements than 'gas' blanks. This increases the LOD and LOQ.
	4. Sample homogenized at dissolution step – no spurious spikes during analysis. Entire analysis integrated for final result – better LOD and LOQ	4. Homogenizing sample potentially loses information on presence of inclusions that might be picked up, although excluded, by online laser ablation.
	5. Little or no inter-element fractionation as ablation is carried out in a sealed ablation cell and all material is recovered during the acid reflux step.	5. Use of acid reagents increases the Total Procedural Blank and increases the LOD and LOQ relative to the online method
	6. Samples spiked with In to correct for instrument drift and matrix suppression. In concentration in samples is user definable and constant – unlike ^{13}C.	6. None
	7. USGS rock standards readily available to set up external calibration. Standards diluted to concentrations that match those typical of diamonds.	7. Calibration standards not an exact matrix match to diamond ablation samples.
	8. Suitable for fibrous *and* gem diamonds.	8. Sample throughput is low *BUT* **quality over quantity**.

Table 2.5 ►. Advantages and disadvantages of the 'online ablation' method to acquire trace elements in diamond. Numbers are correlated, i.e. 1 to 1 and also with Table 1.6.

Table 2.5 Online LA (Rege et al., 2005, 2010)

Advantages	Disadvantages
1. Transfer of ablated material direct to ICP-MS is 'simple' and negates the need for chemistry. Ratio of ablation time/analysis time is obviously fixed at 1:1. Short ablation & analysis times greatly increase sample throughput.	1. 1:1 ablation time/analysis time limits maximum cps signal obtained on all analytes. LOD and LOQ not improved by increasing ablation time. Must increase ablation yield – requires more laser energy/different laser wavelength.
2. None	2. Cannot measure trace element *and* isotope compositions on the same ablated volume
3. Sample introduced as *dry* particulate aerosol. Gas blanks for dry sample introduction are usually lower and more stable than total procedural acid blanks.	3. Gas blank can be higher than acid blank for some elements (e.g. Kr). Gas blanks carried out without an ablation of a blank substrate – not appropriate as blanks for LA of samples. LA introduction not as easy as solution aspiration for enhancing sample transfer efficiency.
4. Time integrated analysis allows 'spurious' spikes to be excluded from final result.	4. Time integrated analysis – only a fraction of the analysis is integrated for final result – throwing away ions.
5. None	5. Inter-element fractionation is a problem throughout analysis – first 10s is particularly serious and is rejected – lost ions.
6. None	6. ^{13}C used as internal 'standard' element to correct for ablation and instrument yield, drift etc. Carbon content of the diamond is *assumed* to be 100% - not true for fibrous stones. Carbon peak to background variable between and within sessions. Carbon peak to background can be very low (~2.5) – background influenced by entrainment of air into plasma and carbon emitting sample transfer tubing.
7. None	7. No accepted diamond ablation stds or silicate stds with certified C concentrations. Calibration strategy complicated and currently uses a cellulose-based pellet doped with trace elements at the 20ppm level – far above the typical concentrations in diamond – essentially a 1 point calibration with non matrix matched std. Ideally ablation std and samples should be ablated under identical or as similar conditions as possible. Cellulose and diamond ablated with completely different laser energies of 0.8mJ and 2.7-8mJ per pulse, respectively – implications for inter element fractionation.
8. Suitable for fibrous diamonds	8. Not suitable for gem diamonds.

The most significant advantage of the offline method is the ability to achieve lower LOD and LOQ for most elements of interest. This is wholly dependent on the greater volume of diamond ablated. Figure 2.24 shows trace element LOD values as ppm in diamond for the offline ablation method based on; 1) a typical ablation pit volume from diamonds in this study ($3*10^8 \mu m^3$); 2) the 3σ LOD based on repeat Total Procedural Blanks. Also shown are the estimated LOD values taken from Fig.1 of Rege et al. (2010) together with LOD values reported in Rege et al. (2005). This figure demonstrates that for the majority of elements, the offline method can acquire lower LOD levels. Figure 2.24 also displays the range over which the LOD changes for the direct method between Rege et al., 2005 and 2010, and highlights why it is difficult to asses the quality of the data reported.

The larger sampling volume of the offline ablation method was specifically identified by Rege et al. (2010) as a disadvantage. Larger ablation pits equals a more destructive method. However, we consider that the improvements in analyte yield and lower LOQ and LOD outweigh this factor. Furthermore, the larger ablation volumes also allow acquisition of isotope data which can provide extremely important constraints on the identity and source of diamond forming fluids. We note also that the production of *any* surface pit on a diamond generated by laser ablation analysis, whether online or offline, leads to that diamond being classified in trade-terms as "treated". Hence the larger pit produced by our method will not lead to grossly different devaluation of any given diamond. Another consequence of our analytical procedure is the greater time taken to analyze samples compared with

direct on-line laser ablation approaches. Clearly, this is a specialized technique designed for low sample throughput, and highest data quality. However, from the database for ‘gem’ diamonds reported in Table A1 (Appendix) and consideration of likely limits of quantification, we suggest that the higher through-put online ablation methods are not yet capable of producing quantitative data (as defined by exceeding a rigorously derived method limit of quantification) for a wide range of trace elements in gem diamonds. We provide a method that has lower limits of quantitation and reports only data that exceeds those values.

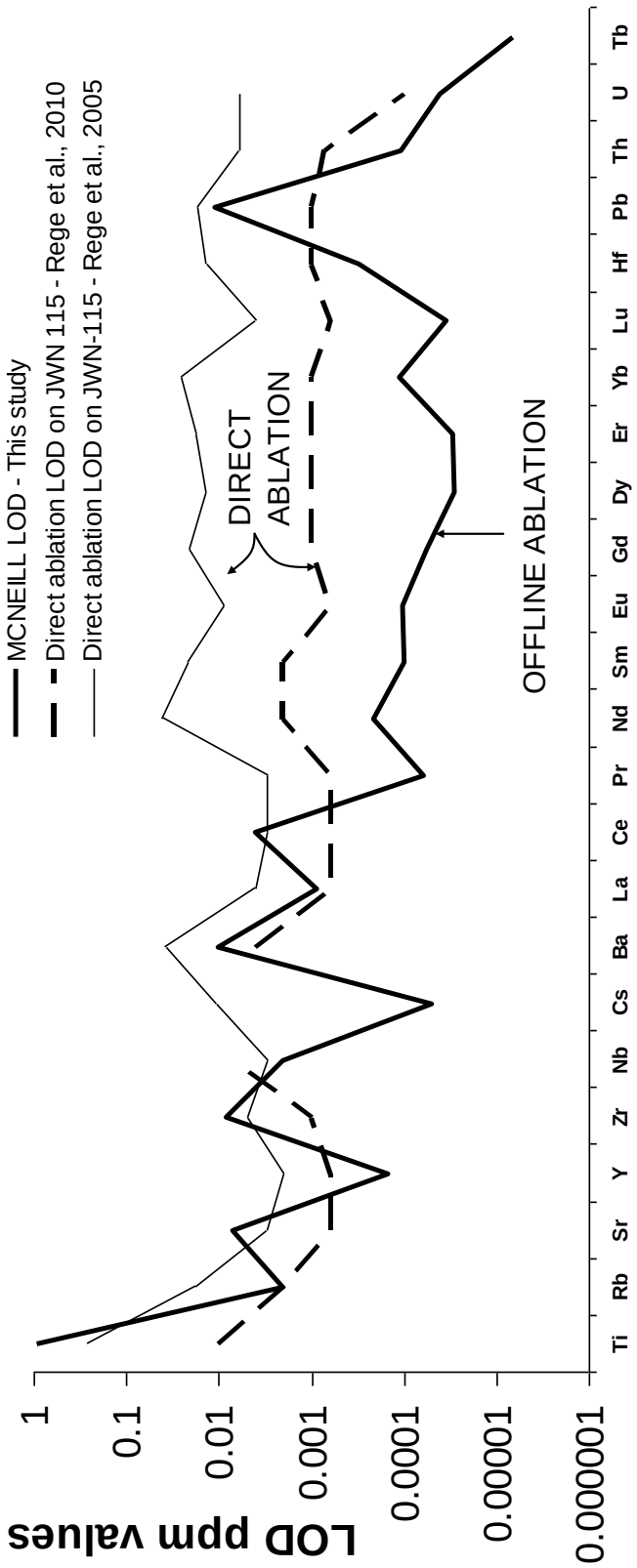

Figure 2.24. Limits of detection comparison. LODs are in ppm. McNeill LOD is an example, calculated using a typical diamond ablation volume and the absolute amount of analyte required to come from that volume to ensure quantitative analyses. A diamond density of 3.52 g cm^{-3} is chosen to calculate the McNeill offline LOD. This will be different for each diamond depending on fluid-inclusions present or whether the diamond is fibrous (lower density) or monocrystalline (higher density). It will also change given the unique volume to each ablation.

2.4 Conclusions

We present a method for the quantitative analysis of trace elements within fibrous *and* monocrystalline diamonds by offline laser ablation using a closed ablation cell followed by a pre-concentrate step and analysis of the sample solution by sector-field ICPMS using multi-point calibration lines based on accepted international rock standards. We evaluate the instrumental/method parameters necessary for the production of quantitative data, and show that the relatively large ablation volumes employed in our offline ablation approach lead to considerably enhanced limits of quantitation necessary for the analysis of gem diamonds. We report some of the first quantitative trace element concentration data for a small number of high-purity 'gem' monocrystalline diamonds and demonstrate the extremely low levels of trace impurity that they contain.

We have compared our offline ablation method to combustion analyses and demonstrated the potential of acquiring radiogenic Sr-Pb-Nd coupled to complement the trace element concentrations of any given diamond. It is clear that diamonds with a low density of fluid inclusions or any other impurity will require an ablation of several hours (>10 hrs) in order to vapourize enough diamond volume and collect enough trace element matrix for isotopic analysis.

Chapter 3 deals with the geological implications of the acquired data but from the samples used in the method development we can observe that the trace element systematics seen in fibrous and monocrystalline diamonds from this study are

common to diamonds from other locations (*See Ch. 3; Section 3.1.3*). In contrast to previous Sr-isotope measurements of Congo fibrous diamonds, e.g. $^{87}Sr/^{86}Sr$ = 0.70360 to 0.70516 (Akagi and Matsuda, 1988; Akagi, 1999) the measured Sr isotope compositions of both fibrous and monocrystalline diamonds in this study show much greater variation from mantle values to much more radiogenic values, $^{87}Sr/^{86}Sr$ = 0.70406±0.00003 to 0.71495±0.00037 (Table A3 (Appendix)).

In the future this method can be developed to further decrease the LOD and to increase the amount of information acquired from a single ablation analysis. The disadvantages of this method can also be addressed and improved upon. These ideas are discussed in detail in ***Chapter 5: Conclusions and Future Work***.

CHAPTER 3

Elemental and isotopic signatures in diamonds from the Diavik, Ekati and Snap Lake mines, Canada and their bearing on diamond genesis and diamond tracing

3.1 Introduction

3.1.1 Nature of the diamond crystallization medium

Diamond is thought to crystallize from a fluid or melt within the Earth's mantle (Sunagawa 1984; Bulanova 1995; Davies et al., 1999; Harte et al., 1999; Navon, 1999; Stachel et al., 2004; Taylor and Anand, 2004; Gurney et al., 2010). Despite intensive work the exact nature of the crystallization medium is unclear. During growth, minute residues of parental fluid can become included within the diamond matrix of some diamonds (Navon, 1988). Understanding the chemistry of these fluids (HDFs = High Density Fluids) provides our best opportunity to characterize the diamond-forming environment and understand the process of diamond formation.

3.1.2 Previous work – Major elements

Major element studies of fluid-bearing diamonds have revealed two wide compositional arrays (Figure 3.1); One array is defined by a range between a silicic endmember rich in Si, Al plus water and a low-Mg carbonatitic endmember, rich in Ca and carbonate. A second array extends between a saline end-member rich in K, Cl plus water and a high-Mg carbonatitic end-member (Izraeli et al., 2001; Klein-BenDavid et al., 2009; Schrauder and Navon, 1994; Weiss et al., 2009). All diamond forming HDFs have significantly higher potassium and volatile contents than kimberlites and carbonatites erupted on the Earth's surface with up to 39 wt.% potassium on a water and carbonate free basis and up to 40 wt.% volatiles (Klein-BenDavid et al., 2007, 2009).

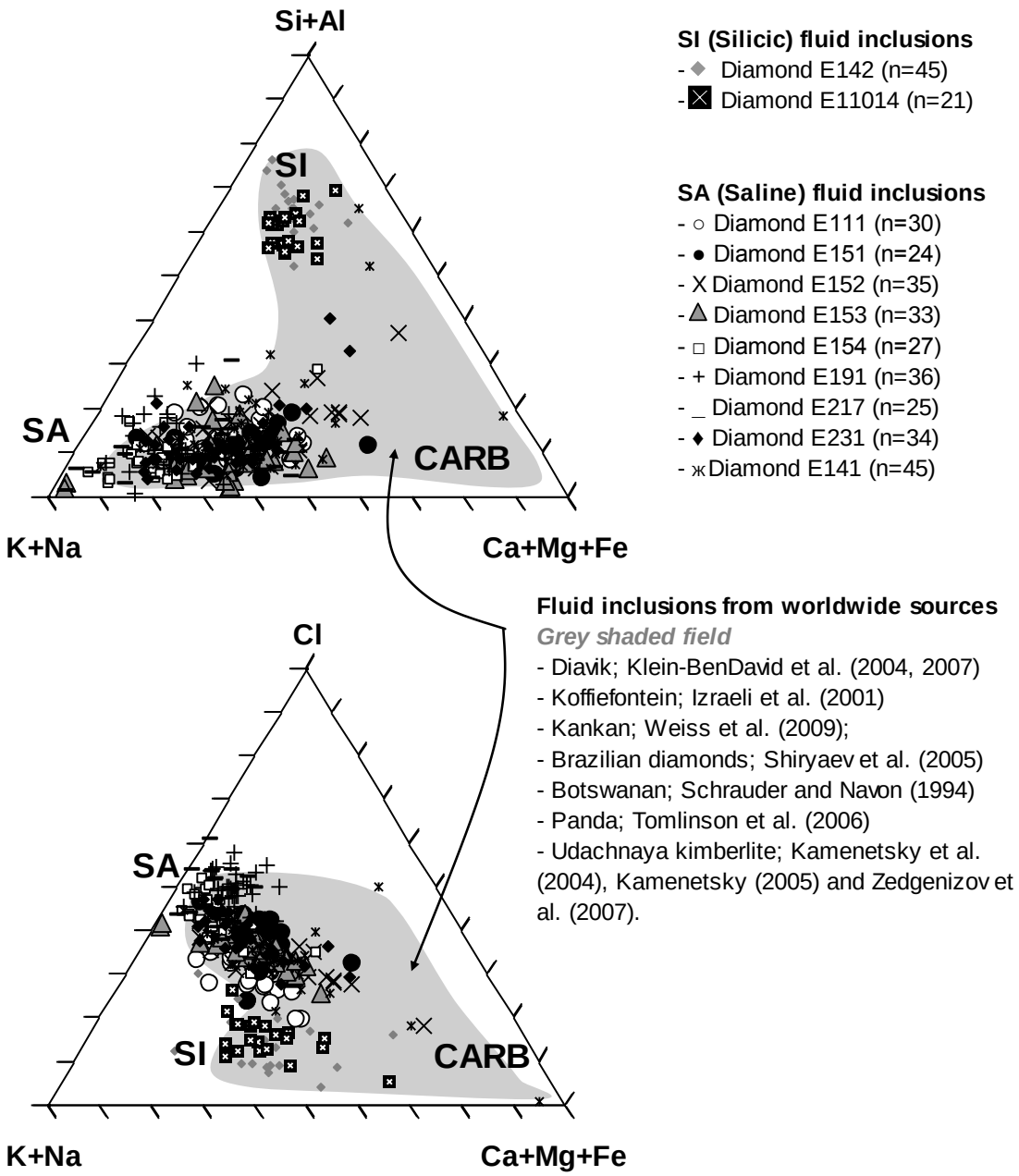

Figure 3.1. The average composition of microinclusions in diamonds from worldwide locations, and from Ekati diamonds in this study. Hydrous silicic fluid/melt endmember compositions fall close to the Si+Al apex **SI**. The carbonatitic fluid/melt falls close to the Ca+Mg+Fe+Na apex **CARB**, and the K+Cl apex represents the brine/saline component **SA**.

Recent studies of daughter minerals in sub-micron fluid-rich inclusions (e.g. Juina - Wirth et al., 2009) have identified a wide range of phases rich in alkali metals, alkaline earths, halogens and water, consistent with crystallization from extremely concentrated fluids (non-UHP diamonds - *pers.comm*. Klein-BenDavid et al., 2010).

3.1.3 Previous work – Trace elements

Until recently, the only available trace-element data on diamonds came from neutron activation analysis (NAA; Fesq et al. 1975; Bibby 1979; Schrauder and Navon 1996) or isotope-dilution analysis of the residues of burned diamonds (Akagi and Masuda 1988). More recently the use of direct laser-ablation-microprobe (LAM-) ICPMS techniques has allowed the analysis of a large number of elements at high sensitivity, and in comparatively small volumes (e.g. Schrauder et al., 1996; Resano et al., 2003; Rege et al., 2005; Tomlinson et al., 2005, 2009; Weiss et al., 2008; Zedgenizov et al., 2007; Klein-BenDavid et al., 2010). Combined, these trace element studies of microinclusion-rich diamonds of fibrous growth form have found a limited range of fluid compositions (Figure 3.2a+b), with a common parental fluid being invoked. The application of the LAM-ICPMS technique to analyzing micro-inclusion poor diamonds of monocrystalline growth should be approached with caution (Rege et al., 2005, 2010; Araujo et al., 2009b). Where limits of quantitation are quoted, they are not fully addressed and are found to be higher than the concentration of many elements reported from ‘gem’ monocrystalline diamonds in this study (See also Table 2.5, Chapter 2).

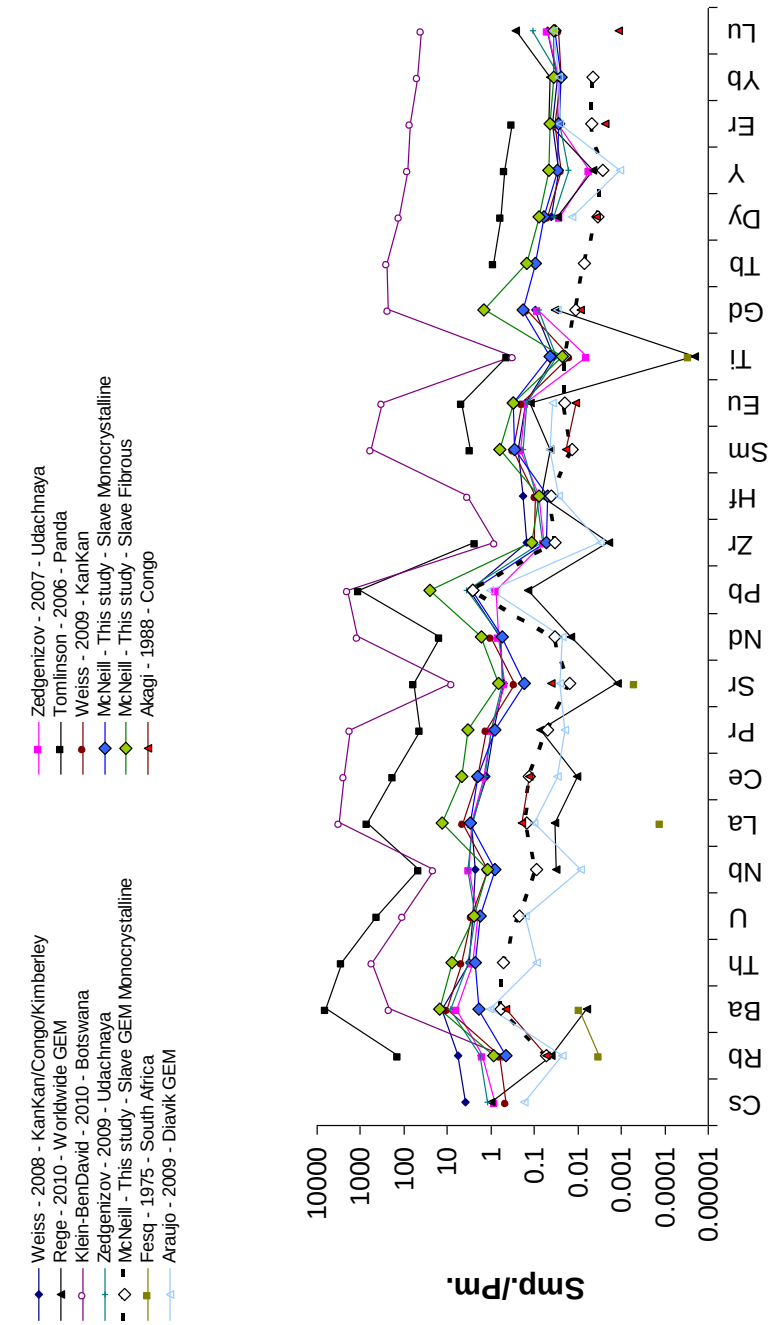

Figure 3.2a. Averaged primitive mantle normalized trace element concentrations in diamonds from several worldwide localities. This data has been collected from the sources indicated on the diagram and have been acquired by those authors with versions of the online LAM-ICPMS technique as demonstrated in Rege et al. (2005). All of the diamonds are fibrous except in Araujo et al. (2009b) and Rege et al. (2010) which represent 'gem' monocrystalline diamonds. Slave fibrous, low-purity monocrystalline and 'gem' monocrystalline averages from this study are included for reference. Pm normalization values from McDonough and Sun, 1995.

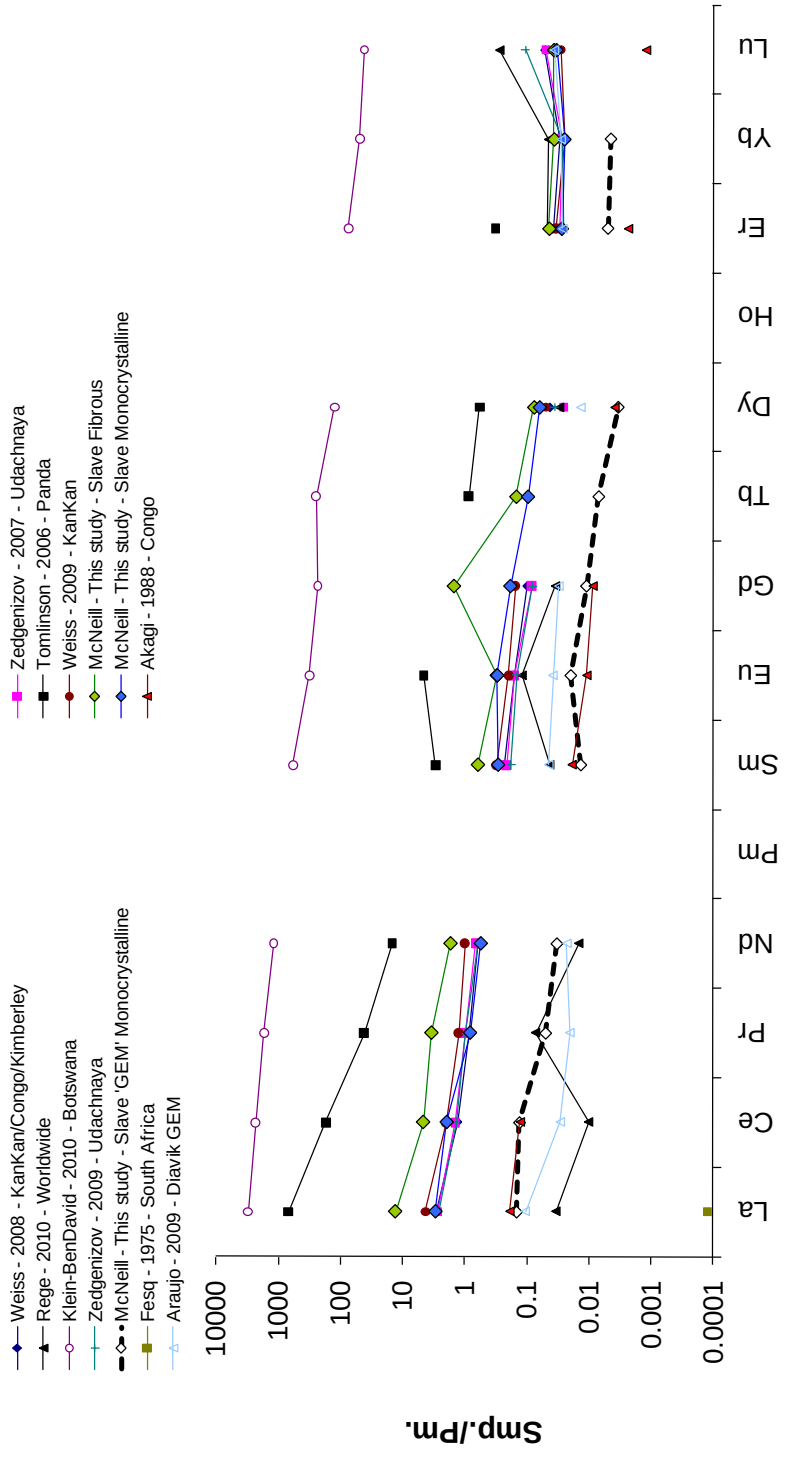

Figure 3.2b. Averaged primitive mantle normalized REE concentrations in diamonds from several worldwide localities. This data has been collected from the sources indicated on the diagram and have been acquired by those authors with versions of the online LAM-ICPMS technique as demonstrated in Rege et al. (2005). All of the diamonds are fibrous except in Araujo et al. (2009b) and Rege et al. (2010) which represent 'gem' monocrystalline diamonds. Slave fibrous, low-purity monocrystalline and 'gem' monocrystalline averages from this study are included for reference.

Results from inclusion-rich coated/fibrous diamonds, for which abundant high quality trace element data exist, support the hypothesis established from major element studies, that there is strong similarity between the HDFs and kimberlites or carbonatites and have led many authors to suggest a direct relationship between these mantle-derived melts and diamond-forming fluids (e.g. Schrauder et al., 1996; Tomlinson et al., 2005, 2009; Zedgenizov et al., 2007; Weiss et al., 2008, 2009). This interpretation is reinforced by the similarity between the restricted carbon isotopic composition of the diamond matrix and convecting mantle values (Boyd and Pillinger, 1994). Early studies of Sr isotopes in small numbers of fibrous diamonds (Akagi and Masuda, 1988) revealed relatively low $^{87}Sr/^{86}Sr$ ratios, consistent with a carbonatitic-kimberlitic link. More recently Klein-BenDavid et al. (2010) made detailed Sr-Nd-Pb isotopic measurements of fibrous diamonds that reveal a broader range of isotopic compositions with $^{87}Sr/^{86}Sr$ ranging to much more radiogenic values than those typical of convecting mantle melts.

3.1.4 The application of a new method for diamond analysis; Offline LA - ICPMS

In this study we have used a novel ICPMS-based method for the analysis of trace element concentrations specifically within low purity monocrystalline diamonds and a small number of fluid-poor high-purity, 'gem' quality diamonds to try to characterize a chemical signature unique to their growth environments. The method employs a closed-system laser ablation cell. Diamonds are ablated and the products trapped for later pre-concentration into solutions that are analyzed by sector-field ICPMS. This technique provides trace element concentrations in each diamond

analyzed and potentially also radiogenic isotope ratios of Sr, Pb and Nd. The methodology is based on that developed by Klein-BenDavid et al, (2010) when analyzing fibrous, micro-inclusion rich diamonds and is described in detail by McNeill et al (2009).

3.1.5 Aims of this study – Understanding diamond forming fluids

The aims of this study are twofold;

- To test the applicability of existing models for diamond genesis, based only on trace element data for fibrous diamonds, to monocrystalline diamonds.
- To propose a model for diamond genesis based on the chemical characteristics observed in both fibrous and monocrystalline diamonds from the Slave craton.

To achieve these aims we present the results of a trace element study with coupled radiogenic isotope information on both fibrous and monocrystalline diamonds from three deposits within Slave craton, the Snap Lake, Ekati and Diavik mines. These results, along with published data from other locations, are used to constrain the nature of the fluid or agent from which the diamonds crystallized and to construct a model for the formation and evolution of diamond-forming fluids.

3.2 Slave Craton Diamonds: Geological Setting

3.2.1 Slave craton

The evolution of the Slave Craton lithosphere has been summarized in recent papers (Aulbach et al., 2004, 2009a,b; Davis et al., 2003; Snyder, 2008; Helmsteadt, 2009; Heaman and Pearson, 2010). The Slave Craton consists of 4 domains. Two of these are major domains: an ancient (4.0 to 2.8 Ga) western-central domain and a juvenile (~2.8 to 2.7 Ga) eastern domain that may have been amalgamated by 2.7 Ga (Kusky, 1989; Bleeker et al., 1999). During this inferred collision event the ancient layered mantle underlying the western domain, consisting of an ultra-depleted shallow and a less depleted deep layer (Griffin et al., 1999), may have been subcreted beneath younger shallow mantle underlying the eastern domain (Aulbach et al., 2005). Multiple accretionary processes occurred on both craton margins between ca 2.1 and 1.8 Ga (summarized in Hoffman, 1989).

3.2.2 Ekati, Diavik and Snap Lake kimberlite fields and their diamonds

The Slave craton has been intruded by over 300 known kimberlites, many of which are diamondiferous (See summary by Kjarsgaard, 2007). General characteristics of Slave diamonds have been described in detailed studies by Stachel et al. (2004) and Gurney et al. (2004). This study will focus on diamonds of unknown parageneses from the Fox and Misery pipes of the Ekati Property, unknown pipes from within the Diavik Property and a suite of diamonds from the Snap/King Lake dyke. The kimberlites of the Ekati and Diavik properties are located in the Lac De Gras Field (Figure 3.3) in the central part of the Slave craton and have reported ages of

emplacement that are focused around 56 Ma (Creaser et al., 2004; Gurney et al., 2005). In contrast, the Snap Lake/King Lake kimberlite dyke emplacement has been dated at 537 ± 11 Ma (Agashev et al., 2008) and is thus thought be the result of an event distinct from that resulting in the central and northern Slave kimberlites.

Slave kimberlites belong to groups in which other surrounding kimberlites are of similar age, defined as domains by Heaman et al. (2003). Domain III – a central Tertiary/Cretaceous domain centred on Lac de Gras contains Ekati and Diavik whereas Domain II – a south-eastern Cambrian domain, contains the Snap Lake dyke (Figure 3.3). Location-specific studies on various aspects of diamonds including ^{13}C, ^{15}N, $^{33,34}S$ stable isotope systematics, colour, morphology, age, and inclusion chemistry have been conducted mostly over the last decade. Ekati diamonds have been described by Gurney et al. (2004) and Cartigny et al. (2009); Diavik diamonds by Stachel et al. (2004) and Araujo (2009); Snap Lake diamonds by Pokhilenko et al. (2004), Yelisseyev et al. (2004) and Promprated et al. (2004).

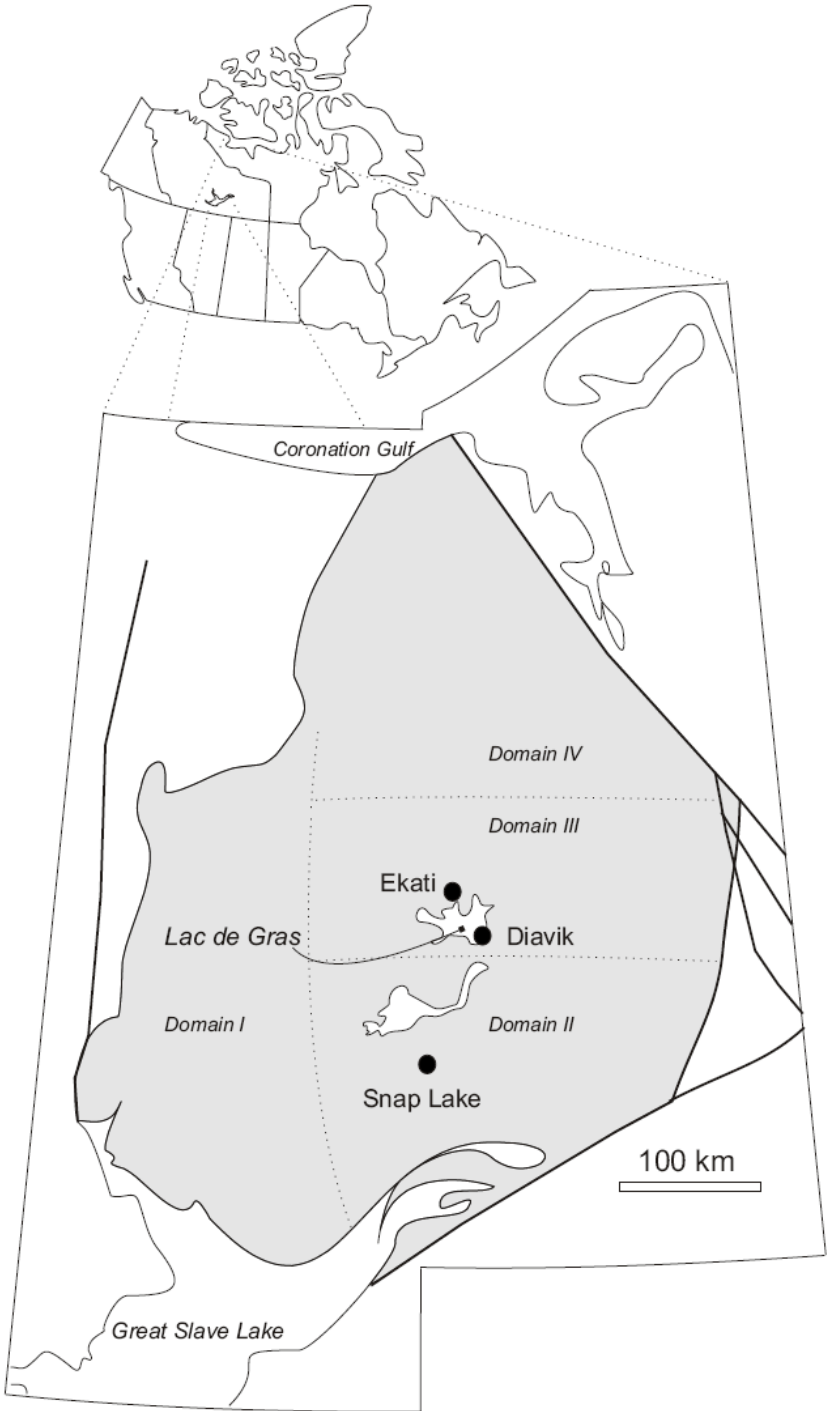

Figure 3.3. Location of the Slave Craton in the North West Territories / Nunavut, Canada with a sketch map of the craton and area north of the Great Slave Lake. The Ekati, Diavik and Snap Lake kimberlite properties are shown within the age-related domains of Heaman et al. (2003).

3.3 Samples

A total of 112 diamonds were analyzed in this study. The suite is a mixture of fibrous/coated, low purity monocrystalline and high-purity 'gem' monocrystalline diamonds from the Diavik, n=27; Ekati, n=42; and Snap Lake, n=43. Details of these diamond suites have been summarized in Table 2.1, Chapter 2. The diamond sample at each mine is not a random sample of run-of-mine production and thus cannot be considered as representative of the total population of central Slave diamonds. All diamonds were supplied as either whole stones or fragments of whole stones (Figures 3.4, 3.5 and 3.6). There is a large range in the size of diamonds analyzed from the Slave craton and also in each of the three mines (Table A.1 (Appendix)). An assumption is made during this study that diamond's size has no correlation to a diamond's chemical signature. Each stone has been analyzed for trace elements only once unless stated otherwise. Five coated diamonds have had their monocrystalline core and fibrous coat analyzed separately to address the question of a genetic link between their respective parental fluids.

Apparent colour varies with density of fluid inclusions present in the diamond and we may expect this to lead to trace element abundance variations. Brown diamonds from Ekati are thought to derive their colour due to vacancy-type defects and heat or stress deformation (Fisher, 2009). Yellow colouration is most often associated with nitrogen impurity (Read 2005). It is therefore unlikely that brown or yellow colours sensu stricto will relate to the measured trace element signature of the diamond.

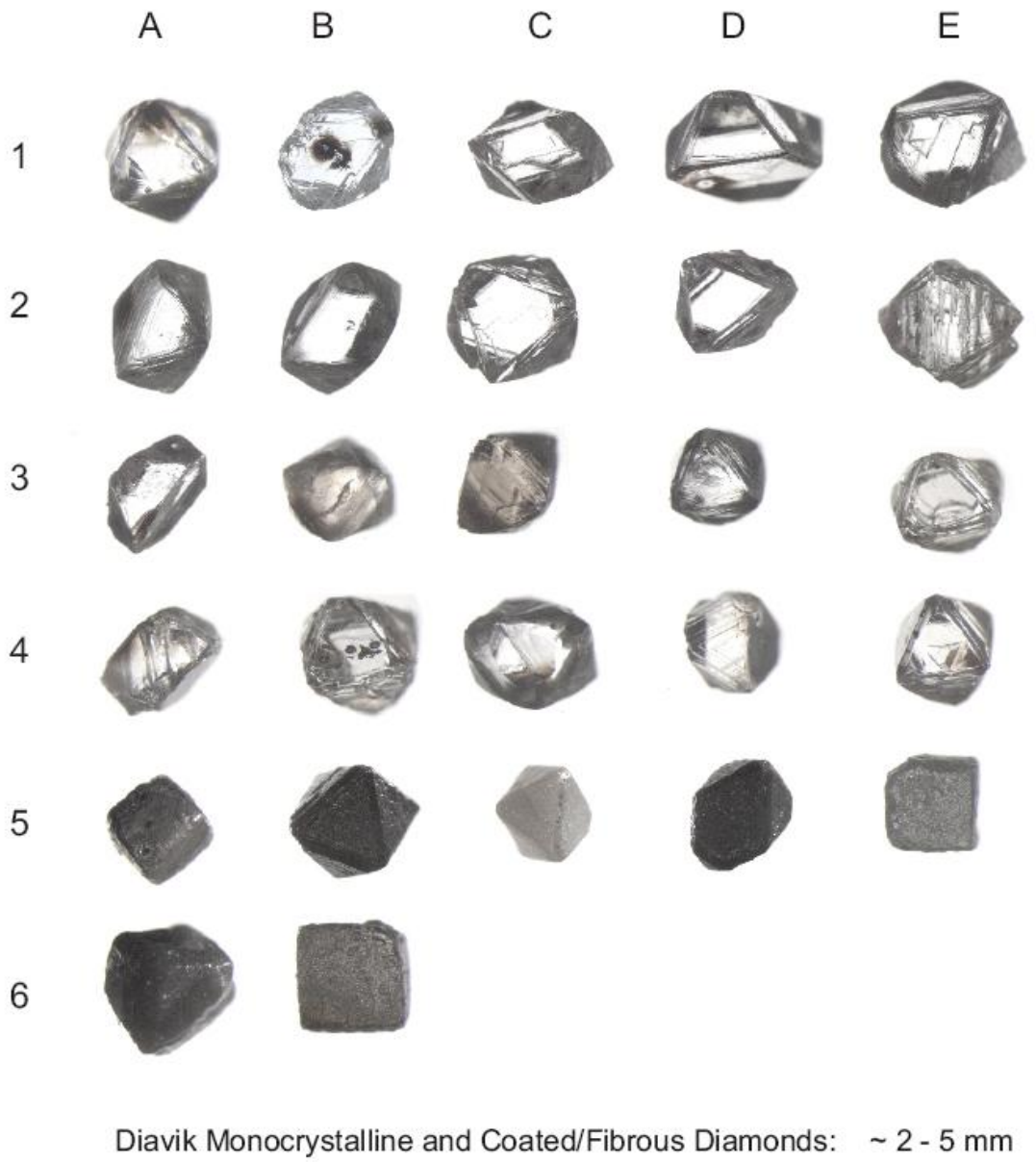

Figure 3.4. Diavik diamonds analyzed in this study. The specific kimberlite source on that property is unknown. Photographs are not to scale relative to one another. See p 252/3 for diamond sample numbers.

Figure 3.5. Ekati diamonds characterized or analyzed in this study. Samples are from the Fox and Misery kimberlite pipes. Photographs are not to scale relative to one another. See p 252/3 for diamond sample numbers.

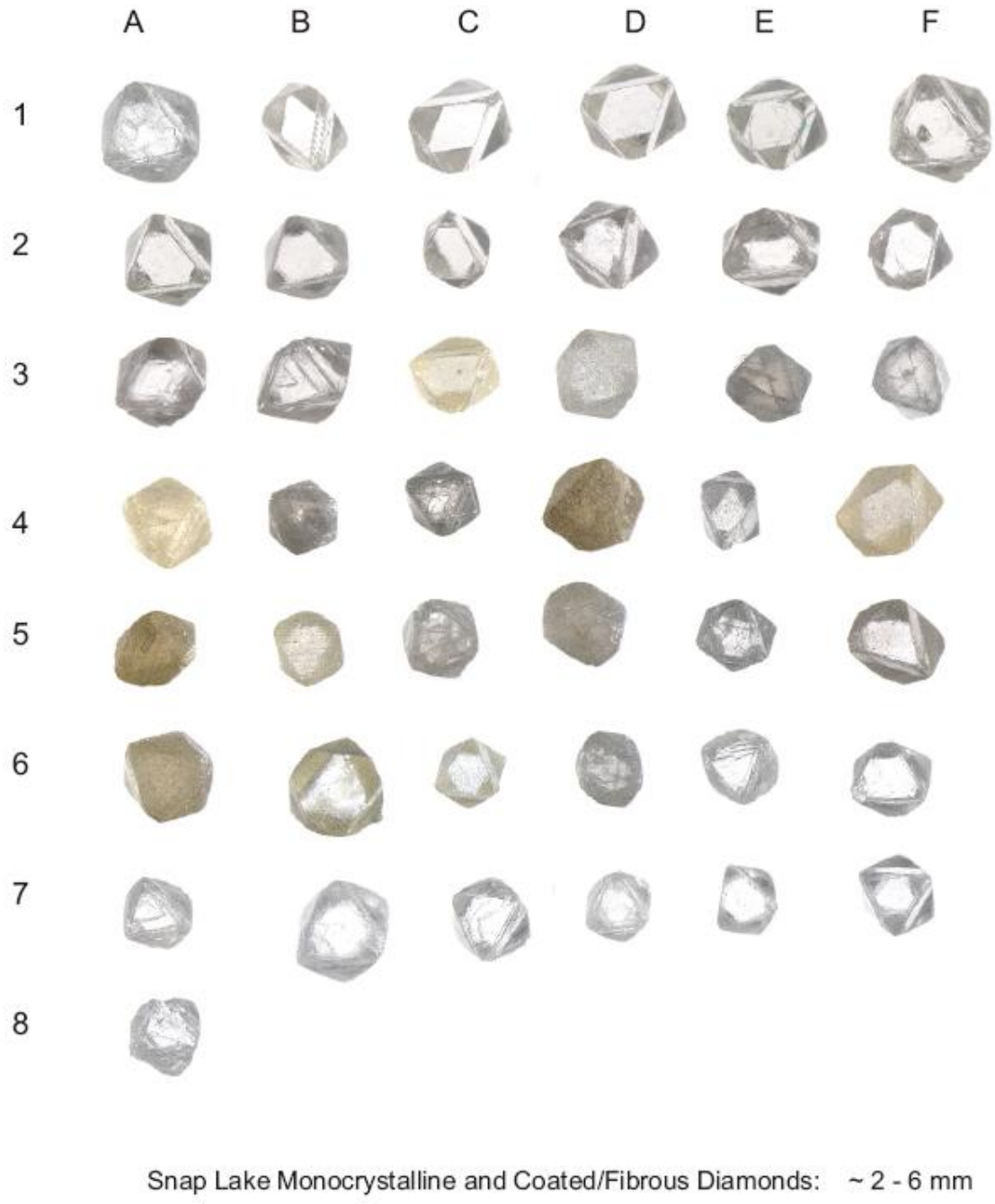

Figure 3.6. Snap Lake diamonds analyzed in this study. Samples are from the Snap Lake/King Lake kimberlite dyke. Photographs are not to scale relative to one another. See p 252/3 for diamond sample numbers.

Monocrystalline diamonds have been separated into two groups; A low-purity group that consists of diamonds that have a high density of fluid inclusions; A high-purity group that has an extremely low density of fluid inclusions. This is a visual classification only. In the text the term *monocrystalline* will refer to both groups, *low-purity* when addressing the first group and '*gem*' is used when referring specifically to the high-purity group for which much more sparse data exist.

The low-purity monocrystalline diamonds are almost exclusively from the Snap Lake mine and they are coats or rims on octahedral 'gem' cores (Figure 3.6 – C3 TO D6). The quality of the coats/rims on the stones is judged to be relatively high and that whilst this layer was probably grown at a higher rate than the 'gem' core, the nucleation rate was not sufficiently high to generate fibrous growth and these are of distinctly monocrystalline growth (*Pers. comm.* Dr David Fisher, Principal Research Scientist, DTC Research Centre, Maidenhead, Uk.). Figure 3.7. displays these diamonds and associated Cl images where available. The monocrystalline coat or rather the last layer of growth can be easily identified as distinct from the 'gem' core which is colourless.

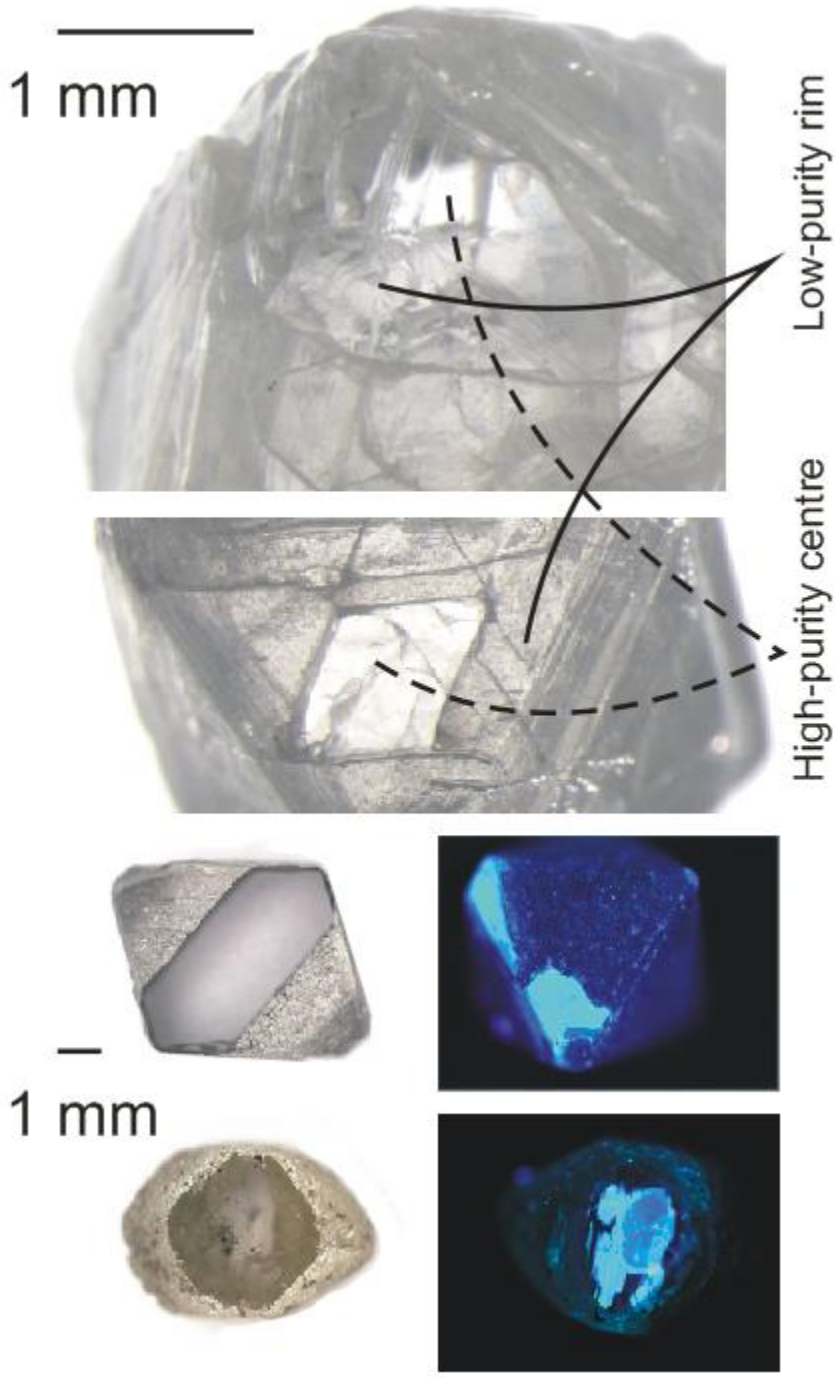

Figure 3.7. Low-purity monocrystalline diamonds from Snap Lake. TOP - The latter stage of growth, coat or rim, is monocrystalline growth that contains a higher density of fluid inclusions than a 'gem' white monocrystalline diamond. The laser analysis sampled the outer, latest stage of growth. BOTTOM - Plate photographs and Cl images highlight by contrast to the core the outer coat.

3.4 Method

3.4.1 Sample preparation and material ablation

All diamonds were processed through two acid baths prior to weighing, as detailed in the previous chapter. This purges the surface of any contaminant or foreign material and also dissolves any exposed inclusions.

Diamonds were ablated in a custom-designed, sealed PTFE ablation cell capped with a laser window that had been previously cleaned with acid (Figure 2.1, Chapter 2). Ablations were performed with a UV-213 New-Wave Laser ablation system, with the custom cell replacing that provided by the manufacturer. A pre-weighed diamond was brought into focus and an ablation was performed using a raster-pattern. Ablation conditions were: scan speed 50 μm/s; raster spacing 80 μm; energy output 5–6 J/cm^2; repetition rate 20 Hz; spot size 160 μm and pass depth 2 μm. Ablation time varied from 3-8 hrs with occasional 10 and 27 hr ablations to collect material for isotope analysis. Following ablation the laser cell is opened in an ultra-clean environment and all ablated material was collected in hydrochloric acid before being dried down prior to further chemistry. The diamond was rinsed in MQ water and dried. Diamonds were re-weighed and the weight loss resulting from the ablation was calculated. Weighing uncertainty is estimated from 100 repeat weighs of both a 'gem' monocrystalline diamond and a fibrous diamond that yielded weights of 148.2570±0.00061 and 28.9163±0.00066 respectively where the uncertainty quoted is one standard deviation and represents an error of approximately <0.01 relative %.

The dried ablation product was taken up in nitric acid. A 20% aliquot is taken by volume for trace element analysis. The remaining sample was processed for Sr isotopic analysis. The Sr separation procedure is based on the method described by Charlier et al. (2006), using Sr-spec resin but with modifications as outlined by Harlou et al. (2009) for sub-ng samples and is described in detail in Chapter 2.

3.4.2 Quantifiable data and background corrections

To obtain a statistically valid view of the "background" corrections for any low-level chemical procedure it is necessary to have adequate knowledge of analytical blanks. Only then can confidence be placed in estimates of the limits of quantification i.e., the ability to report quantitative data. We use the limit of quantification (LOQ) as defined by Currie (1968) as a measure of our ability to quantitatively measure elemental abundances because this parameter is significantly more robust than defining "limits of detection" or LOD, which merely define the ability to qualitatively detect an analyte. The LOQ for a procedure with a well characterized blank is defined by Currie (1968) as: LOQ = 10σ where σ is the standard deviation of the blank for the process (here defined as the total procedural blank or TPB). This approach places clear limits on our ability to quantitatively report concentration data in the diamonds studied. We use a dataset of 20 total procedural blanks (TPBs) performed using the same ablation cells and reagents as used for samples, to determine the LOQ for trace element abundances. Within each batch of samples, between five and ten additional TPBs were also run to monitor whether our LOQ

estimate was applicable from one batch of samples to another. Any analyte below the LOQ is flagged in the data and not used on a concentration plot. LOQ values are given in Table A.1 (Appendix).

In the definition of Currie, data can only be quantitative if it exceeds 10σ of the blank, hence the analyte to blank ratio is a critical parameter to measure. The total amount of analyte and hence the analyte/background ratio is simply a function of the length of the ablation, with the ratio increasing with time.

3.4.3 Multi-element ICP-MS – Trace elements

TPBs and aliquot sample solutions were analyzed for trace element concentrations on the Thermo-Electron Element II ICPMS at Durham University. Each sample aliquot was made to 500 µl with 3% HNO_3. Instrumental conditions were similar to those described by Font et al. (2007). The isotopes measured and the instrumental parameters are shown in Tables A.1 (Appendix) and 2.2 (Chapter 2). Solution concentrations were measured against 9-point calibration lines constructed from appropriately dilute solutions of the international standards AGV-1, BHVO-1 and W-2. All concentrations were corrected for instrument drift using an ^{115}In internal spike. Oxide correction coefficients were determined by running standard solutions of Ba, La, Ce, Pr, Nd, Sm, Gd and Tb at the beginning of each analytical session in order to correct for the daily changes in the oxide production rate. All trace element concentrations were normalized to the diamond weight loss during ablation

.

3.4.4 Thermal Ionization Mass Spectrometry – Radiogenic Sr

With each batch of samples processed for isotopic analysis, between five and ten TPBs were carried out to determine the average size of the blank contribution and its effect on the isotopic composition of the sample. During the course of this study Sr blanks averaged 5 pg (n=12). A Sr isotope blank correction can be performed using the isotopic composition based on combining the equivalent of over 60 TPBs to yield sufficient Sr (~500 pg) for a precise and accurate TIMS analysis. The average $^{87}Sr/^{86}Sr$ composition of the laboratory blank during the course of this work was 0.710853±0.000194 and all Sr samples were blank-corrected based on this value and the average blank set at 5 pg.

Sr samples were loaded using procedures described in detail by Charlier et al. (2006) and Font et al. (2007), employing a purified TaF5 activator. Sr isotope ratios were measured on a ThermoFisher Triton TIMS at Durham University, UK. Sr isotope measurements were carried out using a static multi-collection routine. Each sample measurement achieved between 50 and 300 ratios with an integration time of 4 s per ratio; total analysis time approximately 3 – 20 min. Mass fractionation was corrected using an exponential law and an $^{86}Sr/^{88}Sr$ ratio of 0.1194. Multiple loads (n=43) of NBS987 of between 0.5 and 3 ng size gave an average value of 0.710260±0.00002 (2SD; n=43) which compares well to the long-term values reported of the Durham laboratory for similar sized standards from the same laboratory (Charlier et al., 2006; Font et al., 2007; Harlou et al., 2009; Klein-BenDavid et al., 2010). As the Durham laboratory reports Sr data relative to an $^{87}Sr/^{86}Sr$ ratio of 0.710240 no additional

normalization was performed. Average signal size for the ^{88}Sr for the 0.5 and 3 ng standards were 0.8±0.4 V and 5±1.3 V respectively. Signal sizes for samples were on average 0.2±1 V. We have previously documented in detail the levels of accuracy and repeatability for samples and standards at these low signal intensities (Harlou et al., 2009). There is no systematic relationship between analyte size and Sr isotope composition post blank correction. Hence we conclude that our blank correction procedures adequately correct for our systematic TPB. Uncertainties in the magnitude and isotopic composition of the blank are incorporated into the reported errors on isotopic compositions at the 2σ level. Experiments by Harlou et al. (2009) indicate that for blanks of ~5pg, it is possible to make accurate blank corrections to samples containing as little as 20pg and therefore that level was used as a cut-off for accepting accurate data in this study because similar levels of blank reproduction were achieved.

3.4.5 Major element analyses of fluid inclusions in fibrous diamonds

Analyses on 11 Ekati fibrous diamonds were carried out at the Hebrew University of Jerusalem using EPMA techniques detailed in Weiss et al. (2008) (Figure 3.8). The following is a quote on the method from Klein-BenDavid et al. (2007; Section 3.3):

"Individual, shallow, subsurface micro-inclusions are detected using back-scattered electron images generated using a JEOL JXA 8600 electron probe. Individual inclusions are analyzed using a focused 15 keV, 10 nA electron beam. X-rays are collected for 100 seconds using a Pioneer-Norvar energy-dispersive spectrometer (EDS). The spectral data is reduced using the PROZA correction procedure supplied by Noran (Bastin and Heijligers, 1991) to yield the relative abundances of Si, Ti, Al, Fe, Mg, Ca, Ba, Na, K, P, Sr (S), and Cl. Fluorine was not measured as its concentration in most of the analyzed micro-inclusions was below the level of detection. Where present, it was due to remains of the HF leaching into exposed inclusions and imperfect rinsing. Each EPMA analysis records a single micro-inclusion. As neighbouring micro-inclusions are commonly separated by approximately 1 lm thick diamond matrix (Klein-Ben- David et al., 2006) and as only large, and hence relatively rare micro-inclusions are detected by EPMA, it is unlikely that analyses average multiple micro-inclusions. The inclusion volume is considerably smaller than the volume activated by the electron beam. Moreover, about 30% of the micro-inclusion is filled by low electron-density elements (in water and carbonate), thus totals in this study are, on average, only 3.9 ± 2.1 wt%. In translating counts to weight percentages, the program assumes that the difference to 100% consists of carbon. Later, totals are renormalized to 100% (on a carbon-, water- and carbonate-free basis). Izraeli et al. (2004) demonstrated that in spite of the low totals, the precision is good (about 10% relative) and the estimated accuracy is better than 15% for the major elements in the inclusions. Much of the uncertainty in the average composition of individual diamonds is due to real chemical variability between the various micro-inclusions."

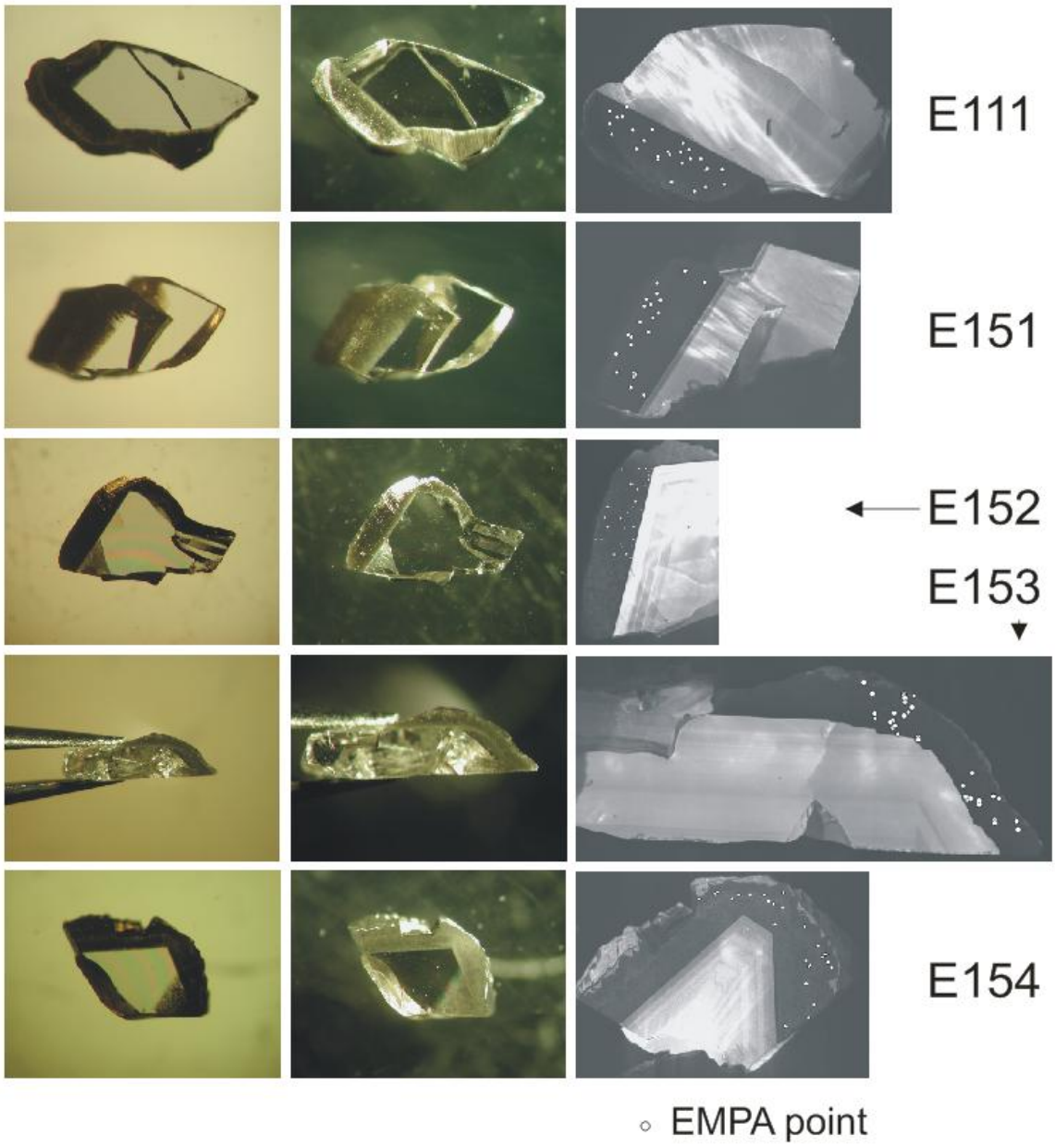

Figure 3.8. Fox diamonds from Ekati displaying the fibrous coat / 'gem' monocrystalline core relationships. From left; Relative fluid inclusion density photograph – Colour photograph – CL image. CL images indicate the number and position of EMP analyses on fluid inclusions within the fibrous coats.

3.5 Results

The important questions about this sample set are focussed around understanding the compositional contrasts and similarities between fibrous, low-purity monocrystalline and 'gem' monocrystalline diamonds and whether diamonds from different sources display distinct chemical signatures unique to their source. As such the results are presented separately for fibrous, low-purity monocrystalline and 'gem' monocrystalline diamonds within each section.

3.5.1 Major Elements

439 microinclusions were analyzed in the fibrous zones/coats exposed on 11 cracked or polished diamonds from Ekati. 346 inclusions are indicative of fluid with compositions varying between carbonatitic melt and a saline or silicic endmember (Figure 3.1 and Table A4. (Appendix)). Nine out of eleven diamond samples contain fluid microinclusions that plot within an array that extends between a saline end-member rich in K, Cl plus water and a high-Mg carbonatitic end-member. Two out of eleven diamonds fall along an array between a silicic endmember rich in Si, Al plus water and a low-Mg carbonatitic endmember, rich in Ca and carbonate. Diamonds on these different arrays display large ranges in Sr isotopic composition. Those on the saline array display $^{87}Sr/^{86}Sr$ = 0.7041±0.00001 to 0.7093±0.0001 (2σ; n=8) whilst those on the silicic array display $^{87}Sr/^{86}Sr$ = 0.707163±0.00005 to 0.712028±0.00004 (2σ; n=2). See Table A3, Appendix. There is no correlation between the average major element compositions of fluid microinclusions in these fibrous diamonds and their Sr isotope composition.

Seven of the 346 analyses display an average MgO > 17 wt. %. 339 fluid inclusions fall below 14 wt. % MgO and are therefore classified as a low-Mg suite (Klein-BenDavid et al., 2009). Major element compositions are summarized in Figure 3.9. Although there are some anomalously high values for BaO, Cr_2O_3, MgO and Al_2O_3, overall the average concentrations for these elements remain low. K_2O reaches up to 48.1 wt. % and is on average 23.5 wt. %, comparable to values found by Navon et al. (1988) and Weiss et al. (2009).

Solid inclusions were also found within the fibrous diamonds. A total of 93 solid inclusions were analyzed and compositions were matched to omphacites, olivines, clinopyroxenes, orthopyroxenes and chromites. The presence of these solid inclusions may be used to constrain diamond paragenetic relationships, information that is not often available in studies of fibrous diamonds due to their general scarcity of solid inclusions. For instance the omphacites in diamond E142 indicate its eclogitic paragenesis whereas olivines and occasional chromite, opx and olivines indicate a peridotitic origin. This is the only one clearly eclogitic example. There is no trace element or isotopic signature in this study that clearly defines eclogitic from peridotitic or otherwise. Most inclusions were ‘clean’ solid minerals but occasionally olivines were mixed with a fluid component. These inclusions were not used in defining the diamond HDFs compositional array.

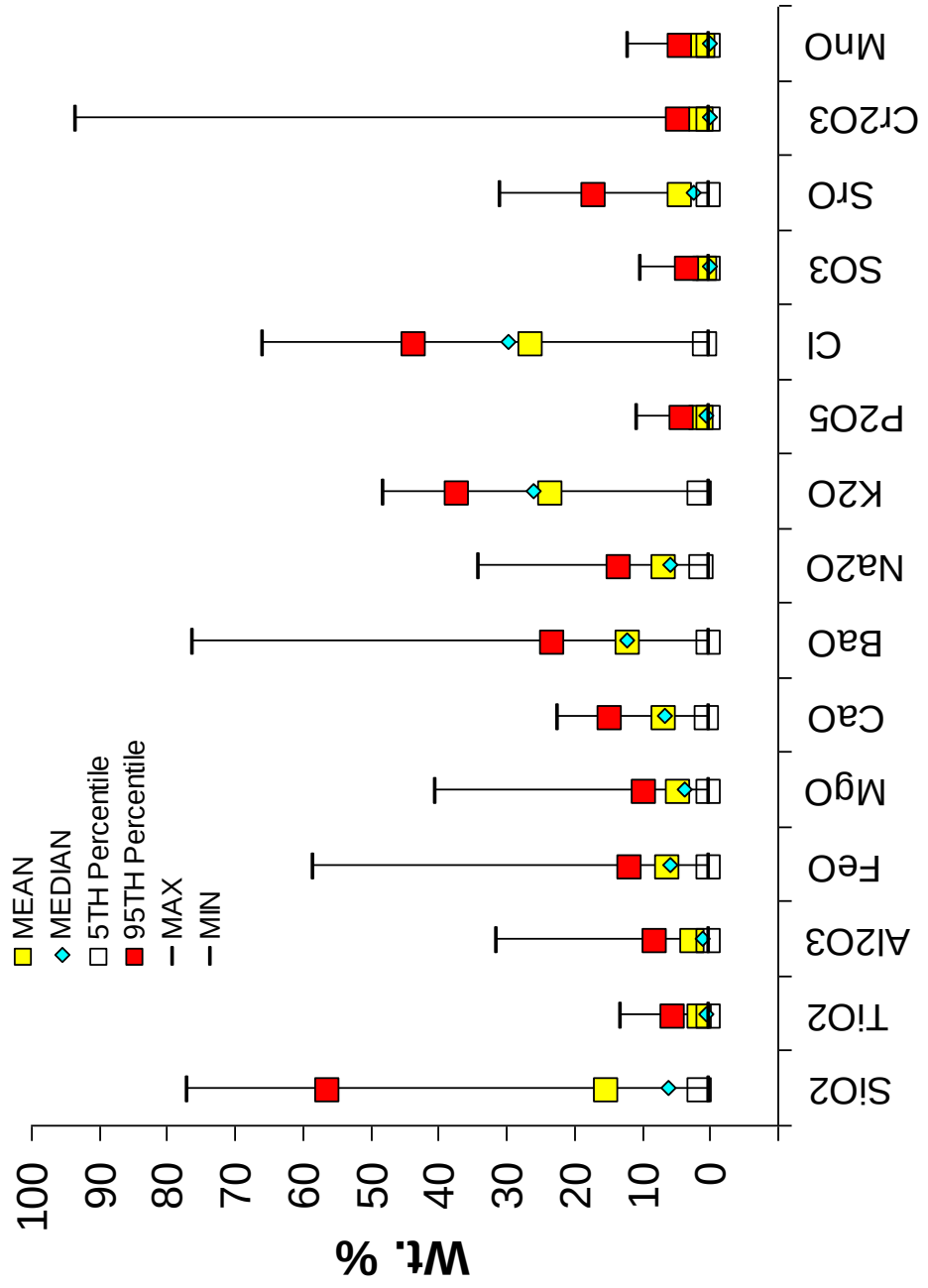

Figure 3.9. Wt.% major elements in fluid inclusions in fibrous diamonds from Ekati (n=11).

3.5.2 Trace elements

Sample concentration are given in Table A.1 (Appendix).

Sample concentration uncertainties are given in Table A.2 (Appendix).

3.5.2.1 Fibrous diamonds

HDFs fom19 fibrous/coated diamonds from Ekati and Diavik display primitive mantle-normalized trace element patterns that show varying levels of incompatible element enrichment but a great degree of similarity (Figure 3.10a+b). In general there is enrichment in LREEs over HREEs, enrichment in Ba, Pb, Sr and relative depletions in Nb, Ti, Zr and Hf. REE patterns are steep with Yb/Er = 441 to 502. There is a moderate depletion in Y relative to Dy and Er but this is not common to every sample.

The incompatible elements range in concentration from 0.1 ppm to 12 ppm with average concentrations of ~ 1 ppm. Ba is one of the more variable LILE elements, with concentrations varying between 19 to 199 ppm. Ti varies between 1.1 to 40 ppm and Sr between 1.2 ppm and 71 ppm but averaging around 4 ppm. HREE concentrations vary widely, from around 1 ppb to several 100 ppb.

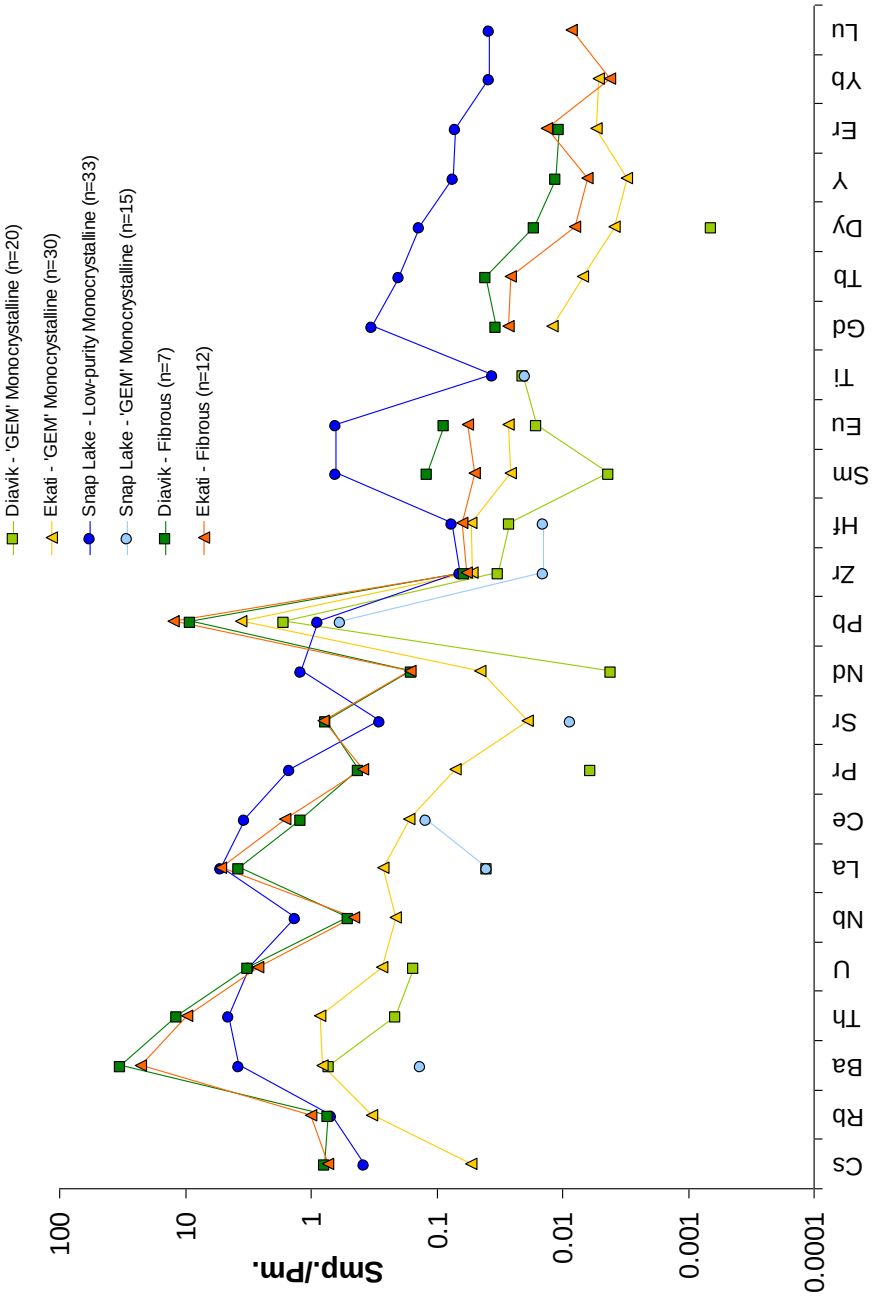

Figure 3.10a. Average trace element concentration in diamonds analyzed in this study. Sample concentrations (normalized to diamond weight loss during ablation) have been primitive mantle normalized (McDonough and Sun, 1995).

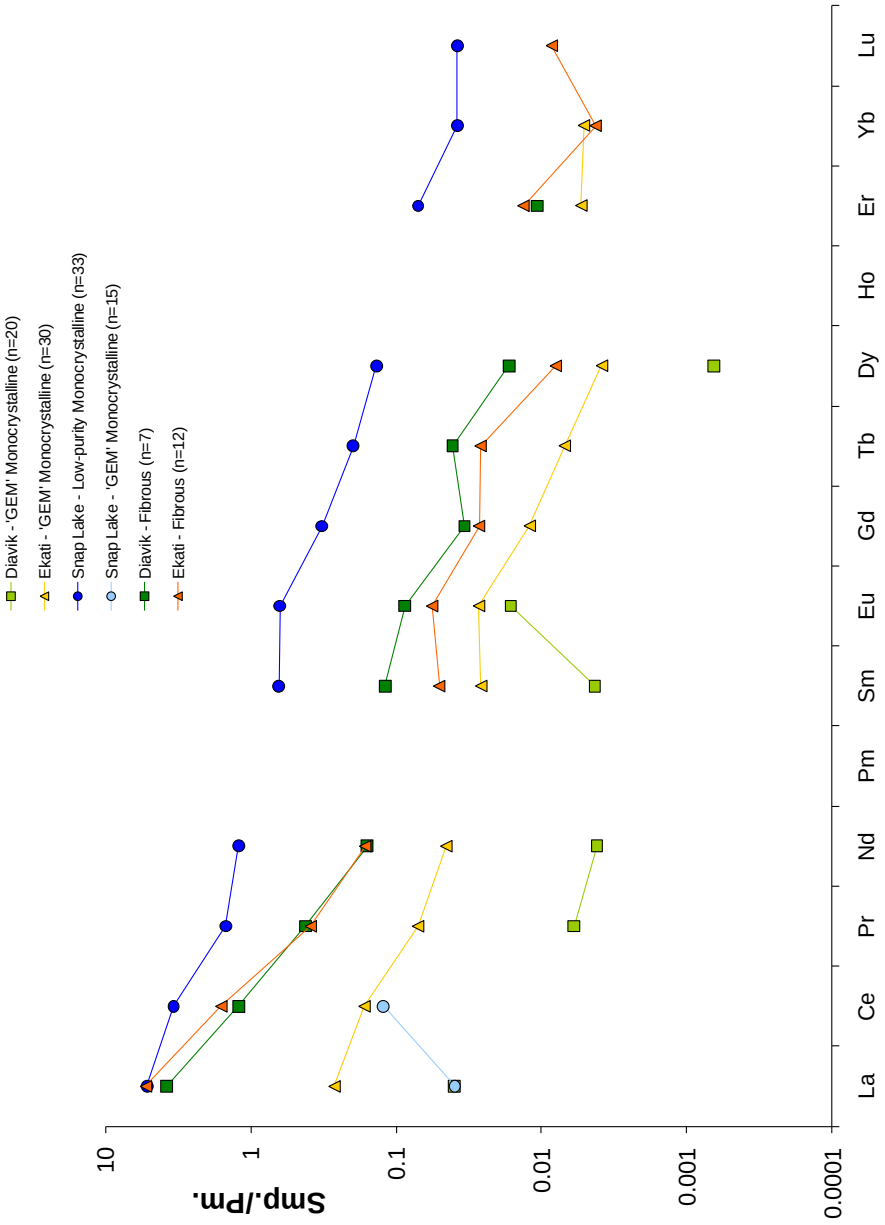

Figure 3.10b. Average REE concentration in diamonds analyzed in this study. Sample concentrations (normalized to diamond weight loss during ablation) have been primitive mantle normalized (McDonough and Sun, 1995).

Ekati and Diavik diamonds display broadly similar Primitive-Mantle normalized concentrations to fibrous diamonds from Snap Lake analyzed by Rege et al. (2010), and share –ve Ti, low Zr-Hf and –ve Y anomalies. Snap Lake diamonds display +ve Nb anomalies and extremely low Pb concentrations in contrast to the Lac de Gras samples studied here (Figure 3.11.). Compared to trace element patterns for fibrous coated diamonds from the Congo, the Ekati and Diavik fibrous diamonds share a common broad Rb-Ba-Th-U peak on a normalized plot yet are even more enriched in Ba. The Congo diamonds are much more enriched in the M- and HREEs yet share the –ve Ti, low Zr-Hf, +ve Pb and –ve Nb anomalies of the Diavik and Ekati fibrous samples. Trace element abundances vary significantly from stone to stone but inter-element ratios show relatively little variability. This is a feature common in other fibrous diamond suites from Africa and Siberia (Weiss et al., 2009; Rege et al., 2010 respectively).

Two diamonds from Ekati, E142 and E11014 (black cubes, Figure 3.5 10B+C) that contain fluid inclusions with silicic compositions display a –ve Sr anomaly (Figure 3.12), manifested as a higher Pr/Sr (2.4 to 3.1) than the saline diamonds (Pr/Sr = 0.6 to 1.2).

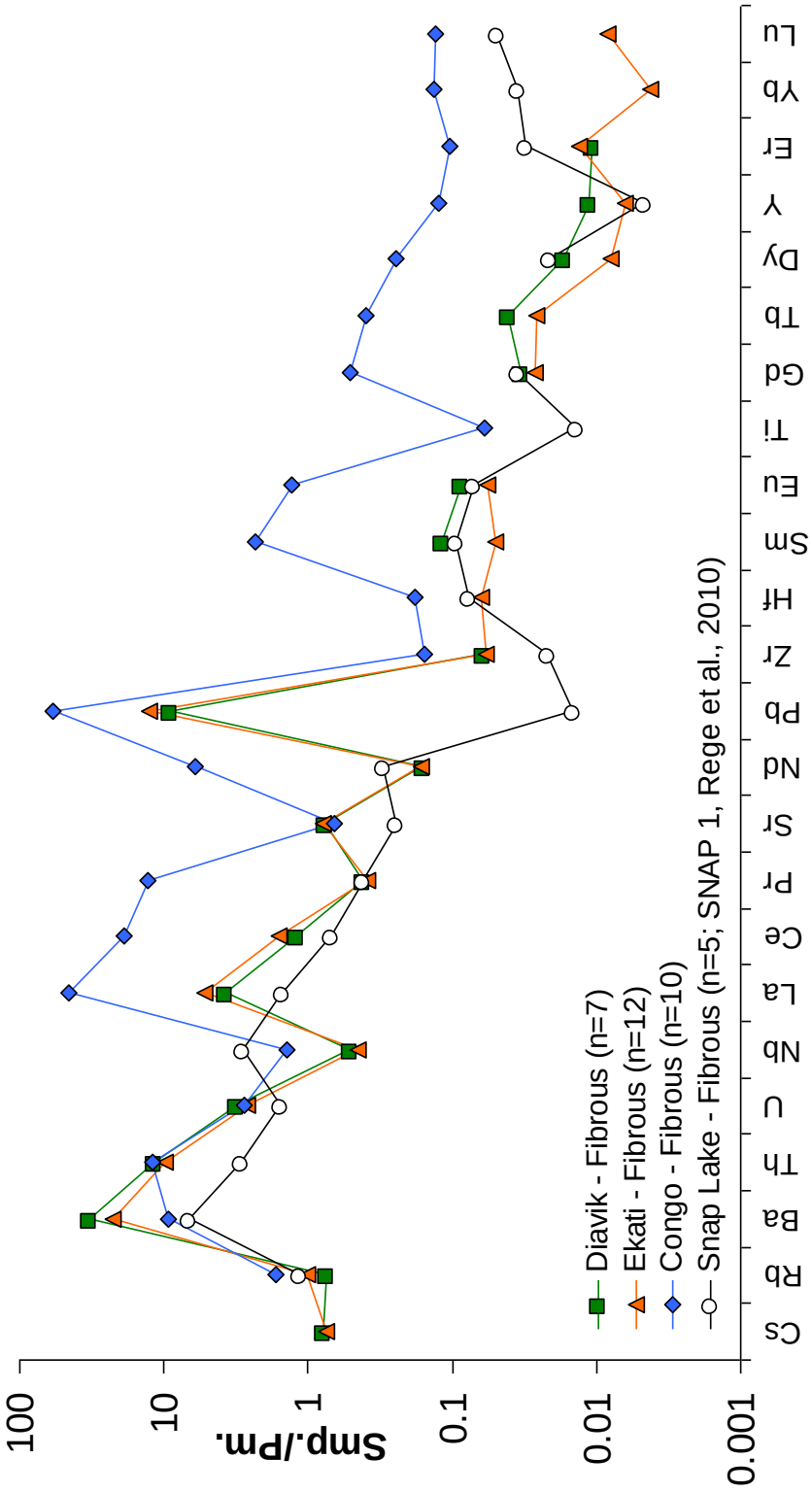

Figure 3.11. Average primitive mantle-normalized trace element concentrations for fibrous diamonds from Diavik and Ekati. Concentrations of fibrous diamonds from the Congo and Snap Lake have been added for reference.

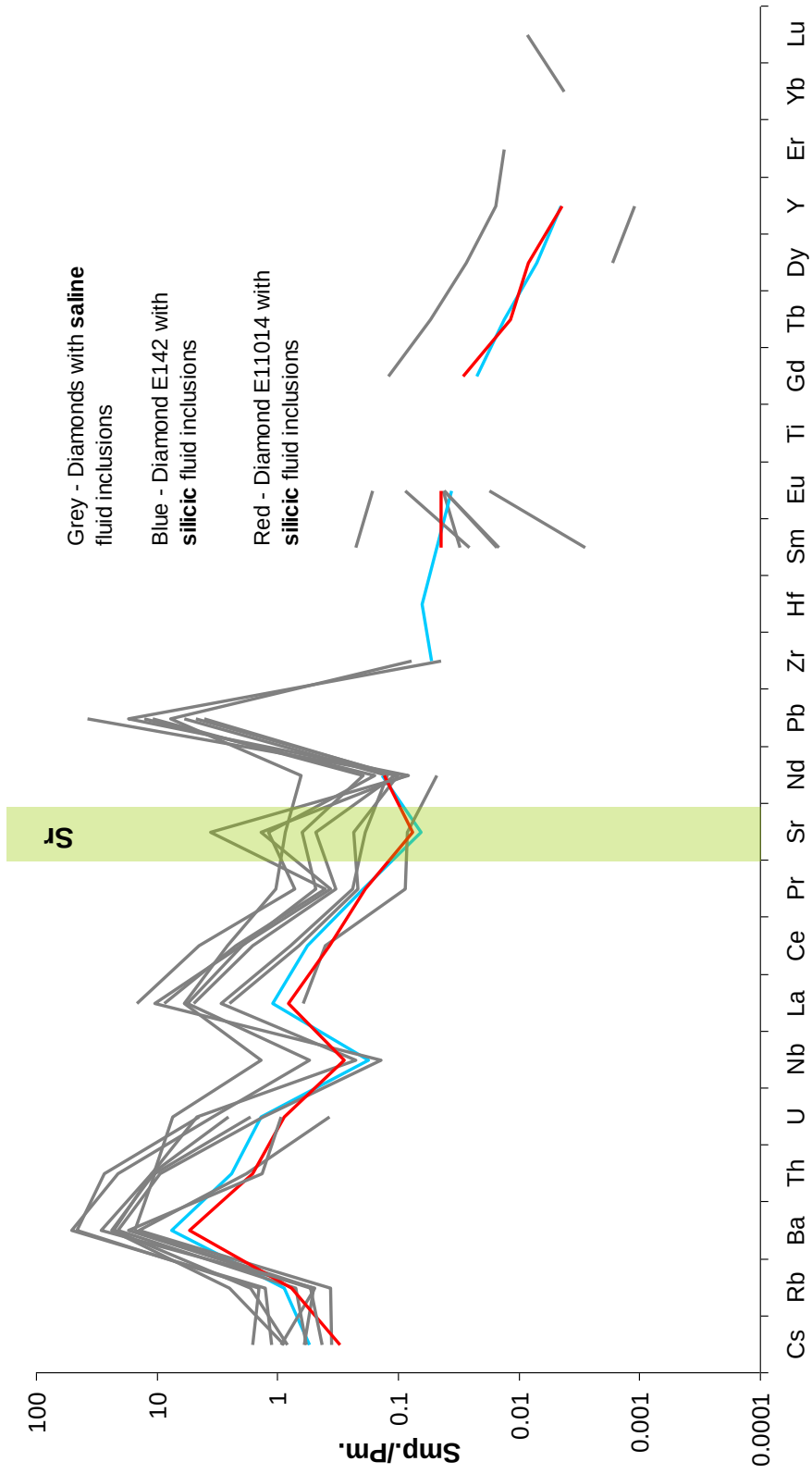

Figure 3.12. Primitive mantle-normalized trace element compositions of diamonds from the Ekati-Fox Kimberlite pipe that are either fibrous cubes or fibrous fragments of coated diamonds.

Overall elemental characteristics displayed in these Slave diamonds are similar to typical multi-element patterns from previous studies o worldwide sources (Figure 3.2; e.g. Schrauder et al., 1996; Resano et al., 2003; Rege et al., 2005; Tomlinson et al., 2005, 2009; Weiss et al., 2008; Zedgenizov et al., 2007; Klein-BenDavid et al., 2010 and references therein).

3.5.2.2 Low-purity monocrystalline diamonds

These samples provide a unique opportunity to study diamonds that are intermediate in "purity" between 'gem' monocrystalline diamonds and fibrous diamonds, but overall show closer morphological links to gem diamonds. Figure 3.13. displays their averaged composition and indicates that these diamonds are LILE and LREE elevated over HFSE. They have –ve Sr anomalies, lower Pb than fibrous diamonds and elevated Th-U. Ba/Th is < 1 which is a feature not seen in other Lac de Gras diamonds but is present in fibrous diamonds from the Congo (Figure 3.11.). These low-purity monocrystalline diamonds are enriched in REEs compared to Ekati and Diavik fibrous diamonds. They display elevated Nd and depletions in Y. All diamonds display a –ve Sr anomaly however diamonds B3 -3, -4 and -17 deviate from the group and bias the average due to their more pronounced –ve Sr. (Figure 3.14).

These low-purity diamonds are free of visible solid inclusions except for six diamonds with the SL prefix (Table A.1 (Appendix)). Diamond SL-50 and -57 show a +ve Ti in a group that is otherwise strongly –ve. These SL- samples differ only in

that they have been previously windowed for microscopy and have a particularly high density of solid microinclusions.

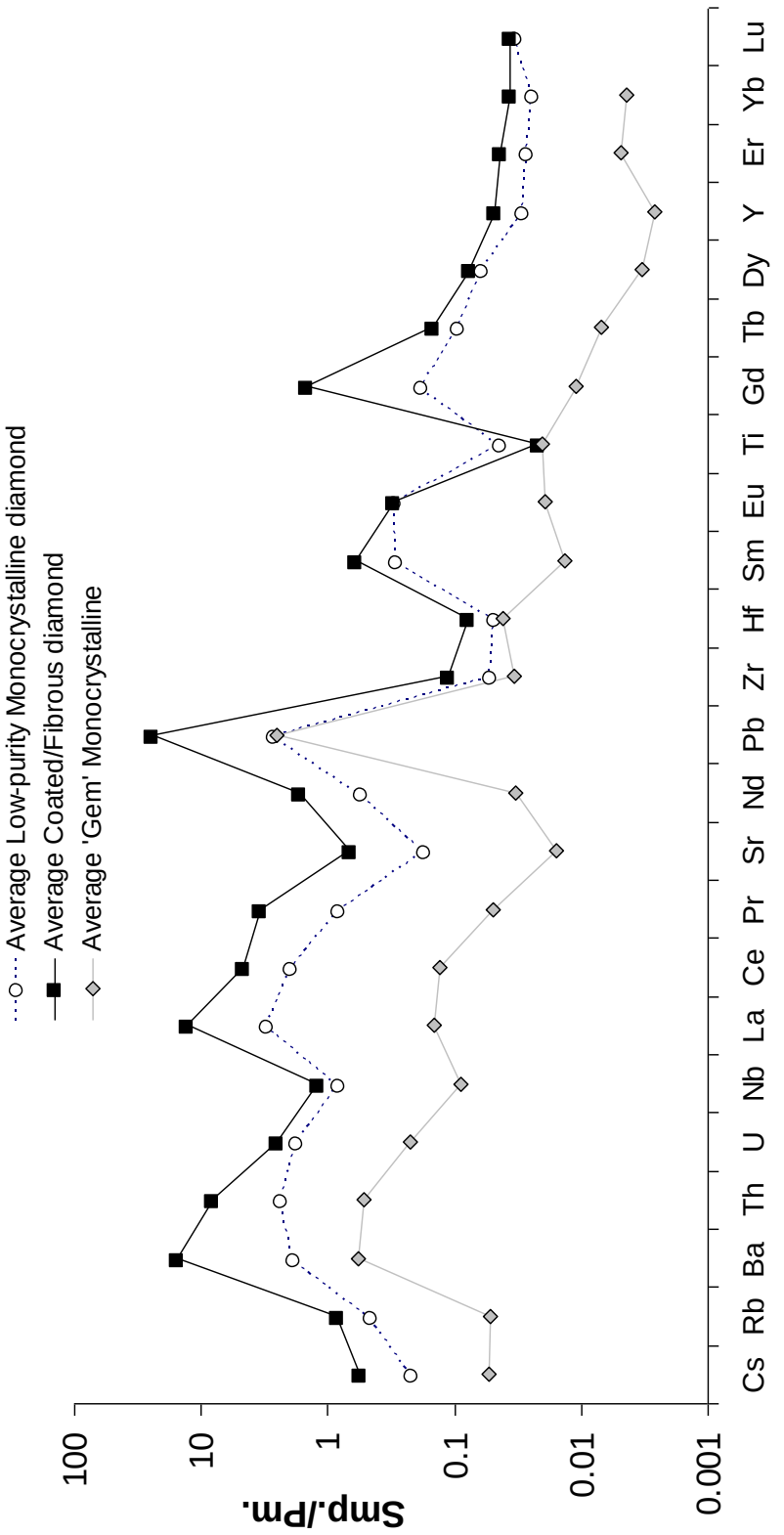

Figure 3.13. Average primitive mantle-normalized trace element concentrations from this study.

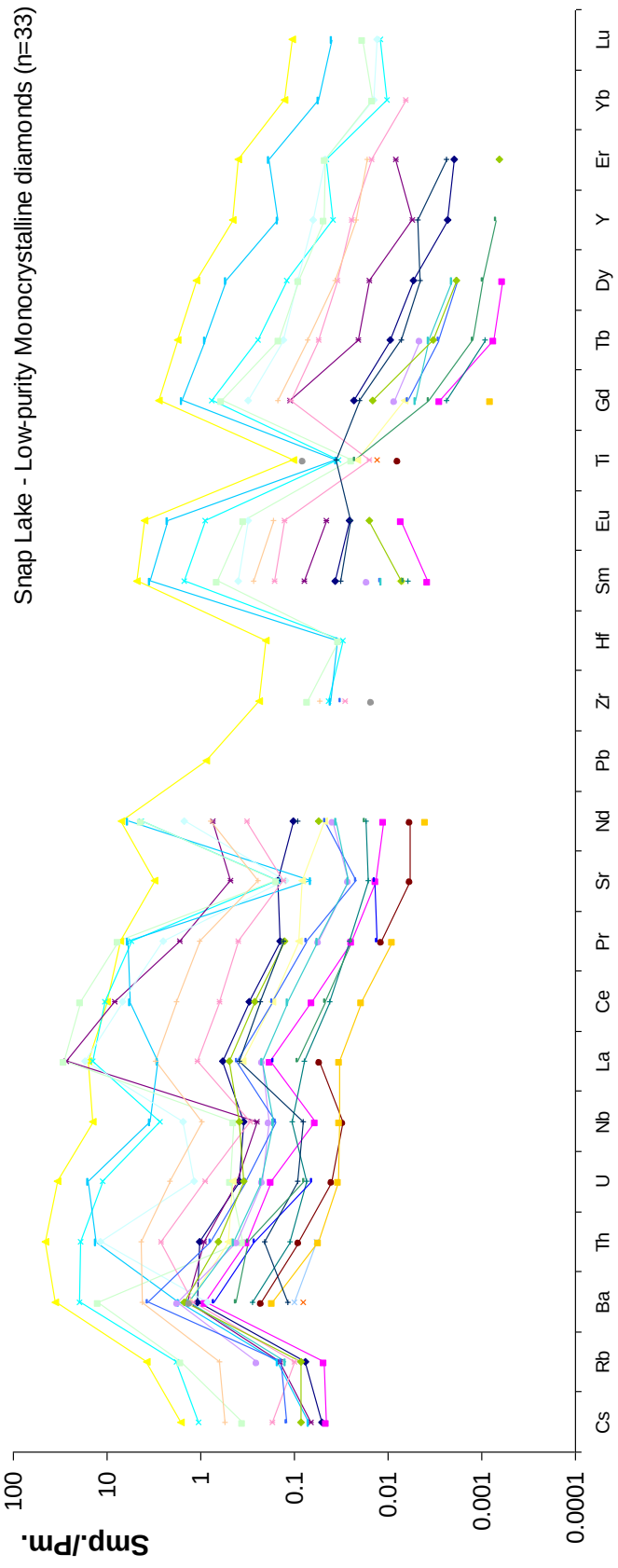

Figure 3.14. Primitive mantle normalized-trace element concentrations from Snap Lake low-purity monocrystalline diamonds from this study. Data points plotted are above the LOQ for this method.

3.5.2.3 High-purity 'gem' monocrystalline diamonds

62 diamonds with extremely low fluid-inclusion density were analyzed from Ekati, Diavik and Snap Lake. The 'gems' from Snap Lake and Diavik are particularly pure with many of the analyzed elements below LOQ and were thus rejected.

Figures 3.15, 3.16 and 3.17. demonstrate the very low levels of trace element concentration in natural 'gem' diamonds. Snap Lake diamonds display a consistent La/Ce < 1 in contrast to the La/Ce > 1 at Ekati and implied at Diavik (due to values below the method LOQ). Ekati 'gem' diamonds display variable systematics but show broad –ve Nb and incompatible enrichment, HFSE depletion and REE depletion The average features in these 'gem' monocrystalline diamonds (Figure 3.13) are consistent with some of the previously published data. For instance, Diavik 'gems' analyzed by Araujo et al. (2009b), Figure 3.2, display strongly –ve Nb and Y, on average –ve Sr, and an average Ba/Th > 1. A Cs/Rb >> 1 is a consistent feature of diamonds in the Araujo study that is in contrast to our reported average Cs/Rb ≤ 1. Rege et al. (2010) report concentrations for 'gem' diamonds from a variety of worldwide locations. The averaged values (Figure 3.2) of elemental ratios are consistent with this study (Figure 3.13) and display -ve Sr, -ve Nb and –ve Y. The main contrast in data is focused on the lack of a reported value for either Th or U (presumably because the concentrations of the elements are below even LOD) and the observation that is Rb/Ba >1 for 27/28 of the diamonds analyzed in that study. Such elemental characteristics are extremely rare, and have not been reported in any other publication except for a single diamond from the Araujo et al

(2009b) study (DVK106-1) and for only 1 diamond from this study (E111). Our LOQ for Rb is ~0.003_{pm} suggesting that the mainly absent Rb measurements represent very low Rb.

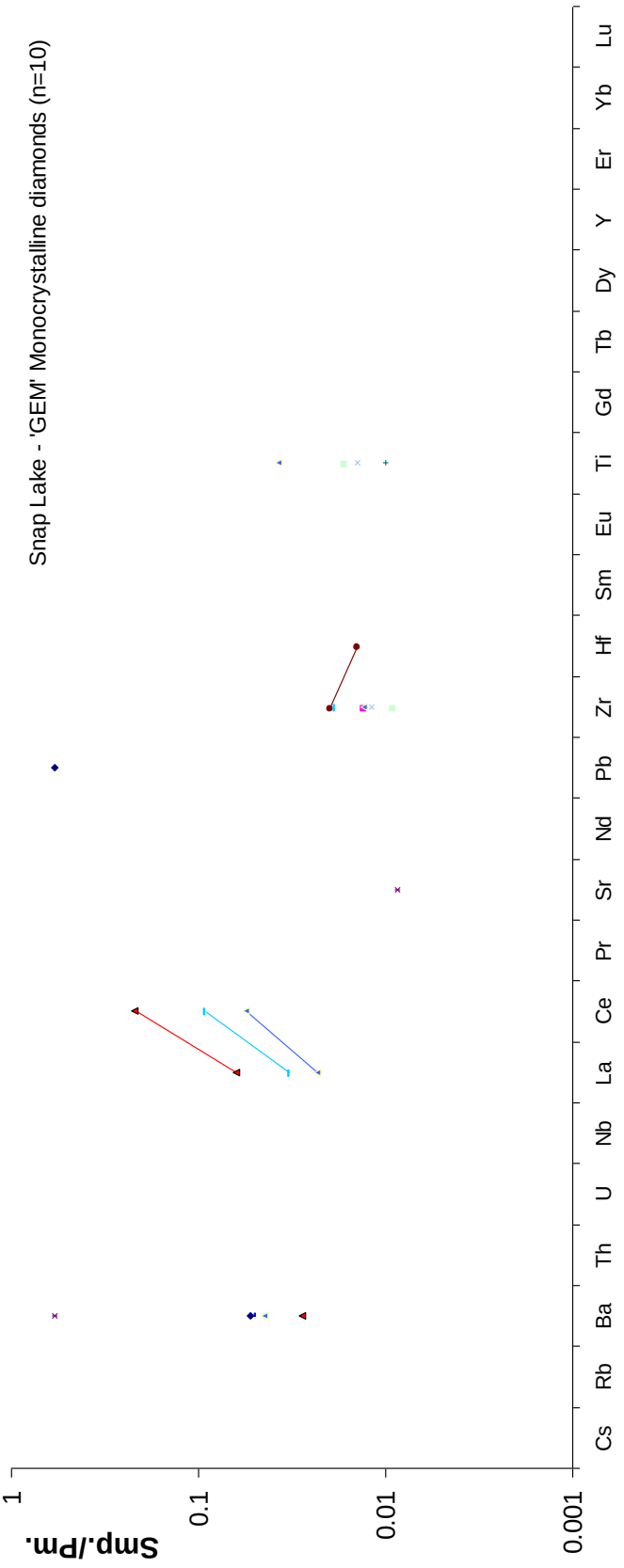

Figure 3.15. Primitive mantle-normalized trace element concentrations for 'gem' quality monocrystalline diamonds from Snap Lake. Data points plotted are above the LOQ for this method.

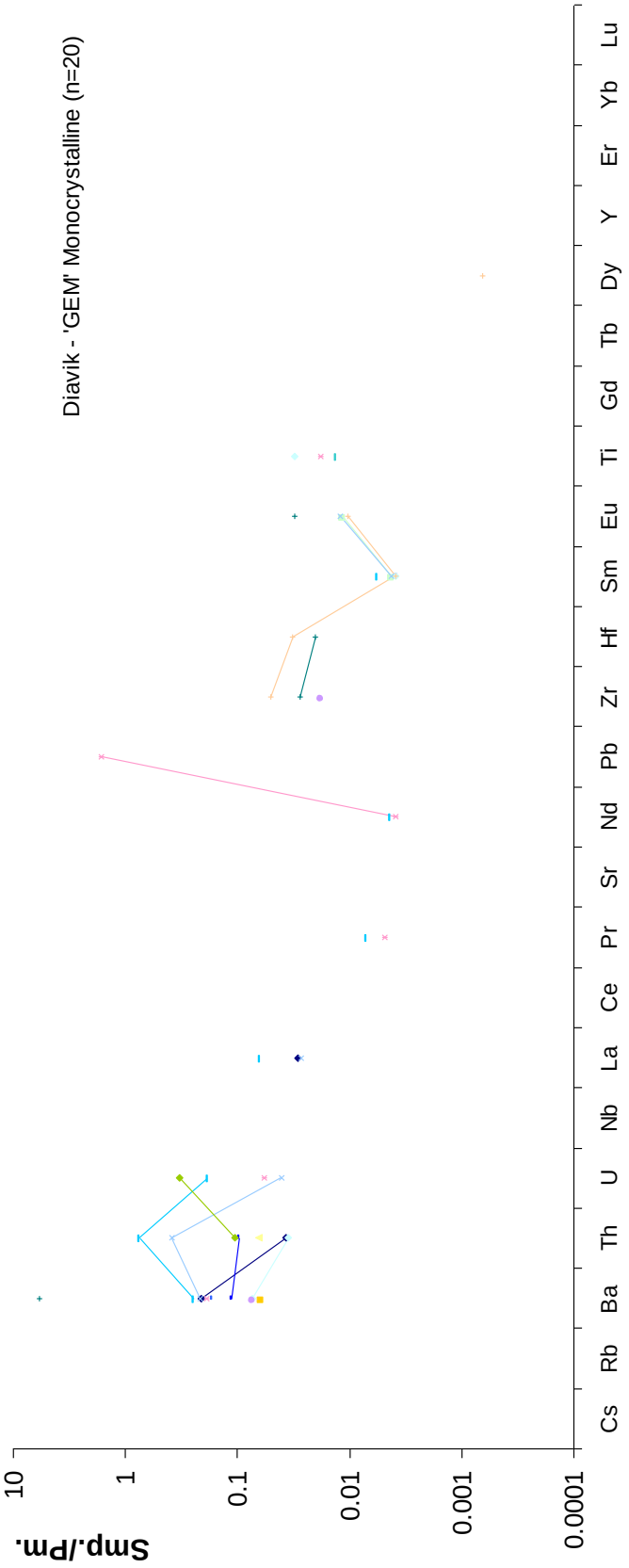

Figure 3.16. Primitive mantle-normalized trace element concentrations for 'gem' quality monocrystalline diamonds from Diavik. Data points plotted are above the LOQ for this method.

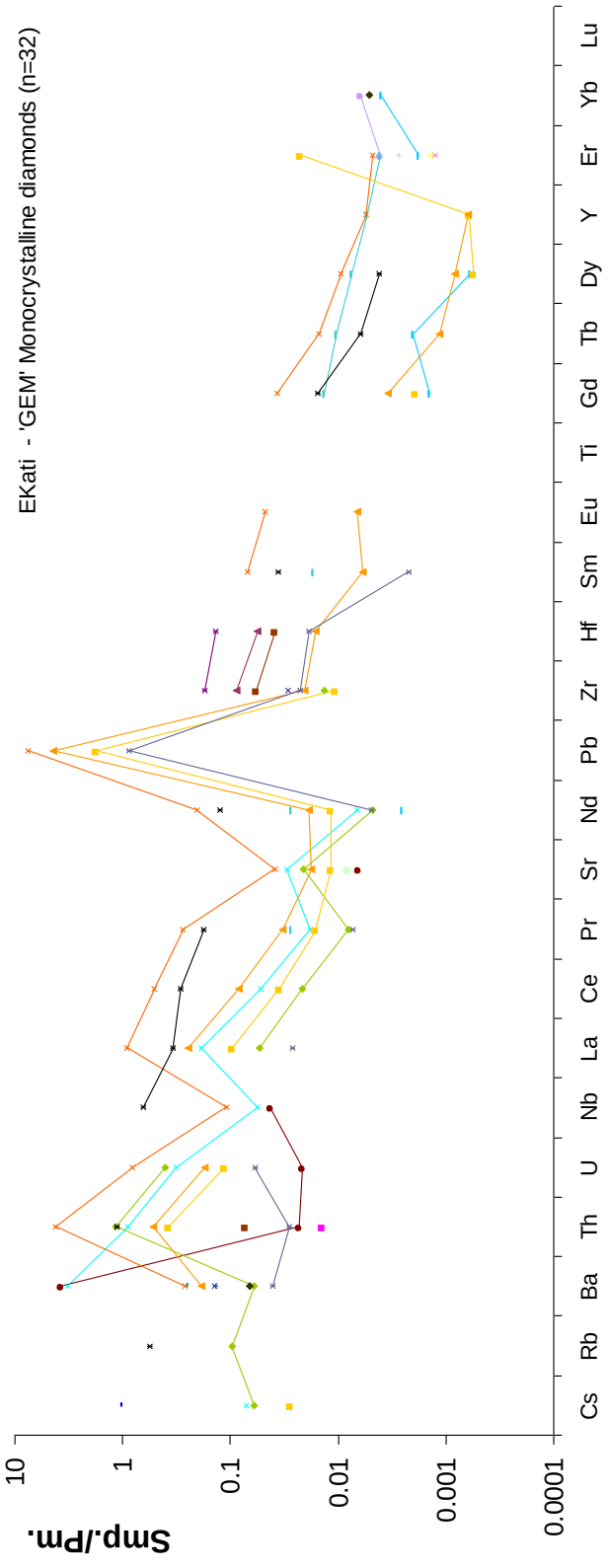

Figure 3.17. Primitive mantle-normalized trace element concentrations for 'gem' quality monocrystalline diamonds from Ekati. Data points plotted are above the LOQ for this method.

3.5.3 Radiogenic Sr isotopes

Measured Sr isotopic compositions vary greatly for the 33 measurements made in this study, with a range of $^{87}Sr/^{86}Sr$ from 0.70406±0.00003 to 0.71495±0.00037. Of these diamonds 16 are low-purity monocrystalline diamonds and only 1, diamond 153, is a 'gem' monocrystalline diamond. Initial Sr isotope compositions calculated at time of eruption (Kimberlite ages from Gurney et al., 2005) vary from $^{87}Sr/^{86}Sr(i)$ = 0.70136±0.001 to 0.71107±0.00021 (Figure 3.18 a+b, Table A.3 (Appendix)). The 'gem' diamond from Ekati has $^{87}Sr/^{86}Sr(i)$ = 0.705996±0.0002, in the middle of the wide range reported for other diamonds. Low-purity monocrystalline diamonds range from $^{87}Sr/^{86}Sr(i)$ = 0.70136±0.001 to 0.70864±0.00004. Fibrous diamonds range from $^{87}Sr/^{86}Sr(i)$ = 0.70386±0.00005 to 0.71107±0.00021. Due to low Rb (ppm) concentrations, *present-day* and *initial* ratios are similar except for two Snap Lake low-purity monocrystalline samples that have Rb/Sr ~ 0.33. These two diamonds have measured $^{87}Sr/^{86}Sr$ = 0.71495±0.00038 and 0.71185±0.00002 that reduce considerably to initial ratios of $^{87}Sr/^{86}Sr(i)$ = 0.70715±0.002 and 0.70510±0.001 respectively. Figures 3.18 c+d demonstrate that 2σ uncertainties are < 0.001 for the majority of diamonds analyzed. No isochronous relationships are observed in the data (Figure 3.19).

The small dataset is not clearly bimodal and displays a high kurtosis indicating that the data cannot be subdivided easily into more than one group in each plot (Figure 3.20).

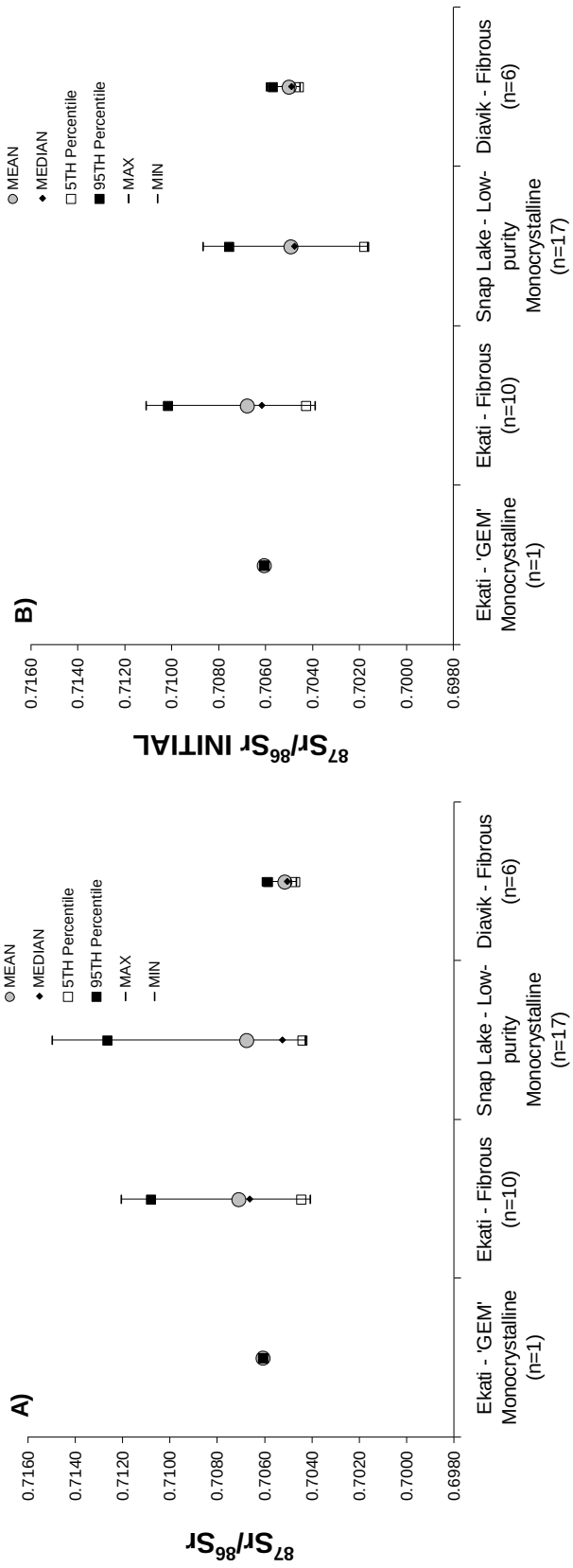

Figure 3.18 a+b. Box plots displaying $^{87}Sr/^{86}Sr$ and $^{87}Sr/^{86}Sr(i)$ characteristics of diamonds from the Slave craton measured for this study. Mean, Median, 5th and 95Th percentiles and maximum/minimum points shown for each location.

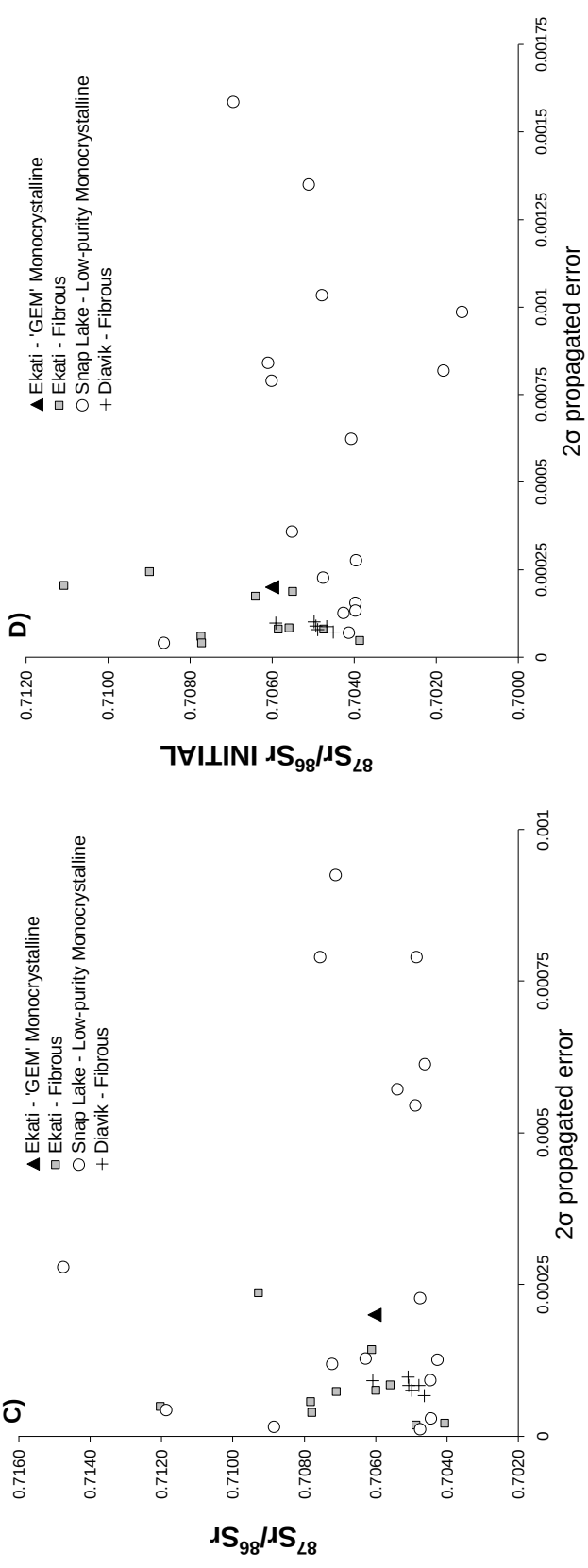

Figure 3.18 c+d. $^{87}Sr/^{86}Sr$ and $^{87}Sr/^{86}Sr(i)$ compositions of diamonds from the Slave craton measured for this study with associated error.

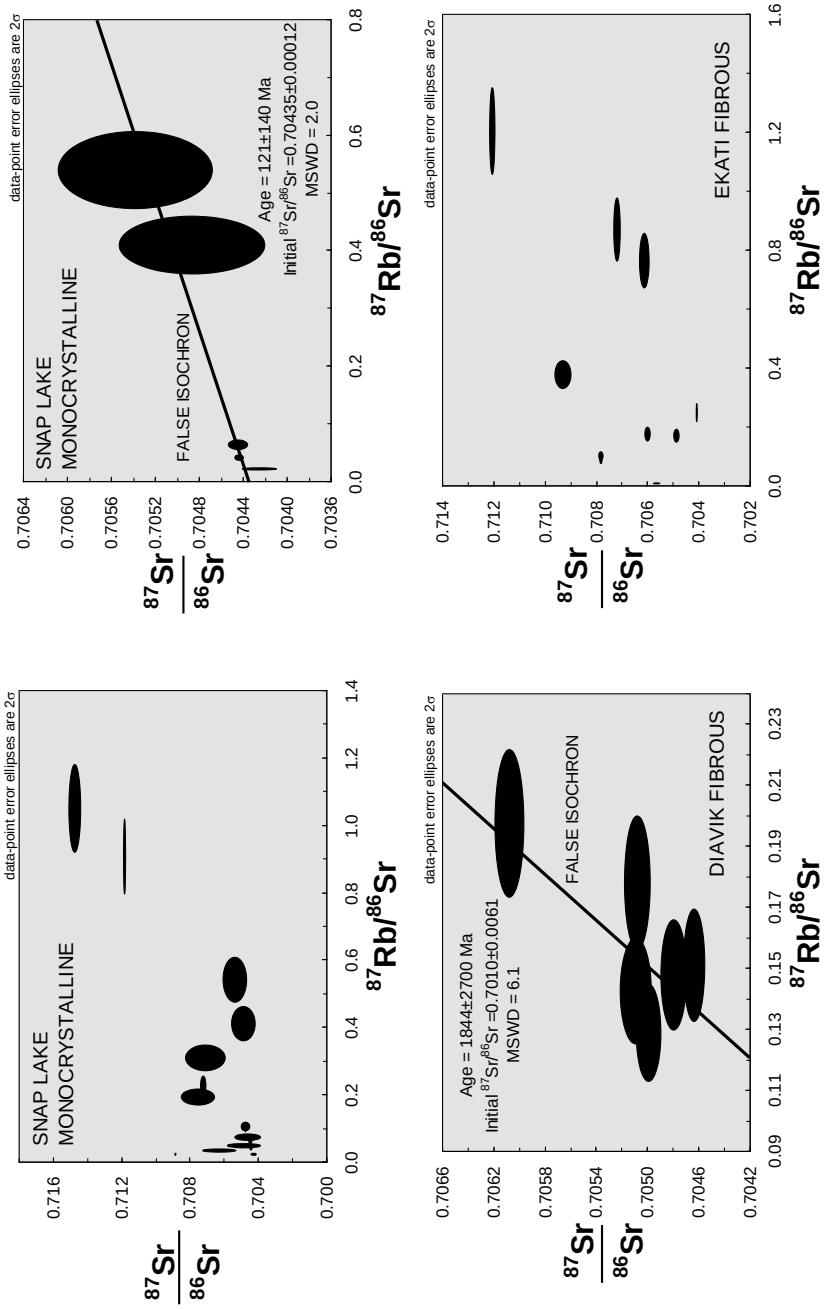

Figure 3.19. Isochron plots for Snap Lake monocrystalline diamonds, and Diavik and Ekati fibrous diamonds. Plots show that no true isochronous relationships exist in the data set. Ages produced by selecting samples with apparent correlation are false (Top right and bottom left for Snap Lake and Diavik respectively). $^{87}Rb/^{86}Sr$ error set at 10%.

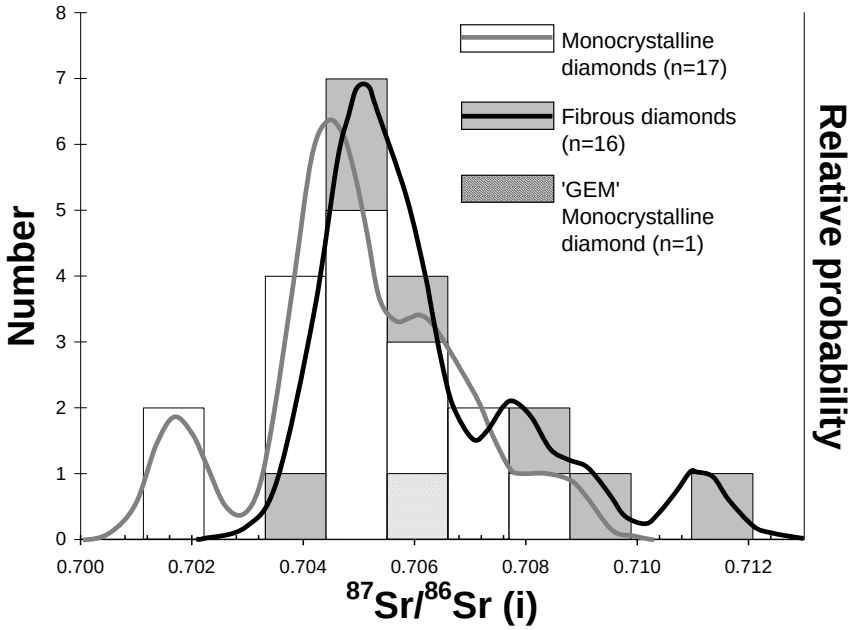

Figure 3.20. Probability density plots of $^{87}Sr/^{86}Sr(i)$ for coated/fibrous and monocrystalline diamonds from the Slave craton. The diamonds do not show bimodal distribution.

Ba/Th, La/Ce and Ti are not correlated with variation in $^{87}Sr/^{86}Sr(i)$, nor is any correlation observed between important mantle ratios such as Sr/Ba, Sr/Nd, and Rb/U vs $^{87}Sr/^{86}Sr$ despite the very broad range of data. This suggests a complex fluid source which may involve mixing of various components with different trace element and isotopic signatures.

3.5.4 Data Summary

Generally, fibrous diamonds contain considerably higher absolute trace element concentrations than 'gem' monocrystalline diamonds due to their higher fluid-inclusion density. In fact, the relative trace element concentrations can, to a first

order, be predicted from their colour, which is a function of fluid inclusion density. Diamonds containing silicic fluid inclusions display Pr/Sr > 1 in contrast to diamonds containing saline fluid inclusions which display Pr/Sr < 1. Diamond 142 contained silicic inclusions as well as some omphacites however there is no clear trace element signature that defines eclogitic diamonds from diamonds from other parageneses.

Using only visual examination of multi-element systematics, diamonds from Snap Lake can be tentatively distinguished from those derived from Diavik and Ekati. Snap Lake 'gem' monocrystalline diamonds uniquely display La/Ce < 1. Snap Lake low-purity monocrystalline diamonds display Nd/Pb > 1. Nd/Pb > 1 is also seen in fibrous diamonds from Snap Lake (Rege et al., 2010). Diavik and Ekati cannot be easily distinguished based on a visual (non statistical) evaluation. A more statistical evaluation of the data is undertaken in the following chapter and will not be dealt with here. Instead, we focus on the petrogenetic information that can be derived from the various geochemical signatures.

Despite the apparent location-specific differences in diamond geochemistry, there is no chemical parameter in our data, based on trace elements and $^{87}Sr/^{86}Sr$ that can unequivocally differentiate between fibrous or monocrystalline diamonds. Where quantitative data has been obtained on monocrystalline diamonds, their average compositions are very similar to fibrous diamonds. Furthermore, statistical treatment of the data (see Chapter 4) cannot differentiate between the two types of

diamonds. As such, the geochemistry of fibrous and monocrystalline diamonds will be discussed together in an attempt to understand the source of their common chemical signature.

3.6 Constraints on diamond source fluids

This section is divided into 4 distinct parts;

- 3.6A Composition of the analyzed diamond volume – What are we measuring?
- 3.6B Processes accounting for the trace element characteristics
- 3.6C Isotope variability and source components of diamond–forming fluids
- 3.6D A model for diamond genesis

3.6A Composition of the analyzed diamond volume

In any given diamond there are often visible solid microinclusions. There will also be fluid inclusions, substitutional lattice impurities and other melt inclusions. As the analytical technique applied here is bulk sampling the diamond volume, great care is taken to locate the ablation site in an area of the diamond which appears 'clean', i.e. where no visible solid inclusions will be consumed in the ablation process.

The overall similarity between signatures measured in fluid-rich fibrous diamonds from worldwide localities is mimicked by monocrystalline diamond signatures in this study (Figure 3.2 and 3.13.). If this phenomenon was to be explained by the presence of solid microinclusions then the assemblage and proportion of each component to one another would need to be non-random and consistent in diamonds worldwide - in both fibrous and monocrystalline diamonds. This is improbable.

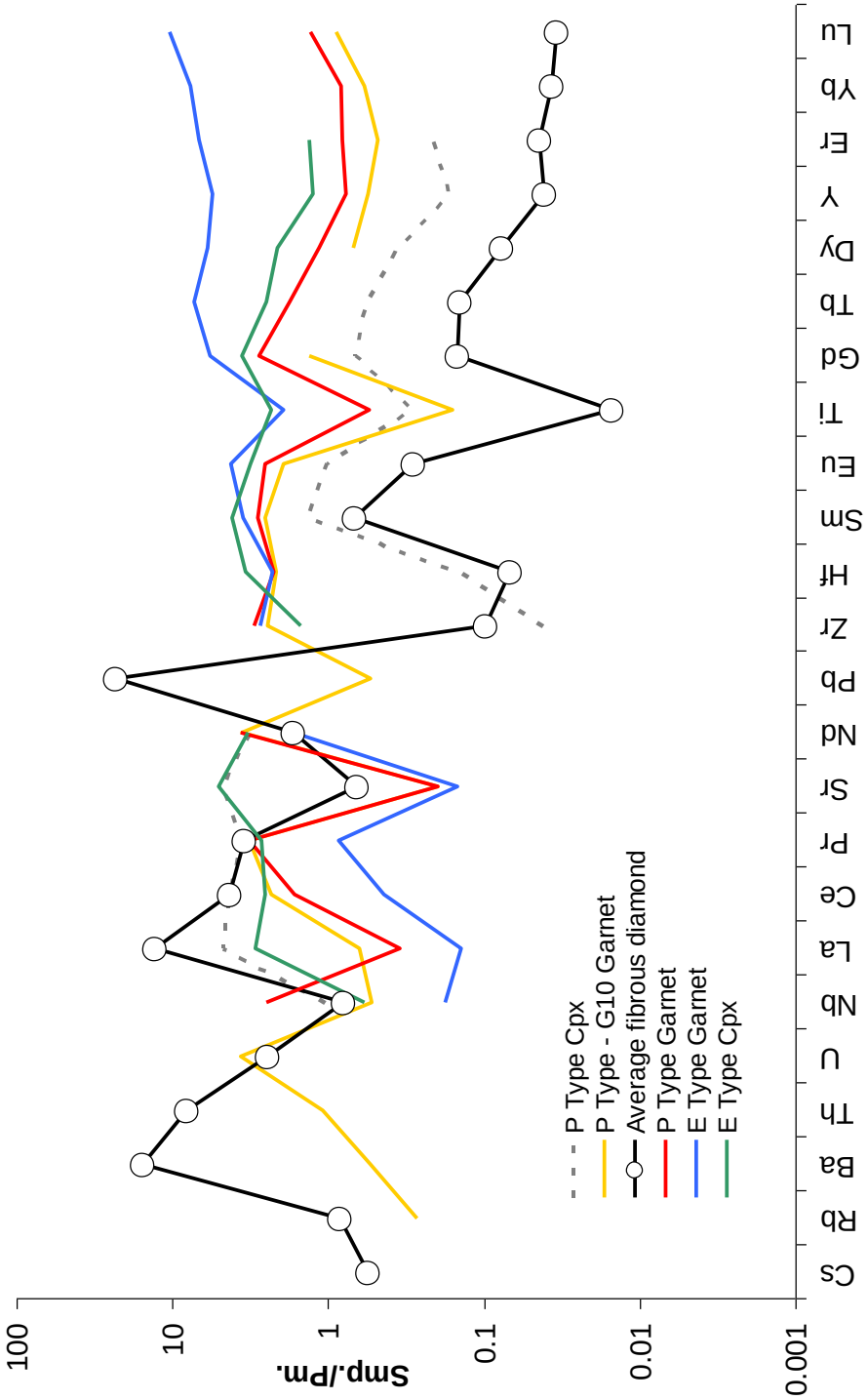

Figure 3.21. Primitive mantle-normalized trace element concentrations in garnet and clinopyroxene inclusions in diamond and average fibrous diamond HDF from this study. G10 Garnet – Shimizu et al. (1995); P+E Garnet and CPX – Stachel et al. (2004).

The data from this study also display a primitive mantle-normalized trace element signature that does not match typical solid inclusions in diamonds. There is some similarity which is to be expected if these diamond inclusions are syngenetic with diamond growth and are in equilibrium with the fluids that they grew from. Figure 3.21 displays trace element patterns for clinopyroxene and garnet inclusions in diamonds (Stachel et al., 2004). Garnets display the same –ve Sr and Ti anomalies displayed by the diamond HDF signature but are depleted in the LILEs and LREEs compared to the HDF. A combination of Cpx and Grt may create a component more enriched in the LILEs but cannot create a component as enriched in LILE, depleted in HFSEs and HREEs as the HDF signature. The extreme La_n/Sr_n ratios displayed in fibrous, low-purity monocrystalline and 'gem' monocrystalline diamonds cannot be achieved by any mix of these solid inclusions.

Figure 3.22 demonstrates the effect of a metasomatic agent on garnet, resulting in a sinusoidal REE pattern, such as those commonly observed in low-Ca, Cr-rich (G10) garnets. While none of the diamond HDFs display the patterns of this type of garnets, the average HDF composition has a fractionated REE pattern that is similar to postulated fluids in equilibrium with these metasomatic garnets (Figure 3.23a+b; partition coefficients for peridotitic garnet / carbonatitic melt from Keshav et al., 2005; typical P-Type G10 garnet from Ekati from Klein-BenDavid and Pearson 2009). The order of magnitude higher in concentration of the calculated fluid in equilibrium with G10 garnets compared with the HDF can be explained as a function of dilution of the HDF abundances by the diamond matrix.

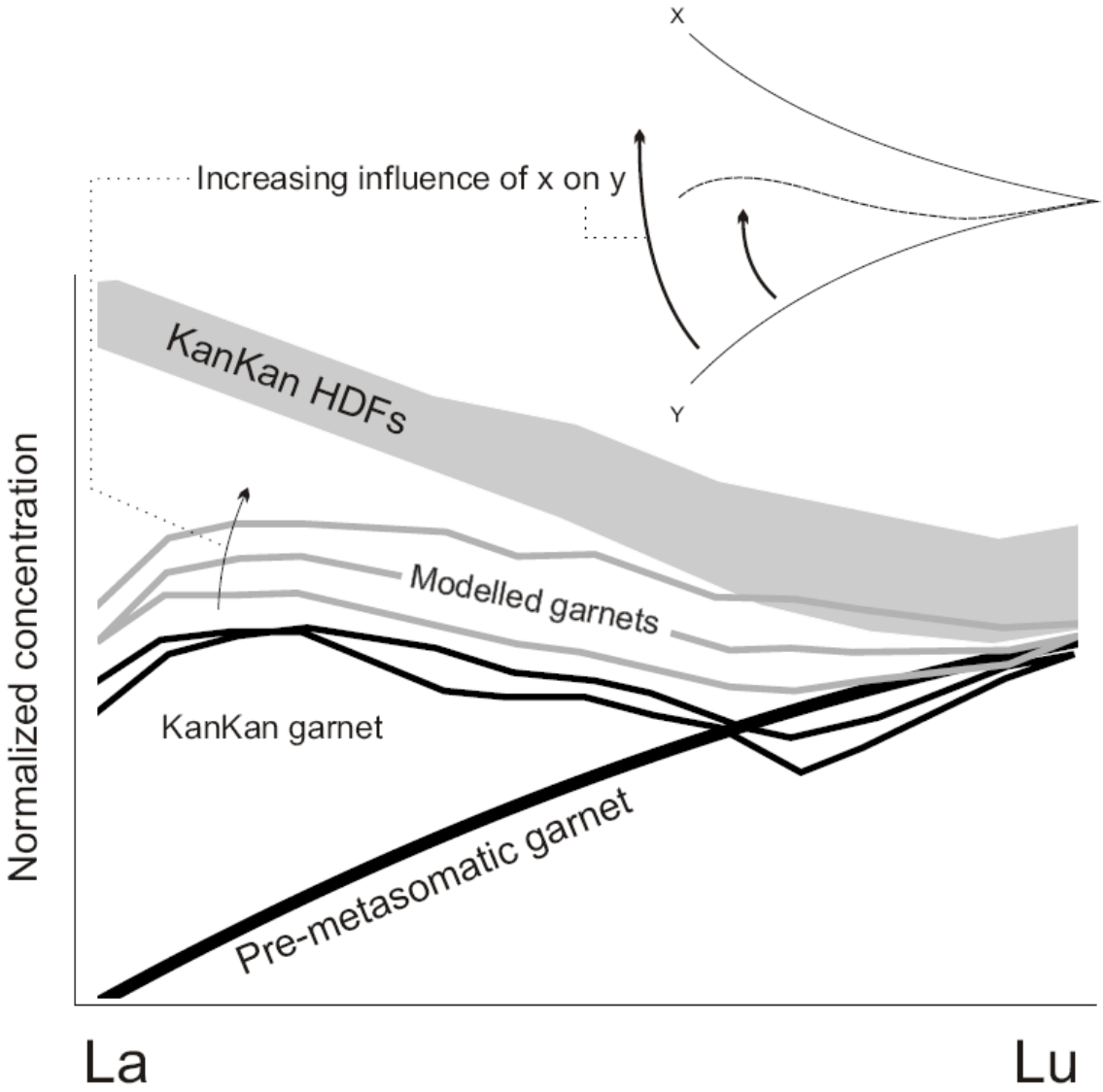

Figure 3.22. Diagram showing the influence of metasomatic fluids such as HDFs on pre-existing garnets. Data and diagram modified from Weiss et al. (2009). Patterns of peridotitic Kankan garnet diamond inclusions (Stachel et al., 2000) can be mimicked by modelling HDF interaction (compositions from Weiss et al., 2009) with pre-metasomatic garnet (Stachel et al., 2004). Garnets develop a sinusoidal REE pattern not observed in the HDFs.

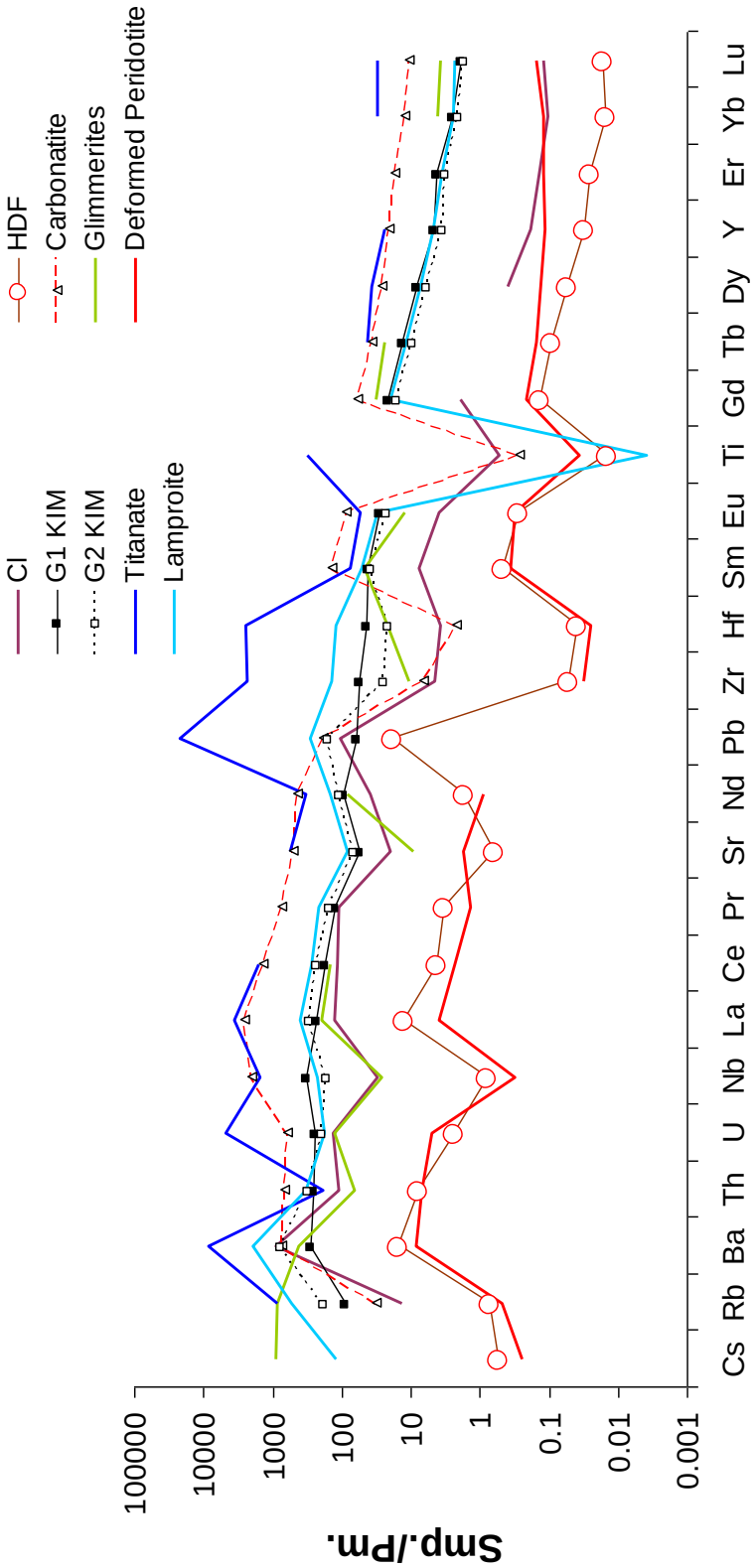

Figure 3.23a. Trace element modelling. Concentration are normalized to primitive mantle (McDonough and Sun, 1995). Fluid in equilibrium with G10 garnet (Cl) is modelled to estimate a fluid in equilibrium with the diamond forming medium. The HDF composition is the fibrous composition in Slave Craton diamonds from this study. Titanate (Jones et al., 1989), Group I and II kimberlites (Becker et al., 2006), Glimmerites (Becker et al., 1999; Klein-BenDavid and Pearson, 2009), Deformed Peridotite (Bedini et al., 1997) and Carbonatite (Bizimis et al., 2003) are included for reference in the discussion. Garnet partition coefficients from Keshav et al., 2005.

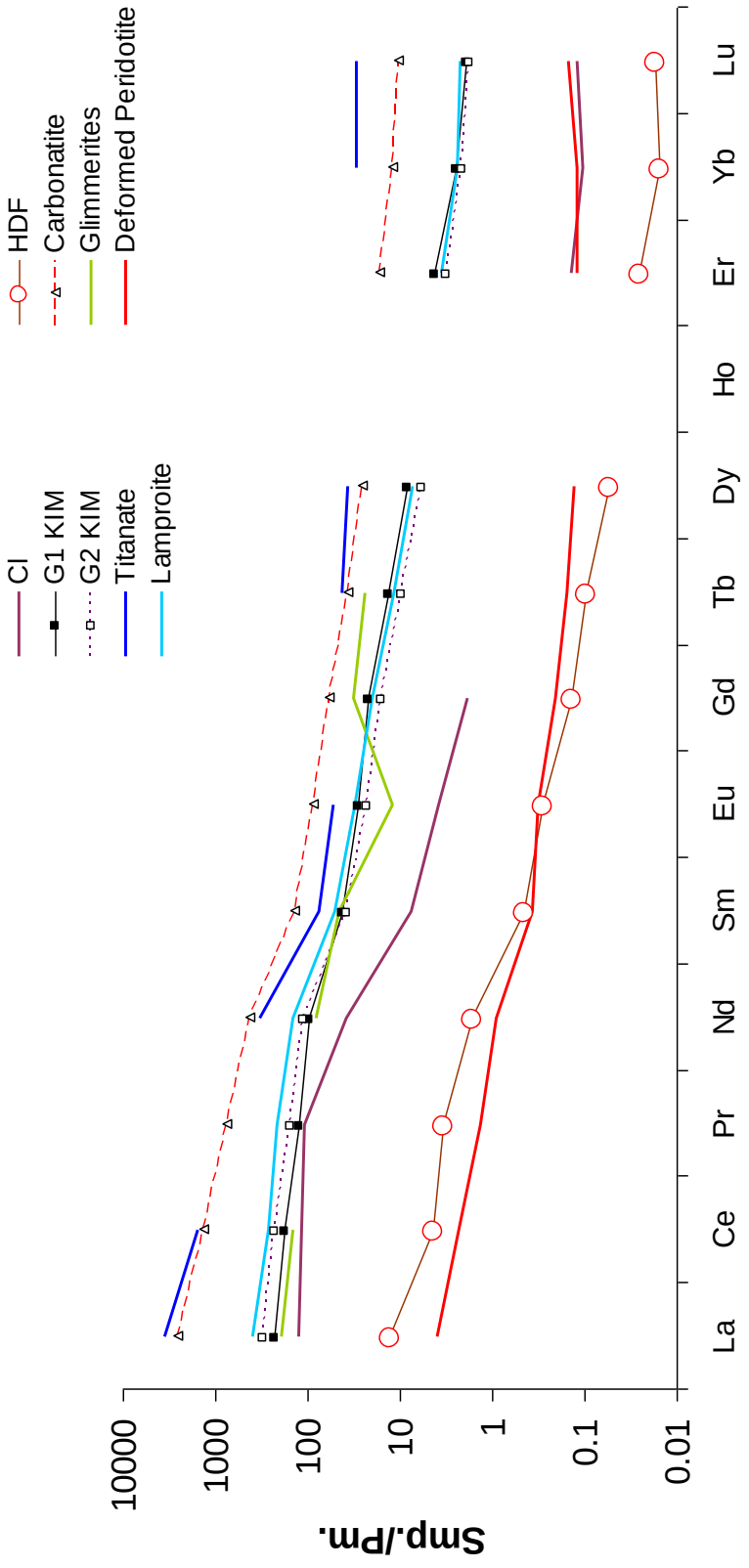

Figure 3.23b. REE modelling. Concentration are normalized to primitive mantle (McDonough and Sun, 1995). Fluid in equilibrium with G10 garnet (Cl) is modelled to estimate a fluid in equilibrium with the diamond forming medium. The HDF composition is the fibrous composition in Slave craton diamonds from this study. Titanate (Jones et al., 1989), Group I and II kimberlites (Becker et al., 2006), Glimmerites (Becker et al., 1999; Klein-BenDavid and Pearson, 2009), Deformed Peridotite (Bedini et al., 1997) and Carbonatite (Bizimis et al., 2003) are included for reference in the discussion. Garnet partition coefficients from Keshav et al., 2005.

We conclude from these considerations that we are, in these circumstances, measuring the signature of a fluid that is broadly in equilibrium with some types of syngenetic diamond inclusions and that this is the fluid from which the diamond precipitates.

3.6B Understanding the processes involved in the diamond forming environment and their relationship to the observed HDF compositions

3.6B.1 Monocrystalline vs. Fibrous/Coated diamond growth environments

The broad trace element and Sr isotope similarities observed in this study between fibrous and monocrystalline diamonds suggests that their associated HDFs may share a chemical link. In addition, Tomlinson et al. (2009) have found that the trace element signatures within silicate inclusions trapped within fibrous diamonds and those trapped within octahedral diamonds are very similar and argue that these inclusions have equilibrated with fluid of similar composition. This is in contrast to the major chemical differences that classically categorize fibrous from monocrystalline diamonds (Table 3.1).

	FIBROUS	**MONCRYSTALLINE**
GENESIS AGE	<350 Ma (Shirey et al., 2002)	1-3 Ga (Shirey et al., 2002)
NITROGEN CONTENT	~ or > 1000 ppm (Cartigny et al., 2003)	< 1000 ppm (Deines et al., 1993)
$\delta^{13}C$	–8.1 to –4.9‰ (Cartigny, 2005)	P-type = –26.4 to +0.2‰ E-type = –38.5 to +2.7‰ (Cartigny, 2005)

Table 3.1. Chemical contrasts between diamonds of fibrous and monocrystalline growth based on age, N and C systematics.

Five diamonds analyzed from the Fox pipe in the Ekati Property suite are fragments consisting of monocrystalline cores that have octahedral fibrous diamond overgrowths (Figure 3.24).

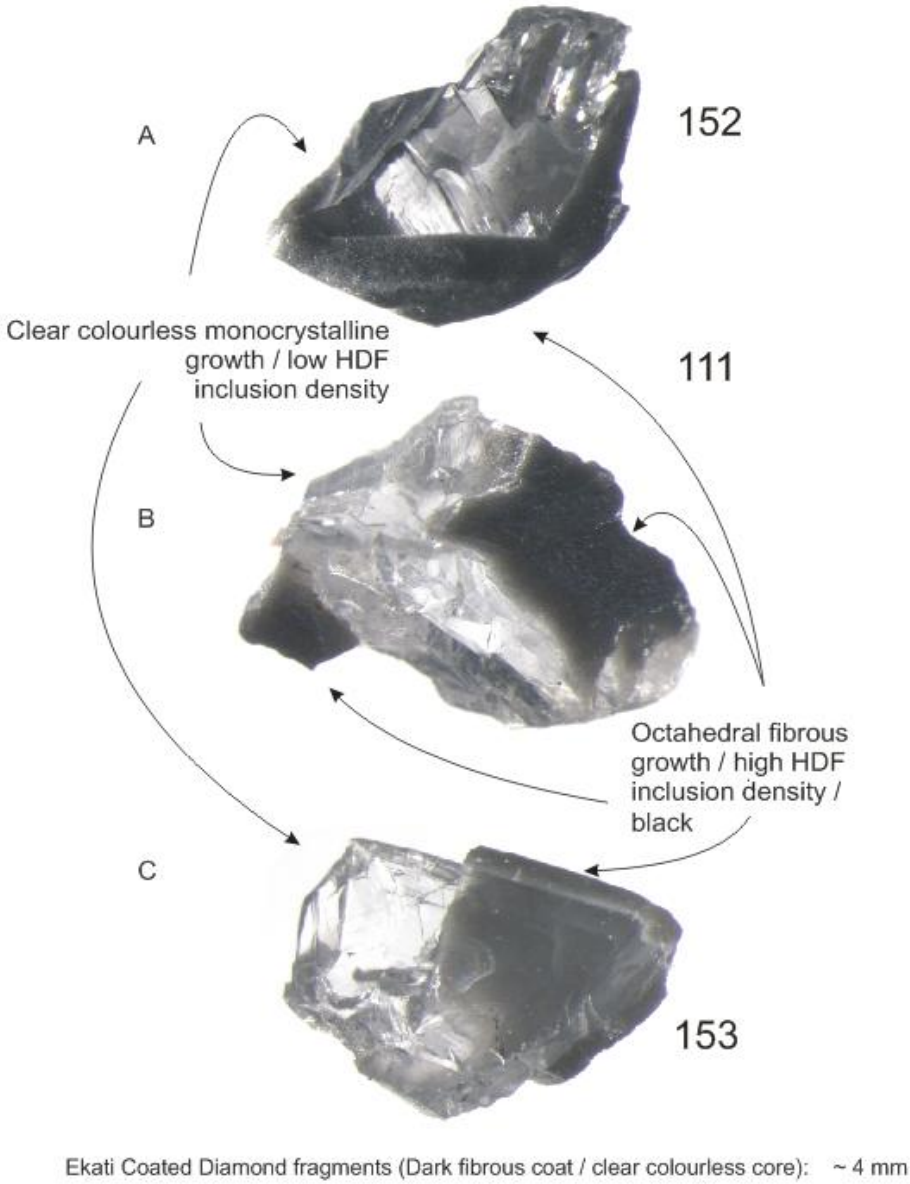

Figure 3.24. Photograph of diamond 152, 111 and 153 from the Fox kimberlite on the Ekati property. A clear monocrystalline core can be seen with an overcoat of fibrous diamond. A sharp boundary between the two forms indicates either a significant time gap or a very immediate change in growth conditions.

The Fox coated diamonds provide an ideal example to investigate the relationship between the two growth forms. Due to analytical difficulties, it has not been previously possible to try to evaluate whether, from a trace element perspective, the composition of fluid in fibrous diamonds could have evolved from that parental to an included monocrystalline diamond core. A specific issue is to determine whether the similarities and contrasts between core and coat could be accounted for by fluid evolution and un-mixing in a closed system. In systems involving fluid – solid equilibria, crystal fractionation and liquid-liquid mixing can create inter element fractionation. The effects of such processes on the evolution of diamond-forming fluids can be modelled most simply by assuming a closed system for diamond growth (Table 3.2). A summary of the similarities and differences between coats and cores for the 5 samples under consideration is presented in Table 3.3.

	FIBROUS COATS	**'GEM' MONOCRYSTALLINE CORES**
HYPOTHESIS	The later growth of the fibrous coat was from an evolved form of the fluid from which the monocrystalline core grew.	
ASSUMPTIONS	• The 5 diamonds were grown in the same diamond-forming events i.e. that these diamonds are of the same population • Closed system for fluid evolution	

Table 3.2. Hypothetical situation in order to test the plausibility of an un-mixing model to account for differences between fibrous coat and monocrystalline core in Fox kimberlite diamonds.

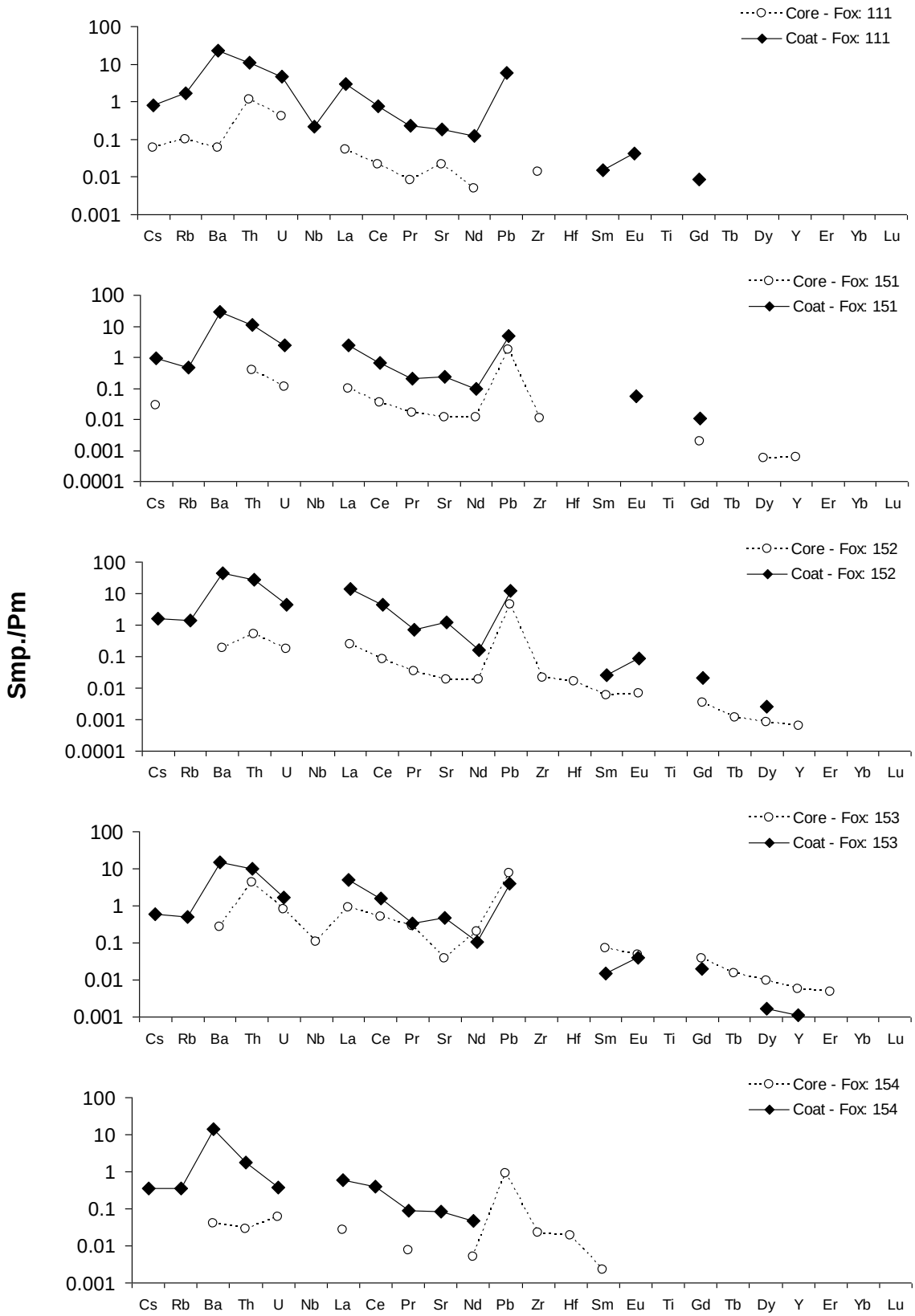
Core - Fox: 111
Coat - Fox: 111
Core - Fox: 151
Coat - Fox: 151
Core - Fox: 152
Coat - Fox: 152
Core - Fox: 153
Coat - Fox: 153
Core - Fox: 154
Coat - Fox: 154
Smp./Pm
Cs Rb Ba Th U Nb La Ce Pr Sr Nd Pb Zr Hf Sm Eu Ti Gd Tb Dy Y Er Yb Lu

Figure 3.25 ◄. Primitive mantle-normalized trace element concentrations for 5 fragments of octahedral coated diamonds from the Fox kimberlite on the Ekati property.

	FIBROUS COATS	'GEM' MONOCRYSTALLINE CORES
SIMILARITIES **Figure 3.25**	• Multi-element fractionation pattern consistently similar • Broad Ba-Th peak • –ve Nb, +ve Pb and low Zr-Hf anomalies	
DIFFERENCES **Figure 3.25**	• +ve Sr anomaly • Lower Zr-Hf concentrations (Values in the coat did not reach above the LOQ values) • Higher Ba/Th • Coat of diamond 153 displays $^{87}Sr/^{86}Sr(i)$ = 0.70770 ± 0.00004 • Coats of other samples $^{87}Sr/^{86}Sr(i)$ = 0.70548 ± 0.0001 to 0.70772 ± 0.00006	• -ve Sr anomaly (except core 111) • Higher Zr-Hf concentrations • Lower Ba/Th • Core of diamond 153 displays $^{87}Sr/^{86}Sr(i)$ = 0.705996±0.0002

Table 3.3. Characteristics of 5 Fox kimberlite diamonds: Contrasts and similarities in the 'gem' monocrystalline core and fibrous outer coat.

Evaluating the closed-system hypothesis, there are several processes that must take place in order to account for the observed differences between the latter-forming coat and earlier cores (Table 3.3). Figure 3.26 in conjunction with Table 3.4 focus on some of the most likely processes that may affect chemical change in the diamond-forming fluids in trying to derive coat fluids from core fluids.

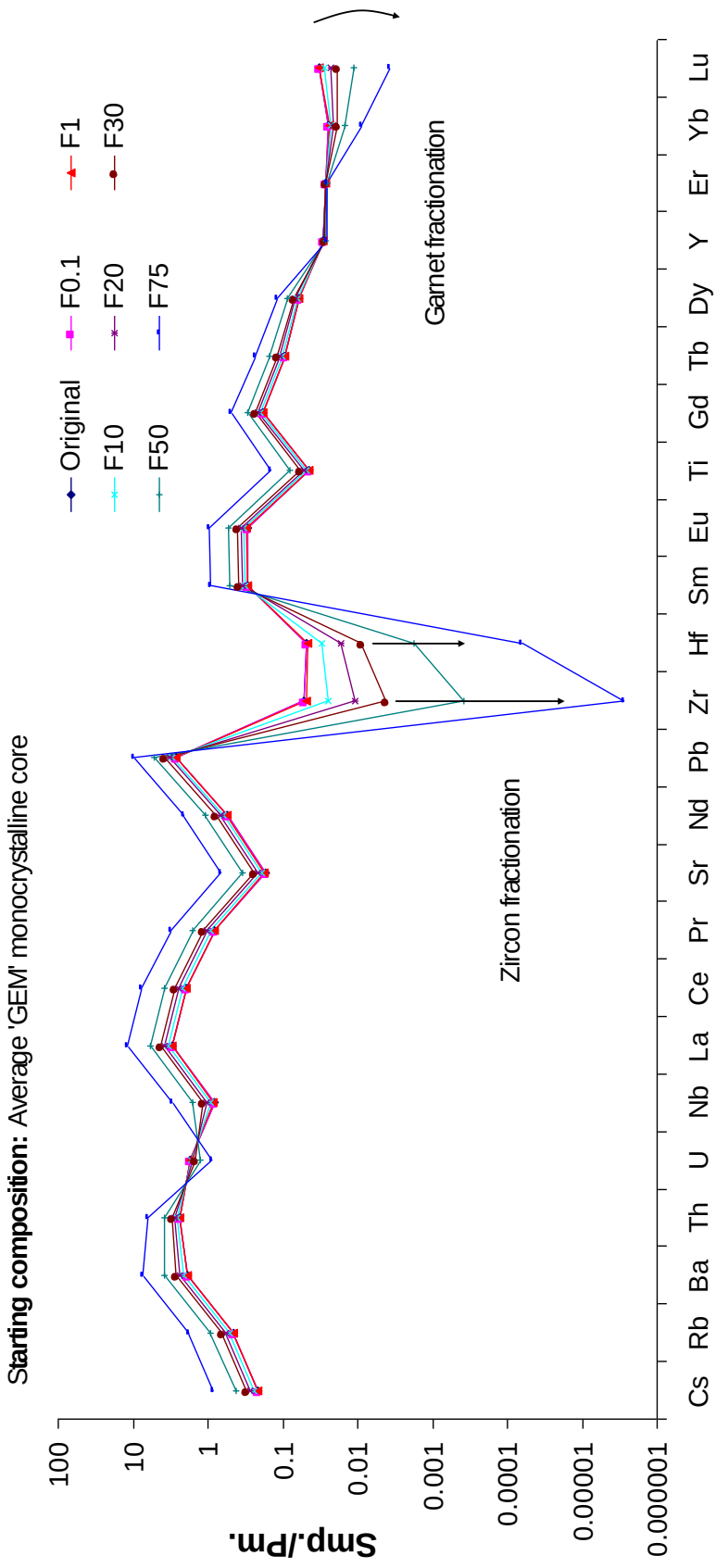

Figure 3.26. Simple fractional crystallization model showing the dramatic effect of zircon fractionation on the Zr-Hf of the residual fluid. F = degree of fractionation, e.g. 10 = 10%. The effect of garnet crystallization is also shown i.e. garnet accommodates the HREEs and thus they progressively become depleted in the residual fluid. Proportions in the crystallizing assemblage = Olivine – 66%, Garnet – 30% and Zircon – 4%. Concentrations are primitive mantle-normalized (McDonough and Sun, 1995).

FEATURE 1: DECREASE IN Zr+Hf CONCENTRATION BETWEEN CORE AND COAT
Crystallizing Zircon (Figure 3.26). Partition coefficients from Klemme et al. (2003) for zircon-melt in a carbonatitic system. With Zircon representing 4% of the fractionating assemblage and garnet, apatite plus olivine in varying proportion accounting for the rest of the assemblage, Zr and Hf will decrease in the HDF below the 0.001 LOQ levels displayed by the Fox coats after 50-75% crystallization of the fractionating assemblage. U/Th fractionation from model not seen in diamonds.
FEATURE 2: +ve Sr AND INCREASED Ba IN FIBROUS COAT
• **Liquid-immiscibility** between co-existing carbonatitic and silicic melts has been invoked as a possible mechanism for driving elemental change in diamond-fluids (Weiss et al., 2009; Rege et al.,2010). Using liquid-liquid distribution coefficients Veksler et al. (1998) we can model un-mixing:- During un-mixing Sr will increase in the carbonatitic fluid ($D_{carbonate\text{-}silicate}$ = 4.77) hence enhanced Sr content consistent with coat growth from an exsolved carbonatitic fluid. Coats enrichment in Ba ($D_{carbonate\text{-}silicate}$ = 4.35) also consistent. • **Apatite dissolution:-** The +ve Sr anomaly displayed by the coats in these diamonds may also be a signature of high degrees of apatite dissolution in the diamond formation environment. Apatite fractionation would have the opposite effect. • **Fractionation or dissolution of other minor phases:-** Fractionation or dissolution and uptake of a phase extremely rich in Sr, e.g., Titante – *2.6B.3* prior to coat formation. Increase Ba/Th in coats may be due to some submicroscopic micaceous inclusion or dissolved by the diamond-forming fluid.

Table 3.4. Features between monocrystalline core and fibrous coat that need to be accounted for in a fluid evolution model and possible explanations.

Several problems arise if an un-mixing process is considered. It is difficult to account for all of the variation seen at the same time without introducing other processes (Table 3.5).

PROBLEMS WITH A CLOSED SYSTEM IMMISCIBILITY MODEL

- Other than Ba, Zr-Hf and Sr, immiscibility does not account for enrichment of other elements in coat ($D_{carbonate\text{-}silicate}$ = 0.24 – 1.39).
- Using available partitioning data unlikely that Zr and Hf would fractionate equally (Zr, Hf $D_{carbonate\text{-}silicate}$ = 0.012 and 0.0075 respectively). Exsolved carbonatitic fluid will evolve to higher Zr/Hf, albeit at lower abundances. Measured Zr/Hf ratios in fibrous, low-purity monocrystalline and 'gem' monocrystalline diamonds in this study very consistent ~ 1.2 hence inconsistent with immiscibility model.

Table 3.5. Set-backs and difficulties that arise when an immiscibility model is used to account for trace element change between a diamond core and coat.

Isotopic constraints: Due to the very low Sr abundances in gem-quality diamond such as that occurring in the cores of the Fox coated diamonds it has only been possible to examine the Sr isotopic composition of one diamond, sample 153. Examining the relationship between the isotopic composition of the two growth forms must be done assuming a common age, that of kimberlite eruption. Assuming any age difference between the two diamond parts automatically invalidates any genetic relationship. The core of this diamond gives $^{87}Sr/^{86}Sr(i_{56})$ = 0.7060±0.0002 whereas the associated coat has $^{87}Sr/^{86}Sr(i_{56})$ = 0.7077±0.00004, i.e., outside of uncertainty. As isotopes in the Sr mass range cannot be significantly fractionated by processes such as mineral crystallization or immiscibility, these differing Sr isotopic

compositions deny any simple closed-system genetic link between the two diamond growth forms. This is in agreement with other studies of coated diamonds where differences in N aggregation and C-isotopic composition have been observed (e.g., Swart et al., 1983; Boyd et al., 1987).

While carbonate-silicate liquid immiscibility may play a role in the development of diamond-forming fluids in genera, it cannot be the dominant process in affecting trace element variation and is incapable of explaining the geochemical differences between fibrous and monocrystalline diamond HDFs.

3.6B.2 The role of percolatory fractionation in source homogenization

Percolatory fractionation in the sense defined by Harte et al. (1993) is a mantle process likely to affect trace element systematics in fluids within the diamond-forming environment. The consequences of melt or fluid percolation through the upper mantle can be modelled as if the environment represented a chromatographic column. Such modeling has been used by Khazan and Fialko (2005) to suggest that similarity in kimberlite trace element concentrations and systematics from provinces around the world may be due to a common physiochemical process operating in the kimberlite source region. By analogy, the conservative range in trace element systematics displayed by our HDFs and their enriched signature may be due in part to a similar percolatory mechanism affecting fluids ascending from the convecting mantle. The location of diamonds towards the base of the lithospheric mantle ostensibly limits such a process because the fluids infiltrating the lithosphere do not

travel far. However, any chemical change is also a function of the fluid-rock ratio and nature of the percolation. Percolative wall-rock interaction can also affect isotopic change although the low Sr concentrations of typical lithospheric low-t peridotites (Pearson & Nowell, 2002) make it unlikely that they will exert much influence on the Sr isotope composition of high Sr diamond-forming fluids invading the base of the lithosphere.

Variations on melt-rock interaction, such as reactive porous flow, are explored in a later section, in terms of their potential to explain the elemental systematics of diamond HDFs.

3.6B.3 The potentially significant role of minor phases in the diamond-forming environment

Because diamond-forming fluids are likely to be of small volume, their trace element concentrations could be very strongly affected by extremely small degrees of crystallization of mantle minerals that accommodate significant amounts of particular elements. Elemental concentrations in such fluids could also be affected by dissolution and/or uptake of elements from such a mineral and thus becoming enriched.

Minerals belonging to the magnetoplumbite mineral group are an example of lithospheric minerals that are highly enriched in specific elements and several have been proposed as diamond associates. A titanate (Sr-magnetoplumbite) associated

with G10 garnets was identified by Sobolev et al. (1988) in a diamond from the Sputnik kimberlite (Yakutia). Five Yimengite inclusions were reported from a natural diamond from the Sese kimberlite (Zimbabwe) by Bulanova et al. (2004) and synthetic Yimengite was found to coexist with a hawthornite phase grown under high pressure (4-5 GPa) and high temperature (1150 – 1350 ^{o}C; Foley et al., 1994). These rare minerals can therefore occur in association with diamond and have been interpreted as resulting from deep mantle metasomatism generated by K- and Ba-rich fluids (Haggerty, 1987; Nixon and Condliffe, 1989).

The recent study by Bulanova et al. (2004) presents a model for Yimengite formation in a restite upper mantle assemblage , consisting mainly of olivine and chromite, which could have been affected by fluids enriched in incompatible elements such as K, Ba, Sr, Ti and REES to form Yimengite i.e., the metasomatic replacement of a cr-spinel.

Trace element concentrations in titanate found in coarse veins of MARID association in peridotite xenoliths from Bulfontein (Jones et al., 1982, 1989) are an example of these minerals occurring in vein-metasomatized lithospheric rock types. In contrast to our diamond HDFs, the titanates display enrichment in Zr-Hf, Ti, and Sr indicating the potential role such a mineral may play in the accommodation of trace elements during fractional crystallization from an enriched mantle fluid (Figure 3.23). Although mineral-melt partition coefficients are not available for these minerals in a carbonatitic environment, it is clear that small degrees of

crystallization of such minerals from a HDF would greatly deplete the fluid in the elements that we observe in diamonds from worldwide sources and thus although extremely rare, they may play an important role in determining the trace element systematics of trace fluid microinclusions.

3.6C Understanding the source of diamond HDF chemistry

3.6C.1 $^{87}Sr/^{86}Sr$ isotope systematics and a multiple component source model

The parental fluids involved in diamond growth must be enriched in LILEs and LREEs however the large range in Sr isotope compositions ($^{87}Sr/^{86}Sr(i)$ up to 0.7110) suggest that this fluid, or a component of it, must have experienced moderate to long-term time-integrated enrichment in Rb/Sr relative to typical asthenospheric/convecting mantle sources. The absence of isochronous relationships together with the unsupported Sr isotope compositions (i.e., highly radiogenic Sr at low Rb/Sr) indicates that the isotopic variation cannot be solely due to ^{87}Sr ingrowth since diamond formation. Klein-BenDavid et al. (2010) also found the same relationships to be true for isotopic variation within single fibrous diamonds from Botswana.

The large range in Sr isotope compositions is present in both fluid-rich fibrous diamonds and fluid-poor monocrystalline diamonds such as those from Snap Lake and Ekati (Fig. 3.27). This observation, together with the similarities in trace element patterns noted above indicate their parental fluids have similar histories, at least as far as is discernable from these geochemical parameters. If we assume that the spectrum of Sr isotope compositions in the diamond HDFs reflect the evolution of the fluid source then initial Sr isotope compositions that range from relatively unradiogenic ($^{87}Sr/^{86}Sr(i) = 0.704$) to extremely radiogenic values must reflect either a source with highly varied Rb/Sr or variation in fluid composition driven by mixing of fluids with varying isotopic compositions. The broad range in initial Sr isotope

ratios coupled with a range in trace element concentration e.g. Sr = ~0.1 - ~10 ppm in the Snap Lake diamonds is consistent with a mixing model where at least two end-members are involved (Figure 3.27), a component akin to convecting mantle and another that is enriched, similar to ancient lithospheric mantle.

Figure 3.27 ►. $^{87}Sr/^{86}Sr$ initial ratios with 2σ error bars for Slave craton diamonds from this study. Each group displays a range of $^{87}Sr/^{86}Sr(i)$ coupled to a range in elemental Sr abundance indicating multi-component source for the measured fluid compositions. A schematic cartoon depicts the mixing scenario. Glimmerites represent an enriched endmember potentially allowing for the radiogenic isotope values whereas kimberlite may be more representative of the convecting mantle signature. Error on Sr ppm is ~10%.

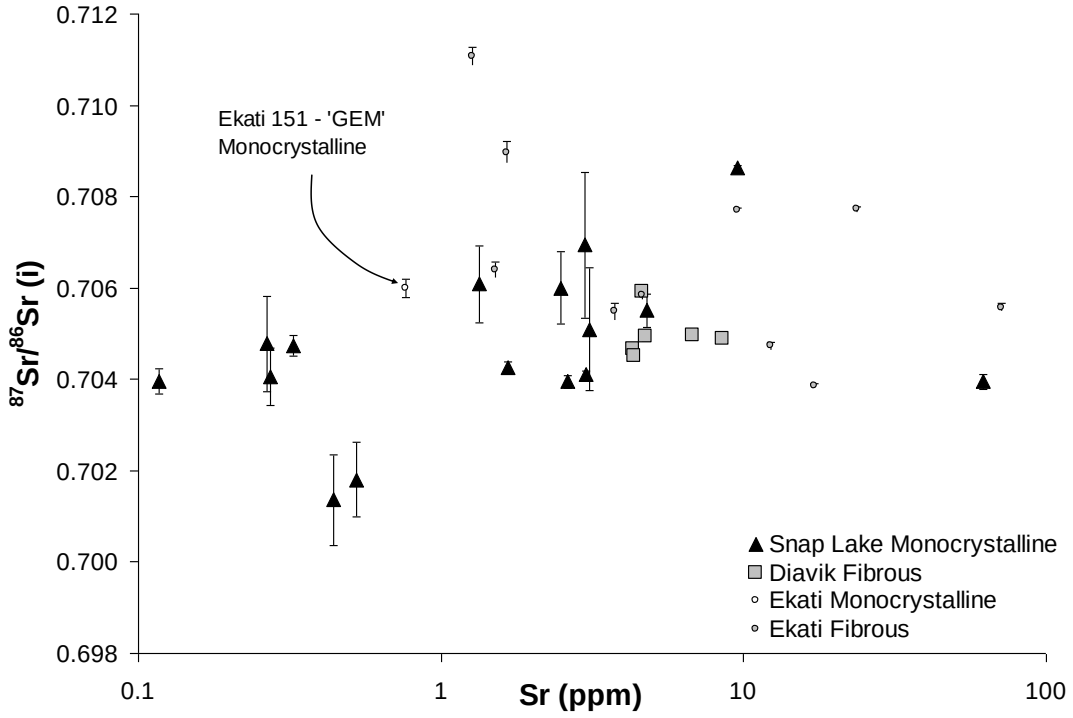
0.712
0.710
0.708
0.706
0.704
0.702
0.700
0.698
$^{87}Sr/^{86}Sr$ (i)
Ekati 151 - 'GEM'
Monocrystalline
Snap Lake Monocrystalline
Diavik Fibrous
Ekati Monocrystalline
Ekati Fibrous
0.1
1
10
100
Sr (ppm)

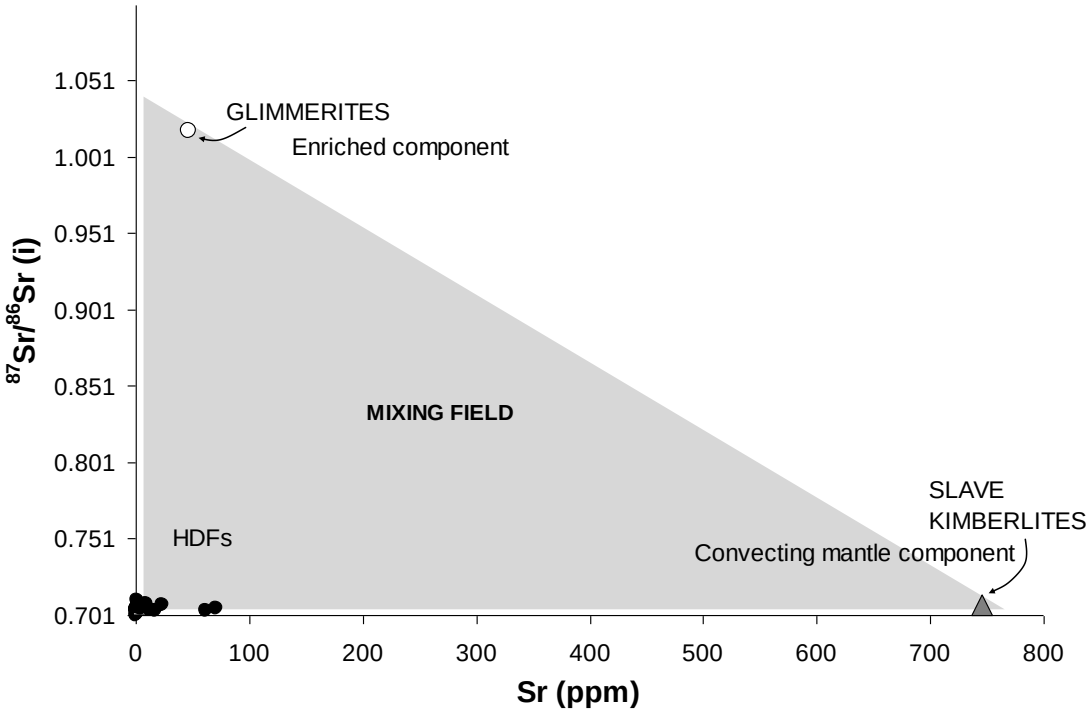
1.051
1.001
0.951
0.901
0.851
0.801
0.751
0.701
$^{87}Sr/^{86}Sr$ (i)
GLIMMERITES
Enriched component
MIXING FIELD
HDFs
SLAVE
KIMBERLITES
Convecting mantle component
0
100
200
300
400
500
600
700
800
Sr (ppm)

3.6C.2 Nature of the enriched fluid source and potential analogues:

A – Group II Kimberlites

A number of authors have suggested kimberlite as a possible diamond-forming melt (Navon et al., 1988; Akagi & Matsuda, 1988). Group I kimberlites have diagnostic incompatible trace element ratios that correspond to those characteristic of OIB (Nb/U = ~ 47; Ce/Pb = ~ 25; Becker and Le Roex, 2006 and references therein). These ratios in the diamond HDFs measured in this study are dramatically different such that Nb/U is typically <1 and Ce/Pb is typically <1, except for a few aberrant samples from the Snap Lake suite. These trace element characteristics are much more akin to Group II kimberlites (Becker and Le Roex, 2006).

Group II kimberlites have $^{87}Sr/^{86}Sr$ (i) between 0.707 and 0.711, similar to the enriched end of the diamond fluid compositions. However, as Group II kimberlites are not reported outside southern Africa then their potential as a source component for Slave diamonds is uncertain. It is possible that similar melts were generated in the basal parts of the Slave lithospheric mantle but have not made it to the surface in other cratons for unknown reasons. Lamproites have similar trace element systematics to Group II kimberlites, with even more extreme Sr isotopic ratios (e.g., Nelson et al., 1989) but are globally ubiquitous, albeit in small volumes (Mitchell & Bergman, 1991). This makes lamproitic melts a similar but more attractive alternative to Group II kimberlites as potential end-members for involvement in diamond formation (Figure 3.23). As the elemental systematics of Group II kimberlites have been studied more closely, using modern instrumentation compared

with lamproites, we will use them to assess the nature of the enriched source components. Calculated trace element compositions of the mantle-source of Group II kimberlites have been calculated by le Roex et al. (2003), Gregoire et al. (2003), Harris et al. (2004), Coe (2004) and Becker and Le Roex (2006). Trace and rare earth element concentrations are not identical to diamonds HDFs but share the –ve Ti and –ve Sr anomalies associated with diamond HDFs. Most notably Group II kimberlites and lamproites display the same strikingly +ve Pb anomalies as the diamond HDFs and this feature is never observed for uncontaminated Group I kimberlites.

The isotope signature of Group II kimberlites and lamproites requires an ancient enrichment of their source regions with subsequent isolation from the convecting mantle to allow development of these compositions. These requirements are shared by the enriched endmember of the diamond HDFs.

While there are isotopic similarities between diamond HDFs and Group II kimberlite/lamproitic melts, some striking elemental differences exist. Most recently Klein-BenDavid et al. (2010) has highlighted the extreme K concentrations in diamond HDF inclusions that are considerably in excess of those typical of kimberlites or lamproites. K concentrations in diamond fluids can reach 50 wt% K_2O, as displayed in the inclusions analyzed from the Fox kimberlite in this study. Kimberlites have much lower K_2O at ~ 4 wt% but it is possible that they may loose some volatile content during ascent. Price et al. (2000) and Le Roex et al. (2003)

argue that CO_2 loss is minimal however Brey et al. (1991) and Girnis et al. (1995, 2005a,b) advocate the formation of kimberlites as saturated melts that degas at sub-crustal pressures. Similarly, Salvioli-Mariani et al. (2004) appeal to a CO_2 release from lamproitic magmas at shallow pressures. Water and Cl may also be lost during degassing (Kamenetsky et al., 2004; Maas et al., 2005). If this is the case, parental melts may be significantly higher, although whether they can reach the K contents of diamond HDFs is uncertain.

B – Phlogopite-rich veins, PICS and Glimmerites

If melts parental to Group II kimberlites/lamproites do not lose volatile content during ascent and actually have initially much lower K_2O than diamond HDFs then other sources need to be appraised. The highly potassic nature of HDFs in fibrous diamonds measured by e.g. Weiss et al. (2008, 2010), Klein-BenDavid et al. (2004, 2007, 2010), Kopylova et al. (2010), Zedgenizov et al. (2007) and in this study maybe accounted for by derivation of fluids from a phlogopite-rich source. This K-rich mineral is stable to depths of 200 km in lithospheric peridotite (Sato et al., 1997), i.e., well into the diamond stability field and is present, albeit very rarely, as inclusions in diamond (Klein-BenDavid et al., 2006; Sobolev et al., 2010). In fact, the low-Al, Si-rich phlogopite mica found included within a diamond HDF by Klein BenDavid et al., 2006 is similar to the residual phlogopite composition observed during phlogopite breakdown reactions at high temperature by Sato et al. (1997).

Phlogopites in MARID (Mica_Phlogopite - Amphibole_K-Richterite – Rutile – Ilmenite – Diopside) suites have been sampled by and are thought to be genetically related to GII kimberlites/lamproites (Waters, 1987; Gregoire et al., 2002). These metasomatic rocks have $^{87}Sr/^{86}Sr$ ranging from 0.71085 – 0.93645 (Kramers et al., 1983; Erlank et al., 1987). Although MARIDs form at depths shallower than the diamond stability field, other such enriched veins that contain stable phlogopite, may be involved in the formation of diamond-forming fluids at depth. Glimmerite veins (Becker et al., 1999) show strongly fractionated REE patterns, negative anomalies of Nb, Ta and Ti and very low Zr and Hf abundances. Glimmerite whole rock $^{87}Sr/^{86}Sr$ ratios reported by Becker et al. (1999b) range from 0.709954 – 0.719658 coupled with 2.6 – 9.1 wt% K_2O. Glimmerites are invoked by Klein-BenDavid et al. (2010) as a possible component in diamond-forming fluids in order to account for the extremely unradiogenic Nd and radiogenic Sr reported in diamonds from that study. Compositions of HDFs from this study also display similarities to glimmerite in their trace element systematics, in particular –ve Sr and Nb anomalies, however the Rb/Ba of average glimmerite is circa 2.0 and hence extreme compared to the average value for HDFs from fibrous diamonds (Rb/Ba = 0.04). This feature is likely to be due to the accommodation of Rb in phlogopite that is a major constituent of glimmerite whereas the diamond HDFs would be a product of phlogopite breakdown and further dilution via mixing with less enriched fluids such as Rb-poor carbonate rich fluids.

These observations indicate that vein phlogopite or at least metasomatic vein rocks may be a major contributor to the radiogenic endmember of our diamond forming HDFs. Phlogopite is capable of rapidly generating radiogenic Sr. For instance, using Rb/Sr values measured in a MARID phlogopite by Kramers et al. (1983) it is possible to evolve from $^{87}Sr/^{86}Sr$ ratios typical of convecting mantle at the time of kimberlite eruption (0.703) to values > 0.93 in the 90 Ma that has elapsed to the present day. Hence, over a short period of time phlogopite can evolve to very radiogenic values due to its high Rb/Sr. Even diamonds that formed 1-3 Ga ago could have been sourced from a fluid that interacted with phlogopites with very radiogenic Sr isotope signatures.

A working model comprising these observations and based on our own dataset proceeds as follows;

(1) Asthenospheric/convecting mantle/GI kimberlite/Carbonatite type fluid enters the base of the continental lithosphere where metasomatized phlogopite-rich rocks and glimmerite veins reside (Figure 3.28 and 3.29)

(2) Heat transfer into these veins from the invading melt at the base of the continental lithosphere leads to phlogopite breakdown into a residual Al-poor, silica-rich mica and K-rich hydrous fluid (Sato et al., 1997)

(3) Diamond precipitates from a fluid that is a mixture of the convecting mantle fluid front and the K-rich hydrous fluid enriched in $^{87}Sr/^{86}Sr$ and K derived from the phlogopite-rich vein (Figure 3.29).

Key support for phlogopite breakdown being the source of the elevated K and radiogenic Sr in the fluids that form diamonds is the observation that, silica-rich, Al-poor mica, similar to that derived by Sato et al. (1997), has been found as microinclusions in several fibrous diamonds (Izraeli et al., 2004; Klein-BenDavid et al., 2006). If carbon in this fluid mixture is dominated by the fluid originating from the carbonate-rich convecting mantle-derived fluid then this scenario is capable of explaining the decoupling of highly enriched elemental and radiogenic isotope systematics from the normal, very restricted mantle-like carbon isotopic compositions seen in fibrous diamonds. Furthermore, even though "gem" diamonds are considerably more variable in their carbon isotope compositions we note that >90% of the population lie within 2 per mille of the typical mantle δ^{13}Cvalue of -5.

C – Highly metasomatized, "Deformed" peridotites

Bedini et al. (1997) use a numerical simulation of reactive porous flow at the transition between adiabatic and conductive geotherms in the mantle to account for unusual trace element signatures in mantle-derived spinel peridotites. In their study, deformed and metasomatized peridotites from Ethiopia (apatite bearing lherzolites and harzburgites) are LILE enriched, HFSE depleted, and display selective enrichment of LREEs relative to HREEs and/or MREEs that are similar to diamond HDFs (Figure 3.30). Bedini ascribes these elemental signatures to extensive reaction and metasomatism with large volumes of basaltic melts, mostly of deep seated origin.

The similarity between the multi-element patterns of diamond HDFs and the deformed peridotites described by Bedini et al. (1997) are striking considering the relatively shallow derivation of the spinel-facies peridotites (Figure 3.23, 3.30). Elevated Ba/Nb and Th/Nb are seen in both sample-types and elemental concentrations are remarkably similar.

Two notable differences are the +ve Sr anomaly in the deformed peridotites and their elevated HREEs. The difference in REEs is most likely related to the diamond HDFs being formed in the presence of highly depleted peridotites whereas the less depleted spinel facies peridotites contain higher HREE than a depleted cratonic peridotite (e.g. Wittig et al., 2008). The addition of apatite to the shallow peridotites has almost certainly created the +ve Sr anomaly and will further enhance HREE abundances.

An additional attraction of melt-rock reaction models that involve some degree of fractionation (e.g., Harte et al., 1993; Burgess and Harte, 2004) is that they give rise to a variety of volatile enriched melts as fractionation proceeds. This is relevant for diamond genesis because it provides a mechanism for volatile and trace element enrichment styles similar to those we observe in our diamond HDFs and provides support for a model where small degree melts and their fluids, from deep seated sources are involved as a source fluid in diamond genesis.

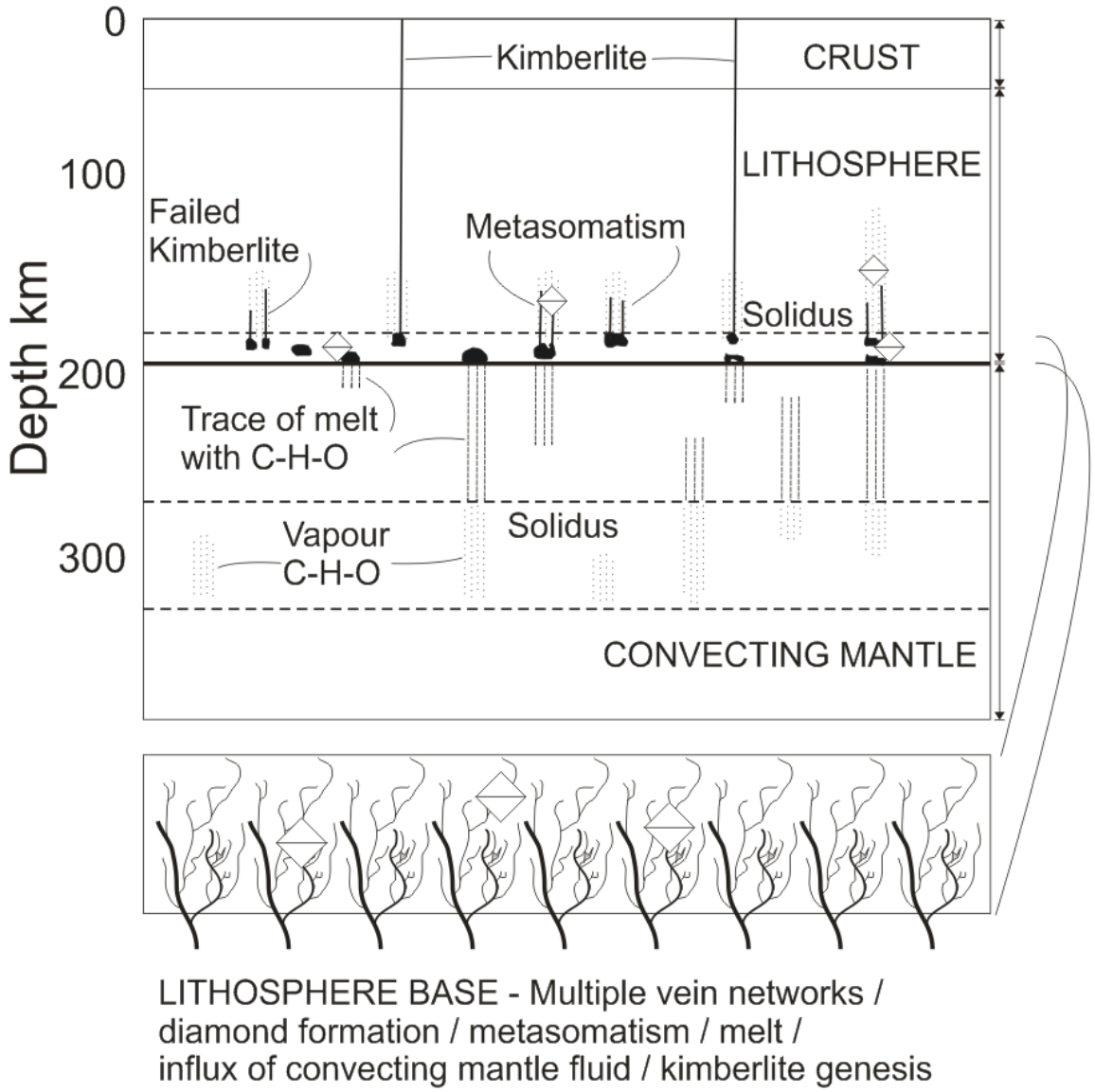

Figure 3.28. Cross section of a craton showing migration of deep volatile components, generation of melts in the asthenosphere, and their entrapment in the lower lithosphere as well as melt generation and vein metasomatism at the base of the lithosphere. Diagram after Wyllie (1989).

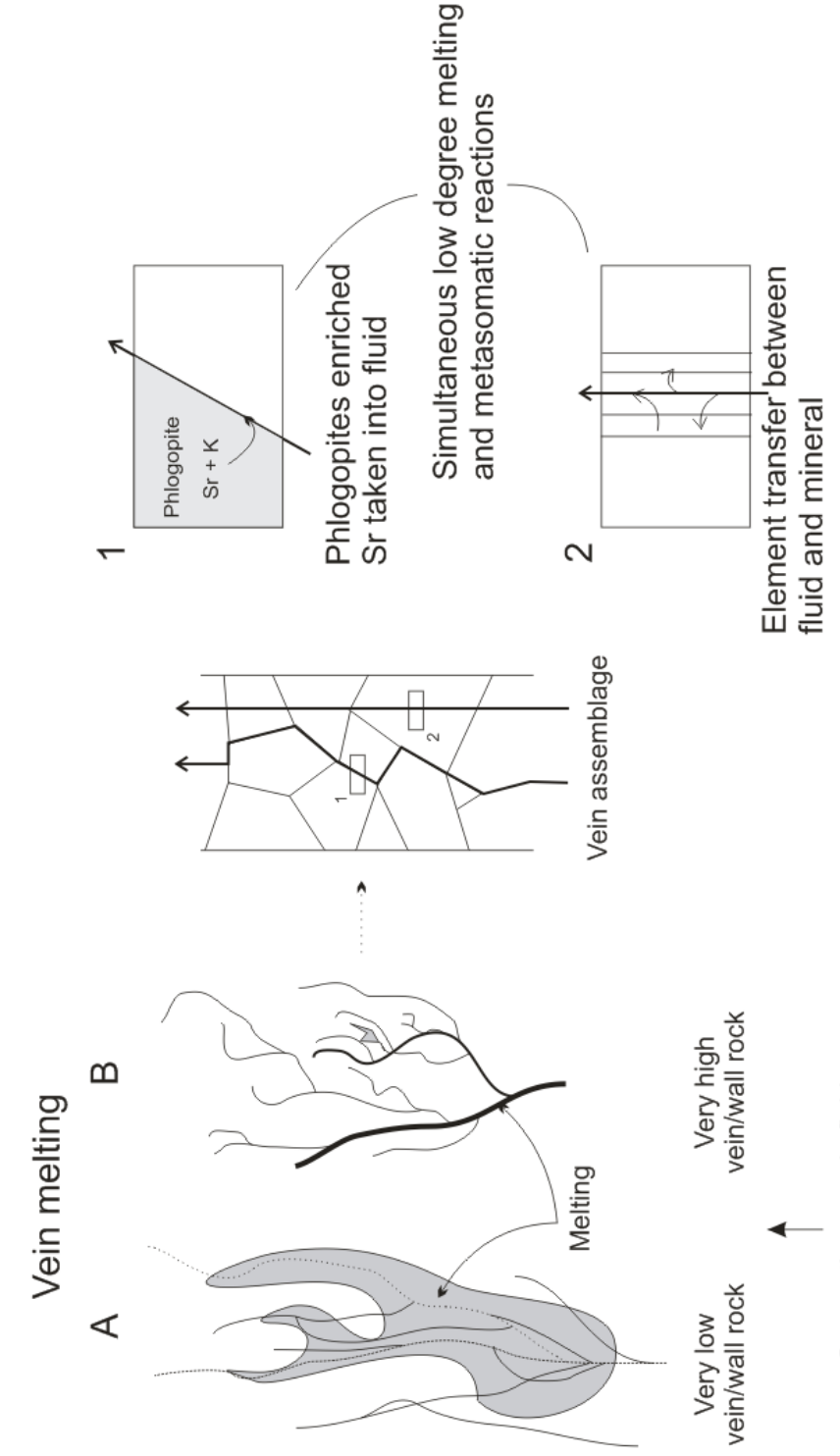

Figure 3.29. A possible vein melting scenario at the base of the lithosphere. Very high vein/wall rock ratios are likely thus limiting the influence of the wall rock. In a vein assemblage such as that for glimmerites (Carlson and Irving, 1994) the presence of phlogopite with radiogenic Sr allows the carbonatitic fluid to acquire the enrichment observed in diamond HDFs.

.

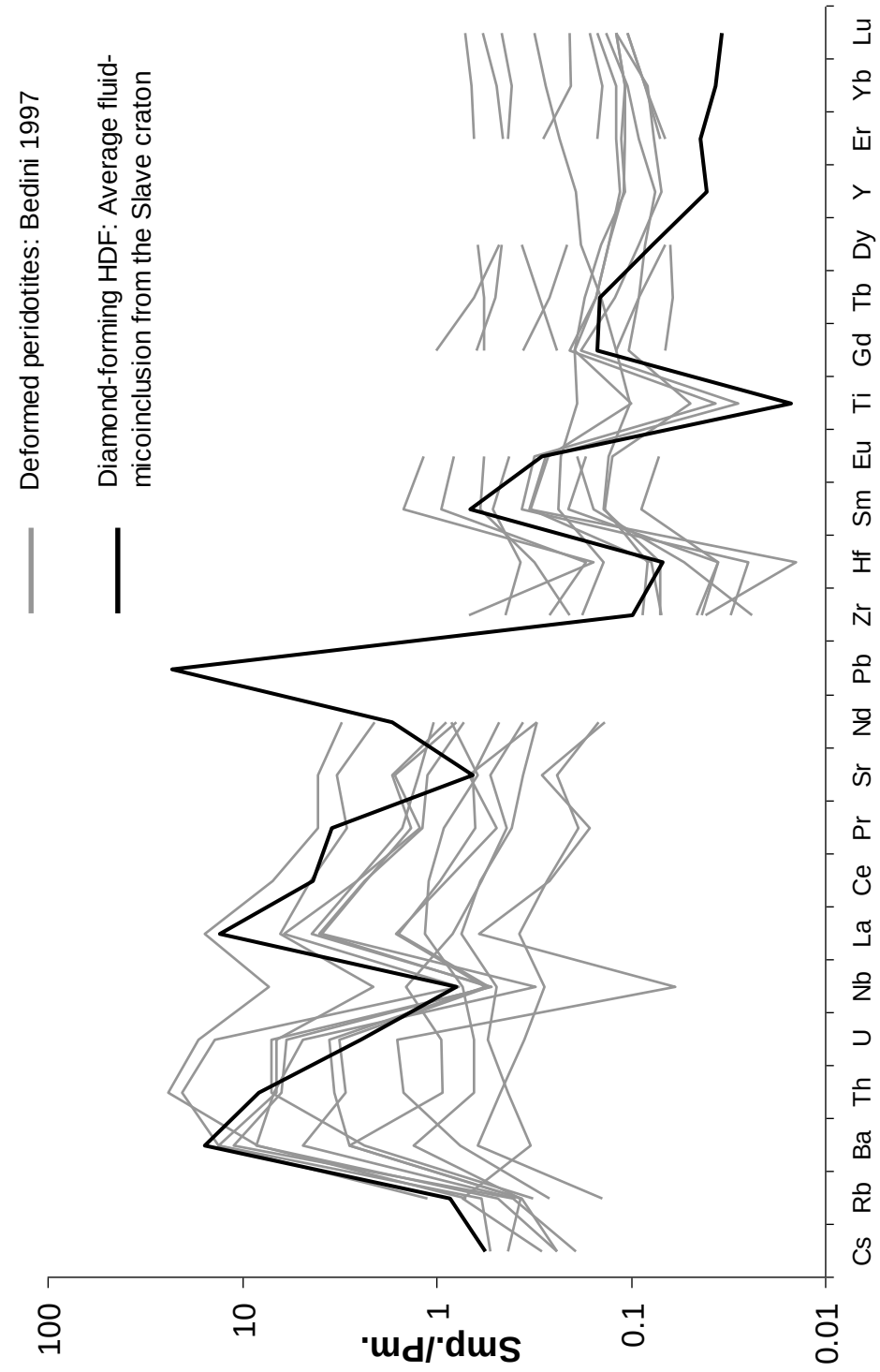

Figure 3.30. Primitive mantle-normalized trace element concentrations of deformed peridotites from Bedini et al. (1997) with average HDF compositions for diamonds from the Slave shown for comparison.

3.6D A model for diamond genesis

3.6D.1 Supercritical fluid, metasomatized-vein and wall-rock reactions

The model of Foley (1992) creates a context for the origin of potassic alkaline magmas, suggesting that metasomatic veins are involved in their formation that are likely to occur at the base of the mechanical boundary layer i.e. the junction between the convecting upper mantle and the overlying rigid lithosphere (Figure 3.28). A consequence is an intensely-veined underside to the channeled flow zone, since the small melt fractions from the porous flow regime in the asthenosphere will be unable to progress far in veins before solidifying due to lack of heat (McKenzie, 1989). Our isotopic evidence requires the isolation of incompatible element enriched reservoirs for substantial time periods and this environment is consistent with that requirement. The metasomatic veins originate by solidification of low-degree melts which are themselves the results of earlier, deeper, multistage melting and metasomatic processes ultimately due to the presence of a transition zone between large-scale channeled and porous flow regimes. Vein fluids and fluids associated with this vein/wall-rock melt may account for some of the characteristics reported on diamond inclusions and HDFs. The melting event producing the ultrapotassic magma begins in the veins due to the concentration of accessory and hydrous phases and incompatible elements.

In terms of diamond genesis, we envisage two temporal diamond-formation scenarios in which a supercritical carbon rich fluid/vapour is always required;

- Diamond may form once the metasomatic veins are in place but before any melting occurs i.e. Si-bearing, CH_4 rich fluids released from sublithospheric melts (asthenospheric component) react with the veins or react with fluid released from the veins (acting as conduits for the fluid) and host mantle wall-rock to create diamond

- Diamond may form when melting occurs with an extreme vein/wall-rock ratio and thus a fluid-melt dominated by the vein signature mixes with the convecting mantle / asthenospheric component (Figure 3.29).

Variations on these scenarios would account for the range observed in $^{87}Sr/^{86}Sr$ providing that diamond precipitation is a direct result of the meeting and interaction of an asthenospheric fluid and an enriched component, either leached from minerals or as a fluid associated with vein-rock mineral melt.

In these diamond-formation models it is important to consider the role of redox. Klein-BenDavid et al. (2010) note that the oxidation state of phlogopite rich veins in the mantle is likely to be two log units over the EMOD buffer. Therefore, as suggested by Malkovets et al. (2007) and Gregoire et al. (2002), diamond will dissolve rather than precipitate in fluid derived solely from such veins. It is therefore essential that if such a fluid is to be involved, it must act as a redox trigger for diamond precipitation upon the influx and oxidation of an asthenospheric component such as CH_4. Even if the lithosphere is too reducing to support methane oxidation, local oxidation states may vary in the presence of some of the K-rich veins we are

describing. Alternatively, diamond may form from reduction of carbonates present in the reaction environment (Stachel and Harris, 2009).

3.6D.2 Support for a mixing model

The role of fluid mixing from different sources has been a central tenet in many models of diamond genesis. Clear evidence of mixing-controlled variation in Sr and Nd isotopes led Richardson et al. (2009) to invoke a multi-component model in the genesis of garnets and diamonds from the Archean Kaapvaal and Zimbabwe cratons. The proposed mixing at Venetia is a simple two component model. Klein-BenDavid et al. (2010) also found clear evidence, on the basis of Sr isotope variations, of mixing in the genesis of individual fibrous diamonds from Botswana. Hence, this process can be involved in both gem and fibrous diamonds. From the system complexity identified above, it seems likely that if mixing is a common feature in diamond forming events, that >2 components would be likely. Among isotope data compiled from a number of studies (Figure 3.31 and references therein) consisting of peridotitic and eclogitic diamond inclusions from a number of locations, the only dataset to display a clear 2-component mixing relationship is the Venetia set (Richardson et al., 2009). Premier (Cullinan) E-Type inclusions display a positive correlation of decreasing Sr with increasing $^{87}Sr/^{86}Sr$ while Premier (Cullinan) P-Type inclusions show no clearly defined endmembers. If the variation were due to mixing then the data would require at least three component endmembers to explain the isotope range displayed (as marked by a dashed '*n*-component' triangle). It is unlikely that a two-component model is applicable to diamond genesis worldwide

and this demonstrates that the environment is complex with several endmembers contributing some chemical component. Defining the detailed characteristics of the endmember fluids unequivocally needs much more research. One problem with defining isotopic mixing trends for diamond fluids and diamond inclusions is that the isotopic compositions reflect at least two processes, mixing and radiogenic ingrowth since the time of mixing. Hence, for clearer resolution it is critical to know the age of diamond formation. Even when these data are available, for well-defined mixing relations to be evident, a pre-requisite is endmembers of relatively restricted concentration and isotopic compositions. Given the isotopic diversity inherent in the lithospheric mantle (e.g. Pearson and Nowell, 2002) these conditions are unlikely to be met often.

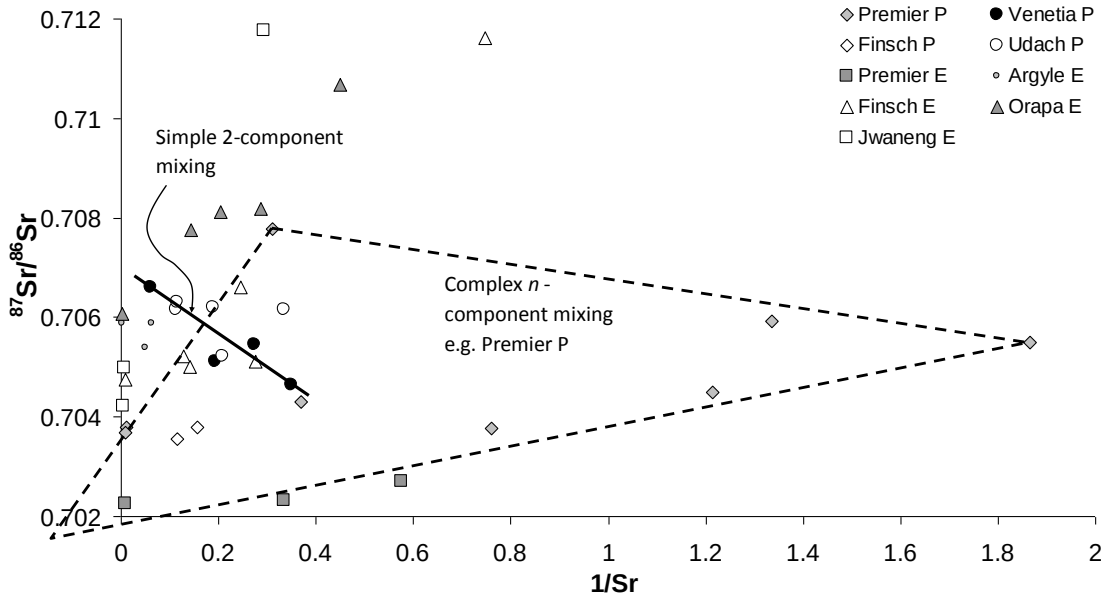

Figure 3.31. Sr isotope composition vs. Sr concentration demonstrating that although simple 2 component mixing is possible, if mixing is occurring then it is likely to be complex and involve many components.: P-Type Subcalcic garnet inclusions from Venetia (Richardson et al., 2009), E-Type garnet inclusions from Finsch (Richardson et al., 1984), Argyle and Premier E-Type garnet and cpx inclusions (Richardson, 1986), Finsch and Orapa E-Type garnet and cpx inclusions (Richardson et al., 1990) Jwaneng E-Type garnet and cpx inclusions (Richardson et al., 1999), Udachnaya (Udach) P-Type garnet inclusions (Richardson et al., 1997) and Premier P-Type garnet and clinopyroxene inclusions (Richardson et al., 1993).

3.7 Summary and Conclusions

The goal of this chapter has been to acquire for the first time, quantitative trace element concentrations in monocrystalline, 'gem'-quality diamonds with coupled radiogenic Sr isotope information. This has allowed a comparison to be made between fibrous/coated diamonds and monocrystalline octahedral diamonds and to thus comment on potential similarities and/or contrasts in their growth environments. The trace element database is the largest to have been established with coupled isotopic information, and has allowed a more rigorous appraisal of early genesis models based in smaller sample sets. The dataset is complex and suffers due to the lack of extra geochemical information on the diamonds analyzed in this study such as N aggregation data and N concentration, C isotopes, mineral inclusion trace element and major element systematics and diamond HDF major element concentrations. However, several conclusions and observations have been suggested from this study that significantly adds to the information known about monocrystalline diamonds and their potential growth environment (Table 3.6).

	FIBROUS	MONOCRSTALLINE
TRACE ELEMENTS	• Primitive mantle normalized diamond concentrations in fibrous *and* monocrystalline diamonds broadly display LILE enrichment and HFSE and HREE depletion. • On average fibrous diamonds display concentrations at least one order of magnitude higher than 'gem' monocrystalline diamonds. •	
MAJOR ELEMENTS	• Diamonds containing silicic fluid inclusions display a -ve Sr anomaly, Pr/Sr > 1 in contrast to diamonds containing saline fluid inclusions which display a +ve Sr anomaly, Pr/Sr < 1. • K_2O in fluid inclusions averages 23.48 wt% but reaches up to 48.08 wt%.	
$^{87}Sr/^{86}Sr$ INITIALS	Ekati fibrous 0.70386±0.00005 to 0.71107±0.0002 Diavik fibrous 0.704513±0.00007 to 0.705917±0.0001	Low-purity monocrystalline 0.70136±0.001 to 0.70864±0.00004 'GEM' monocrystalline (153) 0.705996±0.0002
$^{87}Sr/^{86}Sr$ INITIALS (continued)	• Large Sr isotopic range displayed by both fibrous and	

FIBROUS / MONOCRYSTALLINE LINK	monocrystalline diamonds. Fibrous diamonds containing silicic or saline fluid inclusions cannot be distinguished using $^{87}Sr/^{86}Sr$. • No isochronous relationships observed in this study. The similarities or variation observed between monocrystalline diamonds and fibrous diamonds cannot be accounted for solely by a fluid un-mixing model. An open system of fluid flux is preferred. Processes accounting for chemical variation include mineral fractionation / dissolution, wall-rock interaction and fluid mixing.
SOURCE COMPONENTS	• Radiogenic Sr values and trace element signatures suggests an ancient enriched component such as Lamproites / Group II kimberlites or their sources / Phl-rich assemblages / highly metamorphosed peridotites. • Unradiogenic values suggest a component akin to convecting mantle / MORB / Group I kimberlites. • K_2O is potentially sourced from phlogopite in metasomatic veins. • Diamond formation will occur as a result of the meeting and mixing of an asthenospheric volatile and carbon rich fluid and the constituent endmembers of a multi-component mixing environment. This is thought to be a deep seated process, e.g. at the base of the lithosphere (Figure 3.28).

Table 3.6. Summary conclusions of this study based on observation on trace element and Sr isotope chemistry of fibrous, low-purity monocrystalline and 'gem' monocrystalline diamonds.

CHAPTER 4

Geographic discrimination of diamond using analysis of variance and logistic regression statistics on trace element concentrations

4.1 Introduction

If a trace element signature or rather 'chemical fingerprint' is unique and distinct in each diamond-forming environment, then statistical analysis of a large body of trace-element systematics will test if source discrimination of samples from unknown locations may be possible. Such a tool may have implications for the forensic tracing of illegally traded diamonds.

Previous work on diamonds from different geographic locations has shown that diamonds can have various distinguishing features including their morphology (Harris et al. in Boyd and Meyer 1979; Harris et al., 1992; Robinson 1979; Gurney et al., 2004), mineral-inclusion chemistry (Stachel et al., 2004; Stachel and Harris 2008), N and C isotope systematics (Cartigny et al., 2004) and fluid inclusion trace element chemistry in fibrous diamonds (Rege et al., 2010: Weiss et al., 2010). A variety of instrumentation has been employed in the measurement of these features, including LA-ICPMS, SIMS, microPIXE, IRMS, Cathode-luminescence, Photo-luminescence and FTIR, all of which are powerful tools for distinguishing diamonds from certain well studied areas. However the variation in diamond morphology and chemistry can range to such a degree in a given deposit that on a global scale, source discrimination is extremely difficult.

Of the above approaches, the trace element composition of a diamond offers perhaps the best potential for source discrimination because a single analysis can provide data for 20-30 elements, which can be employed in statistical analysis. Using

information from this study on diamonds from 3 localities in the Slave Craton, Canada and a suite of diamonds from the generic Congo region in Africa, together with significant statistical processing, source discrimination can be attempted given a set of initial criteria. Diavik and Ekati are mine properties defined within the Lac de Gras kimberlite field. Ekati samples are from the Fox and Misery kimberlites. The exact kimberlite from which the Diavik samples originate is not known. While the locus of each property is separated by ~50km, the nearest neighbours from which diamonds are being mined may be as little as 25 km apart. Snap Lake is different in that it is a single mine source. Congo material could be pooled from several different mines within one kimberlite field. They are of unknown source locality.

Two methods have been employed to address the dataset; analysis of variance (ANOVA) and logistic regression. Prior to statistical analysis, the concentration data are normalized to Primitive Mantle values (Sun & McDonough, 1995) to remove variability in concentrations that arise from the well-know differences in nuclear binding energy among isotopes. All statistical calculations performed below were done using the Minitab v.14 statistical package.

4.1A ANOVA and power analysis

Analysis of variance (ANOVA) is a collection of statistical models, and their associated procedures, in which the observed variance in a dataset is partitioned into components due to different sources of variation. In its simplest form ANOVA provides a statistical test of whether or not the means of several groups are all equal, and therefore generalizes Student's two-sample t-test to more than two groups. ANOVAs are helpful because they possess a certain advantage over a two-sample t-test. Performing multiple two-sample t-tests would result in a largely increased chance of committing a type I error i.e. when the hypothesis is inappropriately rejected. For this reason, ANOVAs are useful in comparing three or more means. Furthermore, ANOVAs can test between more than one factor or source of variation without incurring additional risk of type I error. Diamond concentration data in this analysis are blank corrected but not filtered by limits of quantitation as petrogenetic information is not being sought.

Our initial questions are;

(1) Is there sufficient variance in the dataset to attempt further analysis?

(2) Can the geographic source location of a diamond be identified by its trace element chemistry?

The primitive mantle-normalized dataset for both monocrystalline and fibrous diamonds from Snap Lake dyke, Diavik, Ekati and fibrous diamonds from the Congo were first addressed with a multivariate analysis of variance (MANOVA) to test whether mean differences among groups (based on known source location/site) is likely to occur by chance i.e. are there sufficient *a priori* differences within the dataset to grant further analyses. Due to the number of factors and number of different trace elements to be tested even ANOVA may suffer from type I error with such a larger number of repeated ANOVAs being used for each individual trace element. By first performing the MANOVA we can have greater confidence that type I errors will not occur in subsequent ANOVAs. The MANOVA showed that there was significant difference based on 24 independent variants, i.e. the elements analyzed in each diamond. It is not established at this point what the difference is, only that there is a difference.

The next step was to address the potential effect of elements, such as Pb, that are present in much higher concentrations than the other elements and that vary more than other elements and hence may strongly influence the resulting statistical analysis. Pb concentrations may be more variable than other elements if Pb is controlled by a separate factor that does not influence the other elements. In the case of diamond, this factor could be the presence of sub-micrometer sulphide inclusions, an issue raised in previous bulk INAA analytical work by Fesq et al. (1975). Therefore ANOVA with and without Pb as a covariate was performed on a two factor model – Type (gem vs. fibrous) and Site (Snap vs. Ekati vs. Diavik vs.

Congo). Pb was chosen as a covariate as it is a major variant in diamond HDFs, is present in relatively high concentrations in every sample and consistently displays a primitive mantle normalized +ve anomaly on multi-element plots. The large variation in Pb concentrations, ranging from 0.01 times to 250 times primitive mantle values, means that Pb either dominates the signature or masks the effect of the signature in other elements (Table 4.1). Analysis of covariance (ANCOVA) was then employed as a general linear model with a continuous outcome variable i.e. Pb and two or more factors i.e. Type and Site. ANCOVA is a merger of ANOVA and regression analysis for continuous variables. ANCOVA tests whether certain factors have an effect on the outcome variable after removing the variance for which quantitative predictors (covariates) account. The inclusion of covariates can increase statistical power because it accounts for some of the variability. In this analysis we use ANOVA first to see whether a difference between factors exists and then re-analyze for the same trace element including Pb as a covariate. By doing analyses in series it is possible to understand how much of any observed difference between type or site of diamond is due Pb, probably in sulphide inclusions.

The factor Type has only two levels – gem or fibrous, but the factor Site has four levels and so either the ANOVA or ANCOVA analyses may find a significant difference due to Site. This then raises a question of between which levels of this factor a significant difference lays. In order to answer this question post hoc testing used the Tukey test among all levels of the factor Site, in order to assess among which pairs of levels differences lie. Significance of covariates factors or between

levels of a factor are all judged as being significant if they show a 95% or greater probability of not being zero. Where a significant factor or covariate is found, then the proportion of the total variance in the dataset explained by each significant factor or covariate is estimated (Worrall et al., (2001)).

Element	Type	Site	Variance explained	Where is different?
Cs	✓	✓	57%	Congo[1]
Rb	✓	×	19%	None
Ba	✓	✓	61%	Congo
Th	✓	×	20%	None
U	✓	×	7%	None
Nb	×	×	0%	None
La	×	×	0%	None
Ce	×	×	0%	None
Pr	×	×	0%	None
Sr	✓	×	13%	None
Nd	×	×	0%	None
Zr	×	✓	13%	C different from D & E
Zr	-	✓	13%	C different from D & E & S
Hf	×	✓	15%	Congo
Sm	×	×	0%	None
Eu	×	×	0%	None
Ti	×	✓	10%	E & and D & S
Gd	×	×	0%	None
Tb	×	×	0%	None
Dy	×	×	0%	None
Y	×	✓	10%	E & and D & S
Er	×	✓	9%	E & and D & S
Yb	×	✓	13%	Congo
Lu	×	✓	16%	Congo
Pb	×	✓	14%	Congo

Table 4.1. Analysis of variation based on diamond type (fibrous / monocrystalline) and Site (Ekati, Diavik, Snap Lake and Congo). No covariate is used and as such it is difficult to assign the variation in the data to a location or growth form. For example, the variation in Gd both in its concentration range through the data set and in its relation to other elements in the same diamond appears not to be influenced by the source location or diamond type.

[1] This is where Congo is different from all Canadian sites but the Canadian sites are not different from one another

Table 4.1 displays the resulting analyses without Pb as covariate. The predominant effect is that there is a difference among sites based upon ANOVA and that the post hoc tests suggest that this difference is most commonly between the Canadian samples and those from the Congo. The ANOVA rarely finds a significant difference between growth forms (Type). In this analysis, only for the elements Ba and Cs are both Type and Site factors both significant.

Using Pb as a covariate appears to lead to greater discrimination among sites. Table 4.2 highlights that when Pb is used as a covariable along with Type and Site factors then the signature of other elements plays a much more important role than previously suggested by ANOVA without a covariate. This is manifested as an increase in % variance explained by any given element and suggests that Pb concentrations are masking differences among diamond sources.

A key point from this table of values (Table 4.2) is that most of the variance in the data set can be explained by a two factor covariate model involving the LREEs La, Ce, Pr and Nd. The discriminatory power then rapidly decreases to the M- and HREEs. This makes some geochemical sense. In kimberlites, diamond HDFs and small-degree mantle melts in general, REE patterns are steep with enrichment towards the LREEs. As such, if significant chemical variation exists between diamonds from different geographical regions then it will be more evident in the LREE than in the HREE.

Element	Pb	Type	Site	Variance explained	Where is different?
Cs	×	✓	✓	57%	Congo
Rb	✓	✓	✓	52%	Congo
Ba	✓	✓	✓	69%	Congo
Th	✓	✓	✓	57%	Congo
U	✓	✓	×	14%	None
Nb	✓	×	×	11%	None
La	✓	×	✓	95%	Congo[2]
La	✓	-	✓	95%	C, D & E/S[3]
Ce	✓	×	✓	91%	E different from S
Ce	✓	-	✓	91%	S different from E and C
Pr	✓	✓	×	95%	None
Sr	✓	✓	✓	49%	C different from E and S
Nd	✓	✓	×	92%	C different from E and S[4]
Zr	✓	✓	✓	33%	Congo
Hf	✓	✓	✓	55%	Congo
Sm	✓	×	×	80%	None
Eu	✓	×	×	70%	None
Ti	×	×	✓	12%	E and D and S
Gd	×	×	×	0%	None
Tb	✓	×	×	56%	None
Dy	✓	×	×	48%	None
Y	✓	×	×	50%	None
Er	✓	×	×	48%	None
Yb	✓	×	×	67%	None
Lu	✓	×	✓	69%	None

Table 4.2. Analysis of variation based on diamond type (fibrous / monocrystalline) and Site (Ekati, Diavik, Snap Lake and Congo). Pb is used as a covariate and accounts for much of the variance allowing subtle differences to be used to discriminate source.

[2] When type is not significant these are re- analysed to focus on site.
[3] Ekati and Snap are not significantly different from each other
[4] In these types of case the overwhelming effect is due to the Pb covariate and type explains only a small proportion of the variance

Figure 4.1 demonstrates this principal by showing the much greater difference between maximum and minimum values in diamond HDFs for La, Ce, Pr and Nb and the much smaller difference in the HREEs. The LREEs can variably account for differences between each site (Table 4.2) as follows;

i) Congo from Canada; 95% variance explained using La from each Site with Pb as a covariate while including Type as a model factor,

ii) Congo from Diavik from Ekati/Snap Lake; 95% variance explained using La from each Site without the requirement to know or include the diamond Type as a model factor,

iii) Ekati from Snap Lake; 91% variance explained using Ce from each Site with Pb as a covariate including Type as a model factor,

iv) Snap Lake from Ekati from Congo; 91% variance explained using Ce from each Site without the need for knowing Type as a model factor,

v) Congo from Ekati from Snap; 92% variance explained using Nd from Type while including Site as a model factor.

vi) Pr could discriminate Type with 95% of the variance explained but could not distinguish source.

Assessing whether sample size is adequate for statistical approaches is key to evaluating their overall power of discrimination. This can be achieved via a power analysis.

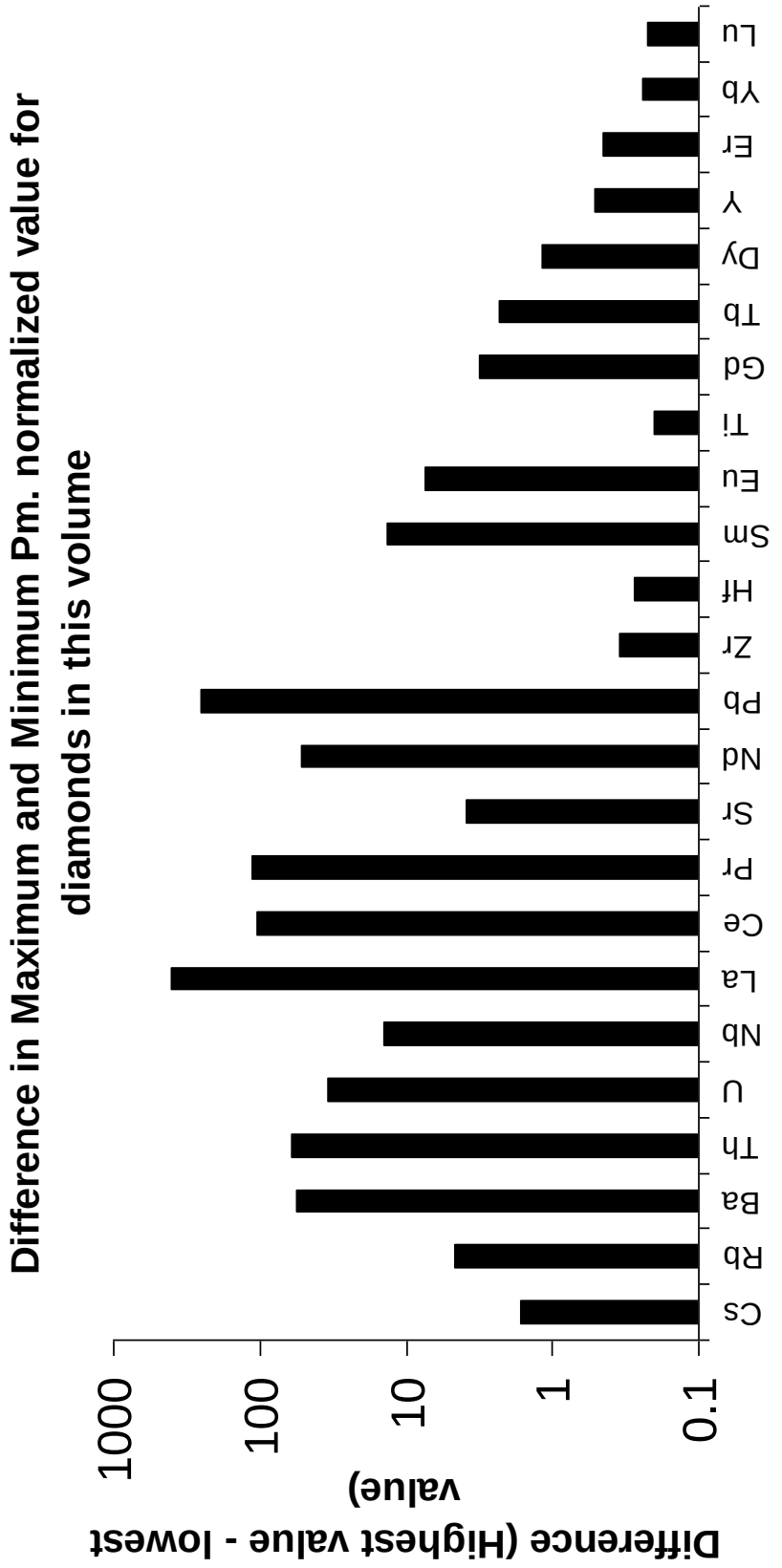

Figure 4.1. Plot demonstrating that the difference between the highest and lowest value reported for any given element in diamond is greater for the more incompatible elements compared to the HREEs. La, Ce, Pr and Nd are strong elements for source discrimination and show the greatest range in values whereas the HREEs display a much more narrow range in difference and as such are a weaker discriminatory tool as suggested by the ANOVA statistics.

Using La with Pb as a covariate, a power analysis was applied in the context of ANOVA in order to assess the probability of successfully rejecting a false null hypothesis (i.e. a Type II error). Power analysis can assist in this study by determining what sample size would be required in order to have a reasonable chance of rejecting the null hypothesis. Given the sample sizes and differences observed above the power is 0.999 i.e. power is equal to 1-β (β=the probability of false negative) and thus if power is 0.999 then the probability of the false negative is very small, hence the confidence that our ANOVA design would reject a false null hypothesis is very good. This suggests that our dataset is more than large enough to have arrived at the conclusions it has. Reversing this question, in terms of the sample size required to make an adequate discrimination between 2 particular localities, it is possible to predict that this methodology could detect a difference as large as that between Snap Lake and Congo with as few as 11 samples from each site.

Determining adequate sample sizes for the differentiation of diamond from different localities is an especially significant issue when using data acquired with the off-line LA-ICPMS method developed in this study. For the statistical techniques described here, and our given sample suite, a relatively small dataset (number of diamonds) is required. This tool will of course only have any merit if any difference exists between the diamonds being analyzed from source X and the source of their 'cover-name' Y. Nonetheless, it is shown above that there is potential for source discrimination to a level between sources that are very close together.

4.1B Logistic regression

Logistic Regression is used for prediction of the probability of occurrence of an event by fitting data to a logit function. It can be used when the target variable is a categorical variable e.g. Site (Snap Lake) with two categories i.e. Yes this sample is from Snap Lake versus No this sample is not from Snap Lake. Also, in our case the logistic regression involves a continuous target variable that has values in the range 0 to 1.0 representing probability values or proportions. A limitation in this application is that the sample has only one alternative to being from Snap Lake, i.e. not being from Snap Lake. The use of logistic regression is therefore not in distinguishing Sites from a dataset but rather eliminating the possibility of that sample being, or not being, from one particular Site.

In this study samples from Snap Lake and Ekati were considered and all trace elements were included in the logistic regression analysis. Logistic regression models are fitted using a maximum likelihood approach rather than the more usual least squares fitting procedure. The procedure included all 24 trace elements in the analyte list but only those significant at 95% level were included in the final model. Inclusion of trace element variables was by a step up and step down procedure to improve stability and physical interpretation of the final model. The fit of any derived linear model was assessed using the percentage concordance of the data at the 50:50 level of classification. For each significant variable included in the final model the odds ratio was also calculated in order to assess the importance of its inclusion. We may pose the question; ‘What is the probability of a sample being

from Snap Lake?' In a dataset that includes Ekati samples, i.e. "false" samples, the logistic regression can predict the probability of a diamond being from Snap Lake with a convincing degree of accuracy. The best-fit model was;

$$\log\left(\frac{\theta}{1-\theta}\right) = 27[Nb] + 677[Eu] - 32[Rb] - 8.4[Th] - 0.89$$

Where θ = the probability of the sample being from Snap Lake; [X] = the concentration of the given element X, primitive mantle normalized.

The model focuses on 4 geochemically distinct elements, Nb, Eu, Rb and Th. This particular equation is 91.2% concordant with n=90, i.e., for this size of sample-set it successfully distinguishes samples from Snap Lake with a 91% success rate. This principal is illustrated in Figure 4.2. The geographical distance between the Snap Lake and Ekati localities is ~200 km and so it is not unreasonable to expect some variation in the character of diamond-forming fluids (that provide the elemental signatures) over that distance.

As a test of the method's ability to discriminate diamonds derived from mines much closer in proximity (50 km), we examined data from the Diavik and Ekati properties, In this situation we can pose the question; 'What is the probability of a sample being from Diavik? Again in a dataset of 65 samples that includes 40 samples from Ekati the logistic regression equation that best separates Diavik from Ekati diamonds is;

$$\log\left(\frac{\theta}{1-\theta}\right) = 7[Nb] + 251[Eu] - 313[Rb] - 0.4[Th] - 1.45$$

Where θ = probability of the sample being from Diavik.

It is significant that the most successful approach utilizes the same 4 elements as in the Snap Lake – Ekati experiment. This equation is 93% concordant for n=65 and demonstrates that with Ekati as a common factor, Diavik is more different from Ekati diamonds than are Snap Lake diamonds. The equation overall has very high predictive power.

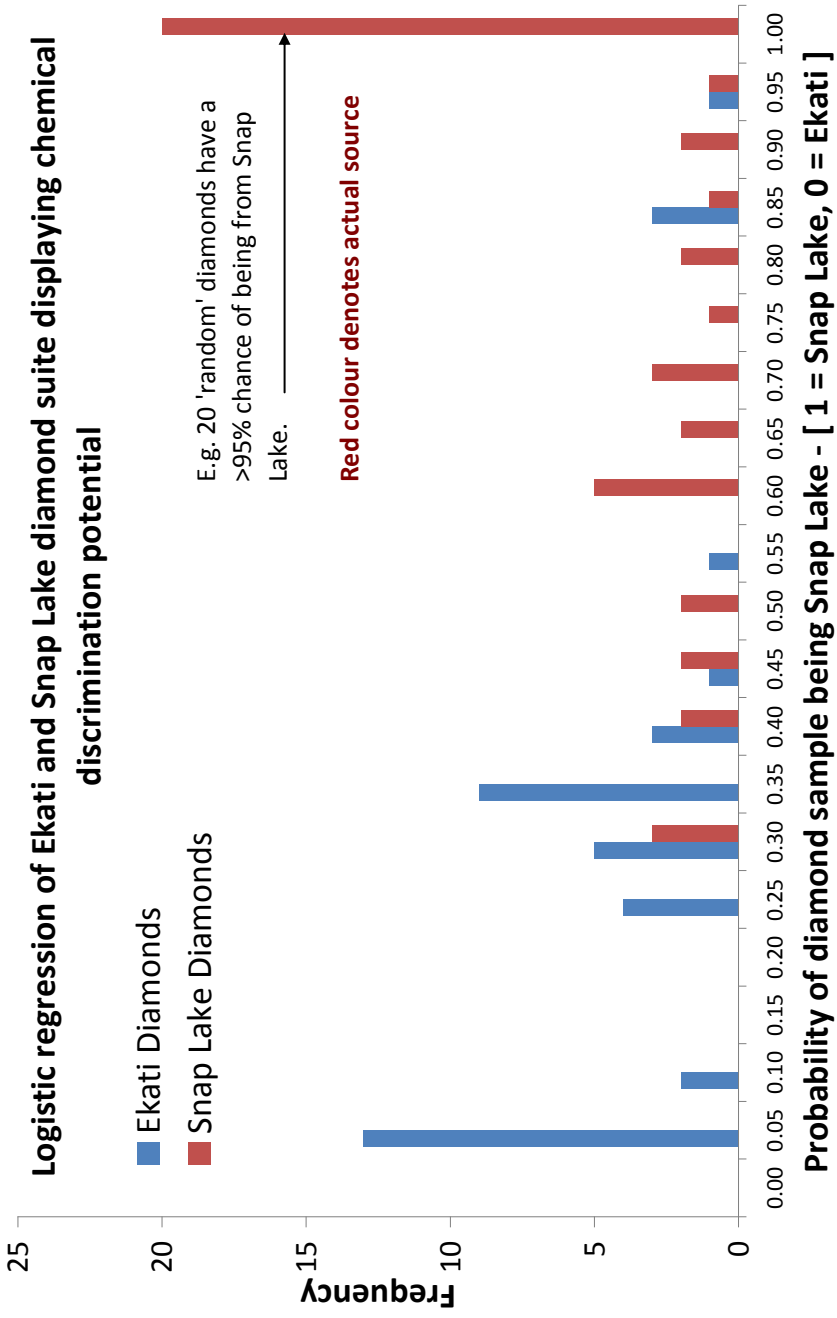

Figure 4.2. Histogram of the probability of a suite of Snap Lake and Ekati diamonds being discriminated from one another based on chemical difference. Blue diamonds, representing Ekati plot mostly towards low probability of being Snap Lake and red diamonds representing Snap Lake plot towards higher probabilities of being different from Ekati i.e. belonging to Snap Lake.

4.2 Summary

Careful application of both ANOVA and logistic regression analysis can be shown to have significant success in distinguishing diamonds form different geographic areas. From the above experiments it is clear that the application of logistic regression has the greatest potential in diamond fingerprinting. As with ANOVA tests, the sample in question can be tested against a known database and the probability of it belonging to that known family of locales can be assessed. These experiments with ANOVA and logistic regression demonstrate that even though geochemical signatures from diamond HDFs are broadly similar worldwide, possibly produced by a common mechanism of formation, there is sufficient systematic variation in particular trace elements to enable carefully applied modern statistical methods to discriminate between localities with high confidence levels. While the ability to resolve among mine productions from groups of kimberlites separated by as little as 50 km may at first be surprising, this probably reflects the multiple sources and processes likely involved in diamond genesis that combine to produce a wide variety of elemental signatures. To assess the full potential of these applications a much larger database needs to be accumulated of trace element concentrations in diamonds from other localities together with application of more rigorous and in-depth statistical approaches. Nonetheless, the method of logistical regression appears to be the most promising way forward in terms of its more straightforward application.

CHAPTER 5

Conclusion: Summary of findings and suggestions for future work

A novel offline laser ablation method has been developed to provide quantitative trace element concentrations in diamond with coupled radiogenic isotope compositions. Lattice impurities and high density fluid inclusions have been bulk sampled in over 120 diamonds. These components represent the diamond-forming fluid. Samples were fibrous cubes, octahedral fibrous coats on monocrystalline cores, low-purity monocrystalline diamonds and higher-purity 'gems' from the Ekati, Diavik and Snap Lake properties in the Slave Craton, Northwest Territories, Canada. Broad LILE enrichment, HFSE depletion and REE depletion is uniformly displayed by all diamonds. Major element compositions of individual fluid inclusions show volatile concentrations up to 50 wt. % and diamonds display $^{87}Sr/^{86}Sr$ initials ranging from 0.70386±0.00005 to 0.71107±0.0002 in fibrous diamonds and 0.70136±0.001 to 0.70864±0.00004 in monocrystalline diamonds. The broad range in $^{87}Sr/^{86}Sr(i)$ between unradiogenic and radiogenic values supports a mixing model between variable proportions of multiple endmembers. Coupled with our observed trace elements compositions these may comprise A] a component akin to convecting mantle, MORB, GI Kimberlites and B] at least one other component more akin to cryptically / modally metasomatized ancient and enriched lithosphere comprising Glimmerite, GII Kimberlites or their sources, Lamproite,

Deformed Peridotites, Phl-rich rock and PIC assemblages. We conclude that diamonds are forming from a primitive, volatile and carbonate-rich, silicate liquid from the convecting mantle that enters an ancient, metasomatically enriched and vein dominated lower lithosphere, interacts with the associated wall-rocks and mixes with locally sourced fluid/melt upon which carbon super-saturation and redox conditions allow carbon to crystallize. The diamond is later exhumed by kimberlitic volcanism. The fluids found in either fibrous, low-purity monocrystalline or 'gem' monocrystalline diamonds display similar trace element patterns, albeit at higher or lower concentration levels and fibrous and monocrystalline diamonds both show a large range in radiogenic $^{87}Sr/^{86}Sr(i)$. This suggests that they are formed from a similar parental fluid that has been derived through a similar mechanism.

There are many questions that have arisen during the method development and applied study. Tables 5.1 and 5.2 address the problems that remain unsolved and suggest directions that a continuation of this work may take. The application of this method as a diamond fingerprinting tool is one that is both feasible and straight-forward. It however assumes that there is a distinguishable difference to be found between diamonds from individual mines. The samples under question would be analyzed and matched to a database which would link the diamond to the source mine or not. We have demonstrated statistically that this can be done with a small database and three selected sources from the Slave craton. The answer will rarely be with 100% confidence due to the range in variation between chemical signatures of

diamonds from individual mines and the mimicking of that trend in diamonds from any given location.

This method reports high quality quantitative data but with low sample throughput. Whether as a petrogenetic tool or a fingerprinting tool, this method will be most powerful when used in conjunction with other techniques to characterize and acquire low-level information on diamond.

	Problem	Proposal
Table 5.1 Offline LA Method Development	1. Components of the diamond e.g. C is converted to CO_2 during ablation, which is not being collected or measured.	1. Modify the ablation cell to collect these components; a valve or port to vent the contents of the cell into another container prior to opening the cell for collection of trace elements.
	2. Bulk ablation of a diamond volume may incorporate both sub-microscopic solid mineral inclusions unrepresentative of the diamond HDF and/or incorporate separate growth events where fluid composition may have changed.	2. Use CL imaging of the diamond to target single event zones for ablation. EMPA results to identify the density of fluid inclusions and location of those inclusions would be extremely useful.
	3. Total procedural acid blanks are higher for most elements than 'gas' blanks. This increases the LOD and LOQ.	3. Increase volume of ablated material / ablation time. Blank contribution will not be increased. This study represents a minimum. Use higher purity acids at all stages including beaker cleaning and all sample processing. This will increase cost but lower TPBs and therefore LOD and LOQ
	. 4. No diamond ablation standard / ablation blank	4. High-purity HPHT synthetic diamonds potentially useful as ablation blank for some elements. Experiment with existing Boron-doped CVD diamond (Tallaire et al., 2010). (Diamond doping is a very cutting edge science and it is not possible for the majority of elements). Experiment with NIST glasses in combustion experiments to further confirm ablation accuracy.
	5. Combustion not confirmed with NIST glass as originally the combustion of diamond was used to confirm ball-park accuracy of ablation.	5. Experiment with NIST glasses to confirm combustion analyses.
	6. Sample throughput is low, limited by the rate at which the UV213 unit can efficiently ablate the diamond.	6. Use an IR laser so that energy can be increased while ablation efficiency is maintained. Greater volumes of diamonds can be ablated in shorter times.
	7. LOQ values based on 103 TPBs run over multiple analytical sessions. Thus is not representative of each analytical run.	7. Run a minimum of 30 TPBs with each analytical session.

Table 5.2 Further research on diamond HDFs using offline LA

	Proposal	Samples / Methods
	1. Confirm or reject the possibility of dating monocrystalline diamonds. Use radiogenic Sr compositions from individual growth zones and show a change in age towards outer zones.	1. CL imaged diamond plates with at least 150µm wide growth zones. Minimum of 3 core to rim analyses on each plate. Ablation volume must increase from this studies average.
	2. Acquire Nd and Pb on a samples.	2. Use PIMMS instrument dedicated to low-level analysis so that background will not swamp analyte signal. OR use TIMS or Nd
	3. Assess how all diamond colour variants affect trace element and/or isotope compositions.	3. From a single mine locality that displays various colours, analyze 20 of each variant. Compare the signature of those variants to samples from classic locations e.g. Pink diamonds from Argyle.
	4. Study the trace element compositions of syngenetic mineral inclusions and input them into a model that involves the host diamond compositions.	4. Samples should contain more than one included mineral phase. The study should encompass both eclogitic and peridotitic samples. Inclusions must be large enough for TE analysis and the diamond sample will need to be cracked.
	5. Evaluate the trace element and isotope systematics of different diamond parageneses, i.e. Websteritic, Eclogitic, Peridotitic, Type IIa (Moore, 2009) and Ultra High Pressure diamonds (Harte, 2010). Distinguish between parageneses if possible. Framesites and Carbonado should be included.	5. Access to these samples is straightforward. They exist in the academic community.
	6. All diamonds should preferably have multiple instrumental analyses performed on them prior to LA analysis. This will enable the detangling of otherwise very uniform trace element signatures. Destructive techniques should be performed post LA analysis.	6. Nitrogen aggregation data, CL imaging, Oxygen, Carbon and N isotopes, Nobel gases and Halogens analysis.
	7. Determine if significant chemical difference exists between diamonds from known civil-war conflict areas, e.g. can diamonds from Sierra Leone be distinguished from near by, cross-border legitimate sources?	7. EU Commissions and other global bodies must facilitate the discrete transfer of known samples of diamonds from conflict zones to the academic research community.

Bibliography

Agashev, A.M., Pokhilenko, N.P., Takazawa, E., McDonald, J.A., Vavilov, M.A., Watanabe, T., and Sobolev, N.V., 2008, Primary melting sequence of a deep (> 250 km) lithospheric mantle as recorded in the geochemistry of kimberlite-carbonatite assemblages, Snap Lake dyke system, Canada: Chemical Geology, v. 255, p. 317-328.

Akagi, T., 1999, Relationship of strontium isotope ratio and chemical composition of micro inclusions in fibrous diamonds: Implication for isotopically different components of the upper mantle: Geochemical Journal, v. 33, p. 101-107.

Akagi, T., and Masuda, A., 1988, Isotopic and elemental evidence for a relationship between kimberlite and Zaire cubic diamonds: Nature, v. 336, p. 665-667.

Anand, M., Taylor, L.A., Misra, K.C., Carlson, W.D., and Sobolev, N.V., 2004, Nature of diamonds in Yakutian eclogites: views from eclogite tomography and mineral inclusions in diamonds: Lithos, v. 77, p. 333-348.

Araújo, D.P., Griffin, W.L., and O'Reilly, S.Y., 2009a, Mantle melts, metasomatism and diamond formation: Insights from melt inclusions in xenoliths from Diavik, Slave Craton: Lithos, v. 112, p. 675-682.

Araújo, D.P., Griffin, W.L., O'Reilly, S.Y., Grant, K.J., Ireland, T., Holden, P., and van Achterbergh, E., 2009b, Microinclusions in monocrystalline octahedral diamonds and coated diamonds from Diavik, Slave Craton: Clues to diamond genesis: Lithos, v. 112, p. 724-735.

Aulbach, S., Griffin, W.L., Pearson, N.J., O'Reilly, S.Y., and Kivi, K., 2005, Os-Hf-Nd isotope Constraints on subcontinental lithospheric mantle evolution, Slave Craton (Canada): Geochimica et Cosmochimica Acta, v. 69, p. A284-A284.

Aulbach, S., Stachel, T., Creaser, R.A., Heaman, L.M., Shirey, S.B., Muehlenbachs, K., Eichenberg, D., and Harris, J.W., 2009, Sulphide survival and diamond genesis during formation and evolution of Archaean subcontinental lithosphere: A comparison between the Slave and Kaapvaal cratons: Lithos, v. 112, p. 747-757.

Becker, H., Jochum, K.P., and Carlson, R.W., 1999a, Constraints from high-pressure veins in eclogites on the composition of hydrous fluids in subduction zones: Chemical Geology, v. 160, p. 291-308.

Becker, H., Wenzel, T., and Volker, F., 1999b, Geochemistry of glimmerite veins in peridotites from lower Austria - Implications for the origin of K-rich magmas in collision zones: Journal of Petrology, v. 40, p. 315-338.

Becker, M., and Le Roex, A.P., 2006, Geochemistry of South African on- and off-craton, Group I and Group II kimberlites: Petrogenesis and source region evolution: Journal of Petrology, v. 47, p. 673-703.

Bedini, R.M., Bodinier, J.L., Dautria, J.M., and Morten, L., 1997, Evolution of LILE-enriched small melt fractions in the lithospheric mantle: a case study from the East African Rift: Earth and Planetary Science Letters, v. 153, p. 67-83.

Bibby, D.M., 1979, Zonal distribution of impurities in diamond: Geochimica et Cosmochimica Acta, v. 43, p. 415-423.

—, 1982, Impurities in Natural Diamond: Chemistry and Physics of Carbon, v. 18, p. 1-91.

Bizimis, M., Salters, V.M., and Dawson, J.B., 2003, The brevity of carbonatite sources in the mantle: evidence from Hf isotopes: Contributions to Mineralogy and Petrology, v. 145, p. 281-300.

Bleeker, W., Ketchum, J., Jackson, V., and Villeneuve, M., 1999, The Central Slave Basement Complex, Part I: its structural topology and autochthonous cover: Canadian Journal of Earth Sciences, v. 36, p. 1083-1109.

Bowen, D.C., Ferraris, R.D., Palmer, C.E., and Ward, J.D., 2009, On the unusual characteristics of the diamonds from Letseng-la-Terae kimberlites, Lesotho: Lithos, v. 112, p. 767-774.

Boyd, F.R., and Nixon, P.H., 1975, Origins of the ultramafic nodules from some kimberlites of northern Lesotho and the Monastery Mine, South Africa: Physics and Chemistry of The Earth, v. 9, p. 431-454.

Boyd, S.R., Mattey, D.P., Pillinger, C.T., Milledge, H.J., Mendelssohn, M., and Seal, M., 1987, Multiple growth events during diamond genesis: an integrated study of carbon and nitrogen isotopes and nitrogen aggregation state in coated stones: Earth and Planetary Science Letters, v. 86, p. 341-353.

Boyd, S.R., and Pillinger, C.T., 1994, A preliminary study of in octahedral growth form diamonds: Chemical Geology, v. 116, p. 43-59.

Boyd, S.R., Pillinger, C.T., Milledge, H.J., Mendelssohn, M.J., and Seal, M., 1992, C and N isotopic composition and the infrared absorption spectra of coated diamonds: evidence for the regional uniformity of CO_2-H_2O rich fluids in lithospheric mantle: Earth and Planetary Science Letters, v. 109, p. 633-644.

Boyd, S.R., Pineau, F., and Javoy, M., 1994, Modelling the growth of natural diamonds: Chemical Geology, v. 116, p. 29-42.

Brenker, F.E., Stachel, T., and Harris, J.W., 2002, Exhumation of lower mantle inclusions in diamond: ATEM investigation of retrograde phase transitions, reactions and exsolution: Earth and Planetary Science Letters, v. 198, p. 1-9.

Brenker, F.E., Vincze, L., Vekemans, B., Nasdala, L., Stachel, T., Vollmer, C., Kersten, M., Somogyi, A., Adams, F., Joswig, W., and Harris, J.W., 2005, Detection of a Ca-rich lithology in the Earth's deep (> 300 km) convecting mantle: Earth and Planetary Science Letters, v. 236, p. 579-587.

Brenker, F.E., Vollmer, C., Vincze, L., Vekemans, B., Szymanski, A., Janssens, K., Szaloki, I., Nasdala, L., Joswig, W., and Kaminsky, F., 2007, Carbonates from the lower part of transition zone or even the lower mantle: Earth and Planetary Science Letters, v. 260, p. 1-9.

Brey, G.P., Bulatov, V., Girnis, A., Harris, J.W., and Stachel, T., 2004, Ferropericlase--a lower mantle phase in the upper mantle: Lithos, v. 77, p. 655-663.

Brey, G.P., Kogarko, L.N., and Ryabchikov, I.D., 1991, Carbon dioxide in kimberlitic melts: Neues Jahrbuch Fur Mineralogie-Monatshefte, p. 159-168.

Bulanova, G.P., 1995, The formation of diamond: Journal of Geochemical Exploration, v. 53, p. 1-23.

Bulanova, G.P., Muchemwa, E., Pearson, D.G., Griffin, B.J., Kelley, S.P., Klemme, S., and Smith, C.B., 2004, Syngenetic inclusions of yimengite in diamond from Sese kimberlite (Zimbabwe) -- evidence for metasomatic conditions of growth: Lithos, v. 77, p. 181-192.

Bulanova, G.P., Pearson, D.G., Hauri, E.H., and Griffin, B.J., 2002, Carbon and nitrogen isotope systematics within a sector-growth diamond from the Mir kimberlite, Yakutia: Chemical Geology, v. 188, p. 105-123.

Burgess, R., Cartigny, P., Harrison, D., Hobson, E., and Harris, J., 2009, Volatile composition of microinclusions in diamonds from the Panda kimberlite, Canada: Implications for chemical and isotopic heterogeneity in the mantle: Geochimica et Cosmochimica Acta, v. 73, p. 1779-1794.

Burgess, R., Johnson, L.H., Mattey, D.P., Harris, J.W., and Turner, G., 1998, He, Ar and C isotopes in coated and polycrystalline diamonds: Chemical Geology, v. 146, p. 205-217.

Burgess, R., Kiviets, G.B., and Harris, J.W., 2004, Ar-Ar age determinations of eclogitic clinopyroxene and garnet inclusions in diamonds from the Venetia and Orapa kimberlites: Lithos, v. 77, p. 113-124.

Burgess, R., Layzelle, E., Turner, G., and Harris, J.W., 2002, Constraints on the age and halogen composition of mantle fluids in Siberian coated diamonds: Earth and Planetary Science Letters, v. 197, p. 193-203.

Burgess, R., Turner, G., Laurenzi, M., and Harris, J.W., 1989, 40Ar39Ar laser probe dating of individual clinopyroxene inclusions in Premier eclogitic diamonds: Earth and Planetary Science Letters, v. 94, p. 22-28.

Butler, J.E., Mankelevich, Y.A., Cheesman, A., Ma, J., and Ashfold, M.N.R., 2009, Understanding the chemical vapor deposition of diamond: recent progress: Journal of Physics-Condensed Matter, v. 21.

Carlson, R.W., and Irving, A.J., 1994, Depletion and enrichment history of subcontinental lithospheric mantle: An Os, Sr, Nd and Pb isotopic study of ultramafic xenoliths from the northwestern Wyoming Craton: Earth and Planetary Science Letters, v. 126, p. 457-472.

Cartigny, P., 2010, Mantle-related carbonados? Geochemical insights from diamonds from the Dachine komatiite (French Guiana): Earth and Planetary Science Letters, v. 296, p. 329-339.

Cartigny, P., De Corte, K., Shatsky, V.S., Ader, M., De Paepe, P., Sobolev, N.V., and Javoy, M., 2001a, The origin and formation of metamorphic microdiamonds from the Kokchetav massif, Kazakhstan: a nitrogen and carbon isotopic study: Chemical Geology, v. 176, p. 265-281.

Cartigny, P., Farquhar, J., Thomassot, E., Harris, J.W., Wing, B., Masterson, A., McKeegan, K., and Stachel, T., 2009, A mantle origin for Paleoarchean peridotitic diamonds from the Panda kimberlite, Slave Craton: Evidence from 13C-, 15N- and 33,34S-stable isotope systematics: Lithos, v. 112, p. 852-864.

Cartigny, P., Harris, J.W., and Javoy, M., 2001b, Diamond genesis, mantle fractionations and mantle nitrogen content: a study of [delta]13C-N concentrations in diamonds: Earth and Planetary Science Letters, v. 185, p. 85-98.

Cartigny, P., Harris, J.W., Phillips, D., Girard, M., and Javoy, M., 1998, Subduction-related diamonds? - The evidence for a mantle-derived origin from coupled $\delta^{13}C$-$\delta^{15}N$ determinations: Chemical Geology, v. 147, p. 147-159.

Cartigny, P., Harris, J.W., Taylor, A., Davies, R., and Javoy, M., 2003, On the possibility of a kinetic fractionation of nitrogen stable isotopes during natural diamond growth: Geochimica et Cosmochimica Acta, v. 67, p. 1571-1576.

Charlier, B.L.A., Ginibre, C., Morgan, D., Nowell, G.M., Pearson, D.G., Davidson, J.P., and Ottley, C.J., 2006, Methods for the microsampling and high-precision analysis of strontium and rubidium isotopes at single crystal scale for petrological and geochronological applications: Chemical Geology, v. 232, p. 114-133.

Chrenko, R.M., McDonald, R.S., and Darrow, K.A., 1967, Infra-red spectra of diamond coat: Nature, v. 213, p. 474-&.

Coe, N., 2004, Petrogenesis of the Swartruggens and Star Group II kimberlite dyke swarms, South Africa, University of Cape Town.

Creaser, R.A., Grütter, H., Carlson, J., and Crawford, B., 2004, Macrocrystal phlogopite Rb-Sr dates for the Ekati property kimberlites, Slave Province, Canada: evidence for multiple intrusive episodes in the Paleocene and Eocene: Lithos, v. 76, p. 399-414.

Currie, L.A., 1968, Limits for qualitative detection and quantitative determination - Application to radiochemistry: Analytical Chemistry, v. 40, p. 586-&.

—, 1999a, Detection and quantification limits: origins and historical overview: Analytica Chimica Acta, v. 391, p. 127-134.

—, 1999b, International recommendations offered on analytical detection and quantification concepts and nomenclature: Analytica Chimica Acta, v. 391, p. 103-103.

—, 1999c, Nomenclature in evaluation of analytical methods including detection and quantification capabilities (IUPAC Recommendations 1995): Analytica Chimica Acta, v. 391, p. 105-126.

Davies, G., 1999, Current problems in diamond: towards a quantitative understanding: Physica B-Condensed Matter, v. 274, p. 15-23.

Davies, R.M., Griffin, W.L., O'Reilly, S.Y., and Andrew, A.S., 2003, Unusual mineral inclusions and carbon isotopes of alluvial diamonds from Bingara, eastern Australia: Lithos, v. 69, p. 51-66.

Davies, R.M., Griffin, W.L., O'Reilly, S.Y., and McCandless, T.E., 2004, Inclusions in diamonds from the K14 and K10 kimberlites, Buffalo Hills, Alberta, Canada: diamond growth in a plume?: Lithos, v. 77, p. 99-111.

Davis, W.J., Jones, A.G., Bleeker, W., and Grütter, H., 2003, Lithosphere development in the Slave craton: a linked crustal and mantle perspective: Lithos, v. 71, p. 575-589.

Deines, P., and Harris, J.W., 1995, Sulfide inclusion chemistry and carbon isotopes of African diamonds: Geochimica et Cosmochimica Acta, v. 59, p. 3173-3188.

Deines, P., Harris, J.W., and Gurney, J.J., 1997, Carbon isotope ratios, nitrogen content and aggregation state, and inclusion chemistry of diamonds from

Jwaneng, Botswana: Geochimica et Cosmochimica Acta, v. 61, p. 3993-4005.

Donnelly, C.L., Stachel, T., Creighton, S., Muehlenbachs, K., and Whiteford, S., 2007, Diamonds and their mineral inclusions from the A154 South pipe, Diavik Diamond Mine, Northwest territories, Canada: Lithos, v. 98, p. 160-176.

Erlank A.J, Waters F.G, Hawkesworth C.J, Haggerty S.F, Allsopp H.L, Rickard R.S, and Menzies, M., 1987, Evidence for mantle metasomatism in peridotite nodules from the Kimberley pipes, South Africa, *in* Menzies M.A, and C.J., H., eds., Mantle Metasomatism: London, New York, Academic Press, p. 221-290.

Fedortchouk, Y., Matveev, S., and Carlson, J.A., 2010, H2O and CO2 in kimberlitic fluid as recorded by diamonds and olivines in several Ekati Diamond Mine kimberlites, Northwest Territories, Canada: Earth and Planetary Science Letters, v. 289, p. 549-559.

Fesq, H.W., Bibby, D.M., Erasmus, C.S., Kable, E.J.D., and Sellschop, J.P.F., 1975, A comparative trace element study of diamonds from Premier, Finsch and Jagersfontein mines, South Africa: Physics and Chemistry of The Earth, v. 9, p. 817-836.

Field, M., Stiefenhofer, J., Robey, J., and Kurszlaukis, S., 2008, Kimberlite-hosted diamond deposits of southern Africa: A review: Ore Geology Reviews, v. 34, p. 33-75.

Fisher, D., Sibley, S.J., and Kelly, C.J., 2009, Brown colour in natural diamond and interaction between the brown related and other colour-inducing defects: Journal of Physics-Condensed Matter, v. 21.

Foley, S., 1992, Vein-plus-wall-rock melting mechanisms in the lithosphere and the origin of potassic alkaline magmas: Lithos, v. 28, p. 435-453.

Foley, S.F., 1994, Gochemical and experimental studies of the origin of ultrapotassic igneous rock: Neues Jahrbuch Fur Mineralogie-Abhandlungen, v. 167, p. 1-55.

Font, L., Nowell, G.N., Pearson, D.G., Ottley,CJ., Willis, S.G., 2007, Sr isotope analysis of bird feathers by TIMS: a tool to trace bird migration paths and breeding sites: J. Anal. At. Spectrom., v. 22, 513–522.

Fujita, N., Jones, R., Öberg, S., and Briddon, P.R., Large spherical vacancy clusters in diamond - Origin of the brown colouration?: Diamond and Related Materials, v. 18, p. 843-845.

Gasparik, T., and Hutchison, M.T., 2000, Experimental evidence for the origin of two kinds of inclusions in diamonds from the deep mantle: Earth and Planetary Science Letters, v. 181, p. 103-114.

Girnis, A.V., Brey, G.P., and Ryabchikov, I.D., 1995, Origin of Group 1A kimberlites: Fluid-saturated melting experiments at 45-55 kbar: Earth and Planetary Science Letters, v. 134, p. 283-296.

Girnis, A.V., Bulatov, V.K., and Brey, G.P., 2005a, Transition from kimberlite to carbonatite melt under mantle parameters: An experimental study: Petrology, v. 13, p. 1-15.

Girnis, A.V., and Ryabchikov, I.D., 2005b, Conditions and mechanisms of generation of kimberlite magmas: Geology of Ore Deposits, v. 47, p. 476-487.

Grégoire, Grégoire, M., Bell, Bell, D., Le, R., and Roex, A.L., 2002, Trace element geochemistry of phlogopite-rich mafic mantle xenoliths: their classification and their relationship to phlogopite-bearing peridotites and kimberlites revisited: Contributions to Mineralogy and Petrology, v. 142, p. 603-625.

Gregoire, M., Bell, D.R., and Le Roex, A.P., 2003, Garnet lherzolites from the Kaapvaal craton (South Africa): Trace element evidence for a metasomatic history: Journal of Petrology, v. 44, p. 629-657.

Grey, I.E., Madsen, I.C., and Haggerty, S.E., 1987, Structure of a new upper mantle, Magnetoplumbite-type phase, Ba Ti3Cr4Fe4Mg O19: American Mineralogist, v. 72, p. 633-636.

Griffin, W.L., Doyle, B.J., Ryan, C.G., Pearson, N.J., O'Reilly, S.Y., Davies, R., Kivi, K., Van Achterbergh, E., and Natapov, L.M., 1999, Layered mantle lithosphere in the Lac de Gras area, Slave Craton: Composition, structure and origin: Journal of Petrology, v. 40, p. 705-727.

Griffin, W.L., Rege, S., O'Reilly, S.Y., Jackson, S.E., Pearson, N.J., Zedgenizov, D., and Kurat, G., 2006, Trace-element patterns of diamond: Toward a unified genetic model: Geochimica et Cosmochimica Acta, v. 70, p. A218-A218.

Gurney, J.J., and Harte, B., 1980, Chemical Variations in Upper Mantle Nodules from Southern African Kimberlites: Philosophical Transactions of the Royal Society of London. Series A, Mathematical and Physical Sciences, v. 297, p. 273-293.

Gurney, J.J., Helmstaedt, H.H., Richardson, S.H., and Shirey, S.B., 2010, Diamonds through Time: Economic Geology, v. 105, p. 689-712.

Gurney, J.J., Helmstaedt, H.H., Le Roux, A.P., Nowicki, T.E., Richardson, S.H. & Westerland, K.J., 2005, Diamonds: crustal distribution and formation processes in time and space and an integrated deposit model: Economic Geology 100th Anniversary Volume, v. 100, p. 143-178.

Gurney, J.J., Hildebrand, P.R., Carlson, J.A., Fedortchouk, Y., and Dyck, D.R., 2004, The morphological characteristics of diamonds from the Ekati property, Northwest Territories, Canada: Lithos, v. 77, p. 21-38.

Guthrie, G.D., Veblen, D.R., Navon, O., and Rossman, G.R., 1991, Submicrometer fluid-inclusion in turbid diamond coat: Earth and Planetary Science Letters, v. 105, p. 1-12.

Haggerty, S.E., 1987, Metasomatic mineral titanates in upper mantle xenoliths, *in* Nixon, P.H., ed., Mantle Xenoliths: Chichester, Wiley, p. 671-690.

Harlou, R., Pearson, D.G., Nowell, G.M., Ottley, C.J., and Davidson, J.P., 2009, Combined Sr isotope and trace element analysis of melt inclusions at sub-ng levels using micro-milling, TIMS and ICPMS: Chemical Geology, v. 260, p. 254-268.

Harris, J.W., 1992, Diamond Geology, *in* Field, J.E., ed., The properties of natural and synthetic diamond: London, Academic Press, p. 345-393.

Harris, J.W., Hawthorne, J.B., Osterweld, M.M., 1979, Regional and local variation in the characteristics of diamonds from some southern african kimberlites, *in*

Boyd, F.R., and Meyer, H.O.A., ed., Kimberlites, diatremes, and diamonds: their geology, petrology, and geochemistry American Geophysical Union, p. 399.

Harris, P.G., and Middlemost, E.A.K., 1970, The evolution of kimberlites: Lithos, v. 3, p. 77-88.

Harte, B., 1983, Mantle peridotites and processes - the kimberlite sample, Continental Basalts and Mantle Xenoliths, Shiva, Nantwich, p. 46-91.

—, 2010, Diamond formation in the deep mantle: the record of mineral inclusions and their distribution in relation to mantle dehydration zones: Mineralogical Magazine, v. 74, p. 189-215.

Harte, B., Hunter, R.H., and Kinny, P.D., 1993, Melt geometry, movement and crystallization, in relation to mantle dykes, veins and metasomatism: Philosophical Transactions of the Royal Society of London Series a-Mathematical Physical and Engineering Sciences, v. 342, p. 1-21.

Harte, B., and Kirkley, M.B., 1997, Partitioning of trace elements between clinopyroxene and garnet: Data from mantle eclogites: Chemical Geology, v. 136, p. 1-24.

Heaman, L.M., Kjarsgaard, B.A., and Creaser, R.A., 2003, The timing of kimberlite magmatism in North America: implications for global kimberlite genesis and diamond exploration: Lithos, v. 71, p. 153-184.

—, 2004, The temporal evolution of North American kimberlites: Lithos, v. 76, p. 377-397.

Heaman, L.M., and Pearson, D.G., 2010, Nature and evolution of the Slave Province subcontinental lithospheric mantle: Canadian Journal of Earth Sciences, v. 47, p. 369-388.

Helmstaedt, H., 2009, Crust-mantle coupling revisited: The Archean Slave craton, NWT, Canada: Lithos, v. 112, p. 1055-1068.

Hoffman, P.F., 1989, Precambrian geology and tectonic history of North America, *in* Bally, A.W.a.P., A.R., ed., The Geology of North America - An Overview: Boulder, Colorado Geological Society of America, p. 447-512.

Hutchison, M.T., Nixon, P.H., and Harley, S.L., 2004, Corundum inclusions in diamonds--discriminatory criteria and a corundum compositional dataset: Lithos, v. 77, p. 273-286.

Ionov, D.A., Dupuy, C., O'Reilly, S.Y., Kopylova, M.G., and Genshaft, Y.S., 1993, Carbonated peridotite xenoliths from Spitsbergen: implications for trace element signature of mantle carbonate metasomatism: Earth and Planetary Science Letters, v. 119, p. 283-297.

Irvine, G.J., Pearson, D.G., Kjarsgaard, B.A., Carlson, R.W., Kopylova, M.G., and Dreibus, G., 2003, A Re-Os isotope and PGE study of kimberlite-derived peridotite xenoliths from Somerset Island and a comparison to the Slave and Kaapvaal cratons: Lithos, v. 71, p. 461-488.

Izraeli, E.S., Harris, J.W., and Navon, O., 1999, Raman barometry of diamond formation: Earth and Planetary Science Letters, v. 173, p. 351-360.

—, 2001, Brine inclusions in diamonds: a new upper mantle fluid: Earth and Planetary Science Letters, v. 187, p. 323-332.

—, 2004, Fluid and mineral inclusions in cloudy diamonds from Koffiefontein, South Africa: Geochimica et Cosmochimica Acta, v. 68, p. 2561-2575.

Johnson, L.H., Burgess, R., Turner, G., and Harris, J.W., 2000, Noble gas and halogen geochemistry of mantle fluids: Comparison of African and Canadian diamonds: Geochimica et Cosmochimica Acta, v. 64, p. 717-732.

Jones, A.P., 1989, Upper-mantle enrichment by kimberlitic or carbonatitic magmatism, *in* Bell, K., ed., Carbonatites; Genesis and Evolution: London, Unwin Hyman, p. 448-463.

Jones, A.P., Smith, J.V., and Dawson, J.B., 1982, Mantle Metasomatism in 14 Veined Peridotites from Bultfontein Mine, South Africa: The Journal of Geology, v. 90, p. 435-453.

Jones, J.H., Walker, D., Pickett, D.A., Murrell, M.T., and Beattie, P., 1995, Experimental investigations of the partitioning of Nb, Mo, Ba, Ce, Pb, Ra, Th, Pa, and U between immiscible carbonate and silicate liquids: Geochimica et Cosmochimica Acta, v. 59, p. 1307-1320.

Kamenetsky, M.B., Sobolev, A.V., Kamenetsky, V.S., Maas, R., Danyushevsky, L.V., Thomas, R., Pokhilenko, N.P., and Sobolev, N.V., 2004, Kimberlite melts rich in alkali chlorides and carbonates: A potent metasomatic agent in the mantle: Geology, v. 32, p. 845-848.

Kaminsky, F.V., and Khachatryan, G.K., 2004a, The relationship between the distribution of nitrogen impurity centres in diamond crystals and their internal structure and mechanism of growth: Lithos, v. 77, p. 255-271.

Kaminsky, F.V., Khachatryan, G.K., Andreazza, P., Araujo, D., and Griffin, W.L., 2009, Super-deep diamonds from kimberlites in the Juina area, Mato Grosso State, Brazil: Lithos, v. 112, p. 833-842.

Kaminsky, F.V., Sablukov, S.M., Belousova, E.A., Andreazza, P., Tremblay, M., and Griffin, W.L., 2010, Kimberlitic sources of super-deep diamonds in the Juina area, Mato Grosso State, Brazil: Lithos, v. 114, p. 16-29.

Kaminsky, F.V., Sablukov, S.M., Sablukova, L.I., and Channer, D.M.D., 2004b, Neoproterozoic anomalous kimberlites of Guaniamo, Venezuela: Mica kimberlites of isotopic transitional type: Lithos, v. 76, p. 565-590.

Kato, T., Ringwood, A.E., and Irifune, T., 1988, Experimental determination of element partitioning between silicate perovskites, garnets and liquids: constraints on early differentiation of the mantle: Earth and Planetary Science Letters, v. 89, p. 123-145.

Keshav, S., Corgne, A., Gudfinnsson, G.H., Bizimis, M., McDonough, W.F., and Fei, Y., 2005, Kimberlite petrogenesis: Insights from clinopyroxene-melt partitioning experiments at 6 GPa in the CaO-MgO-Al_2O_3-SiO_2-CO_2 system: Geochimica et Cosmochimica Acta, v. 69, p. 2829-2845.

Kessel, R., Ulmer, P., Pettke, T., Schmidt, M.W., and Thompson, A.B., 2005, The water-basalt system at 4 to 6 GPa: Phase relations and second critical endpoint in a K-free eclogite at 700 to 1400 °C: Earth and Planetary Science Letters, v. 237, p. 873-892.

Khazan, Y., and Fialko, Y., 2005, Why do kimberlites from different provinces have similar trace element patterns?: Geochemistry Geophysics Geosystems, v. 6.

Kjarsgaard, B.A., 2007, Kimberlite diamond deposits *in* Goodfellow, W.D., ed., Mineral deposits of Canada: A Synthesis of Major Deposit-Types, District Metallogeny, the Evolution of Geological Provences, and Exploration Models, Volume 5, Special Publication, p. 245-272.

Kjarsgaard, B.A., Pearson, D.G., Tappe, S., Nowell, G.M., and Dowall, D.P., 2009, Geochemistry of hypabyssal kimberlites from Lac de Gras, Canada: Comparisons to a global database and applications to the parent magma problem: Lithos, v. 112, p. 236-248.

Klein-BenDavid, O., and Graham Pearson, D., 2009, Origins of subcalcic garnets and their relation to diamond forming fluids--Case studies from Ekati (NWT-Canada) and Murowa (Zimbabwe): Geochimica et Cosmochimica Acta, v. 73, p. 837-855.

Klein-BenDavid, O., Izraeli, E.S., Hauri, E., and Navon, O., 2004, Mantle fluid evolution--a tale of one diamond: Lithos, v. 77, p. 243-253.

—, 2007, Fluid inclusions in diamonds from the Diavik mine, Canada and the evolution of diamond-forming fluids: Geochimica et Cosmochimica Acta, v. 71, p. 723-744.

Klein-BenDavid, O., Logvinova, A.M., Schrauder, M., Spetius, Z.V., Weiss, Y., Hauri, E.H., Kaminsky, F.V., Sobolev, N.V., and Navon, O., 2009, High-Mg carbonatitic microinclusions in some Yakutian diamonds--a new type of diamond-forming fluid: Lithos, v. 112, p. 648-659.

Klein-BenDavid, O., Pearson, D.G., Nowell, G.M., Ottley, C., McNeill, J.C.R., and Cartigny, P., 2010, Mixed fluid sources involved in diamond growth constrained by Sr-Nd-Pb-C-N isotopes and trace elements: Earth and Planetary Science Letters, v. 289, p. 123-133.

Kong, X., and Cheng, P., 2010, Application of Nanodiamonds in Biomolecular Mass Spectrometry: Materials, v. 3, p. 1845-1862.

Kopylova, M., Navon, O., Dubrovinsky, L., and Khachatryan, G., 2010, Carbonatitic mineralogy of natural diamond-forming fluids: Earth and Planetary Science Letters, v. 291, p. 126-137.

Kramers, J.D., Roddick, J.C.M., and Dawson, J.B., 1983, Trace element and isotope studies on veined, metasomatic and "MARID" xenoliths from Bultfontein, South Africa: Earth and Planetary Science Letters, v. 65, p. 90-106.

Kusky, T.M., 1989, Accretion of the Archean Slave Province: Geology, v. 17, p. 63-67.

Laiginhas, F., Pearson, D.G., Phillips, D., Burgess, R., and Harris, J.W., 2009, Re-Os and 40Ar/39Ar isotope measurements of inclusions in alluvial diamonds from the Ural Mountains: Constraints on diamond genesis and eruption ages: Lithos, v. 112, p. 714-723.

Lang, A.R., and Walmsley, J.C., 1983, Apatite inclusions in natural diamond coat: Physics and Chemistry of Minerals, v. 9, p. 6-8.

Le Roex, A.P., Bell, D.R., and Davis, P., 2003, Petrogenesis of group I kimberlites from Kimberley, South Africa: Evidence from bulk-rock geochemistry: Journal of Petrology, v. 44, p. 2261-2286.

Litvin, Y.A., 2009, The physicochemical conditions of diamond formation in the mantle matter: experimental studies: Russian Geology and Geophysics, v. 50, p. 1188-1200.

Malkovets, V.G., Griffin, W.L., O'Reilly, S.Y., and Wood, B.J., 2007, Diamond, subcalcic garnet, and mantle metasomatism: Kimberlite sampling patterns define the link: Geology, v. 35, p. 339-342.

McDonough, W.F., 1990, Constraints on the composition of the continental lithospheric mantle: Earth and Planetary Science Letters, v. 101, p. 1-18.

—, 2001, Chapter 1 The composition of the earth, *in* Roman, T., and Eugeniusz, M., eds., International Geophysics, Volume Volume 76, Academic Press, p. 3-23.

—, 2003, Compositional Model for the Earth's Core, *in* Heinrich, D.H., and Karl, K.T., eds., Treatise on Geochemistry: Oxford, Pergamon, p. 547-568.

McDonough, W.F., and Sun, S.S., 1988, A primitive mantle composition from xenoliths: Chemical Geology, v. 70, p. 12-12.

McDonough, W.F., and Sun, S.s., 1995, The composition of the Earth: Chemical Geology, v. 120, p. 223-253.

McKenzie, D., 1989, Some remarks on the movement of small melt fractions in the mantle: Earth and Planetary Science Letters, v. 95, p. 53-72.

McNeill, J., Pearson, D.G., Klein-BenDavid, O., Nowell, G.M., Ottley, C.J., and Chinn, I., 2009, Quantitative analysis of trace element concentrations in some gem-quality diamonds: Journal of Physics-Condensed Matter, v. 21, 36.

Meyer, H.O.A., 1985, Genesis od diamond - A mantle saga: American Mineralogist, v. 70, p. 344-355.

Meyer, H.O.A., and Boyd, F.R., 1972, Composition and origin of crystalline inclusions in natural diamonds.: Geochimica Cosmochimica Acta, v. 36, p. 18.

Mitchell, R.H., 2008, Petrology of hypabyssal kimberlites: Relevance to primary magma compositions: Journal of Volcanology and Geothermal Research, v. 174, p. 1-8.

Mitchell, R.H., and Bergman, S.C., 1991, Petrology of Lamproites: New York, London, Plenum Press.

Moore, A.E., 2009, Type II diamonds: Flamboyant Megacrysts?: South African Journal of Geology, v. 112, p. 23-38.

Moss, S., Russell, J.K., Brett, R.C., and Andrews, G.D.M., 2009, Spatial and temporal evolution of kimberlite magma at A154N, Diavik, Northwest Territories, Canada: Lithos, v. 112, p. 541-552.

Navon, O., 1999, Formation of diamonds in the Earth's Mantle, *in* Gurney, J.J., Gurney, J.L., Pasque, M.D. and Richardson, S.H., ed., Proc. of the VIIth International Kimberlitic Conference, Red Roof Design, Cape Town, South Africa, p. 584-604.

Navon, O., Hutcheon, I.D., Rossman, G.R., and Wasserburg, G.J., 1988, Mantle-derived fluid in diamond micro-iclusions: Nature, v. 335, p. 784-789.

Navon, O., and Stolper, E., 1987, Geochemical Consequences of Melt Percolation: The Upper Mantle as a Chromatographic Column: The Journal of Geology, v. 95, p. 285-307.

Nelson, D.R., 1989, Isotopic characteristics and petrogenesis of the lamproites and kimberlites of central west Greenland: Lithos, v. 22, p. 265-274.

Nixon, P.H., 1995, A review of mantle xenoliths and their role in diamond exploration: Journal of Geodynamics, v. 20, p. 305-329.

Nixon, P.H., and Condliffe, E., 1989, Yimengite of K-Ti metasomatic origin in kimberlitic rocks from Venezuela: Mineralogical Magazine, v. 53, p. 305-309.

Nixon, P.H., Davies, G.R., Rex, D.C., and Gray, A., 1992, Venezuela kimberlites: Journal of Volcanology and Geothermal Research, v. 50, p. 101-115.

Nowell, G.M., Pearson, D.G., Bell, D.R., Carlson, R.W., Smith, C.B., Kempton, P.D., and Noble, S.R., 2004, Hf isotope systematics of kimberlites and their megacrysts: New constraints on their source regions: Journal of Petrology, v. 45, p. 1583-1612.

Nowicki, T., Crawford, B., Dyck, D., Carlson, J., McElroy, R., Oshust, P., and Helmstaedt, H., 2004, The geology of kimberlite pipes of the Ekati property, Northwest Territories, Canada: Lithos, v. 76, p. 1-27.

Nowicki, T., Porritt, L., Crawford, B., and Kjarsgaard, B., 2008, Geochemical trends in kimberlites of the Ekati property, Northwest Territories, Canada: Insights on volcanic and resedimentation processes: Journal of Volcanology and Geothermal Research, v. 174, p. 117-127.

Olivieri, A.C., Faber, N.K.M., Ferre, J., Boque, R., Kalivas, J.H., and Mark, H., 2006, Uncertainty estimation and figures of merit for multivariate calibration: Pure and Applied Chemistry, v. 78, p. 633-661.

Palyanov, Y.N., Borzdov, Y.M., Bataleva, Y.V., Sokol, A.G., Palyanova, G.A., and Kupriyanov, I.N., 2007, Reducing role of sulfides and diamond formation in the Earth's mantle: Earth and Planetary Science Letters, v. 260, p. 242-256.

Palyanov, Y.N., Borzdov, Y.M., Khokhryakov, A.F., Kupriyanov, I.N., and Sobolev, N.V., 2006, Sulfide melts-graphite interaction at HPHT conditions: Implications for diamond genesis: Earth and Planetary Science Letters, v. 250, p. 269-280.

Palyanov, Y.N., and Sokol, A.G., 2009, The effect of composition of mantle fluids/melts on diamond formation processes: Lithos, v. 112, p. 690-700.

Patterson, M., Francis, D., and McCandless, T., 2009, Kimberlites: Magmas or mixtures?: Lithos, v. 112, p. 191-200.

Pearson, D.G., Canil, D., and Shirey, S.B., 2003, Mantle Samples Included in Volcanic Rocks: Xenoliths and Diamonds, *in* Heinrich, D.H., and Karl, K.T., eds., Treatise on Geochemistry: Oxford, Pergamon, p. 171-275.

Pearson, D.G., and Nowell, G.M., 2002, The continental lithospheric mantle: characteristics and significance as a mantle reservoir: Philosophical Transactions of the Royal Society a-Mathematical Physical and Engineering Sciences, v. 360, p. 2383-2410.

—, 2005, Accuracy and precision in plasma ionisation multicollector mass spectrometry: Constraints from neodymium and hafnium isotope measurements: Plasma Source Mass Spectrometry: Current Trends and Future Developments, p. 284-314.

Pearson, D.G., Shirey, S.B., Harris, J.W., and Carlson, R.W., 1998, Sulphide inclusions in diamonds from the Koffiefontein kimberlite, S Africa: constraints on diamond ages and mantle Re-Os systematics: Earth and Planetary Science Letters, v. 160, p. 311-326.

Pokhilenko, N.P., Sobolev, N.V., Reutsky, V.N., Hall, A.E., and Taylor, L.A., 2004, Crystalline inclusions and C isotope ratios in diamonds from the Snap Lake/King Lake kimberlite dyke system: evidence of ultradeep and enriched lithospheric mantle: Lithos, v. 77, p. 57-67.

Price, S.E., Russell, J.K., and Kopylova, M.G., 2000, Primitive magma from the Jericho Pipe, NWT, Canada: Constraints on primary kimberlite melt chemistry: Journal of Petrology, v. 41, p. 789-808.

Promprated, P., Taylor, L.A., Anand, M., Floss, C., Sobolev, N.V., and Pokhilenko, N.P., 2004, Multiple-mineral inclusions in diamonds from the Snap Lake/King Lake kimberlite dike, Slave craton, Canada: a trace-element perspective: Lithos, v. 77, p. 69-81.

Read, P.G., 2005, Gemmology, Butterworth-Heinemann.

Rege, S., Griffin, W.L., Kurat, G., Jackson, S.E., Pearson, N.J., and O'Reilly, S.Y., 2008, Trace-element geochemistry of diamondite: Crystallisation of diamond from kimberlite-carbonatite melts: Lithos, v. 106, p. 39-54.

Rege, S., Griffin, W.L., Pearson, N.J., Araujo, D., Zedgenizov, D., and O'Reilly, S.Y., 2010, Trace-element patterns of fibrous and monocrystalline diamonds: Insights into mantle fluids: Lithos, v. 118, p. 313-337.

Rege, S., Jackson, S., Griffin, W.L., Davies, R.M., Pearson, N.J., and O'Reilly, S.Y., 2005, Quantitative trace-element analysis of diamond by laser ablation inductively coupled plasma mass spectrometry: Journal of Analytical Atomic Spectrometry, v. 20, p. 601-611.

Reguir, E.P., Chakhmouradian, A.R., Halden, N.M., Malkovets, V.G., and Yang, P., 2009, Major- and trace-element compositional variation of phlogopite from kimberlites and carbonatites as a petrogenetic indicator: Lithos, v. 112, p. 372-384.

Resano, M., Vanhaecke, F., Hutsebaut, D., De Corte, K., and Moens, L., 2003, Possibilities of laser ablation-inductively coupled plasma-mass spectrometry for diamond fingerprinting: Journal of Analytical Atomic Spectrometry, v. 18, p. 1238-1242.

Richardson, S.H., 1986, Latter-day origin of diamonds of eclogitic paragenesis: Nature, v. 322, p. 623-626.

Richardson, S.H., Chinn, I., Harris, J.W., 1999, Age and origin of eclogitic diamonds from the Jwaneng kimberlite, Botswana, *in* Gurney, J.J., Gurney, J. L., Pascoe, M. D., Richardson, S. H. , ed., 8th International Kimberlite Conference: The P.H. Nixon volume: Cape Town, Red Roof Design, p. 734-736.

Richardson, S.H., Erlank, A.J., Harris, J.W., and Hart, S.R., 1990, Eclogitic diamonds of Proterozoic age from Cretaceous kimberlites: Nature, v. 346, p. 54-56.

Richardson, S.H., Gurney, J.J., Erlank, A.J., and Harris, J.W., 1984, Origin of diamonds in old enriched mantle: Nature, v. 310, p. 198-202.

Richardson, S.H., and Harris, J.W., 1997, Antiquity of peridotitic diamonds from the Siberian craton: Earth and Planetary Science Letters, v. 151, p. 271-277.

Richardson, S.H., Harris, J.W., and Gurney, J.J., 1993, 3 generations of diamonds from old enriched mantle: Nature, v. 366, p. 256-258.

Richardson, S.H., Harris, J.W., and Pöml, P.F., 2006, Antiquity of harzburgitic diamonds from the Venetia kimberlite, Limpopo Belt, Kaapvaal craton: Geochimica et Cosmochimica Acta, v. 70, p. A531-A531.

Richardson, S.H., Poml, P.F., Shirey, S.B., and Harris, J.W., 2009, Age and origin of peridotitic diamonds from Venetia, Limpopo Belt, Kaapvaal-Zimbabwe craton: Lithos, v. 112, p. 785-792.

Richardson, S.H., Shirey, S.B., and Harris, J.W., 2004, Episodic diamond genesis at Jwaneng, Botswana, and implications for Kaapvaal craton evolution: Lithos, v. 77, p. 143-154.

Richardson, S.H., Shirey, S.B., Harris, J.W., and Carlson, R.W., 2001, Archean subduction recorded by Re-Os isotopes in eclogitic sulfide inclusions in Kimberley diamonds: Earth and Planetary Science Letters, v. 191, p. 257-266.

Robinson, A.L., 1979, Is a diamond really forever?: Science, v. 206, p. 670-673.

Rondeau, B., Fritsch, E., Moore, M., Thomassot, E., and Sirakian, J.-F., 2007, On the growth of natural octahedral diamond upon a fibrous core: Journal of Crystal Growth, v. 304, p. 287-293.

Royse, K.R., Kempton, P.D. and Darbyshire, D.P.F., 1998, Procedure for the analysis for Rb-Sr and Sm-Nd isotopes at the NERC isotope geosciences laboratory. : NERC Isotope Geosciences Laboratory Report Series, v. 121.

Ryabchikov, I.D., and Girnis, A.V., 2005, Genesis of low-calcium kimberlite magmas: Russian Geology and Geophysics, v. 46, p. 1202-1212.

Safonov, O.G., Chertkova, N.V., Perchuk, L.L., and Litvin, Y.A., 2009, Experimental model for alkalic chloride-rich liquids in the upper mantle: Lithos, v. 112, p. 260-273.

Safonov, O.G., Perchuk, L.L., and Litvin, Y.A., 2007, Melting relations in the chloride-carbonate-silicate systems at high-pressure and the model for formation of alkalic diamond-forming liquids in the upper mantle: Earth and Planetary Science Letters, v. 253, p. 112-128.

Salvioli-Mariani, E., Toscani, L., and Bersani, D., 2004, Magmatic evolution of the Gaussberg lamproite (Antarctica): volatile content and glass composition: Mineralogical Magazine, v. 68, p. 83-100.

Sato, K., Katsura, T., and Ito, E., 1997, Phase relations of natural phlogopite with and without enstatite up to 8 GPa: Implication for mantle metasomatism: Earth and Planetary Science Letters, v. 146, p. 511-526.

Schmidberger, S.S., and Francis, D., 1999, Nature of the mantle roots beneath the North American craton: mantle xenolith evidence from Somerset Island kimberlites: Lithos, v. 48, p. 195-216.

Schmidberger, S.S., Simonetti, A., Heaman, L.M., Creaser, R.A., and Whiteford, S., 2007, Lu-Hf, in-situ Sr and Pb isotope and trace element systematics for mantle eclogites from the Diavik diamond mine: Evidence for

Paleoproterozoic subduction beneath the Slave craton, Canada: Earth and Planetary Science Letters, v. 254, p. 55-68.

Schneider, M.E., and Eggler, D.H., 1986, Fluids in equilibrium with peridotite minerals: Implications for mantle metasomatism: Geochimica et Cosmochimica Acta, v. 50, p. 711-724.

Schrauder, M., Koeberl, C., and Navon, O., 1996, Trace element analyses of fluid-bearing diamonds from Jwaneng, Botswana: Geochimica et Cosmochimica Acta, v. 60, p. 4711-4724.

Schrauder, M., and Navon, O., 1994, Hydrous and carbonatitic mantle fluids in fibrous diamonds from Jwaneng, Botswana: Geochimica et Cosmochimica Acta, v. 58, p. 761-771.

Schulze, D.J., Canil, D., Channer, D.M.D., and Kaminsky, F.V., 2006, Layered mantle structure beneath the western Guyana Shield, Venezuela: Evidence from diamonds and xenocrysts in Guaniamo kimberlites: Geochimica et Cosmochimica Acta, v. 70, p. 192-205.

Scott Smith, B.H., 2008, Canadian kimberlites: Geological characteristics relevant to emplacement: Journal of Volcanology and Geothermal Research, v. 174, p. 9-19.

Shatsky, V., Ragozin, A., Zedgenizov, D., and Mityukhin, S., 2008, Evidence for multistage evolution in a xenolith of diamond-bearing eclogite from the Udachnaya kimberlite pipe: Lithos, v. 105, p. 289-300.

Shimizu, N., and Richardson, S.H., 1987, Trace element abundance patterns of garnet inclusions in peridotite-suite diamonds: Geochimica et Cosmochimica Acta, v. 51, p. 755-758.

Shirey, S.B., Harris, J.W., Richardson, S.H., Fouch, M., James, D.E., Cartigny, P., Deines, P., and Viljoen, F., 2003, Regional patterns in the paragenesis and age of inclusions in diamond, diamond composition, and the lithospheric seismic structure of Southern Africa: Lithos, v. 71, p. 243-258.

Shirey, S.B., Harris, J.W., Richardson, S.H., Fouch, M.J., James, D.E., Cartigny, P., Deines, P., and Viljoen, F., 2002, Diamond genesis, seismic structure, and evolution of the Kaapvaal-Zimbabwe craton: Science, v. 297, p. 1683-1686.

Shirey, S.B., Richardson, S.H., and Harris, J.W., 2004a, Age, paragenesis and composition of diamonds and evolution of the Precambrian mantle lithosphere of southern Africa: South African Journal of Geology, v. 107, p. 91-106.

—, 2004b, Integrated models of diamond formation and craton evolution: Lithos, v. 77, p. 923-944.

Shiryaev, A.A., Izraeli, E.S., Hauri, E.H., Zakharchenko, O.D., and Navon, O., 2005, Chemical, optical and isotopic investigation of fibrous diamonds from Brazil: Russian Geology and Geophysics, v. 46, p. 1185-1201.

Smart, K.A., Heaman, L.M., Chacko, T., Simonetti, A., Kopylova, M., Mah, D., and Daniels, D., 2009, The origin of high-MgO diamond eclogites from the Jericho Kimberlite, Canada: Earth and Planetary Science Letters, v. 284, p. 527-537.

Smit, K.V., Shirey, S.B., Richardson, S.H., le Roex, A.P., and Gurney, J.J., 2010, Re-Os isotopic composition of peridotitic sulphide inclusions in diamonds

from Ellendale, Australia: Age constraints on Kimberley cratonic lithosphere: Geochimica et Cosmochimica Acta, v. 74, p. 3292-3306.

Snyder, D.B., 2008, Stacked uppermost mantle layers within the Slave craton of NW Canada as defined by anisotropic seismic discontinuities: Tectonics, v. 27.

Sobolev, N.V., 1974, Deep-seated Inclusions in Kimberlites and the Problem of the Composition of the Upper Mantle: Nauka, Novosibirsk, p. 264.

Sobolev, N.V., Kaminsky, F.V., Griffin, W.L., Yefimova, E.S., Win, T.T., Ryan, C.G., and Botkunov, A.I., 1997, Mineral inclusions in diamonds from the Sputnik kimberlite pipe, Yakutia: Lithos, v. 39, p. 135-157.

Sobolev, N.V., Logvinova, A.M., and Efimova, E.S., 2009, Syngenetic phlogopite inclusions in kimberlite-hosted diamonds: implications for role of volatiles in diamond formation: Russian Geology and Geophysics, v. 50, p. 1234-1248.

Sobolev, N.V., Yefimova, E.S., Kaminsky, F.V., Lavrentiev, Y.G., Usova, L.V., 1988, Titanate of complex composition and phlogopite in the diamond stability field, *in* Sobolev, N.V., ed., Composition and Processes of Deep Seated Zones of Continental Lithosphere, Nauka, Novosibirsk, p. 185-186.

Spetsius, Z.V., 1995, Occurrence of diamond in the mantle: a case study from the Siberian Platform: Journal of Geochemical Exploration, v. 53, p. 25-39.

Stachel, T., Aulbach, S., Brey, G.P., Harris, J.W., Leost, I., Tappert, R., and Viljoen, K.S., 2004, The trace element composition of silicate inclusions in diamonds: a review: Lithos, v. 77, p. 1-19.

Stachel, T., and Harris, J.W., 2008, The origin of cratonic diamonds -- Constraints from mineral inclusions: Ore Geology Reviews, v. 34, p. 5-32.

Stachel, T., Harris, J.W., and Muehlenbachs, K., 2009, Sources of carbon in inclusion bearing diamonds: Lithos, v. 112, p. 625-637.

Stachel, T., Harris, J.W., Tappert, R., and Brey, G.P., 2003, Peridotitic diamonds from the Slave and the Kaapvaal cratons--similarities and differences based on a preliminary data set: Lithos, v. 71, p. 489-503.

Stachel, T., Viljoen, K.S., Brey, G., and Harris, J.W., 1998, Metasomatic processes in lherzolitic and harzburgitic domains of diamondiferous lithospheric mantle: REE in garnets from xenoliths and inclusions in diamonds: Earth and Planetary Science Letters, v. 159, p. 1-12.

Sunagawa, I., 1984, Morphology of natural and synthetic diamond crystals, *in* Sunagawa, I., ed., Materials science of the Earth's interior: Tokyo, Japan, Terra. Sci. Publ., p. 303-330.

Swart, P.K., Pillinger, C.T., Milledge, H.J., and Seal, M., 1983, Carbon isotopic variation within individual diamonds: Nature, v. 303, p. 793-795.

Tallaire, A., Issaoui, R., Silva, F., Mille, V., Achard, J., Gicquel, A., 2010, Growth of thick highly boron-doped diamond single crystals by CVD, *in* Newton, M., ed., The 61st Diamond Conference (abstracts): Warwick, England.

Taylor, L.A., and Anand, M., 2004, Diamonds: time capsules from the Siberian Mantle: Chemie der Erde - Geochemistry, v. 64, p. 1-74.

Taylor, L.A., and Liu, Y., 2009, Sulfide inclusions in diamonds: not monosulfide solid solution: Russian Geology and Geophysics, v. 50, p. 1201-1211.

Thomassot, E., Cartigny, P., Harris, J.W., Lorand, J.P., Rollion-Bard, C., and Chaussidon, M., 2009, Metasomatic diamond growth: A multi-isotope study

(^{13}C, ^{15}N, ^{33}S, ^{34}S) of sulphide inclusions and their host diamonds from Jwaneng (Botswana): Earth and Planetary Science Letters, v. 282, p. 79-90.

Thomassot, E., Cartigny, P., Harris, J.W., and Viljoen, K.S., 2007, Methane-related diamond crystallization in the Earth's mantle: Stable isotope evidences from a single diamond-bearing xenolith: Earth and Planetary Science Letters, v. 257, p. 362-371.

Tomlinson, E., De Schrijver, I., De Corte, K., Jones, A.P., Moens, L., and Vanhaecke, F., 2005, Trace element compositions of submicroscopic inclusions in coated diamond: A tool for understanding diamond petrogenesis: Geochimica et Cosmochimica Acta, v. 69, p. 4719-4732.

Tomlinson, E.L., Jones, A.P., and Harris, J.W., 2006, Co-existing fluid and silicate inclusions in mantle diamond: Earth and Planetary Science Letters, v. 250, p. 581-595.

Tomlinson, E.L., McMillan, P.F., Zhang, M., Jones, A.P., and Redfern, S.A.T., 2007, Quartz-bearing C-O-H fluid inclusions diamond: Retracing the pressure-temperature path in the mantle using calibrated high temperature IR spectroscopy: Geochimica et Cosmochimica Acta, v. 71, p. 6030-6039.

Tomlinson, E.L., Müller, W., and Eimf, 2009, A snapshot of mantle metasomatism: Trace element analysis of coexisting fluid (LA-ICP-MS) and silicate (SIMS) inclusions in fibrous diamonds: Earth and Planetary Science Letters, v. 279, p. 362-372.

Turner, G., Burgess, R., and Bannon, M., 1990, Volatile-rich mantle fluids inferred from inclusions in diamond and mantle xenoliths: Nature, v. 344, p. 653-655.

van Achterbergh, A.E., Griffin, W.L., Kivi, K., Pearson, N.J., and O'Reilly, S.Y., 2001, Carbonatites at 200 km: quenched melt inclusions in megacrystalline Iherzolite xenoliths, Slave Craton, Canada: Journal of African Earth Sciences, v. 32, p. A35-A35.

Van Rythoven, A.D., and Schulze, D.J., 2009, In-situ analysis of diamonds and their inclusions from the Diavik Mine, Northwest Territories, Canada: Mapping diamond growth: Lithos, v. 112, p. 870-879.

Veksler, I.V., 2004, Liquid immiscibility and its role at the magmatic-hydrothermal transition: a summary of experimental studies: Chemical Geology, v. 210, p. 7-31.

Walmsley, J.C., and Lang, A.R., 1992, Oo submicrometer inclusions in diamond coat - Crystallography and composition of ankerites and related rhombohedral carbonates: Mineralogical Magazine, v. 56, p. 533-543.

Wang, A., Pasteris, J.D., Meyer, H.O.A., and Dele-Duboi, M.L., 1996, Magnesite-bearing inclusion assemblage in natural diamond: Earth and Planetary Science Letters, v. 141, p. 293-306.

Waters, F.G., 1987, A suggested origin of MARID xenoliths in kimberlites by high pressure crystallization of an ultrapotassic rock such as lamproite: Contributions to Mineralogy and Petrology, v. 95, p. 523-533.

Watling, R.J., Herbert, H.K., Barrow, I.S., and Thomas, A.G., 1995, Analysis of diamonds and indicator minerals for diamond exploration by laser ablation inductively coupled plasma mass spectrometry: Analyst, v. 120, p. 1357-1364.

Weiss, Y., Griffin, W.L., Elhlou, S., and Navon, O., 2008, Comparison between LA-ICP-MS and EPMA analysis of trace elements in diamonds: Chemical Geology, v. 252, p. 158-168.

Weiss, Y., Kessel, R., Griffin, W.L., Kiflawi, I., Klein-BenDavid, O., Bell, D.R., Harris, J.W., and Navon, O., 2009, A new model for the evolution of diamond-forming fluids: Evidence from microinclusion-bearing diamonds from Kankan, Guinea: Lithos, v. 112, p. 660-674.

Wirth, R., Kaminsky, F., Matsyuk, S., and Schreiber, A., 2009, Unusual micro- and nano-inclusions in diamonds from the Juina Area, Brazil: Earth and Planetary Science Letters, v. 286, p. 292-303.

Wirth, R., Vollmer, C., Brenker, F., Matsyuk, S., and Kaminsky, F., 2007, Inclusions of nanocrystalline hydrous aluminium silicate "Phase Egg" in superdeep diamonds from Juina (Mato Grosso State, Brazil): Earth and Planetary Science Letters, v. 259, p. 384-399.

Wittig, N., Pearson, D.G., Webb, M., Ottley, C.J., Irvine, G.J., Kopylova, M., Jensen, S.M., and Nowell, G.M., 2008, Origin of cratonic lithospheric mantle roots: A geochemical study of peridotites from the North Atlantic Craton, West Greenland: Earth and Planetary Science Letters, v. 274, p. 24-33.

Wood, B.J., and Corgne, A., 2007, Mineralogy of the Earth - Trace Elements and Hydrogen in the Earth's Transition Zone and Lower Mantle, *in* Gerald, S., ed., Treatise on Geophysics: Amsterdam, Elsevier, p. 63-89.

Worrall, F., 2001, A molecular topology approach to predicting pesticide pollution of groundwater: Environmental Science & Technology, v. 35, p. 2282-2287.

Wyllie, P.J., 1989, Origin of carbonatites: evidence from phase equilibrium studies, *in* Bell, K., ed., Carbonatites; Genesis and Evolution: London, Unwin Hyman, p. 500-545.

Wyllie, P.J., and Ryabchikov, I.D., 2000, Volatile components, magmas, and critical fluids in upwelling mantle: Journal of Petrology, v. 41, p. 1195-1206.

Yelisseyev, A.P., Pokhilenko, N.P., Steeds, J.W., Zedgenizov, D.A., and Afanasiev, V.P., 2004, Features of coated diamonds from the Snap Lake/King Lake kimberlite dyke, Slave craton, Canada, as revealed by optical topography: Lithos, v. 77, p. 83-97.

Zedgenizov, D.A., and Harte, B., 2004, Microscale variations of [delta]13C and N content within a natural diamond with mixed-habit growth: Chemical Geology, v. 205, p. 169-175.

Zedgenizov, D.A., Ragozin, A.L., Shatsky, V.S., Araujo, D., Griffin, W.L., and Kagi, H., 2009, Mg and Fe-rich carbonate-silicate high-density fluids in cuboid diamonds from the Internationalnaya kimberlite pipe (Yakutia): Lithos, v. 112, p. 638-647.

Zedgenizov, D.A., Rege, S., Griffin, W.L., Kagi, H., and Shatsky, V.S., 2007, Composition of trapped fluids in cuboid fibrous diamonds from the Udachnaya kimberlite: LAM-ICPMS analysis: Chemical Geology, v. 240, p. 151-162.

APPENDIX

The following Appendix contains Tables, Photograph Numbers and Laboratory Processes referred to in the main text of the thesis.

○

○

Appendix

Page

Electronic Supplement – *Includes a PDF copy of this volume*

Table A1-A6 is included as excel files. This includes an extended Table A4 including all micro-inclusion analyses.

An additional excel file, entitled 'LOQ file', contains;

A) Blanks from this study and their use in the calculation of LOQ values,

B) Blank corrected but unfiltered ppm concentrations as well as data filtered by LOD and LOQ parameters.

	CANADA, Slave Province											
LOCALITY	Ekati	Ekati	Ekati	Ekati	Ekati	Ekati	Ekati	Ekati	Ekati	Ekati	Ekati	Ekati
KIMBERLITE	Fox	Fox	Misery	Misery	Fox	Fox	Fox	Fox	Fox	Fox	Fox	Fox
Type	Fibrous cube	Fibrous cube	Monocrystalline	Monocrystalline	Monocrystalline	Monocrystalline	Monocrystalline	Monocrystalline	Monocrystalline	Fibrous coat	Monocrystalline	Monocrystalline
Colour	Black	Black	Brown	Brown	Brown	C-less	C-less	C-less	C-less	Yellow	C-less	C-less
Category	F	F	GEM	GEM	GEM	GEM	GEM	GEM	GEM	F	GEM	GEM
Wt. (mg)	7.48	3.06	14.66	14.51	34.47	23.71	22.76	31.28	31.65	82.94	36.52	29.93
Wt. loss (mg)	0.39	0.42	0.36	0.41	0.46	0.41	0.35	0.42	0.42	0.41	0.33	0.35
Ablation (hrs)	3	3	3	3	3	3	3	3	3	3	4	4
SAMPLE #	**E141**	**E142**	**E2108**	**E2101**	**E249**	**E248**	**E242**	**E246**	**E247**	**E221**	**245**	**244**
(ppm)												
Ti												
Rb	0.7485	0.5301								0.4242		
Sr	12.32	1.27				0.5981		0.1286		27.21		
Y		0.01922										
Zr		0.5483					1.817					
Nb	0.3532	0.1166				0.0372		0.02784		0.09109		
Cs	0.02318	0.01146				0.001487				0.0121		
Ba	180.7	27.13				11.62		13.37	0.4934	74.6		
La	3.629	0.7076				0.1193				6.743		
Ce	3.243	0.9398				0.08682				3.353		
Pr	0.1222	0.0497				0.004624				0.09254		
Nd	0.2434	0.1682				0.008329				0.1057	0.003165	
Sm	0.01253	0.01945								0.001141		
Eu	0.006524	0.005514								0.002692		
Gd	0.00672	0.0121								0.002229	0.0007724	
Tb		0.001292									0.0002011	
Dy		0.004729								0.0004837	0.0003963	
Er											0.0007913	
Yb										0.00186	0.001767	
Lu										0.0005697		
Hf		0.0177					0.03869					
Pb	1.6									5.602		
Th	1.644	0.1907		0.001131		0.07084		0.001824		0.7433		
U	0.06925	0.02788				0.00646		0.0004404		0.02647		

NOTES

Category: F - fibrous; LOW-P - low purity monocrystalline: GEM - higher purity monocrystalline (See section 3.3 Chapter 3)

Blank cell - Value below LOQ: See electronic file for unfiltered data

2σ uncertainties in Table A2

NR - Not reported

LOCALITY	Ekati	Ekati	Ekati	Ekati	Ekati	Ekati	Ekati	Ekati	Ekati	Ekati	Ekati	Ekati
KIMBERLITE	Fox	Misery	Fox	Mis	Misery	Fox	Mis	Mis	Fox	Fox	Fox	Fox
Type	Monocrystalline	Monocrystalline	Monocrystalline	Fibrous cube	Monocrystalline	Monocrystalline	Monocrystalline	Monocrystalline	Monocrystalline	Monocrystalline	Fibrous Coat	Fibrous Coat
Colour	C-less	C-less	C-less	C-less	C-less	Brown	C-less	Yellow	C-less	C-less	Grey	Grey
Category	GEM	GEM	GEM	F	GEM	GEM	GEM	GEM	GEM	GEM	F	F
Wt. (mg)	25.17	4.80	20.56	3.71	3.54	8.67	5.89	3.94	29.41	5.70	5.28	34.32
Wt. loss (mg)	0.45	0.39	0.37	0.37	0.39	0.31	0.31	0.10	0.45	0.40	0.41	0.36
Ablation (hrs)	4	4	4	4	4	3	3	4	5	6	5	5
SAMPLE #	**243**	**291**	**241**	**261**	**263**	**131**	**262**	**264**	**111**	**151**	**E151**	**E152**
(ppm)												
Ti												
Rb									0.05773		0.2904	0.8553
Sr	0.162								0.4148	0.2323	4.643	23.6
Y								0.02333		0.002625		
Zr									0.1395	0.1116		
Nb												
Cs									0.001279	0.0005897	0.01947	0.03377
Ba									0.2174		103.1	163.9
La									0.0344	0.0629	1.619	9.387
Ce									0.03608	0.05854	1.104	7.399
Pr								0.006886	0.002014	0.004095	0.05395	0.183
Nd								0.03397	0.005965	0.01443	0.1247	0.1957
Sm								0.00694				0.01029
Eu											0.008758	0.01343
Gd								0.007231		0.001041	0.006023	0.01142
Tb								0.001017				
Dy								0.004985		0.0003766		0.001712
Er		0.0006226		0.000554	0.001788	0.001198		0.001762		0.009886		
Yb					0.002728							
Lu												
Hf												
Pb										0.2624	0.7155	1.897
Th									0.09219	0.03011	0.867	2.149
U									0.008095	0.002293	0.05129	0.09004

NOTES

Category: F - fibrous; LOW-P - low purity monocrystalline: GEM - higher purity monocrystalline (See section 3.3 Chapter 3)

Blank cell - Value below LOQ: See electronic file for unfiltered data

2σ uncertainties in Table A2

NR - Not reported

LOCALITY	Ekati	Ekati	Ekati	Ekati	Ekati	Ekati	Ekati	Ekati	Ekati	Ekati	Ekati	Ekati
KIMBERLITE	Fox	Fox	Fox	Fox	Fox	Fox	Fox	Fox	Fox	Fox	Fox	Misery
Type	Fibrous Coat	Fibrous Coat	Fibrous Coat	Fibrous Cube	Monocrystalline	Monocrystalline	Monocrystalline	Monocrystalline	Monocrystalline	Monocrystalline	Monocrystalline	Monocrystalline
Colour	Grey	Grey	Grey	Brown	C-less	C-less	C-less	C-less	C-less	Brown	C-less	Brown
Category	F	F	F	F	GEM	GEM	GEM	GEM	GEM	GEM	GEM	GEM
Wt. (mg)	15.66	31.16	29.09	5.32	34.68	16.37	31.47	14.12	4.14	23.15	9.08	6.51
Wt. loss (mg)	0.71	0.31	0.32	0.32	0.50	0.21	0.45	0.56	0.54	0.56	0.52	0.28
Ablation (hrs)	4	4	5	4	7	5	4	6	5.5	7	6	3
SAMPLE #	**E153**	**E154**	**E111**	**E11014**	**152**	**153**	**154**	**E121**	**E122**	**E161**	**E171**	**E2104**
(ppm)												
Ti												
Rb	0.3012	0.2179	0.9921	0.4573								
Sr	9.516	1.65	3.733	1.511	0.3549	0.7644						
Y	0.004697			0.01862	0.0027	0.02383						
Zr					0.2177		0.2389					
Nb			0.1474	0.1838		0.07133						
Cs	0.01244	0.007507	0.01729	0.006374								
Ba	55.02	50.16	81.11	19.17	0.6632	0.9431	0.1473			0.8924		0.2372
La	3.164	0.3953	1.901	0.52	0.1584	0.5861	0.01712					
Ce	2.688	0.6751	1.292	0.6133	0.1396	0.8454						
Pr	0.0833	0.02222	0.05998	0.04702	0.008409	0.07103	0.001854					
Nd	0.1315	0.05892	0.1543	0.1616	0.02343	0.2555	0.006121					
Sm	0.005906		0.006203	0.01779	0.002379	0.02811	0.0008892					
Eu	0.006302		0.006375	0.006694	0.001033	0.00726						
Gd	0.01091		0.004754	0.01563	0.001866	0.02003						
Tb				0.001163	0.0001134	0.001488						
Dy	0.001116			0.005592	0.0005497	0.006439						
Er						0.002093						
Yb												0.002286
Lu												
Hf					0.004545		0.005283					
Pb	0.6003		0.8926		0.6587	1.13	0.1299					
Th	0.8148	0.1441	0.8708	0.1278	0.04104	0.3364	0.002245					
U	0.03387	0.007508	0.09449	0.01787	0.003503	0.01644	0.001193					

NOTES

Category: F - fibrous; LOW-P - low purity monocrystalline: GEM - higher purity monocrystalline (See section 3.3 Chapter 3)

Blank cell - Value below LOQ: See electronic file for unfiltered data

2σ uncertainties in Table A2

NR - Not reported

	CANADA, Slave Province									
LOCALITY	Ekati	Ekati	Ekati	Ekati	Ekati	Ekati	Diavik	Diavik	Diavik	Diavik
KIMBERLITE	Fox	Misery	Misery	Misery	Misery	Fox	Unknown	Unknown	Unknown	Unknown
Type	Fibrous Cube	Monocrystalline	Monocrystalline	Monocrystalline	Monocrystalline	Fibrous Cube	Fibrous Coat	Fibrous Coat	Fibrous Coat	Fibrous Cube
Colour	Grey	Brown	C-less	C-less	Brown	Grey	Black	Black	Black	Black
Category	F	GEM	GEM	GEM	GEM	F	F	F	F	F
Wt. (mg)	5.83	6.63	10.31	5.41	54.37	4.40	572.72	142.49	160.91	19.96
Wt. loss (mg)	0.42	0.28	0.26	0.20	0.28	0.40	0.32	0.39	0.45	0.32
Ablation (hrs)	4	3	3	3	3	4	3	3	5	3
SAMPLE #	**E217**	**E2105**	**E2102**	**E2103**	**E21011**	**E191**	**D104**	**D126**	**D131**	**D168**
(ppm)										
Ti										
Rb	1.487				0.3348	0.3161	0.3806	0.3174	0.3361	0.2921
Sr	17.07					71.19	8.517	4.637	6.802	4.734
Y	0.06586						0.03229			
Zr	0.8067	0.5979	0.9204	0.3078		0.4647				
Nb	0.8945				0.4189		0.2062		0.1176	
Cs	0.01853					0.008961	0.01676	0.01674	0.01597	0.01575
Ba	84.2			0.5084		61.11	169.8	100	130.4	92.69
La	3.782				0.2232	5.647	2.645	1.79	1.662	1.544
Ce	4.376				0.4906	3.661	2.437	1.333	1.557	1.132
Pr	0.263				0.04462	0.1009	0.173	0.05738	0.0768	0.07149
Nd	0.7904				0.1574	0.1033	0.5663	0.1179	0.1298	0.1577
Sm	0.09031				0.01447		0.04962		0.005295	
Eu	0.02517					0.005203	0.02453	0.008661	0.008352	0.007546
Gd	0.06528				0.008447	0.01057	0.04246	0.006419	0.005721	0.00474
Tb	0.005302				0.0006137		0.00277			
Dy	0.01841				0.002821		0.01208			
Er	0.005797						0.003558			
Yb										
Lu										
Hf		0.01092	0.01604							
Pb	1.139					2.551	1.368	0.994	0.7307	
Th	0.8346	0.005736			0.0908	0.1068	1.251	0.9242	0.8364	0.6073
U	0.1479					0.01887	0.09424	0.04784	0.04502	0.04216

NOTES

Category: F - fibrous; LOW-P - low purity monocrystalline: GEM - higher purity monocrystalline (See section 3.3 Chapter 3)

Blank cell - Value below LOQ: See electronic file for unfiltered data

2σ uncertainties in Table A2

NR - Not reported

LOCALITY	Diavik	Diavik	Diavik	Diavik	Diavik	Diavik	Diavik	Diavik	Diavik	Diavik	Diavik	Diavik
KIMBERLITE	Unknown	Unknown	Unknown	Unknown	Unknown	Unknown	Unknown	Unknown	Unknown	Unknown	Unknown	Unknown
Type	Fibrous Cube	Fibrous Cube	Monocrystalline	Monocrystalline	Monocrystalline	Monocrystalline	Monocrystalline	Monocrystalline	Monocrystalline	Monocrystalline	Monocrystalline	Monocrystalline
Colour	Black	Black	C-less	C-less	C-less	C-less	C-less	C-less	C-less	C-less	C-less	C-less
Category	F	F	GEM	GEM	GEM	GEM	GEM	GEM	GEM	GEM	GEM	GEM
Wt. (mg)	11.05	12.36	159.59	144.05	175.33	159.25	138.71	146.07	712.80	131.57	171.42	177.73
Wt. loss (mg)	0.39	0.40	0.26	0.20	0.23	0.27	0.02	0.23	0.29	0.25	0.22	0.26
Ablation (hrs)	5	5	3	3	3	3	3	3	3	3	3	3
SAMPLE #	**D169**	**D170**	**D113**	**D116**	**D115**	**D114**	**D110**	**D112**	**D102**	**D118**	**D108**	**D117**
(ppm)												
Ti												37.68
Rb	0.2214	0.2276										
Sr	4.326	4.354										
Y												
Zr									0.2916			
Nb		0.1153										
Cs	0.01599	0.01436										
Ba	120.7	96.56	0.751						20.95	0.4104	0.8846	0.2632
La	1.442	1.104	0.01879								0.04133	
Ce	1.052	0.9348										
Pr	0.05385	0.05272									0.001787	
Nd	0.08179	0.1206									0.005461	
Sm										0.001549	0.002298	0.001578
Eu	0.009166	0.008296							0.004737			
Gd	0.005815	0.00595										
Tb												
Dy												
Er												
Yb												
Lu												
Hf									0.005767			
Pb												
Th	0.9581	0.7115	0.00297							0.007627	0.05987	0.002809
U	0.03051	0.04968									0.003707	

NOTES

Category: F - fibrous; LOW-P - low purity monocrystalline: GEM - higher purity monocrystalline (See section 3.3 Chapter 3)

Blank cell - Value below LOQ: See electronic file for unfiltered data

2σ uncertainties in Table A2

NR - Not reported

LOCALITY	Diavik	Diavik	Diavik	Diavik	Diavik	Diavik	Diavik	Diavik	Diavik	Diavik	Diavik
KIMBERLITE	Unknown	Unknown	Unknown	Unknown	Unknown	Unknown	Unknown	Unknown	Unknown	Unknown	Unknown
Type	Monocrystalline	Monocrystalline	Monocrystalline	Monocrystalline	Monocrystalline	Monocrystalline	Monocrystalline	Monocrystalline	Monocrystalline	Monocrystalline	Fibrous Cube
Colour	C-less	C-less	C-less	C-less	C-less	C-less	C-less	C-less	C-less	C-less	Black
Category	GEM	GEM	GEM	GEM	GEM	GEM	GEM	GEM	GEM	GEM	F
Wt. (mg)	20.21	16.98	15.60	22.12	13.65	20.41	16.47	13.27	21.75	18.60	10.70
Wt. loss (mg)	0.24	0.25	0.24	0.23	0.21	0.26	0.22	0.23	0.25	0.23	0.19
Ablation (hrs)	3	3	3	3	3	3	3	3	3	3	3
SAMPLE #	**D181**	**D200**	**D201**	**D173**	**D199**	**D182**	**D183**	**D185**	**D186**	**D184**	**D167**
(ppm)											
Ti				21.76				15.8			
Rb											0.4081
Sr											
Y											
Zr					0.1899	0.5357					
Nb											
Cs											0.02386
Ba			0.773	0.6738	0.268		0.6004			0.2206	199.8
La			0.01751								2.408
Ce											1.773
Pr				0.001243							0.112
Nd				0.004881							0.2129
Sm	0.001725		0.001739			0.001576					
Eu	0.001766		0.001874			0.001609					0.02388
Gd											0.01857
Tb											
Dy						0.0004385					0.0033
Er											
Yb											
Lu											
Hf						0.009224					
Pb				0.2455							
Th		0.005159	0.03053						0.008473		2.078
U			0.0008264	0.001165					0.006734		0.1019

NOTES

Category: F - fibrous; LOW-P - low purity monocrystalline: GEM - higher purity monocrystalline (See section 3.3 Chapter 3)

Blank cell - Value below LOQ: See electronic file for unfiltered data

2σ uncertainties in Table A2

NR - Not reported

	CANADA, Slave Province											
LOCALITY	Snap Lake	Snap Lake	Snap Lake	Snap Lake	Snap Lake	Snap Lake	Snap Lake	Snap Lake	Snap Lake	Snap Lake	Snap Lake	Snap Lake
KIMBERLITE	Snap/King Lake Dyke	Snap/King Lake Dyke	Snap/King Lake Dyke	Snap/King Lake Dyke	Snap/King Lake Dyke	Snap/King Lake Dyke	Snap/King Lake Dyke	Snap/King Lake Dyke	Snap/King Lake Dyke	Snap/King Lake Dyke	Snap/King Lake Dyke	Snap/King Lake Dyke
Type	Monocrystalline	Monocrystalline	Monocrystalline	Monocrystalline	Monocrystalline	Monocrystalline	Monocrystalline	Monocrystalline	Monocrystalline	Monocrystalline	Mono-Coat	Mono-Coat
Colour	C-less	C-less	C-less	C-less	C-less	C-less	C-less	C-less	C-less	C-less	Yellow	Yellow
Category	GEM	GEM	GEM	GEM	GEM	GEM	GEM	GEM	GEM	GEM	LOW-P	LOW-P
Wt. (mg)	152.11	143.84	175.84	153.29	177.35	156.36	176.05	160.58	141.51	166.01	179.89	174.54
Wt. loss (mg)	2.90	0.45	0.60	0.80	0.29	0.31	0.31	0.32	0.34	0.31	0.53	0.41
Ablation (hrs)	27	6	6	8	5	3	3	3	3	3	6	5
SAMPLE #	B2-1	B2-2	B2-3	B2-4	B2-5	B1-1	B1-2	B1-3	B1-4	B1-5	B3-11	B3-12
(ppm)												
Ti							12.12					
Rb											0.04528	0.02882
Sr					0.1717						3.025	0.2664
Y											0.009844	
Zr		0.1368				0.2063			0.1958			
Nb											0.2277	0.03926
Cs											0.001072	0.000945
Ba	0.1909		0.1009		2.116			0.1788		0.16	3.886	3.273
La			0.04047						0.02126		0.3775	0.1172
Ce			0.3668						0.1555		0.5092	0.1077
Pr											0.03643	0.006147
Nd											0.1278	0.01393
Sm											0.01475	0.00152
Eu											0.003953	0.001112
Gd											0.01265	0.001541
Tb											0.0009403	0.00007332
Dy											0.003583	0.000402
Er											0.0008565	
Yb												
Lu												
Hf						0.004015						
Pb	0.08757											
Th											0.0823	0.02522
U											0.007821	0.003547

NOTES

Category: F - fibrous; LOW-P - low purity monocrystalline: GEM - higher purity monocrystalline (See section 3.3 Chapter 3)

Blank cell - Value below LOQ: See electronic file for unfiltered data

2σ uncertainties in Table A2

NR - Not reported

LOCALITY	Snap Lake	Snap Lake	Snap Lake	Snap Lake	Snap Lake	Snap Lake	Snap Lake	Snap Lake	Snap Lake	Snap Lake	Snap Lake	Snap Lake
KIMBERLITE	Snap/King Lake Dyke	Snap/King Lake Dyke	Snap/King Lake Dyke	Snap/King Lake Dyke	Snap/King Lake Dyke	Snap/King Lake Dyke	Snap/King Lake Dyke	Snap/King Lake Dyke	Snap/King Lake Dyke	Snap/King Lake Dyke	Snap/King Lake Dyke	Snap/King Lake Dyke
Type	Mono-Coat	Mono-Coat	Mono-Coat	Mono-Coat	Mono-Coat	Mono-Coat	Mono-Coat	Mono-Coat	Mono-Coat	Mono-Coat	Mono-Coat	Mono-Coat
Colour	Grey	Grey	C-less	C-less	Yellow	Grey	Grey	Grey	Yellow	Yellow	C-less	Grey
Category	LOW-P	LOW-P	LOW-P	LOW-P	LOW-P	LOW-P	LOW-P	LOW-P	LOW-P	LOW-P	LOW-P	LOW-P
Wt. (mg)	168.50	140.59	148.92	174.22	165.98	171.37	141.43	150.95	174.78	152.66	171.18	179.16
Wt. loss (mg)	0.51	0.35	0.35	0.39	0.38	0.20	0.17	0.18	0.18	0.19	0.15	0.19
Ablation (hrs)	6	4	4	4	5	3	3	3	3	3	3	3
SAMPLE #	B3-13	B3-14	B3-15	B3-16	B3-1	B3-2	B3-3	B3-4	B3-17	B3-18	B3-19	B3-20
(ppm)												
Ti	123.9	40.76		9.48			43.45		29.11	25.94		19.18
Rb	2.262	1.089	0.08556				0.09018		0.9739			0.06043
Sr	61.8	2.993	9.561	0.117	0.3247	0.2728	1.334	2.48	3.094	1.662		2.627
Y	1.977	0.1654	0.0234				0.6494	0.2716	0.2072			0.1045
Zr	2.532	0.4539					0.4309		0.7566			0.3001
Nb	9.289	1.811	0.1671	0.02011	0.06921		2.269	1.012	0.2882			0.1969
Cs	0.03431	0.02201	0.001408				0.001473		0.007402			0.003656
Ba	128	70.57	4.947	0.8125	1.011	2.61	6.209	3.053	44.68	4.859	0.3569	4.33
La	10.37	9.252	17.53	0.03468	0.05139	0.1093	1.876	11.14	18.85	0.231		0.707
Ce	16.75	17.64	13.78		0.07062		9.562	11.58	32.45	0.2917		1.058
Pr	1.838	1.406	0.4227	0.002951	0.006549	0.003311	1.506	0.6408	1.953	0.02299		0.1025
Nd	8.687	5.337	0.939	0.007324	0.02129		7.539	1.873	5.404	0.06094		0.4014
Sm	1.966	0.6107	0.03199		0.002505		1.406	0.1635	0.2679	0.003048		0.06529
Eu	0.6112	0.1367	0.006963				0.3461	0.04851	0.05294			0.01939
Gd	1.512	0.4098	0.06034		0.001297		0.8647	0.1681	0.3261	0.00365		0.05903
Tb	0.1744	0.02418	0.002077		0.00009043		0.08881	0.01299	0.01445			0.005419
Dy	0.7498	0.08081	0.01081				0.3594	0.06173	0.06002			0.02355
Er	0.1765	0.01996	0.003648				0.08203	0.02056	0.02066			0.006514
Yb	0.05612	0.004501					0.02401	0.006337	0.006474			0.002848
Lu	0.007154	0.0008182					0.002711	0.0008745	0.001249			
Hf	0.05693	0.008703					0.009819		0.009636			
Pb	0.1318											
Th	3.606	1.51	0.07278	0.007064	0.008959	0.02126	1.04	0.943	0.02849	0.04023	0.004585	0.2136
U	0.6898	0.2292	0.008379	0.0008051	0.001496	0.0013	0.326	0.02404	0.009721	0.009362		0.01798

NOTES

Category: F - fibrous; LOW-P - low purity monocrystalline: GEM - higher purity monocrystalline (See section 3.3 Chapter 3)

Blank cell - Value below LOQ: See electronic file for unfiltered data

2σ uncertainties in Table A2

NR - Not reported

LOCALITY	Snap Lake	Snap Lake	Snap Lake	Snap Lake	Snap Lake	Snap Lake	Snap Lake	Snap Lake	Snap Lake	Snap Lake	Snap Lake	Snap Lake
KIMBERLITE	Snap/King Lake Dyke	Snap/King Lake Dyke	Snap/King Lake Dyke	Snap/King Lake Dyke	Snap/King Lake Dyke	Snap/King Lake Dyke	Snap/King Lake Dyke	Snap/King Lake Dyke	Snap/King Lake Dyke	Snap/King Lake Dyke	Snap/King Lake Dyke	Snap/King Lake Dyke
Type	Mono-Coat	Mono-Coat	Mono-Coat	Mono-Coat	Mono-Coat	Mono-Coat	Mono-Coat	Mono-Coat	Mono-Coat	Mono-Coat	Mono-Coat	Mono-Coat
Colour	Yellow	Grey	Grey	Yellow	C-less	Yellow	Green	Brown	Grey	Yellow	Brown	Brown
Category	LOW-P	LOW-P	LOW-P	LOW-P	LOW-P	LOW-P	LOW-P	LOW-P	LOW-P	LOW-P	LOW-P	LOW-P
Wt. (mg)	166.34	172.97	151.47	145.57	144.86	162.95	214.13	280.03	258.77	234.38	288.50	304.30
Wt. loss (mg)	0.32	0.30	0.58	0.53	0.50	0.70	0.26	0.25	0.25	0.21	0.24	0.26
Ablation (hrs)	3	3	6	6	5	7	3	3	3	3	3	3
SAMPLE #	B3-5	B3-6a	B3-7a	B3-8	B3-9	B3-10	SL-1	SL-19	SL-38	SL-39	SL-50	SL-57
(ppm)												
Ti								15.61		97.8	43.13	27.44
Rb	0.1512	0.3815	0.08265	0.07529	0.05128							
Sr	0.5342	4.802	0.4408	0.5278								
Y		0.09312									0.02058	0.003001
Zr		0.5585	0.3385							0.1587		
Nb	0.1236	0.6352	0.1029	0.1092	0.2553	0.02173					0.0526	
Cs		0.0115	0.002533		0.001784							
Ba	6.382	15.25	13.38	4.791	5.336	0.6133		0.2867		4.708	0.428	1.525
La	0.1428	1.962	0.2637	0.1415	0.3229	0.02132					0.249	0.05919
Ce		3.049	0.2862	0.1974	0.446	0.03201					0.3886	0.07888
Pr	0.01399	0.2644	0.01874	0.0145	0.03209	0.002258					0.03327	0.006243
Nd	0.04873	0.9733	0.0593	0.04455	0.06912	0.005001					0.1161	0.02193
Sm	0.006789	0.1119	0.004878	0.004809	0.0029						0.01293	0.002761
Eu		0.02575			0.002429						0.003861	#VALUE!
Gd	0.004685	0.08193	0.003309	0.002758	0.0079	0.0004355					0.01103	0.002017
Tb	0.0004543	0.007249	0.0002884	0.0003682	0.0003231						0.0007107	0.0001221
Dy		0.0249	0.001214	0.001411	0.001268						0.003099	0.0006473
Er		0.007265			0.0002872						0.001052	
Yb												
Lu												
Hf												
Pb												
Th	0.03235	0.3426	0.06222	0.03506	0.05195	0.004341					0.0163	0.02497
U	0.004491	0.04299	0.006776	0.004562	0.007123	0.0006858					0.001862	0.001606

NOTES

Category: F - fibrous; LOW-P - low purity monocrystalline: GEM - higher purity monocrystalline (See section 3.3 Chapter 3)

Blank cell - Value below LOQ: See electronic file for unfiltered data

2σ uncertainties in Table A2

NR - Not reported

LOCALITY	Snap Lake	Snap Lake	Snap Lake	Snap Lake	Snap Lake	Snap Lake	Snap Lake	Snap Lake
KIMBERLITE	Snap/King Lake Dyke	Snap/King Lake Dyke	Snap/King Lake Dyke	Snap/King Lake Dyke	Snap/King Lake Dyke	Snap/King Lake Dyke	Snap/King Lake Dyke	Snap/King Lake Dyke
Type	Monocrystalline	Monocrystalline	Monocrystalline	Monocrystalline	Monocrystalline	Monocrystalline	Monocrystalline	Monocrystalline
Colour	C-less	C-less	C-less	C-less	C-less	C-less	C-less	C-less
Category	GEM	GEM	GEM	LOW-P	LOW-P	GEM	GEM	GEM
Wt. (mg)	169.93	161.72	157.29	5.68	16.96	30.05	18.01	54.81
Wt. loss (mg)	0.35	0.33	0.30	0.30	0.30	0.30	0.30	0.30
Ablation (hrs)	3.5	3	3	3	3	3	3	3
SAMPLE #	**B1-6**	**B1-7**	**B1-8**	**B3-6b**	**B3-7b**	**B4-5**	**B4-7**	**B4-10**
(ppm)								
Ti	19.86	45.29	17.04			128.8	208.7	244.7
Rb								
Sr								
Y								
Zr	0.09561	0.1362	0.1245					
Nb				0.04602				
Cs								
Ba		0.1592		4.672	12.27	1.576		
La		0.01508		0.05815				
Ce		0.09382		0.05623				
Pr				0.003833				
Nd				0.007975				
Sm								0.005052
Eu				0.002466				
Gd				0.00122				
Tb								
Dy								
Er								
Yb								
Lu								
Hf								
Pb								
Th				0.01364				
U				0.00206				

NOTES

Category: F - fibrous; LOW-P - low purity monocrystalline: GEM - higher purity monocrystalline (See section 3.3 Chapter 3)

Blank cell - Value below LOQ: See electronic file for unfiltered data

2σ uncertainties in Table A2

NR - Not reported

	DEMOCRATIC REPUBLIC OF CONGO, Congo Craton										
LOCALITY	DR Congo	DR Congo	DR Congo	DR Congo	DR Congo	DR Congo	DR Congo	DR Congo	DR Congo	DR Congo	DR Congo
KIMBERLITE	Unknown	Unknown	Unknown	Unknown	Unknown	Unknown	Unknown	Unknown	Unknown	Unknown	Unknown
Type	Fibrous Coat	Fibrous Coat	Fibrous Coat	Fibrous Coat	Fibrous Coat	Fibrous Coat	Fibrous Coat	Fibrous Coat	Fibrous Coat	Fibrous Coat	Fibrous Coat
Colour	Yellow	Grey	Grey	Yellow/Grey	Brown	Grey	Grey	Grey	Grey	Grey	Green/Brown
Category	F	F	F	F	F	F	F	F	F	F	F
Wt. (mg)	28.66	27.24	21.17	28.92	22.57	22.86	20.60	21.32	19.53	21.50	43.49
Wt. loss (mg)	0.31	0.29	0.25	0.29	0.33	0.29	0.31	0.27	0.26	0.29	0.44
Ablation (hrs)	0.75	0.75	0.75	0.75	0.75	0.75	0.75	0.75	0.75	0.75	3
SAMPLE #	**CNG-1**	**CNG-3**	**CNG-2**	**CNG-4**	**CNG-5**	**CNG-11**	**CNG-7**	**CNG-8**	**CNG-9**	**CNG-10**	**DRC-2**
(ppm)											
Ti						77.38			68.18		21.4
Rb						2.756		0.2733	0.6183	0.4082	0.6194
Sr	1.301			2.943	3.339	76.73	1.012	4.869	4.295	9.235	15
Y	0.07691			0.05484	0.05993	2.183		0.1489	0.6974	0.5603	0.1372
Zr						2.835		1.129		0.9306	1.071
Nb						3.269		0.1475	0.1458	0.1561	1.492
Cs	NR	NR	NR	NR	NR	NR	NR	NR	NR	NR	0.01007
Ba	2.834		1.219	8.745	8.286	136.6	2.601	53.67	25.57	63.69	22.92
La	1.029	0.062	0.1182	0.8623	0.9674	259	0.1697	3.28	5.089	22.49	1.928
Ce	0.5155			1.403	1.598	177.4		4.708	6.972	29.62	4.757
Pr	0.1224	0.01327	0.01625	0.1815	0.1661	28.72	0.02361	0.3771	0.6607	2.383	0.2724
Nd	0.3716	0.05216	0.04897	0.5866	0.5469	64.97	0.06569	1.093	2.004	6.391	0.9724
Sm	0.04191			0.07484	0.06677	5.45		0.08826	0.2769	0.6489	0.09305
Eu	0.008403			0.01379	0.01156	1.13		0.0257	0.06928	0.1528	0.02007
Gd	0.01962	0.004679		0.02938	0.024	1.693		0.02758	0.1826	0.2638	2.87
Tb	0.003392	0.0006405		0.004527	0.003499	0.227		0.008854	0.02782	0.03729	0.006253
Dy	0.0146			0.0154	0.01541	0.8026		0.03604	0.1282	0.1388	0.02952
Er	0.00567			0.004947	0.005238	0.1958		0.007998	0.05671	0.04094	0.01165
Yb						0.1062			0.04446	0.02571	0.01071
Lu						0.01517			0.007317	0.004292	0.001843
Hf						0.07787		0.04028		0.03719	0.02216
Pb	3.627	2.472		1.968		37.58			1.652	5.986	4.226
Th	0.05189		0.01543	0.09218	0.1449	4.802	0.02286	0.7085	0.2784	2.403	0.2646
U	0.006058			0.01329	0.01564	0.2574	0.004192	0.04757	0.03282	0.06912	0.05637

NOTES

Category: F - fibrous; LOW-P - low purity monocrystalline: GEM - higher purity monocrystalline (See section 3.3 Chapter 3)

Blank cell - Value below LOQ: See electronic file for unfiltered data

2σ uncertainties in Table A2

NR - Not reported

	SOUTH AFRICA, Kaapvaal Craton											
LOCALITY	Cullinan	Cullinan	Cullinan	Cullinan	Cullinan	Cullinan	Cullinan	Cullinan	Cullinan	Cullinan	Cullinan	Cullinan
KIMBERLITE	Unknown	Unknown	Unknown	Unknown	Unknown	Unknown	Unknown	Unknown	Unknown	Unknown	Unknown	Unknown
Type	Monocrystalline	Monocrystalline	Monocrystalline	Monocrystalline	Monocrystalline	Monocrystalline	Monocrystalline	Monocrystalline	Monocrystalline	Monocrystalline	Monocrystalline	Monocrystalline
Colour	C-less	C-less	C-less	C-less	C-less	C-less	C-less	C-less	C-less	C-less	C-less	C-less
Category	GEM	GEM	GEM	GEM	GEM	GEM	GEM	GEM	GEM	GEM	GEM	GEM
Wt. (mg)	47.67	39.28	93.36	53.63	56.54	64.47	44.49	39.37	49.22	52.94	47.24	38.87
Wt. loss (mg)	0.37	0.46	0.46	0.44	0.42	0.43	0.41	0.47	0.44	0.44	0.44	0.40
Ablation (hrs)	3	3	3	3	3	3	3	3	3	3	3	3
SAMPLE #	**AP 25a**	**AP 26a**	**AP 28a**	**AP 30a**	**AP 31a**	**AP 34a**	**AP 35a**	**AP36a**	**AP 37a**	**AP 38a**	**AP 25b**	**AP 26b**
(ppm)												
Ti												25.61
Rb											0.05257	
Sr												
Y		0.003475			0.004438		0.002592	0.001705		0.001457	0.01087	0.002855
Zr												
Nb							0.01886				0.01852	
Cs	0.0009548			0.0004589	0.0006875		0.0006132	0.0004327		0.0004552		
Ba												
La						0.01592						
Ce						0.0974						
Pr		0.003317			0.003873		0.003306	0.001018		0.001907		
Nd		0.001881	0.007046		0.07063		0.008231			0.2738	0.002736	0.002335
Sm		0.002777			0.003701		0.003199	0.0008592		0.001968		
Eu		0.002829			0.003302		0.002809					
Gd		0.002524			0.003543		0.00244					0.0005645
Tb	0.0002016	0.002803		0.0001707	0.003344		0.002912	0.0008196	0.0004015	0.0001116		
Dy		0.002607			0.003427		0.00253	0.0008765	0.0004252			
Er		0.002394			0.002927		0.002564	0.000744	0.0002682		0.0007561	0.000845
Yb		0.002739			0.00373		0.002854					
Lu		0.002675			0.003485		0.002683	0.0008618	0.0003969			0.0007805
Hf		0.00509			0.003577		0.02037					
Pb	0.2466	0.1143								0.1117	0.3722	0.1182
Th		0.00342			0.003201		0.004694	0.001037				
U		0.002026			0.001636		0.003426	0.0004254				

NOTES

Category: F - fibrous; LOW-P - low purity monocrystalline: GEM - higher purity monocrystalline (See section 3.3 Chapter 3)

Blank cell - Value below LOQ: See electronic file for unfiltered data

2σ uncertainties in Table A2

NR - Not reported

								BRAZIL, Sao Luiz Province		
LOCALITY	Cullinan	Cullinan	Cullinan	Jwaneng	Monastery	Monastery	Monastery	Mato Grosso	Mato Grosso	Mato Grosso
KIMBERLITE	Unknown	Unknown	Unknown	Unknown	Unknown	Unknown	Unknown	Juina	Juina	Juina
Type	Monocrystalline	Monocrystalline	Monocrystalline	Fibrous Coat	Mono-UHP	Mono-UHP	Mono-UHP	Mono-UHP	Mono-UHP	Mono-UHP
Colour	C-less	C-less	C-less	Grey	C-less	C-less	C-less	C-less	C-less	C-less
Category	GEM	GEM	GEM	F	GEM	GEM	GEM	GEM	GEM	GEM
Wt. (mg)	92.93	53.19	52.48	291.18	4.81	6.21	3.72	1.14	14.39	175.94
Wt. loss (mg)	0.41	0.43	0.46	0.42	0.47	0.52	0.37	0.82	0.88	0.66
Ablation (hrs)	3	3	3	3	7	6	6	3	3	7
SAMPLE #	**AP 28b**	**AP 30b**	**AP 38b**	**0N-JWN-110**	**A4-03**	**B9-15**	**B9-17**	**J-5103**	**J-5102**	**JUa2**
(ppm)										
Ti				37.93				11.32		
Rb		0.09893	0.01913	0.335					0.02353	
Sr				73.67				0.08805	0.3683	
Y		0.005436	0.007822	0.1418	0.00845			0.007392	0.214	
Zr				0.5155				0.1073	0.3892	
Nb				0.14		0.08988		0.1082	0.1133	
Cs				0.008367						
Ba		0.1351		8.096				0.05009	1.016	3.039
La				0.2957				0.1045	1.818	
Ce				0.7879				0.09573	1.419	
Pr				0.06398				0.009902	0.192	
Nd		0.004218	0.007469	0.2703				0.02255	0.4977	
Sm				0.05515				0.002763	0.07594	
Eu				0.01529					0.007289	
Gd				0.05828				0.001546	0.05279	
Tb				0.005822				0.0002883	0.009363	
Dy				0.03117	0.001298			0.001664	0.0585	
Er	0.0004354	0.000932	0.001073	0.01389	0.001363			0.0009341	0.03083	
Yb				0.007693				0.0009429	0.03647	
Lu				0.001012				0.0001726	0.005596	
Hf				0.01328				0.001893	0.005914	
Pb		0.2883		1.763				0.05907	1.52	
Th				0.05135				0.008163	0.2233	
U		0.00193		0.03105				0.009375	0.08003	

NOTES

Category: F - fibrous; LOW-P - low purity monocrystalline: GEM - higher purity monocrystalline (See section 3.3 Chapter 3)

Blank cell - Value below LOQ: See electronic file for unfiltered data

2σ uncertainties in Table A2

NR - Not reported

LOCALITY	Mato Grosso	Mato Grosso	Mato Grosso	Mato Grosso	Mato Grosso	Mato Grosso	Mato Grosso
KIMBERLITE	Juina	Juina	Juina	Juina	Juina	Juina	Juina
Type	Mono-UHP	Mono-UHP	Mono-UHP	Mono-UHP	Mono-UHP	Mono-UHP	Mono-UHP
Colour	C-less	C-less	C-less	C-less	C-less	C-less	C-less
Category	GEM	GEM	GEM	GEM	GEM	GEM	GEM
Wt. (mg)	45.71	135.80	7.70	7.08	8.41	31.06	2.75
Wt. loss (mg)	0.62	0.56	0.43	0.26	0.22	0.26	0.22
Ablation (hrs)	7	6	8	3	3	3	3
SAMPLE #	**JUc34**	**JUs41**	**2.8**	**J-104**	**J5-101**	**J5-102**	**J4-104**
(ppm)							
Ti							
Rb							
Sr							
Y	0.005286					0.2273	
Zr							
Nb							
Cs							
Ba			0.8769			1.099	2.584
La	0.05754					7.762	
Ce						6.356	
Pr	0.007424					0.6068	
Nd	0.01801	0.008323				1.083	
Sm						0.09512	
Eu						0.008923	
Gd	0.00215					0.1525	
Tb	0.0003103	0.0002631				0.009557	
Dy	0.001771	0.00107				0.05517	
Er						0.02863	
Yb						0.02926	
Lu						0.004404	
Hf							
Pb							
Th						0.16	
U							

NOTES

Category: F - fibrous; LOW-P - low purity monocrystalline: GEM - higher purity monocrystalline (See section 3.3 Chapter 3)

Blank cell - Value below LOQ: See electronic file for unfiltered data

2σ uncertainties in Table A2

NR - Not reported

	SYNTHETIC ORIGIN								
LOCALITY	Laboratory	Laboratory	Laboratory	Laboratory	Laboratory	Laboratory	Laboratory	Laboratory	Laboratory
KIMBERLITE	N/a	N/a	N/a	N/a	N/a	N/a	N/a	N/a	N/a
Type	CVD	CVD	CVD	HPHT	CVD	CVD	CVD	HPHT	Inknown
Colour	C-less	Black	C-less	Yellow	C-less	Black	C-less	Yellow	C-less
Category									
Wt. (mg)	21.67	80.93	94.97	24.78	21.67	80.93	94.97	24.78	7.75
Wt. loss (mg)	0.73	0.3	0.42	0.31	0.51	0.35	0.36	0.37	0.25
Ablation (hrs)	3	5	5	3	5	3	3	3	3
SAMPLE #	**s16a**	**0843818-F1a**	**0743817-L1a**	**S407-27a**	**s16b**	**0843818-F1b**	**0743817-L1b**	**S407-27b**	**ADMPD2JKS**
(ppm)									
Ti	15.99				11.08				28
Rb									
Sr									
Y		0.002255							
Zr					0.4506				
Nb									
Cs						0.001122			
Ba	0.06638		0.3515	0.1598	0.1863				0.1792
La									
Ce									
Pr									
Nd									
Sm									
Eu									
Gd									
Tb						0.00008628			
Dy									
Er									
Yb	0.002857								
Lu	0.00114								
Hf					0.0103				
Pb		0.8168		0.2615		1.048			
Th	0.0006346				0.001628				
U					0.0003627				

NOTES

Category: F - fibrous; LOW-P - low purity monocrystalline: GEM - higher purity monocrystalline (See section 3.3 Chapter 3)

Blank cell - Value below LOQ: See electronic file for unfiltered data

2σ uncertainties in Table A2

NR - Not reported

	RUSSIAN FEDERATION, Siberian Craton		VENEZUELA	LOQ	LOQ
LOCALITY	Udachnaya	Mir	Venezuela		
KIMBERLITE	Unknown	Unknown	Unknown		
Type	Monocrystalline	Monocrystalline	Monocrystalline		
Colour	C-less	C-less	C-less		
Category	GEM	GEM	GEM		
Wt. (mg)	148.25	99.76	19.99		
Wt. loss (mg)	0.71	0.55	0.69		**Estimate**
Ablation (hrs)	3.00	3.00	3.00		**See section**
SAMPLE #	**3812P**	**1581**	**5921**	**$10\sigma_{Blank}$**	**2.3.2 Chapter 2**
	(ppm)			pg/g	(ppm)
Ti				3806	3.067
Rb	0.016260	0.020790		8.412	0.006789
Sr	0.054860	0.228000		29.29	0.02364
Y		0.004661		0.619	0.0004995
Zr			0.07253	34.43	0.02779
Nb		0.100500		8.261	0.006667
Cs	NR	NR	NR	0.205	0.0001654
Ba	0.087600	0.09523		42.53	0.03433
La		0.100800		3.654	0.002949
Ce		0.195100		16.42	0.01325
Pr		0.0243		0.2479	0.0002001
Nd		0.08893		0.8906	0.0007188
Sm		0.01138		0.4085	0.0003297
Eu		0.002788		0.4304	0.0003474
Gd		0.004727		0.2288	0.0001847
Tb		0.0005984		0.02785	0.00002248
Dy		0.002657		0.1154	0.00009317
Er		0.0006718		0.1208	0.0000975
Yb		0.0009781		0.4654	0.0003757
Lu				0.1449	0.0001169
Hf				1.276	0.001029
Pb		0.1724		45.99	0.03712
Th		0.009457		0.4492	0.0003625
U		0.003943		0.1692	0.0001365

NOTES

Category: F - fibrous; LOW-P - low purity monocrystalline: GEM - higher purity monocrystalline (See section 3.3 Chapter 3)

Blank cell - Value below LOQ: See electronic file for unfiltered data

2σ uncertainties in Table A2

NR - Not reported

	COMBUSTIONS									
LOCALITY	DR Congo	DR Congo	DR Congo	DR Congo	DR Congo	DR Congo	Snap Lake	Snap Lake	Snap Lake	Snap Lake
KIMBERLITE	Unknown	Unknown	Unknown	Unknown	Unknown	Unknown	Snap/King Lake Dyke	Snap/King Lake Dyke	Snap/King Lake Dyke	Snap/King Lake Dyke
Type	Fibrous Coat	Fibrous Coat	Fibrous Coat	Fibrous Coat	Fibrous Coat	Fibrous Coat	Monocrystalline	Monocrystalline	Monocrystalline	Monocrystalline
Colour	Green/Brown	Green/Brown	Green/Brown	Yellow	Yellow	Yellow	C-less	C-less	C-less	C-less
Category	F	F	F	F	F	F	GEM	GEM	GEM	GEM
Wt. (mg)	-	-	-	-	-	-	-	-	3.45	-
Wt. loss (mg)	1.36	3.25	1.58	7.47	4.13	2.85	1.89	2.78	8.23	7.84
Ablation (hrs)	1.00	1.50	1.00	2.00	2.00	2.00	2.00	2.50	2.00	4.00
SAMPLE #	DRC-2a	DRC-2b	DRC-2c	CNG-1a	CNG-1b	CNG-1c	B4-5 a	B4-5 b	B3-6b	B3-7b
(ppm)										
Ti	19.23	7.594	6.059	21	4.535	12.43		7.501		
Rb	0.1106	0.1257	0.09771	0.07136	0.024	0.007397			0.01343	
Sr	8.935	8.305	9.354	2.126	0.9189	0.2619				
Y	0.1337	0.04264	0.06997	0.1557	0.05498	0.02061	0.08067	0.0726	0.002796	0.0008698
Zr				3.657	0.5902	1.336	2.844	2.011	0.2592	0.2074
Nb	0.6121	0.9247	0.905	0.02798	0.005322		0.112	0.06158	0.07755	0.04409
Cs	0.002269	0.001305	0.0007362	0.001432	0.001157	0.0003551			0.00068	
Ba	6.472	13.39	18.09	19.78	12.55	1.157	12.04	11.64	3.662	3.662
La	2.382	0.9543	1.246	2.496	0.7366	0.2873	1.094	0.9502	0.1509	0.146
Ce	3.552	1.485	1.948	3.494	0.9271	0.3873	1.538	1.324	0.1564	0.1105
Pr	0.3094	0.1356	0.176	0.3309	0.1112	0.04288	0.1417	0.1232	0.01211	0.006294
Nd	1.055	0.4566	0.6101	0.9907	0.3189	0.1309	0.4182	0.369	0.02967	0.01173
Sm	0.1217	0.05646	0.0728	0.1217	0.04048	0.0166	0.05484	0.04899	0.002933	0.0008367
Eu	0.02394	0.008218	0.01262	0.03078	0.01107	0.004086	0.0112	0.01241	0.001167	0.0008076
Gd	0.0697	0.0231	0.03402	0.07943	0.02794	0.0106	0.05119	0.04641	0.003111	0.001352
Tb	0.007269	0.002215	0.003579	0.008055	0.002815	0.001076	0.004377	0.003888	0.0002074	0.00007226
Dy	0.03013	0.009516	0.0154	0.03426	0.01191	0.004702	0.0209	0.01815	0.0009016	0.0003093
Er	0.01018	0.003148	0.005439	0.01087	0.003819	0.001614	0.007987	0.006861	0.0003496	0.0001233
Yb	0.006936	0.002157	0.003969	0.007407	0.002588	0.001124	0.005156	0.004687		
Lu	0.0009772	0.0003566	0.0005904	0.001137	0.0003804	0.0002163	0.0008665	0.0007039		
Hf	0.008617	0.002413	0.005846	0.03023	0.003662	0.005043	0.03766	0.02213	0.0009713	
Pb	2.08	2.836	0.4931	1.244	2.408	1.601	0.5771	1.002	0.2657	0.5244
Th	0.2972	0.1531	0.187	0.229	0.0604	0.02952	0.1773	0.1299	0.02788	0.03764
U		0.01651	0.03061	0.03832	0.008947	0.005659	0.01934	0.009806	0.01429	0.00355
									Gem Core of LOW-P B3-6/7	

NOTES

Category: F - fibrous; LOW-P - low purity monocrystalline: GEM - higher purity monocrystalline (See section 3.3 Chapter 3)

Blank cell - Value below LOQ: See electronic file for unfiltered data

2σ uncertainties in Table A2

NR - Not reported

	CANADA, Slave Province											
LOCALITY	Ekati	Ekati	Ekati	Ekati	Ekati	Ekati	Ekati	Ekati	Ekati	Ekati	Ekati	Ekati
KIMBERLITE	Fox	Fox	Misery	Misery	Fox	Fox	Fox	Fox	Fox	Fox	Fox	Fox
Type	Fibrous cube	Fibrous cube	Monocrystalline	Monocrystalline	Monocrystalline	Monocrystalline	Monocrystalline	Monocrystalline	Monocrystalline	Monocrystalline	Monocrystalline	Monocrystalline
Colour	Black	Black	Brown	Brown	Brown	C-less	C-less	C-less	C-less	Yellow	C-less	C-less
Category	F	F	GEM	GEM	GEM	GEM	GEM	GEM	GEM	F	GEM	GEM
Wt. (mg)	7.48	3.06	14.66	14.51	34.47	23.71	22.76	31.28	31.65	82.94	36.52	29.93
Wt. loss (mg)	0.39	0.42	0.36	0.41	0.46	0.41	0.35	0.42	0.42	0.41	0.33	0.35
Ablation (hrs)	3	3	3	3	3	3	3	3	3	3	4	4
SAMPLE #	E141	E142	E2108	E2101	E249	E248	E242	E246	E247	E221	245	244
(2σ,ppm) Ti												
Rb	5.E-02	4.E-02								6.E-02		
Sr	7.E-01	5.E-02				7.E-02		1.E-02		3.E+00		
Y		4.E-04										
Zr		4.E-02					2.E-01					
Nb	2.E-02	3.E-03				4.E-03		2.E-03		1.E-02		
Cs	3.E-03	1.E-03				4.E-04				1.E-03		
Ba	7.E+00	7.E-01				9.E-01		1.E+00	4.E-02	7.E+00		
La	2.E-01	7.E-03				9.E-03				6.E-01		
Ce	1.E-01	2.E-02				9.E-03				3.E-01		
Pr	5.E-03	2.E-03				2.E-04				7.E-03		
Nd	2.E-02	2.E-02				3.E-03				1.E-02	3.E-03	
Sm	9.E-03	8.E-03								4.E-04		
Eu	9.E-03	3.E-03								1.E-03		
Gd	7.E-03	1.E-02								2.E-03	7.E-04	
Tb		2.E-04									8.E-05	
Dy		1.E-03								6.E-04	5.E-04	
Er											5.E-04	
Yb										3.E-04	5.E-04	
Lu										2.E-04		
Hf		3.E-03					2.E-03					
Pb	5.E-02									2.E-01		
Th	2.E-02	6.E-03		3.E-04		3.E-03		5.E-05		4.E-02		
U	3.E-03	9.E-04				4.E-04		2.E-05		1.E-03		

NOTES

Category: F - fibrous; LOW-P - low purity monocrystalline: GEM - higher purity monocrystalline (See section 3.3 Chapter 3)

Blank cell - Sample value below LOQ: See electronic file for unfiltered data

Sample concentrations in Table A1

NR - Not reported

Appendix - Table A2. 2σ uncertainties on sample concentrations in Table A1.

LOCALITY	Ekati	Ekati	Ekati	Ekati	Ekati	Ekati	Ekati	Ekati	Ekati	Ekati	Ekati	Ekati
KIMBERLITE	Fox	Misery	Fox	Mis	Misery	Fox	Mis	Mis	Fox	Fox	Fox	Fox
Type	Monocrystalline	Monocrystalline	Monocrystalline	Fibrous cube	Monocrystalline	Monocrystalline	Monocrystalline	Monocrystalline	Monocrystalline	Monocrystalline	Fibrous Coat	Fibrous Coat
Colour	C-less	C-less	C-less	C-less	C-less	Brown	C-less	Yellow	C-less	C-less	Grey	Grey
Category	GEM	GEM	GEM	GEM	GEM	GEM	GEM	GEM	GEM	GEM	F	F
Wt. (mg)	25.17	4.80	20.56	3.71	3.54	8.67	5.89	3.94	29.41	5.70	5.28	34.32
Wt. loss (mg)	0.45	0.39	0.37	0.37	0.39	0.31	0.31	0.10	0.45	0.40	0.41	0.36
Ablation (hrs)	4	4	4	4	4	3	3	4	5	6	5	5
SAMPLE #	243	291	241	261	263	131	262	264	111	151	E151	E152
(2σ,ppm)												
Ti												
Rb									6.E-03		4.E-02	9.E-02
Sr	3.E-02								4.E-02	2.E-02	5.E-01	3.E+00
Y								9.E-03		2.E-03		
Zr									2.E-02	3.E-02		
Nb												
Cs									5.E-04	9.E-05	4.E-03	5.E-03
Ba									1.E-02		1.E+01	2.E+01
La									5.E-03	3.E-03	2.E-01	1.E+00
Ce									5.E-03	4.E-03	2.E-01	1.E+00
Pr								9.E-04	3.E-04	8.E-04	7.E-03	2.E-02
Nd								1.E-02	2.E-03	3.E-03	1.E-02	3.E-02
Sm								1.E-02				6.E-03
Eu											3.E-03	4.E-03
Gd								4.E-03		5.E-04	2.E-03	5.E-03
Tb								1.E-04				
Dy								3.E-03		6.E-04		1.E-03
Er		2.E-04		2.E-04	4.E-04	7.E-04		7.E-04		5.E-04		
Yb					9.E-04							
Lu												
Hf												
Pb										1.E-02	1.E-01	2.E-01
Th									1.E-02	1.E-03	9.E-02	2.E-01
U									1.E-03	3.E-04	7.E-03	1.E-02

NOTES

Category: F - fibrous; LOW-P - low purity monocrystalline: GEM - higher purity monocrystalline (See section 3.3 Chapter 3)

Blank cell - Sample value below LOQ: See electronic file for unfiltered data

Sample concentrations in Table A1

NR - Not reported

Appendix - Table A2. 2σ uncertainties on sample concentrations in Table A1.

LOCALITY	Ekati	Ekati	Ekati	Ekati	Ekati	Ekati	Ekati	Ekati	Ekati	Ekati	Ekati	Ekati
KIMBERLITE	Fox	Fox	Fox	Fox	Fox	Fox	Fox	Fox	Fox	Fox	Fox	Misery
Type	Fibrous Coat	Fibrous Coat	Fibrous Coat	Fibrous Cube	Monocrystalline	Monocrystalline	Monocrystalline	Monocrystalline	Monocrystalline	Monocrystalline	Monocrystalline	Monocrystalline
Colour	Grey	Grey	Grey	Brown	C-less	C-less	C-less	C-less	C-less	Brown	C-less	Brown
Category	F	F	F	F	GEM	GEM	GEM	GEM	GEM	GEM	GEM	GEM
Wt. (mg)	15.66	31.16	29.09	5.32	34.68	16.37	31.47	14.12	4.14	23.15	9.08	6.51
Wt. loss (mg)	0.71	0.31	0.32	0.32	0.50	0.21	0.45	0.56	0.54	0.56	0.52	0.28
Ablation (hrs)	4	4	5	4	7	5	4	6	5.5	7	6	3
SAMPLE #	**E153**	**E154**	**E111**	**E11014**	**152**	**153**	**154**	**E121**	**E122**	**E161**	**E171**	**E2104**
(2σ,ppm)												
Ti												
Rb	3.E-02	3.E-02	1.E-01	5.E-02								
Sr	1.E+00	2.E-01	5.E-01	1.E-01	2.E-02	6.E-02						
Y	2.E-03			6.E-03	6.E-04	2.E-03						
Zr					8.E-03		2.E-02					
Nb			2.E-02	3.E-02	#VALUE!	4.E-03						
Cs	1.E-03	2.E-03	4.E-03	2.E-03	#VALUE!							
Ba	7.E+00	7.E+00	1.E+01	2.E+00	4.E-02	2.E-02	1.E-02			4.E-02		2.E-02
La	4.E-01	5.E-02	3.E-01	6.E-02	8.E-03	2.E-02	9.E-04					
Ce	3.E-01	8.E-02	2.E-01	7.E-02	7.E-03	3.E-02						
Pr	1.E-02	4.E-03	8.E-03	6.E-03	4.E-04	3.E-03	3.E-04					
Nd	2.E-02	8.E-03	2.E-02	3.E-02	1.E-03	1.E-02	4.E-04					
Sm	3.E-03		4.E-03	4.E-03	7.E-04	4.E-03	2.E-04					
Eu	1.E-03		4.E-03	3.E-03	2.E-04	3.E-04						
Gd	9.E-04		2.E-03	7.E-03	7.E-04	3.E-03						
Tb				7.E-04	5.E-05	2.E-04						
Dy	6.E-04			2.E-03	2.E-04	2.E-03						
Er						2.E-04						
Yb												5.E-04
Lu												
Hf					6.E-04		7.E-04					
Pb	6.E-02		1.E-01		5.E-02	5.E-02	8.E-03					
Th	6.E-02	7.E-03	1.E-01	8.E-03	4.E-03	1.E-02	3.E-04					
U	3.E-03	2.E-03	1.E-02	2.E-03	2.E-04	1.E-03	3.E-03					

NOTES

Category: F - fibrous; LOW-P - low purity monocrystalline: GEM - higher purity monocrystalline (See section 3.3 Chapter 3)

Blank cell - Sample value below LOQ: See electronic file for unfiltered data

Sample concentrations in Table A1

NR - Not reported

Appendix - Table A2. 2σ uncertainties on sample concentrations in Table A1.

	CANADA, Slave Province									
LOCALITY	Ekati	Ekati	Ekati	Ekati	Ekati	Ekati	Diavik	Diavik	Diavik	Diavik
KIMBERLITE	Fox	Misery	Misery	Misery	Misery	Fox	Unknown	Unknown	Unknown	Unknown
Type	Fibrous Cube	Monocrystalline	Monocrystalline	Monocrystalline	Monocrystalline	Fibrous Cube	Fibrous Coat	Fibrous Coat	Fibrous Coat	Fibrous Cube
Colour	Grey	Brown	C-less	C-less	Brown	Grey	Black	Black	Black	Black
Category	F	GEM	GEM	GEM	GEM	F	F	F	F	F
Wt. (mg)	5.83	6.63	10.31	5.41	54.37	4.40	572.72	142.49	160.91	19.96
Wt. loss (mg)	0.42	0.28	0.26	0.20	0.28	0.40	0.32	0.39	0.45	0.32
Ablation (hrs)	4	3	3	3	3	4	3	3	5	3
SAMPLE #	**E217**	**E2105**	**E2102**	**E2103**	**E21011**	**E191**	**D104**	**D126**	**D131**	**D168**
(2σ ppm)										
Ti										
Rb	2.E-01				3.E-02	4.E-02	3.E-02	5.E-02	4.E-02	4.E-02
Sr	2.E+00					6.E+00	6.E-01	6.E-01	9.E-01	7.E-01
Y	1.E-02						4.E-03			
Zr	7.E-02	5.E-02	3.E-02	4.E-02		4.E-02				
Nb	1.E-01				4.E-02		2.E-02		2.E-02	
Cs	3.E-03					1.E-03	2.E-03	3.E-03	3.E-03	2.E-03
Ba	1.E+01			6.E-02		6.E+00	1.E+01	1.E+01	2.E+01	1.E+01
La	5.E-01				3.E-02	5.E-01	2.E-01	3.E-01	2.E-01	2.E-01
Ce	5.E-01				6.E-02	3.E-01	1.E-01	2.E-01	2.E-01	2.E-01
Pr	3.E-02				8.E-03	8.E-03	1.E-02	1.E-02	1.E-02	9.E-03
Nd	9.E-02				4.E-02	2.E-02	1.E-02	2.E-02	2.E-02	3.E-02
Sm	2.E-02				7.E-03		4.E-03		3.E-03	
Eu	2.E-03					2.E-03	4.E-03	2.E-03	2.E-03	3.E-03
Gd	1.E-02				5.E-03	2.E-03	3.E-03	3.E-03	6.E-03	3.E-03
Tb	2.E-03				4.E-04		3.E-04			
Dy	4.E-03				2.E-03		4.E-03			
Er	3.E-03						2.E-03			
Yb										
Lu										
Hf		2.E-03	7.E-04							
Pb	1.E-01					2.E-01	1.E-01	1.E-01	1.E-01	
Th	9.E-02	8.E-04			8.E-03	6.E-03	7.E-02	8.E-02	8.E-02	3.E-02
U	3.E-02					1.E-03	8.E-03	8.E-03	8.E-03	9.E-03

NOTES

Category: F - fibrous; LOW-P - low purity monocrystalline: GEM - higher purity monocrystalline (See section 3.3 Chapter 3)

Blank cell - Sample value below LOQ: See electronic file for unfiltered data

Sample concentrations in Table A1

NR - Not reported

Appendix - Table A2. 2σ uncertainties on sample concentrations in Table A1.

LOCALITY	Diavik	Diavik	Diavik	Diavik	Diavik	Diavik	Diavik	Diavik	Diavik	Diavik	Diavik	Diavik
KIMBERLITE	Unknown	Unknown	Unknown	Unknown	Unknown	Unknown	Unknown	Unknown	Unknown	Unknown	Unknown	Unknown
Type	Fibrous Cube	Fibrous Cube	Monocrystalline	Monocrystalline	Monocrystalline	Monocrystalline	Monocrystalline	Monocrystalline	Monocrystalline	Monocrystalline	Monocrystalline	Monocrystalline
Colour	Black	Black	C-less	C-less	C-less	C-less	C-less	C-less	C-less	C-less	C-less	C-less
Category	F	F	GEM	GEM	GEM	GEM	GEM	GEM	GEM	GEM	GEM	GEM
Wt. (mg)	11.05	12.36	159.59	144.05	175.33	159.25	138.71	146.07	712.80	131.57	171.42	177.73
Wt. loss (mg)	0.39	0.40	0.26	0.20	0.23	0.27	0.02	0.23	0.29	0.25	0.22	0.26
Ablation (hrs)	5	5	3	3	3	3	3	3	3	3	3	3
SAMPLE #	**D169**	**D170**	**D113**	**D116**	**D115**	**D114**	**D110**	**D112**	**D102**	**D118**	**D108**	**D117**
(2σ,ppm)												
Ti												6.E+00
Rb	2.E-02	3.E-02										
Sr	4.E-01	4.E-01										
Y												
Zr									4.E-03			
Nb		2.E-02										
Cs	3.E-03	2.E-03										
Ba	2.E+01	9.E+00	3.E-02						6.E-01	1.E-02	3.E-02	2.E-02
La	2.E-01	1.E-01	6.E-04								2.E-03	
Ce	1.E-01	7.E-02										
Pr	8.E-03	5.E-03									3.E-04	
Nd	1.E-02	1.E-02									3.E-03	
Sm										8.E-04	1.E-03	6.E-04
Eu	2.E-03	2.E-03							9.E-04			
Gd	2.E-03	2.E-03										
Tb												
Dy												
Er												
Yb												
Lu												
Hf									1.E-03			
Pb												
Th	6.E-02	5.E-02	5.E-04							6.E-04	3.E-03	5.E-04
U	4.E-03	5.E-03									7.E-04	

NOTES

Category: F - fibrous; LOW-P - low purity monocrystalline: GEM - higher purity monocrystalline (See section 3.3 Chapter 3)

Blank cell - Sample value below LOQ: See electronic file for unfiltered data

Sample concentrations in Table A1

NR - Not reported

Appendix - Table A2. 2σ uncertainties on sample concentrations in Table A1.

LOCALITY	Diavik	Diavik	Diavik	Diavik	Diavik	Diavik	Diavik	Diavik	Diavik	Diavik	Diavik
KIMBERLITE	Unknown	Unknown	Unknown	Unknown	Unknown	Unknown	Unknown	Unknown	Unknown	Unknown	Unknown
Type	Monocrystalline	Monocrystalline	Monocrystalline	Monocrystalline	Monocrystalline	Monocrystalline	Monocrystalline	Monocrystalline	Monocrystalline	Monocrystalline	Fibrous Cube
Colour	C-less	C-less	C-less	C-less	C-less	C-less	C-less	C-less	C-less	C-less	Black
Category	GEM	GEM	GEM	GEM	GEM	GEM	GEM	GEM	GEM	GEM	F
Wt. (mg)	20.21	16.98	15.60	22.12	13.65	20.41	16.47	13.27	21.75	18.60	10.70
Wt. loss (mg)	0.24	0.25	0.24	0.23	0.21	0.26	0.22	0.23	0.25	0.23	0.19
Ablation (hrs)	3	3	3	3	3	3	3	3	3	3	3
SAMPLE #	**D181**	**D200**	**D201**	**D173**	**D199**	**D182**	**D183**	**D185**	**D186**	**D184**	**D167**
(2σ ppm)											
Ti				4.E+00				4.E+00			
Rb											1.E-02
Sr											
Y											
Zr					6.E-03	3.E-02					
Nb											
Cs											4.E-03
Ba			4.E-02	2.E-02	2.E-02		2.E-02			1.E-02	3.E+00
La			1.E-03								7.E-02
Ce											9.E-02
Pr				2.E-04							4.E-03
Nd				2.E-03							2.E-02
Sm	1.E-03		2.E-03			1.E-03					
Eu	7.E-04		8.E-04			7.E-04					5.E-03
Gd											2.E-03
Tb											
Dy						4.E-04					3.E-03
Er											
Yb											
Lu											
Hf						2.E-03					
Pb				2.E-03							
Th		3.E-04	1.E-03						8.E-04		6.E-02
U			1.E-04	3.E-04					3.E-04		8.E-03

NOTES

Category: F - fibrous; LOW-P - low purity monocrystalline: GEM - higher purity monocrystalline (See section 3.3 Chapter 3)

Blank cell - Sample value below LOQ: See electronic file for unfiltered data

Sample concentrations in Table A1

NR - Not reported

Appendix - Table A2. 2σ uncertainties on sample concentrations in Table A1.

	CANADA, Slave Province											
LOCALITY	Snap Lake	Snap Lake	Snap Lake	Snap Lake	Snap Lake	Snap Lake	Snap Lake	Snap Lake	Snap Lake	Snap Lake	Snap Lake	Snap Lake
KIMBERLITE	Snap/King Lake Dyke	Snap/King Lake Dyke	Snap/King Lake Dyke	Snap/King Lake Dyke	Snap/King Lake Dyke	Snap/King Lake Dyke	Snap/King Lake Dyke	Snap/King Lake Dyke	Snap/King Lake Dyke	Snap/King Lake Dyke	Snap/King Lake Dyke	Snap/King Lake Dyke
Type	Monocrystalline	Monocrystalline	Monocrystalline	Monocrystalline	Monocrystalline	Monocrystalline	Monocrystalline	Monocrystalline	Monocrystalline	Monocrystalline	Mono-Coat	Mono-Coat
Colour	C-less	C-less	C-less	C-less	C-less	C-less	C-less	C-less	C-less	C-less	Yellow	Yellow
Category	GEM	GEM	GEM	GEM	GEM	GEM	GEM	GEM	GEM	GEM	LOW-P	LOW-P
Wt. (mg)	152.11	143.84	175.84	153.29	177.35	156.36	176.05	160.58	141.51	166.01	179.89	174.54
Wt. loss (mg)	2.90	0.45	0.60	0.80	0.29	0.31	0.31	0.32	0.34	0.31	0.53	0.41
Ablation (hrs)	27	6	6	8	5	3	3	3	3	3	6	5
SAMPLE #	B2-1	B2-2	B2-3	B2-4	B2-5	B1-1	B1-2	B1-3	B1-4	B1-5	B3-11	B3-12
(2σ; ppm)												
Ti							3.E+00					
Rb											1.E-03	1.E-03
Sr					2.E-02						3.E-02	3.E-03
Y											2.E-03	
Zr		8.E-03				3.E-02			3.E-02			
Nb											1.E-02	2.E-03
Cs											2.E-04	3.E-04
Ba	4.E-03		7.E-03		1.E-01			1.E-02		1.E-02	9.E-02	2.E-02
La			2.E-03						1.E-03		1.E-02	3.E-03
Ce			2.E-02						7.E-03		6.E-03	2.E-03
Pr											1.E-03	3.E-04
Nd											3.E-03	2.E-03
Sm											2.E-03	5.E-04
Eu											7.E-04	3.E-04
Gd											1.E-03	8.E-04
Tb											2.E-04	7.E-05
Dy											4.E-04	3.E-04
Er											4.E-04	
Yb												
Lu												
Hf						3.E-04						
Pb	2.E-03											
Th											2.E-03	1.E-03
U											1.E-04	1.E-04

NOTES

Category: F - fibrous; LOW-P - low purity monocrystalline: GEM - higher purity monocrystalline (See section 3.3 Chapter 3)

Blank cell - Sample value below LOQ: See electronic file for unfiltered data

Sample concentrations in Table A1

NR - Not reported

Appendix - Table A2. 2σ uncertainties on sample concentrations in Table A1.

LOCALITY	Snap Lake	Snap Lake	Snap Lake	Snap Lake	Snap Lake	Snap Lake	Snap Lake	Snap Lake	Snap Lake	Snap Lake	Snap Lake	Snap Lake
KIMBERLITE	Snap/King Lake Dyke	Snap/King Lake Dyke	Snap/King Lake Dyke	Snap/King Lake Dyke	Snap/King Lake Dyke	Snap/King Lake Dyke	Snap/King Lake Dyke	Snap/King Lake Dyke	Snap/King Lake Dyke	Snap/King Lake Dyke	Snap/King Lake Dyke	Snap/King Lake Dyke
Type	Mono-Coat	Mono-Coat	Mono-Coat	Mono-Coat	Mono-Coat	Mono-Coat	Mono-Coat	Mono-Coat	Mono-Coat	Mono-Coat	Mono-Coat	Mono-Coat
Colour	Grey	Grey	C-less	C-less	Yellow	Grey	Grey	Grey	Yellow	Yellow	C-less	Grey
Category	LOW-P	LOW-P	LOW-P	LOW-P	LOW-P	LOW-P	LOW-P	LOW-P	LOW-P	LOW-P	LOW-P	LOW-P
Wt. (mg)	168.50	140.59	148.92	174.22	165.98	171.37	141.43	150.95	174.78	152.66	171.18	179.16
Wt. loss (mg)	0.51	0.35	0.35	0.39	0.38	0.20	0.17	0.18	0.18	0.19	0.15	0.19
Ablation (hrs)	6	4	4	4	5	3	3	3	3	3	3	3
SAMPLE #	**B3-13**	**B3-14**	**B3-15**	**B3-16**	**B3-1**	**B3-2**	**B3-3**	**B3-4**	**B3-17**	**B3-18**	**B3-19**	**B3-20**
(2σ; ppm)												
Ti	1.E+01	3.E+00		3.E+00			1.E+01		7.E+00	7.E+00		5.E+00
Rb	2.E-01	7.E-02	1.E-02				2.E-02		3.E-02			4.E-03
Sr	3.E+00	2.E-01	7.E-01	8.E-04	5.E-03	7.E-03	2.E-01	1.E-01	6.E-02	1.E-01		1.E-01
Y	1.E-01	9.E-03	4.E-03				7.E-02	3.E-03	9.E-03			5.E-03
Zr	3.E-01	8.E-02					1.E-01		5.E-02			5.E-02
Nb	5.E-01	6.E-02	3.E-03	2.E-03	3.E-03		3.E-01	4.E-02	3.E-03			1.E-02
Cs	2.E-03	2.E-04	2.E-04				8.E-04		4.E-04			5.E-04
Ba	5.E+00	3.E+00	2.E-01	1.E-02	3.E-02	5.E-02	5.E-01	7.E-02	5.E-01	2.E-01	9.E-03	1.E-01
La	4.E-01	3.E-01	8.E-01	4.E-03	3.E-03	6.E-03	2.E-01	4.E-01	2.E-01	7.E-03		1.E-02
Ce	5.E-01	6.E-01	4.E-01		3.E-03		8.E-01	3.E-01	7.E-01	5.E-03		2.E-02
Pr	6.E-02	4.E-02	2.E-02	2.E-04	2.E-04	7.E-04	1.E-01	1.E-02	4.E-02	1.E-03		4.E-03
Nd	3.E-01	1.E-01	4.E-02	1.E-03	2.E-03		5.E-01	6.E-02	1.E-01	3.E-03		1.E-02
Sm	5.E-02	2.E-02	7.E-03		3.E-04		1.E-01	1.E-02	2.E-02	4.E-03		6.E-03
Eu	2.E-02	3.E-03	1.E-03				2.E-02	4.E-03	3.E-03			2.E-03
Gd	6.E-02	7.E-03	6.E-03		4.E-04		5.E-02	1.E-02	2.E-02	6.E-04		2.E-03
Tb	4.E-03	9.E-04	6.E-04		6.E-05		5.E-03	1.E-03	2.E-03			5.E-04
Dy	2.E-02	8.E-03	1.E-03				1.E-02	3.E-03	5.E-03			3.E-03
Er	9.E-03	4.E-03	1.E-03				5.E-03	2.E-03	3.E-03			7.E-04
Yb	3.E-03	1.E-03					3.E-03	1.E-03	3.E-03			1.E-03
Lu	2.E-04	3.E-04					4.E-04	3.E-04	2.E-04			
Hf	4.E-03	2.E-03					2.E-03		1.E-03			
Pb	4.E-03											
Th	5.E-02	2.E-02	3.E-03	5.E-04	6.E-04	7.E-04	2.E-02	9.E-03	1.E-03	5.E-04	9.E-04	5.E-03
U	1.E-02	6.E-03	3.E-04	2.E-04	2.E-04	4.E-04	5.E-03	1.E-03	8.E-04	1.E-03		2.E-03

NOTES

Category: F - fibrous; LOW-P - low purity monocrystalline: GEM - higher purity monocrystalline (See section 3.3 Chapter 3)

Blank cell - Sample value below LOQ: See electronic file for unfiltered data

Sample concentrations in Table A1

NR - Not reported

Appendix - Table A2. 2σ uncertainties on sample concentrations in Table A1.

LOCALITY	Snap Lake	Snap Lake	Snap Lake	Snap Lake	Snap Lake	Snap Lake	Snap Lake	Snap Lake	Snap Lake	Snap Lake	Snap Lake	Snap Lake
KIMBERLITE	Snap/King Lake Dyke	Snap/King Lake Dyke	Snap/King Lake Dyke	Snap/King Lake Dyke	Snap/King Lake Dyke	Snap/King Lake Dyke	Snap/King Lake Dyke	Snap/King Lake Dyke	Snap/King Lake Dyke	Snap/King Lake Dyke	Snap/King Lake Dyke	Snap/King Lake Dyke
Type	Mono-Coat	Mono-Coat	Mono-Coat	Mono-Coat	Mono-Coat	Mono-Coat	Mono-Coat	Mono-Coat	Mono-Coat	Mono-Coat	Mono-Coat	Mono-Coat
Colour	Yellow	Grey	Grey	Yellow	C-less	Yellow	Green	Brown	Grey	Yellow	Brown	Brown
Category	LOW-P	LOW-P	LOW-P	LOW-P	LOW-P	LOW-P	LOW-P	LOW-P	LOW-P	LOW-P	LOW-P	LOW-P
Wt. (mg)	166.34	172.97	151.47	145.57	144.86	162.95	214.13	280.03	258.77	234.38	288.50	304.30
Wt. loss (mg)	0.32	0.30	0.58	0.53	0.50	0.70	0.26	0.25	0.25	0.21	0.24	0.26
Ablation (hrs)	3	3	6	6	5	7	3	3	3	3	3	3
SAMPLE #	**B3-5**	**B3-6a**	**B3-7a**	**B3-8**	**B3-9**	**B3-10**	**SL-1**	**SL-19**	**SL-38**	**SL-39**	**SL-50**	**SL-57**
(2σ: ppm)												
Ti								3.E+00		2.E+01	8.E+00	3.E+00
Rb	2.E-02	5.E-02	1.E-02	8.E-03	7.E-03							
Sr	6.E-02	6.E-01	5.E-02	5.E-02								
Y		8.E-03									3.E-03	2.E-04
Zr		6.E-02	6.E-02							1.E-02		
Nb	2.E-02	7.E-02	2.E-02	7.E-03	3.E-02	2.E-03					4.E-03	
Cs		4.E-03	9.E-04		1.E-04							
Ba	8.E-01	2.E+00	1.E+00	3.E-01	7.E-01	7.E-02		7.E-03		1.E-01	2.E-02	4.E-02
La	1.E-02	2.E-01	3.E-02	1.E-02	4.E-02	2.E-03					8.E-03	1.E-03
Ce		4.E-01	3.E-02	2.E-02	6.E-02	4.E-03					1.E-02	3.E-03
Pr	3.E-03	4.E-02	1.E-03	1.E-03	5.E-03	3.E-04					2.E-03	5.E-04
Nd	2.E-02	7.E-02	1.E-02	1.E-02	5.E-03	3.E-03					7.E-03	2.E-03
Sm	9.E-04	1.E-02	6.E-04	1.E-03	2.E-03						2.E-03	6.E-04
Eu		4.E-03			3.E-04						4.E-04	
Gd	5.E-03	9.E-03	1.E-03	1.E-03	1.E-03	2.E-04					1.E-03	2.E-04
Tb	3.E-04	1.E-03	2.E-04	4.E-04	5.E-05						1.E-04	4.E-05
Dy		7.E-03	9.E-05	1.E-03	5.E-04						4.E-04	1.E-04
Er		3.E-03			2.E-04						8.E-04	
Yb												
Lu												
Hf												
Pb												
Th	4.E-03	2.E-02	1.E-03	3.E-03	5.E-03	3.E-04					4.E-04	8.E-04
U	1.E-03	5.E-03	1.E-03	1.E-03	5.E-04	1.E-04					4.E-04	2.E-04

NOTES

Category: F - fibrous; LOW-P - low purity monocrystalline: GEM - higher purity monocrystalline (See section 3.3 Chapter 3)

Blank cell - Sample value below LOQ: See electronic file for unfiltered data

Sample concentrations in Table A1

NR - Not reported

Appendix - Table A2. 2σ uncertainties on sample concentrations in Table A1.

LOCALITY	Snap Lake	Snap Lake	Snap Lake	Snap Lake	Snap Lake	Snap Lake	Snap Lake	Snap Lake
KIMBERLITE	Snap/King Lake Dyke	Snap/King Lake Dyke	Snap/King Lake Dyke	Snap/King Lake Dyke	Snap/King Lake Dyke	Snap/King Lake Dyke	Snap/King Lake Dyke	Snap/King Lake Dyke
Type	Monocrystalline	Monocrystalline	Monocrystalline	Monocrystalline	Monocrystalline	Monocrystalline	Monocrystalline	Monocrystalline
Colour	C-less	C-less	C-less	C-less	C-less	C-less	C-less	C-less
Category	GEM	GEM	GEM	LOW-P	LOW-P	GEM	GEM	GEM
Wt. (mg)	169.93	161.72	157.29	5.68	16.96	30.05	18.01	54.81
Wt. loss (mg)	0.35	0.33	0.30	0.30	0.30	0.30	0.30	0.30
Ablation (hrs)	3.5	3	3	3	3	3	3	3
SAMPLE #	**B1-6**	**B1-7**	**B1-8**	**B3-6b**	**B3-7b**	**B4-5**	**B4-7**	**B4-10**
(2σ, ppm)								
Ti	4.E+00	2.E+01	3.E+00			2.E+01	4.E+01	5.E+01
Rb								
Sr								
Y								
Zr	1.E-02	4.E-02	2.E-02					
Nb				6.E-03				
Cs								
Ba		3.E-02		5.E-01	1.E+00	1.E-01		
La		3.E-03		7.E-03				
Ce		2.E-02		7.E-03				
Pr				3.E-04				
Nd				2.E-03				
Sm								5.E-03
Eu				1.E-03				
Gd				1.E-03				
Tb								
Dy								
Er								
Yb								
Lu								
Hf								
Pb								
Th				9.E-04				
U				2.E-04				

NOTES

Category: F - fibrous; LOW-P - low purity monocrystalline: GEM - higher purity monocrystalline (See section 3.3 Chapter 3)

Blank cell - Sample value below LOQ: See electronic file for unfiltered data

Sample concentrations in Table A1

NR - Not reported

Appendix - Table A2. 2σ uncertainties on sample concentrations in Table A1.

	DEMOCRATIC REPUBLIC OF CONGO, Congo Craton										
LOCALITY	DR Congo	DR Congo	DR Congo	DR Congo	DR Congo	DR Congo	DR Congo	DR Congo	DR Congo	DR Congo	DR Congo
KIMBERLITE	Unknown	Unknown	Unknown	Unknown	Unknown	Unknown	Unknown	Unknown	Unknown	Unknown	Unknown
Type	Fibrous Coat	Fibrous Coat	Fibrous Coat	Fibrous Coat	Fibrous Coat	Fibrous Coat	Fibrous Coat	Fibrous Coat	Fibrous Coat	Fibrous Coat	Fibrous Coat
Colour	Yellow	Grey	Grey	Yellow/Grey	Brown	Grey	Grey	Grey	Grey	Grey	Green/Brown
Category	F	F	F	F	F	F	F	F	F	F	F
Wt. (mg)	28.66	27.24	21.17	28.92	22.57	22.86	20.60	21.32	19.53	21.50	43.49
Wt. loss (mg)	0.31	0.29	0.25	0.29	0.33	0.29	0.31	0.27	0.26	0.29	0.44
Ablation (hrs)	0.75	0.75	0.75	0.75	0.75	0.75	0.75	0.75	0.75	0.75	3
SAMPLE #	**CNG-1**	**CNG-3**	**CNG-2**	**CNG-4**	**CNG-5**	**CNG-11**	**CNG-7**	**CNG-8**	**CNG-9**	**CNG-10**	**DRC-2**
(2σ ppm)											
Ti						7.E+00			7.E+00		4.E-01
Rb						2.E-01		2.E-02	6.E-02	4.E-02	5.E-02
Sr	1.E-01			2.E-01	3.E-01	6.E+00	9.E-02	4.E-01	3.E-01	8.E-01	1.E+00
Y	1.E-02			1.E-02	1.E-02	2.E-01		1.E-02	4.E-02	6.E-02	1.E-02
Zr						2.E-01		4.E-02		6.E-02	8.E-02
Nb						2.E-01		7.E-03	1.E-02	1.E-02	1.E-01
Cs	NR	NR	NR	NR	NR	NR	NR	NR	NR	NR	2.E-03
Ba	4.E-01		8.E-02	4.E-01	3.E-01	8.E+00	3.E-01	3.E+00	1.E+00	4.E+00	1.E+00
La	8.E-02	6.E-03	1.E-02	5.E-02	9.E-02	2.E+01	1.E-02	2.E-01	9.E-02	2.E+00	1.E-01
Ce	5.E-02			6.E-02	9.E-02	1.E+01		2.E-01	3.E-01	1.E+00	3.E-01
Pr	1.E-02	9.E-04	3.E-03	2.E-02	6.E-03	2.E+00	2.E-03	1.E-02	3.E-02	1.E-01	2.E-02
Nd	2.E-02	7.E-03	9.E-03	5.E-02	4.E-02	3.E+00	2.E-02	3.E-02	1.E-01	4.E-01	6.E-02
Sm	7.E-03			1.E-02	1.E-02	2.E-01		1.E-02	9.E-03	7.E-02	1.E-02
Eu	2.E-03			5.E-03	3.E-03	6.E-02		3.E-03	5.E-03	1.E-02	2.E-03
Gd	6.E-03	4.E-03		9.E-03	9.E-03	1.E-01		8.E-03	4.E-02	4.E-02	2.E-01
Tb	7.E-04	3.E-04		7.E-04	7.E-04	1.E-02		7.E-04	4.E-03	1.E-03	6.E-04
Dy	3.E-03			3.E-03	7.E-03	3.E-02		3.E-03	1.E-02	1.E-02	3.E-03
Er	7.E-04			1.E-03	1.E-03	1.E-02		1.E-03	7.E-03	1.E-02	6.E-04
Yb						4.E-03			5.E-03	6.E-03	1.E-03
Lu						1.E-03			2.E-03	3.E-04	8.E-05
Hf						5.E-03		5.E-03		5.E-03	2.E-03
Pb	3.E-01	4.E-01		3.E-01		1.E+01			3.E-01	1.E+00	2.E-01
Th	3.E-03		3.E-03	7.E-03	9.E-03	1.E-01	1.E-03	2.E-02	9.E-03	7.E-02	1.E-02
U	5.E-04			1.E-03	2.E-03	1.E-02	1.E-03	2.E-03	1.E-03	4.E-03	3.E-03

NOTES

Category: F - fibrous; LOW-P - low purity monocrystalline: GEM - higher purity monocrystalline (See section 3.3 Chapter 3)

Blank cell - Sample value below LOQ: See electronic file for unfiltered data

Sample concentrations in Table A1

NR - Not reported

Appendix - Table A2. 2σ uncertainties on sample concentrations in Table A1.

	SOUTH AFRICA, Kaapvaal Craton											
LOCALITY	Cullinan	Cullinan	Cullinan	Cullinan	Cullinan	Cullinan	Cullinan	Cullinan	Cullinan	Cullinan	Cullinan	Cullinan
KIMBERLITE	Unknown	Unknown	Unknown	Unknown	Unknown	Unknown	Unknown	Unknown	Unknown	Unknown	Unknown	Unknown
Type	Monocrystalline	Monocrystalline	Monocrystalline	Monocrystalline	Monocrystalline	Monocrystalline	Monocrystalline	Monocrystalline	Monocrystalline	Monocrystalline	Monocrystalline	Monocrystalline
Colour	C-less	C-less	C-less	C-less	C-less	C-less	C-less	C-less	C-less	C-less	C-less	C-less
Category	GEM	GEM	GEM	GEM	GEM	GEM	GEM	GEM	GEM	GEM	GEM	GEM
Wt. (mg)	47.67	39.28	93.36	53.63	56.54	64.47	44.49	39.37	49.22	52.94	47.24	38.87
Wt. loss (mg)	0.37	0.46	0.46	0.44	0.42	0.43	0.41	0.47	0.44	0.44	0.44	0.40
Ablation (hrs)	3	3	3	3	3	3	3	3	3	3	3	3
SAMPLE #	AP 25a	AP 26a	AP 28a	AP 30a	AP 31a	AP 34a	AP 35a	AP36a	AP 37a	AP 38a	AP 25b	AP 26b
(2σ,ppm)												
Ti												7.E+00
Rb											9.E-03	
Sr												
Y		3.E-04			7.E-04		6.E-04	3.E-04		3.E-04	3.E-03	3.E-03
Zr												
Nb							3.E-03				2.E-03	
Cs	3.E-04			1.E-04	1.E-04		2.E-04	1.E-04		1.E-04		
Ba												
La						1.E-03						
Ce						8.E-03						
Pr		1.E-04			2.E-04					2.E-04		
Nd		5.E-04	8.E-04		5.E-03		1.E-03			3.E-03	3.E-03	3.E-03
Sm		4.E-04			1.E-03		9.E-04	2.E-04		6.E-04		
Eu		6.E-04			4.E-04		4.E-04					
Gd		6.E-04			5.E-04		8.E-04					4.E-04
Tb				1.E-04	4.E-04		4.E-04	1.E-04	1.E-04	1.E-04		
Dy		3.E-04			5.E-04		7.E-04	1.E-04	1.E-04			
Er		4.E-04			6.E-04		5.E-04	2.E-04	1.E-04		6.E-04	1.E-03
Yb		5.E-04			1.E-04		7.E-04					
Lu		2.E-04			4.E-04		1.E-04	1.E-04				1.E-04
Hf		2.E-04			5.E-04		1.E-03					
Pb	5.E-03	2.E-03								2.E-03	2.E-02	5.E-03
Th		6.E-04			4.E-04		4.E-04	#NUM!				
U		1.E-04			1.E-04		1.E-04	1.E-04				

NOTES

Category: F - fibrous; LOW-P - low purity monocrystalline: GEM - higher purity monocrystalline (See section 3.3 Chapter 3)

Blank cell - Sample value below LOQ: See electronic file for unfiltered data

Sample concentrations in Table A1

NR - Not reported

Appendix - Table A2. 2σ uncertainties on sample concentrations in Table A1.

								BRAZIL, Sao Luiz Province		
LOCALITY	Cullinan	Cullinan	Cullinan	Jwaneng	Monastery	Monastery	Monastery	Mato Grosso	Mato Grosso	Mato Grosso
KIMBERLITE	Unknown	Unknown	Unknown	Unknown	Unknown	Unknown	Unknown	Juina	Juina	Juina
Type	Monocrystalline	Monocrystalline	Monocrystalline	Fibrous Coat	Mono-UHP	Mono-UHP	Mono-UHP	Mono-UHP	Mono-UHP	Mono-UHP
Colour	C-less	C-less	C-less	Grey	C-less	C-less	C-less	C-less	C-less	C-less
Category	GEM	GEM	GEM	F	GEM	GEM	GEM	GEM	GEM	GEM
Wt. (mg)	92.93	53.19	52.48	291.18	4.81	6.21	3.72	1.14	14.39	175.94
Wt. loss (mg)	0.41	0.43	0.46	0.42	0.47	0.52	0.37	0.82	0.88	0.66
Ablation (hrs)	3	3	3	3	7	6	6	3	3	7
SAMPLE #	**AP 28b**	**AP 30b**	**AP 38b**	**0N-JWN-110**	**A4-03**	**B9-15**	**B9-17**	**J-5103**	**J-5102**	**JUa2**
(2σ ppm)										
Ti				5.E+00				2.E+00		
Rb		2.E-02	2.E-03	4.E-02					2.E-03	
Sr				1.E+01				1.E-02	2.E-02	
Y		1.E-03	5.E-03	3.E-02	3.E-03			6.E-04	8.E-03	
Zr				8.E-02				7.E-03	3.E-02	
Nb				2.E-02		7.E-03		1.E-02	4.E-03	
Cs				2.E-03						
Ba		3.E-02		1.E+00				7.E-03	3.E-02	2.E-01
La				5.E-02				8.E-03	7.E-02	
Ce				1.E-01				7.E-03	4.E-02	
Pr				1.E-02				5.E-04	5.E-03	
Nd		4.E-03	1.E-03	5.E-02				1.E-03	2.E-02	
Sm				9.E-03				8.E-04	4.E-03	
Eu				2.E-03					6.E-04	
Gd				1.E-02				5.E-04	6.E-03	
Tb				1.E-03				1.E-04	4.E-04	
Dy				7.E-03	3.E-04			7.E-04	4.E-03	
Er	4.E-04	8.E-04	1.E-03	2.E-03	1.E-03			3.E-04	3.E-03	
Yb				2.E-03				2.E-04	2.E-03	
Lu				2.E-04				1.E-04	7.E-04	
Hf				2.E-03				4.E-04	5.E-04	
Pb		2.E-02		3.E-01				2.E-03	2.E-02	
Th				9.E-03				1.E-03	2.E-02	
U		7.E-05		6.E-03				2.E-04	1.E-03	

NOTES

Category: F - fibrous; LOW-P - low purity monocrystalline: GEM - higher purity monocrystalline (See section 3.3 Chapter 3)

Blank cell - Sample value below LOQ: See electronic file for unfiltered data

Sample concentrations in Table A1

NR - Not reported

Appendix - Table A2. 2σ uncertainties on sample concentrations in Table A1.

LOCALITY	Mato Grosso	Mato Grosso	Mato Grosso	Mato Grosso	Mato Grosso	Mato Grosso	Mato Grosso
KIMBERLITE	Juina	Juina	Juina	Juina	Juina	Juina	Juina
Type	Mono-UHP	Mono-UHP	Mono-UHP	Mono-UHP	Mono-UHP	Mono-UHP	Mono-UHP
Colour	C-less	C-less	C-less	C-less	C-less	C-less	C-less
Category	GEM	GEM	GEM	GEM	GEM	GEM	GEM
Wt. (mg)	45.71	135.80	7.70	7.08	8.41	31.06	2.75
Wt. loss (mg)	0.62	0.56	0.43	0.26	0.22	0.26	0.22
Ablation (hrs)	7	6	8	3	3	3	3
SAMPLE #	**JUc34**	**JUs41**	**2.8**	**J-104**	**J5-101**	**J5-102**	**J4-104**
(2σ ppm)							
Ti							
Rb							
Sr							
Y	2.E-03					2.E-02	
Zr							
Nb							
Cs							
Ba			3.E-02			4.E-02	2.E-01
La	1.E-03					1.E-01	
Ce						9.E-02	
Pr	3.E-04					1.E-02	
Nd	6.E-03	2.E-03				3.E-02	
Sm						1.E-02	
Eu						3.E-03	
Gd	7.E-04					1.E-02	
Tb	2.E-04	2.E-04				1.E-03	
Dy	4.E-04	5.E-04				9.E-03	
Er						3.E-03	
Yb						6.E-03	
Lu						8.E-04	
Hf							
Pb							
Th						7.E-03	
U							

NOTES

Category: F - fibrous; LOW-P - low purity monocrystalline: GEM - higher purity monocrystalline (See section 3.3 Chapter 3)

Blank cell - Sample value below LOQ: See electronic file for unfiltered data

Sample concentrations in Table A1

NR - Not reported

Appendix - Table A2. 2σ uncertainties on sample concentrations in Table A1.

	SYNTHETIC ORIGIN								
LOCALITY	Laboratoty	Laboratoty	Laboratoty	Laboratoty	Laboratoty	Laboratoty	Laboratoty	Laboratoty	Laboratoty
KIMBERLITE	N/a	N/a	N/a	N/a	N/a	N/a	N/a	N/a	N/a
Type	CVD	CVD	CVD	HPHT	CVD	CVD	CVD	HPHT	Inknown
Colour	C-less	Black	C-less	Yellow	C-less	Black	C-less	Yellow	C-less
Category									
Wt. (mg)	21.67	80.93	94.97	24.78	21.67	80.93	94.97	24.78	7.75
Wt. loss (mg)	0.73	0.3	0.42	0.31	0.51	0.35	0.36	0.37	0.25
Ablation (hrs)	3	5	5	3	5	3	3	3	3
SAMPLE #	**s16a**	**0843818-F1a**	**0743817-L1a**	**S407-27a**	**s16b**	**0843818-F1b**	**0743817-L1b**	**S407-27b**	**ADMPD2JKS**
(2σ ppm)									
Ti	9.E+00				2.E+00				1.E+01
Rb									
Sr									
Y		1.E-02							
Zr					1.E-02				
Nb									
Cs						3.E-04			
Ba	6.E-03		2.E-02	2.E-02	1.E-02				1.E-02
La									
Ce									
Pr									
Nd									
Sm									
Eu									
Gd									
Tb						5.E-05			
Dy									
Er									
Yb	1.E-03								
Lu	6.E-04								
Hf					9.E-04				
Pb		1.E-01		3.E-02		3.E-02			
Th	3.E-04				4.E-04				
U					7.E-04				

NOTES

Category: F - fibrous; LOW-P - low purity monocrystalline: GEM - higher purity monocrystalline (See section 3.3 Chapter 3)

Blank cell - Sample value below LOQ: See electronic file for unfiltered data

Sample concentrations in Table A1

NR - Not reported

Appendix - Table A2. 2σ uncertainties on sample concentrations in Table A1.

	RUSSIAN FEDERATION, Siberian Craton		VENEZUELA	LOQ
LOCALITY	Udachnaya	Mir	Venezuela	
KIMBERLITE	Unknown	Unknown	Unknown	
Type	Monocrystalline	Monocrystalline	Monocrystalline	
Colour	C-less	C-less	C-less	
Category	GEM	GEM	GEM	
Wt. (mg)	148.25	99.76	19.99	
Wt. loss (mg)	0.71	0.55	0.69	
Ablation (hrs)	3.00	3.00	3.00	
SAMPLE #	**3812P**	**1581**	**5921**	**$10\sigma_{Blank}$**
(2σ ppm)				**pg/g**
Ti				2.E+02
Rb	2.E-03	9.E-04		4.E-01
Sr	4.E-03	6.E-03		1.E+00
Y		3.E-04		3.E-02
Zr			3.E-03	2.E+00
Nb		1.E-03		4.E-01
Cs	NR	NR	NR	1.E-02
Ba	2.E-02	2.E-03		2.E+00
La		3.E-03		2.E-01
Ce		5.E-03		8.E-01
Pr		1.E-03		1.E-02
Nd		3.E-03		4.E-02
Sm		9.E-04		2.E-02
Eu		1.E-04		2.E-02
Gd				1.E-02
Tb		1.E-04		1.E-03
Dy		5.E-04		6.E-03
Er		1.E-04		6.E-03
Yb		2.E-04		2.E-02
Lu				7.E-03
Hf				6.E-02
Pb		2.E-03		2.E+00
Th		3.E-04		2.E-02
U		2.E-04		8.E-03

NOTES

Category: F - fibrous; LOW-P - low purity monocrystalline: GEM - higher purity monocrystalline (See section 3.3 Chapter 3)

Blank cell - Sample value below LOQ: See electronic file for unfiltered data

Sample concentrations in Table A1

NR - Not reported

Appendix - Table A2. 2σ uncertainties on sample concentrations in Table A1.

	COMBUSTIONS									
LOCALITY	DR Congo	DR Congo	DR Congo	DR Congo	DR Congo	DR Congo	Snap Lake	Snap Lake	Snap Lake	Snap Lake
KIMBERLITE	Unknown	Unknown	Unknown	Unknown	Unknown	Unknown	Snap/King Lake Dyke	Snap/King Lake Dyke	Snap/King Lake Dyke	Snap/King Lake Dyke
Type	Fibrous Coat	Fibrous Coat	Fibrous Coat	Fibrous Coat	Fibrous Coat	Fibrous Coat	Monocrystalline	Monocrystalline	Monocrystalline	Monocrystalline
Colour	Green/Brown	Green/Brown	Green/Brown	Yellow	Yellow	Yellow	C-less	C-less	C-less	C-less
Category	F	F	F	F	F	F	GEM	GEM	GEM	GEM
Wt. (mg)	-	-	-	-	-	-	-	-	3.45	-
Wt. loss (mg)	1.36	3.25	1.58	7.47	4.13	2.85	1.89	2.78	8.23	7.84
Ablation (hrs)	1.00	1.50	1.00	2.00	2.00	2.00	2.00	2.50	2.00	4.00
SAMPLE #	DRC-2a	DRC-2b	DRC-2c	CNG-1a	CNG-1b	CNG-1c	B4-5 a	B4-5 b	B3-6b	B3-7b
(2σ,ppm)										
Ti	3.E+00	1.E+00	7.E-01	2.E+00	9.E-01	1.E+00		5.E-01		
Rb	5.E-02	5.E-02	4.E-02	6.E-03	6.E-03	5.E-04			9.E-04	
Sr	7.E-01	9.E-01	7.E-01	2.E-01	3.E-01	3.E-02				
Y	1.E-02	4.E-03	5.E-03	2.E-02	2.E-02	2.E-03	9.E-04	3.E-03	3.E-04	1.E-04
Zr				4.E-01	2.E-01	3.E-01	1.E-01	7.E-02	6.E-03	7.E-03
Nb	7.E-02	9.E-02	5.E-02	1.E-02	3.E-03		2.E-03	1.E-03	4.E-03	1.E-02
Cs	4.E-04	2.E-04	2.E-04	2.E-04	3.E-04	6.E-05			1.E-04	
Ba	4.E-01	1.E+00	7.E-01	2.E+00	4.E+00	1.E-01	3.E-01	2.E-01	7.E-02	1.E-01
La	1.E-01	1.E-01	5.E-02	3.E-01	3.E-01	4.E-02	2.E-02	2.E-02	4.E-03	4.E-03
Ce	2.E-01	1.E-01	6.E-02	3.E-01	3.E-01	5.E-02	3.E-02	3.E-02	4.E-03	3.E-03
Pr	2.E-02	1.E-02	8.E-03	4.E-02	4.E-02	6.E-03	2.E-03	2.E-03	2.E-04	3.E-04
Nd	8.E-02	5.E-02	2.E-02	1.E-01	1.E-01	2.E-02	1.E-02	6.E-03	7.E-04	3.E-04
Sm	1.E-02	1.E-02	4.E-03	1.E-02	1.E-02	3.E-03	4.E-03	2.E-03	2.E-04	3.E-04
Eu	2.E-03	1.E-03	9.E-04	4.E-03	4.E-03	5.E-04	3.E-04	2.E-04	2.E-04	5.E-05
Gd	3.E-03	2.E-03	3.E-03	7.E-03	9.E-03	2.E-03	3.E-03	3.E-03	2.E-04	2.E-04
Tb	4.E-04	3.E-04	2.E-04	9.E-04	8.E-04	1.E-04	1.E-04	3.E-04	2.E-05	2.E-05
Dy	4.E-03	1.E-03	2.E-03	4.E-03	4.E-03	2.E-04	3.E-04	2.E-03	1.E-04	8.E-05
Er	1.E-03	2.E-04	5.E-04	2.E-03	1.E-03	7.E-05	8.E-04	4.E-04	9.E-05	7.E-05
Yb	8.E-04	5.E-04	5.E-04	8.E-04	1.E-03	1.E-04	6.E-04	4.E-04		
Lu	2.E-04	4.E-05	9.E-05	8.E-05	2.E-04	4.E-05	9.E-05	7.E-05		
Hf	7.E-04	6.E-05	2.E-04	3.E-03	1.E-03	1.E-03	2.E-03	8.E-04	4.E-05	
Pb	9.E-02	3.E-01	2.E-02	1.E-01	7.E-01	2.E-01	1.E-02	1.E-02	8.E-03	2.E-03
Th	2.E-02	2.E-02	1.E-02	3.E-02	2.E-02	4.E-03	4.E-03	1.E-03	6.E-04	2.E-04
U		2.E-03	2.E-03	4.E-03	3.E-03	6.E-04	7.E-04	3.E-04	2.E-04	2.E-04
									Gem Core of LOW-P B3-6/7	

NOTES

Category: F - fibrous; LOW-P - low purity monocrystalline: GEM - higher purity monocrystalline (See section 3.3 Chapter 3)

Blank cell - Sample value below LOQ: See electronic file for unfiltered data

Sample concentrations in Table A1

NR - Not reported

Appendix - Table A2. 2σ uncertainties on sample concentrations in Table A1.

	CANADA, Slave Province											
LOCALITY		**Snap Lake**	**Snap Lake**	**Snap Lake**	**Snap Lake**	**Snap Lake**	**Snap Lake**	**Snap Lake**	**Snap Lake**	**Snap Lake**	**Snap Lake**	**Snap Lake**
KIMBERLITE		**Snap/King Lake Dyke**	**Snap/King Lake Dyke**	**Snap/King Lake Dyke**	**Snap/King Lake Dyke**	**Snap/King Lake Dyke**	**Snap/King Lake Dyke**	**Snap/King Lake Dyke**	**Snap/King Lake Dyke**	**Snap/King Lake Dyke**	**Snap/King Lake Dyke**	**Snap/King Lake Dyke**
SAMPLE		**B3-11**	**B3-12**	**B3-13**	**B3-14**	**B3-15**	**B3-16**	**B3-1**	**B3-2**	**B3-3**	**B3-4**	**B3-17**
Rb-Sr												
Analysis date	**▼ SNAP LAKE DIAMONDS**	19-Jun-10	19-Jun-10	19-Jun-10	19-Jun-10	19-Jun-10	19-Jun-10	19-Jun-10	19-Jun-10	19-Jun-10	19-Jun-10	19-Jun-10
Analysis method		TIMS - 742	TIMS - 742	TIMS - 742	TIMS - 742	TIMS - 742	TIMS - 742	TIMS - 742	TIMS - 742	TIMS - 742	TIMS - 742	TIMS - 742
Standard average		0.710274	0.710274	0.710274	0.710274	0.710274	0.710274	0.710274	0.710274	0.710274	0.710274	0.710274
+/- 2σ		2.2E-05	2.2E-05	2.2E-05	2.2E-05	2.2E-05	2.2E-05	2.2E-05	2.2E-05	2.2E-05	2.2E-05	2.2E-05
Rb (ppm)		0.05	0.03	2.26	1.09	0.09	0.002	0.01	0.01	0.09	0.03	0.97
Sr (ppm)		3.0	0.3	61.8	3.0	9.6	0.1	0.3	0.3	1.3	2.5	3.1
$^{87}Rb/^{86}Sr$		0.0433	0.3130	0.1059	1.0537	0.0259	0.0619	0.1060	0.0836	0.1956	0.0360	0.9110
$^{87}Sr/^{86}Sr$		0.704432	0.707097	0.704735	0.714747	0.708826	0.704830	0.704739	0.704602	0.707537	0.706265	0.711846
+/- 2SE		3.0E-05	9.3E-04	1.3E-05	2.8E-04	1.7E-05	7.9E-04	2.3E-04	6.1E-04	7.9E-04	1.3E-04	4.4E-05
$^{87}Sr/^{86}Sr_i$		0.704111	0.704777	0.703951	0.706938	0.708635	0.704464	0.704738	0.704052	0.706087	0.705998	0.705095
+/- 2SE		7.1E-05	1.0E-03	1.6E-04	1.6E-03	4.2E-05	7.9E-04	2.3E-04	6.2E-04	8.4E-04	7.9E-04	1.4E-03
FIELD	**Snap Lake**	**Snap Lake**	**Snap Lake**	**Snap Lake**	**Snap Lake**		**Diavik**	**Diavik**	**Diavik**	**Diavik**	**Diavik**	**Diavik**
LOCALITY	**Snap/King Lake Dyke**	**Snap/King Lake Dyke**	**Snap/King Lake Dyke**	**Snap/King Lake Dyke**	**Snap/King Lake Dyke**		**Unknown**	**Unknown**	**Unknown**	**Unknown**	**Unknown**	**Unknown**
SAMPLE	**B3-18**	**B3-20**	**B3-6**	**B3-7**	**B3-8**		**D104**	**D126**	**D131**	**D168**	**D169**	**D170**
Analysis date	19-Jun-10	19-Jun-10	26-Jun-10	26-Jun-10	26-Jun-10		10/12-Jun-10	10/12-Jun-10	10/12-Jun-10	10/12-Jun-10	10/12-Jun-10	10/12-Jun-10
Analysis method	TIMS - 742	TIMS - 742	TIMS - 744	TIMS - 744	TIMS - 744		TIMS - 738/9	TIMS - 738/9	TIMS - 738/9	TIMS - 738/9	TIMS - 738/9	TIMS - 738/9
Standard average	0.710274	0.710274	0.710272	0.710272	0.710272	**▼ DIAVIK DIAMONDS**	0.710260	0.710260	0.710260	0.710260	0.710260	0.710260
+/- 2σ	2.2E-05	2.2E-05	3.4E-05	3.4E-05	3.4E-05		4.1E-05	4.1E-05	4.1E-05	4.1E-05	4.1E-05	4.1E-05
Rb (ppm)	0.01	0.06	0.38	0.08	0.08		0.38	0.32	0.34	0.29	0.22	0.23
Sr (ppm)	1.7	2.6	4.8	0.4	0.5		8.5	4.6	6.8	4.7	4.3	4.4
$^{87}Rb/^{86}Sr$	0.0244	0.0665	0.2299	0.5425	0.4126		0.1293	0.1980	0.1429	0.1784	0.1480	0.1512
$^{87}Sr/^{86}Sr$	0.704250	0.704443	0.707207	0.705379	0.704864		0.704987	0.706075	0.705085	0.705073	0.704789	0.704634
+/- 2SE	1.3E-04	9.3E-05	1.2E-04	5.7E-04	5.5E-04		7.6E-05	9.2E-05	9.8E-05	8.4E-05	8.4E-05	6.7E-05
$^{87}Sr/^{86}Sr_i$	0.704069	0.703950	0.705504	0.701359	0.701806		0.704884	0.705917	0.704972	0.704931	0.704671	0.704513
$\varepsilon_{Sr\,i}$	1.3E-04	1.4E-04	3.6E-04	9.9E-04	8.2E-04		7.9E-05	9.7E-05	1.0E-04	8.9E-05	8.7E-05	7.1E-05
FIELD		**Ekati**	**Ekati**	**Ekati**	**Ekati**	**Ekati**	**Ekati**	**Ekati**	**Ekati**	**Ekati**	**Ekati**	**Ekati**
LOCALITY		**Fox**	**Fox**	**Fox**	**Fox**	**Fox**	**Fox**	**Fox**	**Fox**	**Fox**	**Fox**	**Fox**
SAMPLE		**E141**	**E142**	**E151**	**E152**	**E153**	**E154**	**E111**	**E11014**	**153**	**E217**	**E191**
Analysis date		25-Aug-09	25-Aug-09	10/12-Jun-10	10/12-Jun-10	10/12-Jun-10	10/12-Jun-10	10/12-Jun-10	10/12-Jun-10	10/12-Jun-10	10/12-Jun-10	10/12-Jun-10
Analysis method		TIMS - 0644	TIMS - 0644	TIMS - 738/9	TIMS - 738/9	TIMS - 738/9	TIMS - 738/9	TIMS - 738/9	TIMS - 738/9	TIMS - 738/9	TIMS - 738/9	TIMS - 738/9
Standard average	**▼ EKATI DIAMONDS**	0.710254	0.710254	0.710260	0.710260	0.710260	0.710260	0.710260	0.710260	0.710260	0.710260	0.710260
+/- 2σ		2.3E-05	2.3E-05	4.1E-05	4.1E-05	4.1E-05	4.1E-05	4.1E-05	4.1E-05	4.1E-05	4.1E-05	4.1E-05
Rb (ppm)		0.75	0.53	0.29	0.86	0.30	0.22	0.99	0.46	0.01	1.49	0.32
Sr (ppm)		12.32	1.27	4.64	23.60	9.52	1.65	3.73	1.51	0.76	17.07	71.19
$^{87}Rb/^{86}Sr$		0.1757	1.2079	0.1809	0.1049	0.0916	0.3822	0.7688	0.8758	0.0384	0.2520	0.0128
$^{87}Sr/^{86}Sr$		0.704860	0.712028	0.705978	0.707800	0.707780	0.709275	0.706095	0.707090	0.706026	0.704055	0.705609
+/- 2SE		2.0E-05	5.0E-05	7.7E-05	5.9E-05	4.1E-05	2.4E-04	1.4E-04	7.5E-05	2.0E-04	3.0E-05	1.0E-04
$^{87}Sr/^{86}Sr_i$		0.704726	0.711072	0.705834	0.707717	0.707707	0.708971	0.705483	0.706394	0.705996	0.703855	0.705598
+/- 2SE		8.2E-05	2.1E-04	8.2E-05	6.1E-05	4.3E-05	2.5E-04	1.9E-04	1.8E-04	2.0E-04	5.0E-05	1.0E-04

Appendix - Table A3. Sr isotope data for fibrous and monocrystalline diamonds

	DEMOGRATIC REPUBLIC OF CONGO, Congo Craton											
LOCALITY		Congo	Congo	Congo	Congo	Congo	Congo	Congo	Congo	Congo	Congo	Congo
KIMBERLITE		Unknown	Unknown	Unknown	Unknown	Unknown	Unknown	Unknown	Unknown	Unknown	Unknown	Unknown
SAMPLE		**CNG-1**	**CNG-4**	**CNG-7**	**CNG-8**	**CNG-9**	**CNG-10**	**CNG 1 B**	**CNG 1 C**	**DRC 2**	**DRC 2**	**DRC 2**
Rb-Sr								*Combustion	*Combustion	*Combustion	*Combustion	*Combustion
Analysis date		19-Jun-08	19-Jun-08	19-Jun-08	19-Jun-08	19-Jun-08	19-Jun-08	25-Aug-09	25-Aug-09	25-Aug-09	25-Aug-09	25-Aug-09
Analysis method		TIMS - 0511	TIMS - 0511	TIMS - 0511	TIMS - 0511	TIMS - 0511	TIMS - 0511	TIMS - 0644	TIMS - 0644	TIMS - 0644	TIMS - 0644	TIMS - 0644
Standard average	▼ CONGO DIAMONDS	0.710240	0.710240	0.710240	0.710240	0.710240	0.710240	0.710254	0.710254	0.710254	0.710254	0.710254
+/- 2σ		1.8E-05	1.8E-05	1.8E-05	1.8E-05	1.8E-05	1.8E-05	2.3E-05	2.3E-05	2.3E-05	2.3E-05	2.3E-05
Rb (ppm)		0.03	0.06	0.04	0.28	0.63	0.42	0.02	0.01	0.11	0.10	0.13
Sr (ppm)		1.3	2.9	1.0	4.9	4.3	9.2	0.9	0.3	8.9	9.4	8.3
$^{87}Rb/^{86}Sr$		0.0743	0.0604	0.1016	0.1679	0.4237	0.1314	0.0756	0.0817	0.0361	0.0303	0.0440
$^{87}Sr/^{86}Sr$		0.705597	0.705650	0.705663	0.706016	0.707339	0.712539	0.710252	0.710110	0.705292	0.705292	0.704508
+/- 2SE		1.8E-04	6.9E-05	1.5E-04	6.3E-05	5.2E-05	6.1E-05	9.2E-06	4.6E-05	1.2E-05	1.0E-05	1.1E-05
$^{87}Sr/^{86}Sr_i$		0.705591	0.705645	0.705654	0.706002	0.707304	0.712528	0.710246	0.710104	0.705289	0.705290	0.704505
+/- 2SE		1.8E-04	6.9E-05	1.5E-04	6.3E-05	5.2E-05	6.1E-05	9.3E-06	4.6E-05	1.2E-05	1.0E-05	1.1E-05

	CANADA, Slave Province										
FIELD	Lac de Gras	Lac de Gras	Lac de Gras	Lac de Gras	Lac de Gras	Lac de Gras	Lac de Gras	Lac de Gras	Lac de Gras	Lac de Gras	Lac de Gras
LOCALITY	Ekati - Fox	Ekati - Fox	Ekati - Fox	Ekati - Fox	Ekati - Fox	Ekati - Fox	Ekati - Fox	Ekati - Fox	Ekati - Fox	Ekati - Fox	Ekati - Fox
SMP-INC.#	E111	E151	E152	E153	E154	E141	E142	E191	E217	E231	E11014
E- or P-Type	?	P	P	P	P	P	E	P	P	P	?
# of inclusions	29	24	36	36	28	46	20	37	26	35	22
(%)*											
SiO_2	6.67	4.67	7.07	3.53	3.38	6.62	46.66	3.43	4.18	5.32	41.58
TiO_2	1.19	1.10	1.34	1.39	1.78	1.09	2.63	1.46	0.90	1.84	1.93
Al_2O_3	1.07	0.93	1.09	1.17	0.85	0.96	6.01	0.81	0.70	1.06	5.35
FeO	5.01	7.67	6.79	4.60	4.51	4.53	4.18	4.19	5.08	5.96	5.34
MgO	5.35	3.75	4.41	4.18	1.45	4.54	2.74	1.38	2.80	2.59	2.63
CaO	7.55	5.52	6.35	6.45	2.05	7.59	5.04	2.02	4.98	4.89	4.68
BaO	10.95	12.94	12.09	12.26	13.77	11.04	2.89	11.40	14.35	12.31	5.63
Na_2O	9.81	5.77	5.01	6.06	8.94	5.98	3.04	3.73	6.04	8.52	1.95
K2O	24.19	25.06	24.48	26.51	25.84	24.57	13.43	22.19	25.19	22.82	16.50
P_2O_5	1.01	0.80	0.53	0.79	0.52	1.11	3.23	1.28	0.82	0.83	3.61
Cl	22.67	28.24	25.01	27.63	33.14	26.61	4.49	31.97	30.44	28.84	5.70
SO_3	0.61	0.31	0.92	0.60	0.24	0.62	0.62	0.63	0.40	0.74	1.13
SrO	2.37	1.93	3.21	3.84	1.61	2.42	2.98	13.24	2.65	2.50	2.27
Cr_2O_3	0.92	0.60	0.74	0.38	0.71	1.14	1.03	0.96	0.68	1.09	0.80
MnO	0.62	0.71	0.90	0.54	1.06	1.12	1.02	1.30	0.70	0.69	0.77
F	0.00	0.00	0.06	0.07	0.14	0.08	0.00	0.01	0.08	0.00	0.13
Uncertainty +/- 10%											
TOTAL	100.00	100.00	100.00	100.00	100.00	100.00	100.00	100.00	100.00	100.00	100.00

*** Values averaged and normalized to 100%: See section 3.4.2 Chapter 3**

Appendix - Table A4. Average bulk major element composition of micro-inclusions in individual diamonds

Resolution Mode	Low 1	Runs Passes	4 3	Estimated Total Time: [hr:min:sec]	00:01:50

	Isotope	Accurate Mass	Mass Window	Mass Range	Magnet Mass	Settling Time	Sample Time	Samples Per Peak	Segment Duration	Search Window	Integration Window	Scan Type	Detection Mode	Integration Type	IS Index	IS Name	Regression Type
1	Ti47	46.9512	60	46.904 - 46.998	43.955	0.001	0.0100	20	0.12	80	40	Escan	Both	Average	9	In115	Thru Zero
2	Ti48	47.9474	60	47.899 - 47.995	43.955	0.001	0.0100	20	0.12	80	40	Escan	Both	Average	9	In115	Thru Zero
3	Ti49	48.9473	60	48.898 - 48.996	43.955	0.001	0.0200	20	0.24	80	40	Escan	Both	Average	9	In115	Thru Zero
4	Rb85	84.9113	60	84.826 - 84.996	84.911	0.040	0.0600	20	0.72	80	40	Escan	Both	Average	9	In115	Thru Zero
5	Sr88	87.9051	60	87.817 - 87.993	84.911	0.001	0.0600	20	0.72	80	40	Escan	Both	Average	9	In115	Thru Zero
6	Y89	88.9053	60	88.816 - 88.994	84.911	0.001	0.0100	20	0.12	80	40	Escan	Both	Average	9	In115	Thru Zero
7	Zr90	89.9042	60	89.814 - 89.994	84.911	0.001	0.0150	20	0.18	80	40	Escan	Both	Average	9	In115	Thru Zero
8	Nb93	92.9058	60	92.813 - 92.999	84.911	0.001	0.0300	20	0.36	80	40	Escan	Both	Average	9	In115	Thru Zero
9	In115	114.9033	60	114.788 - 115.018	114.903	0.022	0.0100	20	0.12	80	40	Escan	Both	Average			Thru Zero
10	Cs133	132.9049	60	132.772 - 133.038	132.905	0.012	0.0200	20	0.24	80	40	Escan	Both	Average	9	In115	Thru Zero
11	Ba137	136.9053	60	136.768 - 137.042	132.905	0.001	0.0150	20	0.18	80	40	Escan	Both	Average	9	In115	Thru Zero
12	La139	138.9058	60	138.767 - 139.045	132.905	0.001	0.0150	20	0.18	80	40	Escan	Both	Average	9	In115	Thru Zero
13	Ce140	139.9049	60	139.765 - 140.145	132.905	0.001	0.0150	20	0.18	80	40	Escan	Both	Average	9	In115	Thru Zero
14	Pr141	140.9071	60	140.766 - 141.048	132.905	0.001	0.0100	20	0.3	80	40	Escan	Both	Average	9	In115	Thru Zero
15	Nd143	142.9093	60	142.766 - 143.052	132.905	0.001	0.0150	20	0.18	80	40	Escan	Both	Average	9	In115	Thru Zero
16	Nd145	144.912	60	144.767 - 145.057	132.905	0.001	0.0100	20	0.12	80	80	Escan	Both	Average	9	In115	Thru Zero
17	Nd146	145.9126	60	145.767 - 146.058	132.905	0.001	0.0100	20	0.12	80	80	Escan	Both	Average	9	In115	Thru Zero
18	Sm147	146.9144	60	146.767 - 147.061	132.905	0.001	0.0150	20	0.18	80	40	Escan	Both	Average	9	In115	Thru Zero
19	Sm149	148.9167	60	148.768 - 149.066	132.905	0.001	0.0150	20	0.18	80	40	Escan	Both	Average	9	In115	Thru Zero
20	Eu151	150.9193	60	150.768 - 157.080	132.905	0.001	0.0150	20	0.18	80	40	Escan	Both	Average	9	In115	Thru Zero
21	Gd157	156.9234	60	156.767 - 157.080	156.923	0.014	0.0200	20	0.24	80	40	Escan	Both	Average	9	In115	Thru Zero
22	Dy161	160.9264	60	160.765 - 161.087	156.923	0.001	0.0200	20	0.24	80	40	Escan	Both	Average	9	In115	Thru Zero
23	Er166	165.9298	60	165.764 - 166.096	156.923	0.001	0.0200	20	0.24	80	40	Escan	Both	Average	9	In115	Thru Zero
24	Yb172	171.9359	60	171.764 - 172.108	156.923	0.001	0.0200	20	0.24	80	40	Escan	Both	Average	9	In115	Thru Zero
25	Lu175	174.9402	60	174.765 - 175.115	156.923	0.001	0.0100	20	0.3	60	40	Escan	Both	Average	9	In115	Thru Zero
26	Hf179	178.9453	60	178.766 - 179.124	156.923	0.001	0.0300	20	0.9	60	40	Escan	Both	Average	9	In115	Thru Zero
27	Pb208	207.9761	60	207.768 - 208.184	207.976	0.026	0.0100	20	0.3	60	40	Escan	Both	Average	9	In115	Thru Zero
28	Th232	232.0375	60	231.805 - 232.270	207.976	0.001	0.0100	20	0.3	60	40	Escan	Both	Average	9	In115	Thru Zero
29	U238	238.0502	60	237.812 - 238.288	207.976	0.001	0.0100	20	0.3	60	40	Escan	Both	Average	9	In115	Thru Zero
30	Tb159	158.9248	60	158.766 - 159.084	156.923	0.001	0.0100	20	0.3	60	40	Escan	Both	Average	9	In115	Thru Zero
31	Ca44	43.9549	60	43.911 - 43.999	43.955	0.300	0.0100	20	0.12	80	40	Escan	Both	Average	9	In115	Thru Zero
32	Sn118	117.9011	60	117.783 - 118.019	114.903	0.001	0.0100	20	0.12	80	40	Escan	Both	Average	9	In115	Thru Zero

Appendix - Table A5. Method file parameters for trace element analysis on Element2 ICPMS

	Isotope	Accurate Mass	Programmed Equation	Correction Equation	Apended For Correction	Equation Active
1	Ti47	46.9512				No
2	Ti48	47.9474	Ca	-0.0909*Ca44		No
3	Ti49	48.9473				No
4	Rb85	84.9113				No
5	Sr88	87.9051				No
6	Y89	88.9053				No
7	Zr90	89.9042				No
8	Nb93	92.9058				No
9	In115	114.9033	Sn	-0.0149*Sn118		No
10	Cs133	132.9049				No
11	Ba137	136.9053			use	No
12	La139	138.9058			use	No
13	Ce140	139.9049			use	No
14	Pr141	140.9071			use	No
15	Nd143	142.9093			use	No
16	Nd145	144.912				No
17	Nd146	145.9126				No
18	Sm147	146.9144			use	No
19	Sm149	148.9167				No
20	Eu151	150.9193	Ba	-0.000388*Ba137		Yes
21	Gd157	156.9234	La, Ce, Pr	-0.000061*La139-0.000514*Ce140-0.015565*Pr141	use	Yes
22	Dy161	160.9264	Nd	-0.010694*Nd143		Yes
23	Er166	165.9298	Nd, Sm	-0.007217*Nd143-0.001461*Sm147		Yes
24	Yb172	171.9359	Gd (La, Ce, Pr)	-0.01205*Gd157		Yes
25	Lu175	174.9402	Gd (La, Ce, Pr), Tb (Ce, Pr, Nd)	-0.000589*Gd157-0.006315*Tb159		Yes
26	Hf179	178.9453				No
27	Pb208	207.9761				No
28	Th232	232.0375				No
29	U238	238.0502				No
30	Tb159	158.9248	Ce, Pr, Nd	-0.000106*Ce140-0.000059*Pr141-0.016199*Nd143	app	Yes
31	Ca44	43.9549			app	No
32	Sn118	117.9011			app	No

Appendix - Table A6. Method file parameters for trace element analysis on Element2 ICPMS

Diamond Numbers (*Referencing Figures 3.4, 3.5 and 3.6*)

Referencing Figure 3.4 – Diavik Diamonds

	A	**B**	**C**	**D**	**E**
1	D201	D102	D108	D110	D112
2	D113	D114	D115	D116	D117
3	D118	D173	D181	D182	D183
4	D184	D183	D186	D199	D200
5	D170	D104	D126	D131	D167
6	D168	D169			

Referencing Figure 3.5 – Ekati Diamonds

	A	**B**	**C**	**D**	**E**	**F**
1	E/154	E/111	E/151	E/152	E/153	
2	E2105	E121	E122	E161	E171	E2104
3	E1101	E1102	E1103	E1104	E1105	E2103
4	E1106	E1107	E1108	E1109	E11010	E2102
5	E11011	E11012	E241	E242	E243	E291
6	E244	E245	E246	E247	E248	E274
7	E251	E262	E271	E272	E273	
8	E2108	E131	E172	E221	E249	E2101
9	E252	E264				
10	E261	E141	E142	E191	E11013	E231
11	E11014	E11015	E216	E217		

Referencing Figure 3.6 – Snap Lake Diamonds

	A	**B**	**C**	**D**	**E**	**F**
1	B4-10	B1-1	B1-2	B1-3	B1-4	B1-5
2	B1-6	B1-7	B1-8	B2-1	B2-2	B2-3
3	B2-4	B2-5	B3-1	B3-2	B3-3	B3-4
4	B3-5	B3-6	B3-7	B3-8	B3-9	B3-10
5	B3-11	B3-12	B3-13	B3-14	B3-15	B3-16
6	B3-17	B3-18	B3-19	B3-20	B4-1	B4-2
7	B4-3	B4-4	B4-5	B4-6	B4-7	B4-8
8	B4-9					

PROCESS 1: BEAKER CLEANING

3ml, 7ml, 30ml SAVILLEX and WHITE PTFE ABLATION CELLS

Introduction:
It is of the utmost importance that all the beakers used in the acquisition of diamond material through laser ablation and subsequent chemistry is ultra-clean and thus will contribute as little contaminant as possible to the sample analytes.

Hazards:
This process uses concentrated acid and as such it is mandatory to read any relevant substance handling sheets before undertaking this procedure.

Acids used for 10 beakers:

UpA 6N HCl	20 mls
SpA 6N HCl	20 mls
SpA 16N HNO_3	150 mls

Procedure: Beaker Cleaning **1-12: Standard clean lab hood**
13-20: Ultra-clean hood

1. Each beaker to be cleaned should have any remaining contents emptied into a waste beaker for disposal. After this is done rinse the inside of the beaker and cap with MQ H_2O from a MQ dispensing bottle (**Keep all beakers and MQ bottle resting on clean Clingfilm to avoid picking up unnecessary 'dirt'**). Using white Sontara micropure tissues and some ethanol from a dispensing bottle, wipe off any label ink from the outer surface of the beaker.
2. Using a SpA 6N HCl dispensing bottle, add approx. 1ml to cover the base of the beaker sealing it with the screw cap. Place on a hotplate at 120^0C for at least 7hrs (or overnight).
3. Remove the beakers from the hotplate, decant the HCl to a waste beaker, rinse the beaker and its screw cap with MQ H_2O as described in step 1.
4. Repeat steps 3. and 4.
5. Take a designated 1 litre Savillex beaker. Fill this ¾ full with dilute (~2N) SpA HNO_3. This concentration is achieved by first adding MQ H_2O from the mechanical MQ dispenser and then adding SpA HNO_3 from the glass stock bottles in a 7:1 ratio. **Note that the MQ from the mechanical dispenser should only be taken once the resistivity has reached 18.2Ω.** The 1l beaker must be filled before adding the smaller beakers to be washed as to avoid the possibility of creating air pockets.
6. Add as many of the beakers and their removed screw caps to the dilute HNO_3 as will fit without overflowing the 1l Savillex beaker. **Leave at least 1.5cm between the top of the dilute HNO_3 and the upper lip of the beaker.** Cap

the 1L beaker and place it on a hotplate at 80^0C for at least 7hrs (or overnight).

7. Decant the dilute HNO_3 from the 1l beaker to waste within an extraction hood. Shake the beaker towards the end to dispense as much liquid as possible from inside the smaller beakers being washed.
8. Empty the beakers being cleaned into a Clingfilm lined tray. Rinse the 1L Savillex beaker with MQ H_2O, cap and put away.
9. Take another designated 1 litre Savillex beaker and ¾ fill it with MQ H_2O from the mechanical MQ dispenser. Add as many of the beakers and their removed screw caps to the MQ H_2O as will fit without over flowing the 1L Savillex beaker. **Leave at least 1.5cm between the top of the MQ H_2O and the upper lip of the beaker.** Cap the 1L beaker and place it on a CL hotplate at 80^0C for at least 7hrs (or overnight).
10. Decant the MQ H_2O from the 1l beaker to waste within an extraction hood. Shake the beaker towards the end to dispense as much liquid as possible from inside the smaller beakers being washed.
11. Repeat steps 9. 10. 11. and once again 9.

* *

12. Take the tray of beakers into an ultraclean hood and replace the caps onto the beakers, *first* shaking off any excess MQ H_2O with a controlled flick of the wrist over a waste beaker.
13. Using an UpA 6N HCl dispensing bottle, add approx. 1ml to cover the base of the beaker sealing it with the screw cap. Place on a hotplate at 120^0C for 3hrs.
14. Remove from the hotplate, decant HCl to waste and rinse with MQ H_2O from the dispensing bottle. Then add approx. 1ml MQ H_2O to cover the base of the beaker sealing it with the screw cap. Place on a hotplate at 80^0C for 30mins.
15. Remove from the hotplate, decant H_2O to waste and rinse with MQ H_2O from the dispensing bottle. Then add approx. 1ml UpA 6N HCl to cover the base of the beaker sealing it with the screw cap. Place on a hotplate at 120^0C for 3hrs.
16. Repeat step 15.
17. Remove from the hotplate, decant H_2O to waste.
18. Replace the caps onto the beakers, *first* shaking off any excess MQ H_2O with a controlled flick of the wrist over a waste beaker.
19. Beakers are now clean and ready for use.

COMPLETION TIME: ~ 5-7 DAYS

PROCESS 2: PRE-ABLATION PROCEDURES

SAMPLE WASHING, WEIGHING AND LOADING

Introduction:
Fluid-inclusions trapped within the diamond matrix are accessed via laser ablation of the diamond surface. As this may concern sub-ppt levels of analyte, the utmost care must be taken to ensure accurate weight measurements and the avoidance of any contamination sources.

Hazards:
This process will involve the use of HF and as such it is mandatory to read any relevant substance handling sheets before undertaking this procedure.

Acids used for 10 samples:

UpA 6N HCl	25 mls
UpA 29N HF	2.5 mls
UpA 16N HNO_3	2.5 mls

Procedure: Sample Washing
(Each sample for ablation in a separate 3ml labelled microtube)

1. Decant UpA 29N HF from its stock bottle into a clean 7ml Savillex beaker. Also decant UpA 16N HNO_3 from its stock bottle into a separate clean 7ml Savillex beaker. **How much you decant depends on how many samples you wish to wash. A filled 7ml Savillex will allow for 28 samples to be washed.**
2. With the sample microtubes placed in a rack, use a designated 0.1-1ml pipettor with a cleaned, blue 1ml pipette tip to transfer 0.25mls UpA 16N HNO_3 from the 7ml Savillex beaker into each of the microtubes. **Before transferring the acid into the microtubes, 2 x 0.25mls should be passed to the waste beaker to ensure the pipette is clean.** When dispensing the acid from the pipettor into the microtube the tip of the pipette should not come closer than 1cm to the top of the microtube.
3. Discard the pipette tip to the bin.
4. In the manner of step 2., using a new pipette tip add 0.25mls of UpA 29N HF to the sample microtubes. **Replenish the 7ml Savillex beakers with the required acid if need be.**
5. Discard the pipette tip to the bin.
6. Close the sample microtubes and shake to ensure the acids are mixed around the diamond.
7. Making sure that the microtubes are closed, arrange them in a microtube tray with an open base and then place them in the bottom of an ultrasonic bath. The water level should cover the bottom 5mm of each microtube. **Use Rho-H_2O class water.**

8. Sonicate for 180 minutes without heat.
9. Remove the sample microtubes from the tray into their rack. Using the designated 0.1-1ml pipettor with a cleaned, blue 1ml pipette tip remove the acid and discard it to the waste beaker. **A clean pipette tip should be used for each sample.**
10. Using the MQ H_2O dispenser bottle, rinse the diamond by adding approx. 2.5mls of MQ H_2O to the sample microtube. Close the microtube and shake the diamond to fully rinse.
11. Using the designated 0.1-1ml pipettor with a cleaned, blue 1ml pipette tip remove the MQ H_2O and discard it to the waste beaker.
12. Repeat step 10 AND 11.
13. Using the UpA 6N HCl dispensing bottle add approx. 2.5mls to the sample microtube.
14. Close microtube and leave for 48 hours.
15. Repeat steps 9., 10., 11. and 12.
16. With the microtubes open place them horizontally on a hotplate at $100^{O}C$ for 90 minutes to be sure the diamonds are dry. **Take care not to allow the diamond to fall out from the microtube.**
17. Close the microtubes. The diamonds are now ready to be weighed.

COMPLETION TIME: 3 DAYS

<u>Procedure</u>: Sample Weighing

Gold boats should have been pre-cleaned having been covered in UpA 6N HCl in a 3ml beaker and put on a hotplate at $120^{O}C$ for 180 minutes before being rinsed twice with MQ H_2O and then dried.

The tips of PTFE coated tweezers should have been pre-cleaned in UpA 1N HCl and rinsed with MQ H_2O.

1. Each sample microtube should have an appropriate batch number. **All samples numbers with their respective batch numbers and weights should be recorded in a log book.**
2. Take one of the gold boats and place it on the Mettler 7 figure balance using the PTFE coated tweezers.
3. Close the door of the balance and then tare (zero) the balance.
4. Open the door and using the tweezers transfer the diamond from the microtube onto the gold boat. Close the door.
5. Record the weight. Remove the sample back to the microtube. Close the door and tare the balance.
6. Repeat steps 4. and 5. for a total of five times. Take the average of those five measurements as the weight of the diamond.
7. The diamonds are now ready to be loaded into the ablation cells.

Measurements taken on the Mettler Toledo™ UMT2 Micro Balance are reported with an uncertainty of +/- 0.1 μg on the diamond weight (1 std deviation; determined on 200 replicates).

Procedure: Sample Loading

Ablation cells are leached in SpA 6N HCl (2 x 24 hrs) at 120°C to remove any memory of a previous sample. The main compartment and parts are then immersed in 2N HNO_3 for 24 hrs at 80°C followed by a Milli-Q H_2O bath (2 x 24hrs). The last stage involves a further 120°C leach in UpA 6N HCl (2 x 24 hrs). **(See PROCESS 1).**

Laser glasses should have been pre-cleaned for 24 hrs in dilute UpA HNO_3 and rinsed in MQ H_2O. Early experiments found that significant Ce contamination can arise due to Ce-based polishing compounds used in the glass manufacture. Cleaning of laser glasses therefore must be thorough prior to any analysis session. Immediately prior to use the laser glass is dried in a high-purity argon gas-steam.

1. A clean ablation cell is taken for each diamond. The screw top is removed and the cell cap is taken off and placed on the screw top.
2. Using the clean PTFE tweezers (wiped with MQ H_2O and Sontara 100 paper) transfer the diamond from the sample microtube onto the plinth in the ablation cell. **If the diamond weighs above 20mg then it should hold under its own weight during laser impact. If the diamond weighs less than this it should be held down with pre-cut parafilm squares (2x2mm) that have been leaching in MQ H_2O for at least 5 days.**
3. Replace the cap onto the cell.
4. Rinse a laser glass in MQ H_2O and hold it with your fingers on the outer rim while drying it completely in the high purity argon gas line. **You will need to take care to have the gas stream hit the glass perpendicular to its flat surface to ensure any material on the surface is directed away.**
5. Place the glass in its covered white teflon transfer tray.
6. Remove the cap from the ablation cell and immediately replace with the clean laser glass. Put the cap in the transfer tray.
7. Replace the screw top onto the cell.
8. The cell is now ready to be taken to the laser.

PROCESS 3: POST-ABLATION PROCEDURES

SAMPLE COLLECTION

Introduction:
The collected sample can either be run fully for Trace-elements on the *Element2* (ICPMS) or aliquoted for Sr columns and subsequent Isotope analysis on the *Triton* (TIMS) also. This procedure will detail the steps involved in getting the sample from the ablation cell to a solution stage ready for instrumental analysis.

Hazards:
This process uses concentrated acid and as such it is mandatory to read any relevant substance handling sheets before undertaking this procedure.

Acids used for 10 samples plus 10 blanks:

UpA 6N HCl (made with UpA H_2O)	160 mls
3N UpA HNO_3 (made with UpA H_2O)	4 mls
3% UpA HNO_3 (made with UpA H_2O)	up to 10 mls

Procedure: Sample Collection

1. Take 2 clean 7ml Savillex beakers. Into 1 beaker pipette 1ml of UpA 6N HCl (made from UpA H_2O) and replace the cap. **The HCl should be taken from a clean 7ml Savillex beaker that the acid has been previously dispensed into.**
2. Remove the screw top from the ablation cell but not yet the laser glass.
3. Replace the cap of the 7ml Savillex beaker containing the 1ml HCl with a PTFE glass holder from the clean teflon box. The beaker cap should be placed 'right-way-up' on a strip of parafilm to the side.
4. Take the laser glass off the ablation cell with one hand and replace immediately with the original cell cap from the other hand.
5. Place the laser glass on the PTFE teflon glass holder. To secure the glass add a screw top from the clean teflon box. Place this 'glass collection' beaker onto a hot plate for 30 minutes at 80^{O}C.
6. During this time pipette enough UpA 6N HCl (made from UpA H_2O) into the ablation cell to cover the diamond and its plinth. With the cell cap on and secured with the screw top, vigorously shake the cell to agitate any settled material.
7. Place the ablation cell in an ultrasonic bath covering the base 10mm of the cell for 40 minutes without heat. It is important that this time frame is not overstepped. If the ablated material and diamond are left in acid for several hours in the closed ablation cell two problems may occur. It is possible that material is then being leached out from the diamond itself that does not represent a part of the ablated material. When the trace element concentrations are normalized to the weight loss of the diamond then an inaccurate value will be reported. Secondly, if the density of ablated material

is significant, some of that material may adhere to the walls of the teflon beaker. This occurs when ~ >600 µg of ablated material is in solution. The site of adherence is where the surface film of the acid meets then teflon wall and results in a ring of ablated material being deposited around the cell that is difficult to collect.

8. During this time return to the 'glass collection' beaker. Take off the screw cap and lift the glass so that MQ H_2O from the dispensing bottle can be used to 'squirt' MQ H_2O on the undersurface of the glass so that it drops back into the collection cell. A short 'squirt' amounting to 2ml will suffice.
9. The laser glass should then be place back into its Teflon storage tray for cleaning.
10. Remove the PTFE glass holder from the 7ml 'glass collection' beaker and replace the cap.
11. Once the 40 minutes of sonication is complete on the ablation cell, tip upside down to collection condensation from the roof of the cell.
12. Remove the screw top, pipette out the HCL and transfer it into the second clean 7ml Savillex beaker. **Care should be taken to make sure that all the acid is collected from the cell and that during collection the pipette tip should move across as much of the surface of the cell and the diamond as possible. It is also useful to reflux some of the acid in the pipette tip over the diamond surface repeatedly to loosen and collect any material not fully taken up by the acid.**
13. The ablated diamond should be rinsed multiple times in MQ H_20, dried at 100°C over 60 minutes and re-weighed.
14. The solution from each beaker is not combined in case of contamination from the glass. *Both solutions can analyzed and concentrations added only if any analyte was present in the 'glass' beaker solution*.
15. Both solutions should be dried down on a hot plate at 120°C until a 3mm drop of liquid is left. Turn the heat then down to 100^{O}C and over see the dry down to completion. This ensures the samples are not baked which may make it difficult for the next acid stage to uptake the material in the beaker fully.
16. **Trace elements only:** To the dried down residue add X µl 3% UpA HNO_3 (made with UpA H_2O) and allow to digest fully for 48 hrs on a hot plate at 120°C before being transferred to pre-leached 3 ml micro-tubes. (X µl can change to the calculated amount likely to be taken up during analysis by the ICPMS in different labs therefore maximizing the volume of material in the analysis).
17. **Trace elements and Isotopic analysis:** To the dried down residue add 200 µl 3N UpA HNO_3 (made with UpA H_2O) and allow to digest fully for 48 hrs on a hot plate at 120°C before transferring 40 µl to clean 3ml Savillex beakers. This 20% is dried down and prepared for trace elements, step 16. The remaining 80% is used for Isotopic analysis and so must undergo column chemistry **(See PROCESS 4, 5)**.

The ablated diamond was rinsed multiple times and re-weighed. The weight loss of the diamond was used to calculate trace element concentrations. For a typical 180 minute ablation of a gem diamond using a 500 x 500 μm raster, the mass loss was ~ 300 μg.

PROCESS 4: SAMPLE ALIQUOTTING

<u>Procedure</u>: Extension of Step 17 of PROCESS 3

1. Add 200 ml UpA 3 N HNO3 acid to the dry sample residue remaining after diamond ablation.
2. Tightly seal the beaker and place on a hot plate at 120^0C for 48 hrs. **Approximately each twelve hours shake the beaker vigorously to encourage dissolution.** Allow the beaker to cool to room temperature and agitated several times, to make sure that any sample condensate on the sides and cap of the beaker are collected into the bottom of the beaker.
3. Take a 20% (by volume) aliquot of the acid solvent, and eject the material into a micro-centrifuge tube, previously leached for 72 hrs using UpA 6 N HCl**. The ~ 300 μg of matrix material is assumed to be homogeneously distributed in solution. Aliquotting by volume is preferred because sample masses are small and weighing errors are relatively high.** A 20% aliquot is 40 μl of the 200 μl solution containing the ablated material. *The micro-pipettor was calibrated by altering the volume control until it was dispensing exactly 40 μl of MQ H_2O as 40 μg weight MQ H_2O at 20^oC.*
4. Dry the 40 μl sample solution down and take up in X μl 3% HNO_3 ready for trace element analysis. **The remaining 160 μl sample solution was then ready to go through the column chemistry procedure for Sr, Pb and Nd separation. (See PROCESS 5)**.

PROCESS 5: Sr-Nd-Pb SEPARATION

Procedure: Column chemistry
(Columns have been pre-cleaned in an UpA 1N HCl leach for at least 5 days)

1. Holding the clean columns up with pre-cleaned plastic tweezers rinse columns in MQ H_2O to waste and place columns in a column rack.
2. Wash columns alternately with several column volumes of UpA 6N HCl and MQ H_2O to waste
3. Add 60 µl of Sr Spec resin from 50 ml FEP dropper bottle.
4. Wash the resin with a column volume of UpA 6N HCl then MQ H_2O to waste.
5. Pass 2 x 100µl 3N HNO_3 to waste. **This nitric medium will 'activate' the resin prior to sample being passed through the column.**
6. Remove waste beaker from below the column.
7. Load the column with the sample in 160 µl 3N HNO3 (*Step 4, PROCESS 4)* and allow the material to pass back into its own beaker.
8. Repeat Step 7. however allow solution to pass into a new pre-cleaned collection beaker (**CB1**).
9. Pass an additional 400 µl 3N HNO_3 in 2 x 200 µl stages. **These collected fractions contain (among other matrix elements) Rb and Ca both of which are important elements to be removed for Sr isotope analysis. For Nd isotope composition determinations, these eluted fractions are collected for further separation.** The Sr fraction of the sample now resides in the resin.
10. Following this, new pre-cleaned collection beakers (**CB2**) are placed under the columns and Sr is eluted from the column in 200 µl MQ H_2O in 2 x 100 µl stages. **The Sr fraction is then dried ready for TIMS analysis (PROCESS 6).**
11. 200 µl UpA 2.5 N HCl is passed through the columns to collect any remaining REEs. This is collected with the previous **Nd** fraction (**CB1)**.
12. Finally, 100 µl (2 x 50 µl) of 8N HCl is eluted and collected in separate beakers (**CB3**). This column fraction contains the **Pb** fraction.

Once the columns are cleaned and ready for loading, the separation procedure occupies about 2h. In order to maintain low blank levels, we discard both columns and resin after each use to avoid possible memory effects.

- **CB1** – Nd fraction dried down and taken up in 1N HCl ready for Nd separation chemistry (See below, PROCESS 7).
- **CB2** – Sr fraction dried down and taken up in 16N HNO_3 ready for TIMS analysis (See below, PROCESS 6).
- **CB3** – Pb fraction dried down and taken up in 3% HNO_3 for PIMMS analysis.

PROCESS 6: Sr LOADING FOR TIMS

<u>Procedure</u>: Sample loading on Re filament

1. Pass a current of ~1A through the filament while Parafilm is melted in two bands onto its surface, leaving a gap of ca. 2mm at the centre of the filament. Turn the current off.
2. Load 1 µl of TaF_5 activator into the gap with a micro-pipettor.
3. Take up the sample in 1µl of 16N HNO_3 and add to the filament before the activator has completely dried.
4. Pass a current of ~1.2 A through the filament to dry the loaded solution. **The Parafilm on either side of the droplet helps to constrain the droplet to the centre of the filament as it dries. Convection within the droplet causes the sample to mix efficiently with the activator.**
5. Once the sample is dry, slowly increase the current to ~1.9 A to burn off the Parafilm, then increase further until a dull red glow is achieved for 1 second.
6. Turn off the current and load the filament directly onto the magazine for loading into the mass spectrometer.

PROCESS 7: Nd SEPARATION

Procedure: Column chemistry

Re-usable Nd column resin needs to be thoroughly washed prior to a new chemistry session. Resin remains in the column and is cleaned in situ.

1. Place columns in the column rack and pass 5 mls 29N HF, followed by 10 mls MQ H_2O, followed by 10 mls 6N HCl, to waste. **Cover each column top or store the columns if they are not to be used within 24 hrs.**
2. Pass a column volume (10 mls) of MQ H_2O followed by a column volume of 1N HF – 1N HCl.
3. Load the sample (**CB1** – PROCESS 5) in 1 ml of 1N HCl. Allow solution to pass to waste.
4. Pass 5 mls 1N HF – 1N HCl to elute Hf to waste.
5. Pass 10 mls 2.5N HCl to elute Sr (of which there should be very little having been removed in PROCESS 5) to waste.
6. Pass 5 mls 2N HNO_3 to elute Ba to waste.
7. **Remove waste beaker and replace with a collection beaker.**
8. Pass 12 mls 6N HCl (10 followed by 2) to elute Nd to collection.

The collected Nd fraction can then be dried down and taken up in 3% HNO_3 for PIMMS analysis.